Structural analysis of carbohydrate – protein interactions under special consideration of lipopolysaccharide fragments, hyaluronic acid, sulfated polysaccharides and sialic acids

DISSERATION

zur Erlangung des Doktorgrades

der Mathematisch-Naturwissenschaftlichen Fakultät

der Christian-Albrechts-Universität zu Kiel

vorgelegt von

Ruiyan Zhang

aus China

Kiel, 2016

Examination date: 15.02.2017

Supervisor: Prof. Dr. Axel Scheidig

Supervision Group: Prof. Dr. Axel Scheidig
Prof. Dr. Dr. habil. Hans-Christian Siebert
Prof. Dr. med. Dipl. Biochem. Roland Schauer

Abstract

Carbohydrate – protein interactions play very important roles in many biological functions. For example, cell-cell recognition, cell adhesion, signal transduction, fertilization, infection and inflammation etc. The better understanding of these binding activities could help to develop more cutting-edge treatment strategies. With the progress of science and technology, more and more new structural analyses of carbohydrate-protein interactions are published. Within this thesis, the focus was on analyzing carbohydrate – protein interactions under special consideration of LPS fragments, hyaluronic acid, sulfated saccharides and sialic acids, with biophysical (NMR, X-ray, SPR), biochemical and cell-biological methods. The main findings are as follows.

In *chapter I*, the SPR (Surface Plasmon Resonance) study indicates the saccharide part of LPS determines the specific interactions with lysozymes. For this reason we focus on a defined building block of a LPS glycosidic chain and started with the disaccharide fragment of *Klebsiella pneumoniae*. The data mining analysis of protein-carbohydrate complexes in the Protein Data Bank (PDB) with GlyVicinity revealed that Trp (W), Tyr (Y), Asn (N) and Asp (D) are the most overrepresented amino acids in the vicinity of α-D-Galp residues. Furthermore, the NMR studies suggested that mixtures of human lysozyme (HL) and the disaccharide building block (repeating unit) of the *Klebsiella pneumoniae* LPS yielded only at pH 5.5 observable changes in the chemical shift values. The two helices and in particular the catalytic residue Glu35 respond to the addition of the disaccharide. In addition, a change of chemical shift is also observed on the β-domain in the center of the first strand (Asn44). A strong reduction of line broadening for Hal shift values. The two helices and in particular the catalytic residue Glu35 respond to the addition of the disaccharide. In abohydrate chain packing close to the A, B, C and D binding sites of HL, which primarily occurred through residue-specific, direct or water-mediated hydrogen bonds and hydrophobic contacts. Overall, these results support a crucial role of the Glu35/Asp53/Trp63/Asp102 residues in HL binding to the tetrasaccharide. These observations suggest an unknown glycan-guided mechanism that underlies recognition of the bacterial cell wall by lysozyme and may complement the HL immune defense function.

In *chapter II*, data mining approaches for a general analysis of all protein - sialic acid complexes in the Protein Data Bank (PDB) showed that Arg (R), Tyr (Y) and Trp (W) residues are the most frequently occurring amino acid residues in the vicinity of bound sialic acids. When focusing on sulfate groups of glycan, the data mining approach shows that Lys (K) is

overrepresented in the vicinity of this functional group. Besides Lys (K) residues, Arg (R) residues are likely to primarily bind such residues due to their vicinity preferably to sulfate groups and uronic acid in the corresponding complexes found in the protein data bank. Our data mining approach was supported by NMR experiments. Our NMR results clearly show that the addition of polySia to the MARCKS-ED peptide causes spectral changes, suggesting that protons from the MARCKS-ED peptide are involved in binding with polySia. In addition, NMR experiments using SHL-1 or the human α-defensins HNP1,2,3 as receptors and polySia fragments from colominic acid used as ligands revealed that three aromatic amino acid residues and an Arg residue play a major role in carbohydrate binding. In our studies we were able to combine the structural analysis with cell-biological experiments. Compared to a control group (poly-L-lysine), the sulfated polysaccharides from algae show a statistically significant enhancement of neurite outgrowth at concentrations from 0.0001 to 0.1 mg/ml. However, at concentrations that were higher than 1 mg/ml, the sulfated polysaccharides exhibit inhibitory effects on neurite outgrowth.

In *chapter III*, a new ImageJ analyzing method was developed and successfully applied to determine the molecular weight distribution of hyaluronic acid (HA). By horizontal agarose gel electrophoresis, compared with control synovial fluid (SF), the molecular weight of hyaluronic acid shifted toward the lower range in osteoarthritis and rheumatoid arthritis SF. The percentage of HA in the upper range of 3.1-6.1 MDa was highest in control SF, followed by early-stage osteoarthritis and late-stage osteoarthritis, and bottoming in rheumatoid arthritis. In the lower ranges of 0.5-1.1 MDa and <0.5 MDa, the relative HA concentrations were significantly higher in early-stage osteoarthritis, late-stage osteoarthritis, and rheumatoid arthritis SF versus control SF.

Zusammenfassung

Kohlenhydrat - Protein - Wechselwirkungen spielen bei vielen biologischen Funktionen eine sehr wichtige Rolle. Beispiele sind die Zell-Zell-Erkennung, die Zelladhäsion, die Signaltransduktion, sowie Fertilisationsprozesse, die Infektions- und die Entzündungsbekämpfung. Das bessere Verständnis dieser biochemischen Aktivitäten kann dazu beitragen, innovative Behandlungsstrategien zu entwickeln. Der Fortschritt von Wissenschaft und Technik ermöglicht die Aufklärung neuer Strukturen von Kohlenhydrat-Protein-Komplexen. Im Rahmen dieser Arbeit wurde der Schwerpunkt auf die Analyse von Kohlenhydrat-Protein-Wechselwirkungen unter besonderer Berücksichtigung von LPS (Lipopolysaccharid) - Fragmenten, Hyaluronsäure, sulfatierten Sacchariden und Sialinsäuren mit biophysikalischen (NMR, Röntgen, SPR) und biochemischen Methoden gelegt. Die wichtigsten Ergebnisse sind in den folgenden Textpassagen zusammengefasst.

In Kapitel I wird mit Hilfe einer die SPR-Studie gezeigt, dass der Saccharidteil von LPS spezifische Wechselwirkungen mit Lysozymen eingeht. Aus diesem Grund wurde der Fokus auf einem definierten Baustein einer LPS-glykosidischen Kette (dem Disaccharidfragment von Klebsiella pneumoniae.) gelegt. Die Analyse von Protein-Kohlenhydrat-Wechselwirkungen in der Proteindatenbank (PDB) erfolgte mit dem Data-Mining-Programm GlyVicinity und zeigte, dass Trp (W), Tyr (Y), Asn (N) und Asp (D) Reste die am häufigsten überrepräsentierten Aminosäuren in der Nähe von α-D-Galp-Saccharideinheiten sind. Weiterhin ging aus den NMR-Studien hervor, dass Mischungen aus HL (human lysozyme) und dem Saccharidbaustein (Wiederholungseinheit) der *Klebsiella pneumoniae* LPS Kohlenhydratkette nur bei zu pH 5.5 beobachtbaren Veränderungen der chemischen Verschiebungswerte führten. Die beiden Helices und insbesondere der katalytische Rest Glu35 reagieren auf die Addition des Disaccharids. Zusätzlich wird eine Änderung der chemischen Verschiebung auch auf der β-Domäne in der Mitte des ersten Strangs beobachtet (Asn44). Es ergibt sich eine signifikante Verringerung der Linienverbreiterung für Hε1 von Trp109 in Gegenwart des Saccharids. Die Kristallstruktur des HL-Tetrasaccharid-Komplexes stellt die Kohlenhydratkettenpackung nahe bei die A, B, C und D Bindungsstellen von HL dar, die primär durch restspezifische, direkte oder wasservermittelte Wasserstoffbrücken und hydrophobe Kontakte gebildet wird. Insgesamt unterstützen diese Ergebnisse, die Annahme, dass die Reste Glu35 / Asp53 / Trp63 / Asp102 eine entscheidende Rolle bei der der HL-Bindung an das Tetrasaccharid spielen.

Diese Beobachtungen deuten auf einen unbekannten Glycan-geführten Mechanismus hin, der der Erkennung der bakteriellen Zellwand durch Lysozym unterliegt und die HL-Immunabwehrfunktion ergänzen kann.

In Kapitel II haben Data Mining - Ansätze für eine allgemeine Analyse aller Protein - Sialinsäure - Komplexe in der Protein Data Bank (PDB) gezeigt, dass Arg (R), Tyr (Y) und Trp (W) die am häufigsten vorkommende Aminosäure - Reste in der Nähe von gebundenen Sialinsäuren sind. Bei einer Fokussierung auf Sulfatgruppen von Glycan zeigt der Data-Mining-Ansatz, dass Lys (K) in der Nähe dieser funktionellen Gruppe überrepräsentiert ist. Neben Lys (K) - Resten sind Arg (R) - Reste überrepräsentiert und zwar aufgrund ihrer Fähigkeit bevorzugt Sulfatgruppen und Uronsäure zu binden. Diese Data-Mining Ergebnisse unterstützen die Interpretation unserer NMR Daten. Unsere NMR-Resultate zeigen in deutlicher Weise, dass die Bindung von polySia an das MARCKS-ED-Peptid spektrale Veränderungen bewirkt, was darauf hindeutet, dass Protonen aus dem MARCKS-ED-Peptid an der Bindung mit polySia beteiligt sind. Darüber hinaus belegen die Ergebnisse aus den NMR-Experimenten mit dem Spinnenlektin SHL-1 sowie den humanen α-Defensinen HNP1,2,3, die als Sialinsäure-Minirezeptoren dienen, dass polySia-Fragmente aus Colominsäure spezifisch bindende Liganden sind. Drei aromatische Aminosäurereste und ein Arg-Rest spielen eine wichtige Rolle bei der Sialinsäurbindung. Es war uns möglich die strukturbiologischen Resultate mit zellbiologischen Ansätzen zu verbinden. Im Vergleich zu einem MARCKS-ED-Kontrollpeptid (Poly-L-Lysin) bewirken sulfatierte Polysaccharide aus Algen eine statistisch signifikante Verbesserung des Neuritenwachstums bei Konzentrationen von 0,0001 bis 0,1 mg / ml. Jedoch zeigen die sulfatierten Polysaccharide. Bei Konzentrationen, die höher als 1 mg / ml sind, hemmende Wirkungen auf das Auswachsen von Neuriten.

In Kapitel III wurde ein neues Image-J-Analyseverfahren entwickelt und erfolgreich angewandt, um die Molekulargewichtsverteilung von Hyaluronsäure (HA) zu bestimmen. Durch horizontale Agarosegelelektrophorese, die mit Kontroll-Synovialflüssigkeit (SF) verglichen wurde, verschob sich das Molekulargewicht (MW) von Hyaluronsäure (HA) in Richtung des unteren Bereichs, der für Osteoarthritis und rheumatoider Arthritis signifikant ist. Der prozentuale Anteil von HA im oberen Bereich von 3.1-6.1 MDa war am höchsten in der Kontrollgruppe, gefolgt von Daten einer frühzeitigen Osteoarthritis und Daten die für eine späte Osteoarthritis und/ oder eine rheumatoide Arthritis sprechen. In den unteren Bereichen der Gele von 0,5-1,1 MDa und <0,5 MDa waren die relativen HA-Konzentrationen einer frühen Osteoarthritis sowie der späten Osteoarthritis und der rheumatoiden Arthritis in Bezug auf die untersuchte SF

gegenüber der SF Kontrolle signifikant höher. Mit Hilfe des Image-J-Analyseverfahren konnte so der optimale Analysebericht in den angefertigten Gelen eingegrenzt bzw. bestimmt werden.

Contents

Abbreviations and acronyms

2D	Two-Dimensional
AFM	Atomic Force Microscopy
BMRB	Biological Magnetic Resonance Bank
CPS	Capsular Polysaccharide
CDC	Centers for Disease Control and Prevention
CRDs	Carbohydrate Recognition Domains
CA	Colominic Acid
DOSY	Diffusion-Ordered Spectroscopy
DFT	Density Functional Theory
HL	Human Lysozyme
HEWL	Hen Egg White Lysozyme
HNK1	Human Natural Killer-1
HD5	Human Alpha Defensin 5
HA	Hyaluronic Acid
ICU	Intensive Care Units
CPKP	Carbapenemase-producing *Klebsiella pneumoniae*
KTS	*K. Pneumonia* Tetrasaccharides
LPS	Lipopolysaccharides
LGA	Lamarckian Genetic Algorithm
MW	Molecular Weight
MARCKS	Myristoylated Alanine-rich C Kinase Substrate

NMR	Nuclear Magnetic Resonance
NCAM	Neural Cell Adhesion Molecule
Neu5Ac	N-Acetylneuraminic Acid
NOESY	Nuclear Overhauser Effect Spectroscopy
O-PS	O-antigenic Polysaccharide
OS	Oligosaccharide
PLL	Poly-L-Lysine
PDB	Protein Data Bank
polySia	Polysialic Acid
RMSD	Root-Mean-Square Deviation
RU	Response Units
SPR	Surface Plasmon Resonance
Sia	Sialic Acids
SHL-1	*Selenocosmia huwena* Lectin-I
STD	Saturation Transfer Difference
SF	Synovial Fluid
TOCSY	Total Correlation Spectroscopy

Chapter I: Interaction studies between carbohydrate residues of bacterial lipopolysaccharides (LPS) and lysozymes as revealed by a combination of biophysical methods under special consideration of the pH conditions

1. Introduction

1.1 Lipopolysaccharide from *Klebsiella pneumoniae*

Klebsiella pneumoniae, also called Friedländer's Bacillus, is a Gram-negative, encapsulated, cylindrical rod and non-motile bacterium of the Enterobacteriaceae family, which was first isolated from the lungs of patients who died from pneumoniae and was described by German pathologist Carl Friedländer in 1882. Then it was renamed by *Klebsiella* in 1886 in honor of the German bacteriologist Edwin Klebs (Fig. 1)[1-3]. As a well-known causative pathogen of various severe diseases, it accounts for pneumonia, urinary tract infections, osteomyelitis, septicemia, as well as wound infections and pyogenic liver abscesses, etc.[4,5]. As leading cause of nosocomial opportunistic infections, *Klebsiella pneumoniae* peculiarly infects immunocompromised patients, suffering from chronic alcoholism, diabetes mellitus, chronic pulmonary obstruction, malignancy, liver disease, and people with debilitating diseases[6,7]. The β-lactam drugs have been effectively used for treating *Klebsiella pneumoniae* infections. However, since initially discovered in 1996 in North Carolina, the strains of carbapenemase-producing *Klebsiella pneumoniae* (CPKP) are only susceptible to limited antibiotics, and resulted in high mortality rates of more than 50%. Moreover, they have widely disseminated in the United State and worldwide during the last decades[8-11]. Therefore, the development of new alternative therapeutic strategies is urgently required.

Fig. 1. Scanning electron graph of *Klebsiella pneumoniae*. Janice Carr/Centers for Disease Control and Prevention (CDC) (Image Number: 6834)

Lipopolysaccharide (LPS), also known as endotoxin that is localized at the surface of almost all Gram-negative bacteria (Fig. 2), is a major constituent part of the outer membrane of *Klebsiella pneumonia*. It plays a crucial role in keeping the structural integrity and stability of the microbacillary membrane, and therefore provides the protection for Gram-negative bacteria from attack (e.g. bile salts and lipophilic antibiotics)[12]. LPS can elicit host defense system responses and acts as the endotoxin causing a diversity of pathophysiologic reactions, including fever, shock, hypotension, disseminated intravascular coagulation, and leukocytosis[13]. Together with the capsular polysaccharide (CPS), they are important factors in the pathogenicity of *Klebsiella pneumonia* infection and are responsible for pneumonia and bacteremia[14-16]. LPS is composed of three kinds of structural domains: the long chain O antigenic polysaccharide (O-PS; O-antigen), the core oligosaccharide (OS), and lipid A. The O-antigen is the outermost component of LPS. Among clinical *Klebsiella pneumonia* isolates from different sources and countries, the O1 antigen is the most prevalent O-antigen[17,18]. It has been reported to be expressed on the surface of most strains, and the antibodies against the O1 antigen can protect animal models from *Klebsiella pneumonia* infection[19,20]. The O1 antigen contains two different O-PS components, D-galactan I and D-galactan II (Fig. 3a)[21,22]. The repeating unit, the disaccharide [-3)-β-D-Galf-(1-3)-α-D-Galp-(1-] was identified as the building block of the D-galactan I (Fig. 3b). It has been artificially synthesized by Nikolay E. Nifantiev and his colleagues[23]. In our study, we utilized this synthetic di- and tetrasaccharide as the binding ligand to analyse the interaction properties of *Klebsiella pneumonia* D-galactan I with human lysozyme.

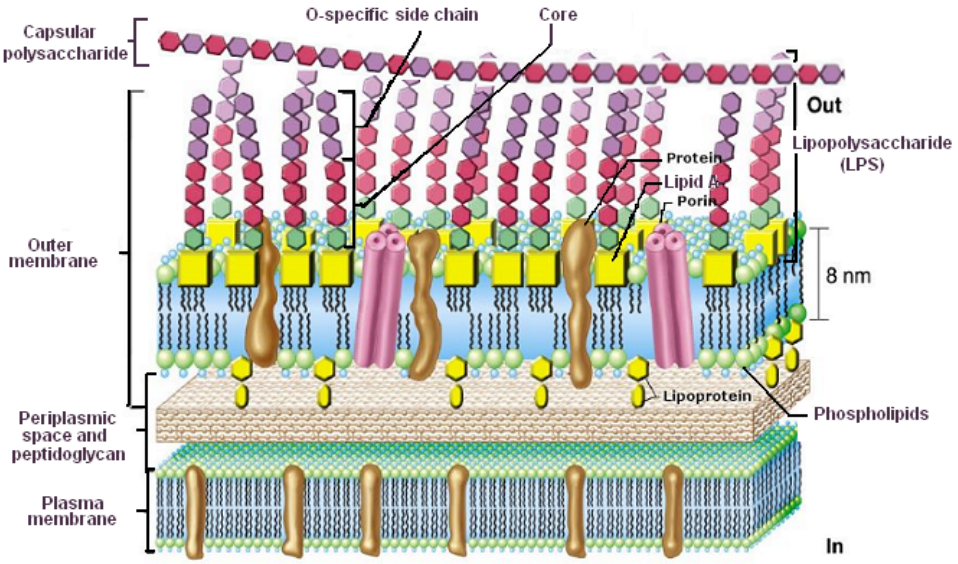

Fig. 2. Lipopolysaccharide (LPS) of Gram-negative bacteria[24].

a

→3)-β-D-Gal*f*-(1→3)-α-D-Gal*p*-(1→ D-galactan I

→3)-α-D-Gal*p*-(1→3)-β-D-Gal*p*-(1→ D-galactan II

b

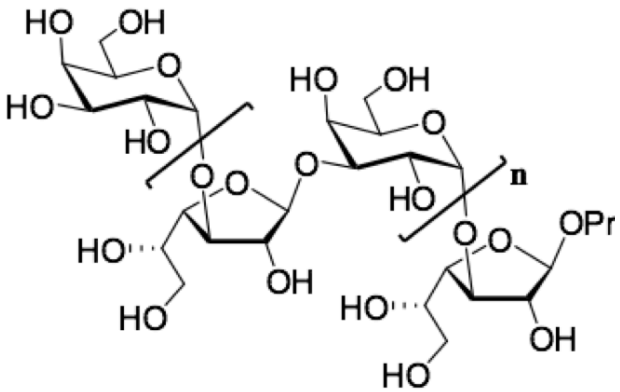

Fig. 3. a The repeating unit structures of the *Klebsiella pneumoniae* O1 LPS consists of two structurally different O-polysaccharides, named D-galactan I and D-galactan II[21]. **b** Structure of synthetic di- and tetrasaccharides related to the glycan chain of the D-galactan I lipopolysaccharide (LPS) from *Klebsiella pneumoniae*.

1.2 Lysozymes

Lysozymes also named as muraminidases of the innate immune system are the lytic enzymes which destroy the peptidoglycans of bacterial cell wall via hydrolysis of β-(1,4)-glycosidic bonds. The antimicrobial activity of lysozymes explains the great interest in their structure and function both for pharmaceutical applications and for food preservation[25]. Lysozymes are occurring in most living organisms. In the animal kingdom three types of lysozymes are distinguished according to amino acid sequence and biochemical properties: c-type (chicken), g-type (goose) and i-type (invertebrate)[26]. C-type lysozymes are found in mammals, birds, reptiles, fish and insects etc.; they consist of ~129 residues, including four conserved disulfide bonds, and form two domains, one built from α-helices and one containing a β-sheet (Fig. 4)[27]. The structure of hen egg white lysozyme was among the first protein crystal structures to be determined[28] and, similarly, this enzyme was among the earliest NMR structures[29]. Since then many X-ray, NMR and other studies have been performed to characterise the structure, dynamics, folding (and misfolding) properties and function of various lysozymes. Of particular interest in food and health related applications are the adaptations of lysozymes to different environments. Thus, while mammals typically show high concentration of lysozyme in the respiratory tract and in milk, birds often exploit lysozyme as an antimicrobial agent in eggs, and fish on the surface of their skin and in the gastrointestinal tract[26]. C-type lysozymes such as human lysozyme (HL) or hen egg white lysozyme (HEWL) all share a conserved sequence (with 30% or higher identity) with strictly conserved disulfide bridges, and similar fold with helices A (residues 5-14), B (25-35), C (90-99) and D (110-116) in the α-domain, and a three-stranded antiparallel β-sheet (42-46, 51-56, 59-61) in the β-domain (Fig. 4)[28,29]. An inter-domain cleft contains six binding pockets (labelled A-F in Fig. 4), with the strictly conserved catalytic residue Glu35 located between the sites D and E[30]. Details of the enzymatic mechanism have been described for HEWL[31] and involve a covalent intermediate with another strictly conserved residue, Asp52, which is provided by the α-domain. This mechanism requires residue Glu35 to be protonated, and indeed its pK_a was found to be unusually high: 6.8 for HL and 5.9 for HEWL[32].

The structural variations between 15 different c-type lysozymes obtained from the Protein Data Bank (PDB)[33] are small. The average RMSD value between all structure pairs, calculated for the backbone of 104 residues, is 0.9 Å (these calculations exclude insertions/deletions, as well as 12 residues in loops adjacent to the latter). The most different structures belong to 3 insect lysozymes that differ by ~1.2 Å RMSD from the other 12 proteins[34]. The more than 20 structures of human lysozymes found in the PDB are overall

even more similar (exceptions are due to perturbations by covalently bound ligands or originating from temperature variations). Nonetheless, it has been noticed for HEWL that the α-domain exhibits increased flexibility when compared to the β-domain, e.g. from studies varying temperature[35] or pressure[36]. Furthermore, a crystal structure of HL with (non-covalent) binding of a tetrasaccharide plus a disaccharide in subsites A-D and E-F, respectively, shows a measurable movement of helix D, which was described as a 'closing' movement leading to tighter lysozyme-ligand interactions. NMR relaxation measurements have shown that the dynamic response indeed varies upon binding of a trisaccharide near the active site (residue 100-115, i.e. helix D plus preceding loop) in HL and HEWL[37] and the authors suggest that ligand binding entails immobilisation of interacting residues and the ensuing penalty is compensated by increased flexibility of other residues. Other NMR studies comparing human lysozyme structures at different temperatures (35°C and 4°C) report that high and low temperature induces 'closing' and 'opening' of the binding cleft, respectively[38].

Besides the presence of interacting ligands and the influence of temperature, pH is also an important determinant for the structure of lysozymes. Thus, for example, deprotonation of Glu35 completely inactivates the enzyme[31]. Structure expansion as a function of pH, in particular far from the isoelectric point, has been reported for HEWL. An interesting application of the pH response of lysozymes is their potential use as "valves" in nanoparticles allowing pH-controlled release of guest molecules[39]. Comparison of surfaces of various c-type lysozymes indicates modulation of the binding affinity to polysaccharides, in particular in sites A-D, by changes of the electrostatic potential.

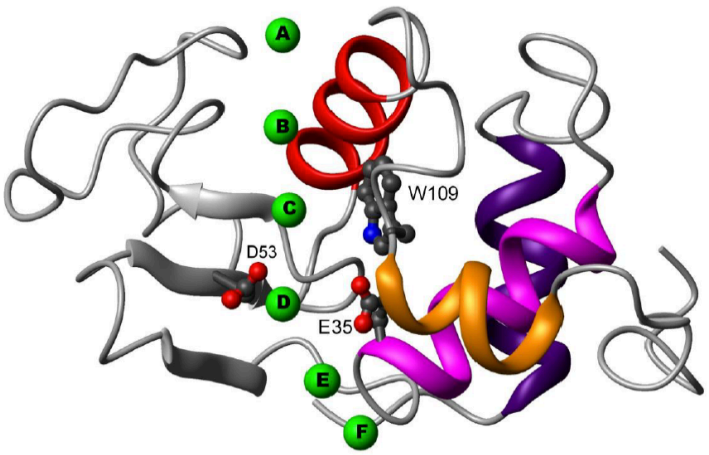

Fig. 4. Structure of human lysozyme (HL; PDB code 1LZS) with selected residues (Glu35, Asp53, Trp109). Binding sites A – F are indicated by letters in green circles, helices are colored as follows: A violet, B magenta, C red and D orange. In the orientation shown, the α-domain is to the right of the binding cleft, the β-domain to the left[27].

1.3 Lysozyme against *Klebsiella pneumoniae* infection

The lysozymes from mice, lysozyme M and lysozyme P, have been assessed and showed the ability to directly kill the *K. pneumonia in vitro*. The further *in vivo* research has elucidated that the enhanced expression of lysozyme in the airways of transgenic mice reduced bacterial burden and increased survival rate of mice, which were intratracheally infected by *K. pneumoniae*. Whereas targeting knockout the lysozyme M gene of mice led to lower effect on *K. pneumoniae* killing and significantly increased susceptibility to *K. pneumoniae* infection[40]. Moreover, intraperitoneal administration of lysozyme could also decrease the pathology resulting from a *Klebsiella pneumoniae* infection in mice[41]. These results suggest that lysozyme plays a very crucial role against *Klebsiella pneumoniae* infection and could be considered as a very promising pharmaceutical agent.

2. Experimental research

2.1 Research topics and methods

In order to reveal the specific non-enzymatic carbohydrate-protein interactions between building blocks of the glycan chain from *K. pneumoniae* and human as well as hen egg white lysozyme, we performed a systematic NMR and X-ray crystallographic study of the response of the HL structure towards pH variation in the range from pH 3-8, which is supported by other biophysical methods (SPR, AFM, Thioflavin T fluorescence assay) and *in silico* approaches. We also analyse the relation between (de)protonation of residue Glu35 and movements of the adjacent residue Trp109 as well as of surrounding helices. Due to the strong pH dependence of the structural properties of lysozymes these results have to be considered as essential prerequisites for a detailed affinity study of HL and HEWL interacting with the weakly binding di- and tetrasaccharids **1** and **2**, the units of the glycan chain of the lipopolysaccharide (LPS) from *K. pneumoniae*.

My part within this study was to perform the X-ray crystallography, Molecular modelling and data mining experiments and analyse the related results.

2.2 The main experimental results

1) Using SPR studies, we could show that the saccharide part of LPS determines the specific interactions with the lysozymes. For this reason we have focused our research on defined

building blocks of the LPS glycosidic chain and started with the disaccharide fragment of *Klebsiella pneumoniae*.

2) Molecular modelling has shown that dimerization of human lysozyme monomers is very likely. However, we have found no evidence for these *in silico* results when human lysozyme was analyzed with NMR methods at different pH values.

3) When comparing the X-ray structures of the human lysozyme from which we have grown crystals in the absence and in the presence of disaccharide **1** at different pH values we have found that a certain amino acid residue (i.e. Trp63) plays a crucial role in the carbohydrate interaction process.

4) The analysis of protein-carbohydrate interactions in the Protein Data Bank (PDB) with GlyVicinity reveals that Trp (W), Tyr (Y), Asn (N) and Asp (D) are the most overrepresented amino acids in the vicinity of α-D-Galp residues.

5) The differences in the patterns of the electrostatic surface potentials argue in favour of variations in ligand binding as well as deviations in the aggregation/ fibrillation behaviour when comparing the human with the avian lysozyme.

6) The NMR studies suggested that mixtures of HL and the disaccharide building block (repeating unit) of the *Klebsiella pneumoniae* LPS (compound **1**) yielded only at pH 5.5 observable changes in the chemical shift values; at pH 3.8 no intermolecular interactions could be detected. Both helices and in particular also the catalytic residue Glu35 respond to the addition of compound **1**. In addition, a change of chemical shift is also observed on the β-domain in the center of the first strand. Noteworthy is the strong reduction of line broadening for Hε1 of Trp109 in the presence of the sugar.

7) In contrast to HL, intermolecular interactions of HEWL could be observed both at pH 3.8 and 5.5. At the lower pH, chemical shift changes due to binding are wider spread than with HL, involving a larger number of residues and covering the length of the entire enzymatic cleft, i.e. all six subsites: Asn44 H, Asp52 H, Gln57 H, Asn59 HN and H, Lys97 and Asp101 H, Ala107 and Ala110 HN. At lower pH, the β-domain is strongly affected by the presence of sugar. At the higher pH the binding is similar to that in HL, affecting Glu35 HN and H, Asn44 H, Trp108 H1 and Hε1, Trp111 HN and Arg112 HN, i.e. only subsites D-F.

8) The crystal structure of the HL-tetrasaccharide complex revealed carbohydrate chain packing close to the A, B, C and D binding sites of HL, which primarily occurred through

residue-specific, direct or water-mediated hydrogen bonds and hydrophobic contacts. Overall, these results support a crucial role of the Glu35/Asp53/Trp63/Asp102 residues in HL binding to the tetrasaccharide (compound **2**). These observations suggest an unknown glycan-guided mechanism that underlies recognition of the bacterial cell wall by lysozyme and may complement the HL immune defense function.

3. Research manuscript

The detailed experimental methods, material, results as well as conclusion are presented in our following manuscript.

3.1 Lysozyme's lectin-like characteristics facilitates its immune defense function

Lysozyme's Lectin-like Characteristics Facilitates its Immune Defense Function

Ruiyan Zhang[1,2], Lisha Wu[3], Thomas Eckert[4,5], Monika Burg-Roderfeld[5], Miguel A. Rojas-Macias[5], Thomas Lütteke[5], Vadim B. Krylov[6], Dmitry A. Argunov[6], Aritreyee Datta[7], Philipp Markart[8,9], Andreas Günther[10], Bengt Norden[3], Roland Schauer[9], Anirban Bhunia[7], Mushira Abdelaziz Enani[11], Martin Billeter[12*], Axel J. Scheidig[2]*, Nikolay E. Nifantiev[6]*, Hans-Christian Siebert[1]*

[1]RI-B-NT Research Institute of Bioinformatics and Nanotechnology, Franziusallee 177, 24148 Kiel, Germany. [2]Institute of Zoology, Department of Structural Biology, Christian-Albrechts-University, Am Botanischen Garten 1-9, 24118 Kiel, Germany. [3]Department of Chemical and Biological Engineering, Chalmers University of Technology, 41296 Gothenburg, Sweden. [4]Clinic of Obstetrics, Gynecology and Andrology for Small and Large Animals, Justus-Liebig-University, Justus-Liebig-University Giessen, Frankfurter Str. 106, 35392 Giessen, Germany. [5]Institute for Veterinary Physiology and Biochemistry, Justus-Liebig-University, Frankfurter Str.100, 35392 Giessen, Germany. [6]Laboratory of Glycoconjugate Chemistry, N.D. Zelinsky Institute of Organic Chemistry, Russian Academy of Sciences, Leninsky prospect 47, 119991 Moscow, Russian Federation. [7]Department of Biophysics, Bose Institute, P-1/12 CIT Scheme VII (M), Kolkata 700054, India. [8]Pneumology, Heart-Thorax-Center Fulda, Pacelliallee 4 - 36043 Fulda, Germany. [9]Institute of Biochemistry, Christian-Albrechts-University, Olshausenstrasse 40, 24098 Kiel, Germany. [10]Medical Clinic II, Justus-Liebig-University, Klinikstraße 33, 35392 Giessen, Germany. [11]Infectious Diseases Division, Department of Medicine, King Fahad Medical City, PO Box 59046, Riyadh 11525, Kingdom of Saudi Arabia. [12]Department of Chemistry and Molecular Biology, University of Gothenburg, 40530 Gothenburg, Sweden.

*To whom correspondence should be addressed:

Martin Billeter - martin.billeter@chem.gu.se;

Axel Scheidig - axel.scheidig@strubio.uni-kiel.de;

Nikolay Nifantiev - nen@ioc.ac.ru;

Hans-Christian Siebert - hcsiebert@aol.com

Abstract

Interactions between human lysozyme (HL) and the lipopolysaccharide (LPS) of *Klebsiella pneumoniae* O1, a causative agent of lung infection, were identified by surface plasmon resonance (SPR). To characterize the molecular mechanism of this interaction, HL binding to synthetic disaccharides and tetrasaccharides representing one and two repeating units, respectively, of the O-chain of this LPS were studied. pH-dependent structural rearrangements of HL after interaction with the disaccharide were observed through NMR. The crystal structure of the HL-tetrasaccharide complex revealed carbohydrate chain packing into the A, B, C and D binding sites of HL, which primarily occurred through residue-specific, direct or water-mediated hydrogen bonds and hydrophobic contacts. Overall, these results support a crucial role of the Glu35/Asp53/Trp63/Asp102 residues in HL binding to the tetrasaccharide. These observations suggest an unknown glycan-guided mechanism that underlies recognition of the bacterial cell wall by lysozyme and may complement the HL immune defense function.

Lower respiratory tract infections are among the top ten causes of death worldwide and are of particular relevance in chronic lung diseases. Lysozyme is one of the most abundant antimicrobial proteins in the airways and alveoli. The concentration of this enzyme in the surface liquid of the human airway is estimated to be 20–100 μg/ml, which is sufficient to kill important pulmonary pathogens such as Gram-positive *Staphylococcus aureus* and Gram-negative *Pseudomonas aeruginosa*[1]. *Klebsiella pneumoniae*, which is a frequent cause of nosocomial infection and may be responsible for up to 20% of the respiratory infections in neonatal intensive care units[2], is also specifically attacked by lysozyme[3].

Human lysozyme (HL, also known as muramidase, *N*-acetyl muramide glycanohydrolase, or EC 3.2.1.17; Figure 1A) is a 130-amino acid cationic protein that cleaves the glycosidic bonds of *N*-acetyl-muramic acid (Figure 1B), thereby damaging the bacterial cell wall and ultimately killing bacteria by lysis in cooperation with defensins. An inter-domain cleft in HL contains six binding pockets (labeled A-F in Figure 1A), and a strictly conserved catalytic residue Glu35 is located between the D and E sites[4]. Co-crystallization of HL with N-acetyl-chitohexaose $(GlcNAc)_6$ (Figure 1B) has revealed a crystal structure with non-covalently linked $(GlcNAc)_4$ and $(GlcNAc)_2$ in subsites A-D and E-F, respectively[5].

In addition to the well-known muramidase activity of HL, increasing evidence suggests the existence of non-enzymatic and/or nonlytic modes of action against Gram-negative and Gram-positive bacteria[6, 7]. Furthermore, lysozyme has antitumor[8] and antiviral activities[7], and it enhances the immune system[9]. The mechanisms of these activities remain unclear, and the dominant questions involve how HL recognizes pathogenic microbes. The ability of lysozyme to interact with lipopolysaccharides (LPSs) was demonstrated in the late 1980s[10, 11]. However, the details of this interaction (i.e., how binding specificity is established between specific parts of the lysozyme protein and the LPS carbohydrate units) have not been examined. The attraction between lysozyme and LPS has been largely attributed to non-specific hydrophobic interactions of lysozyme with lipid A, which is the innermost hydrophobic component of LPS and is primarily responsible for its toxicity. To examine whether lysozyme specifically interacts with bacterial LPS and particularly with the O-chains that form the outer layer of the bacterial cell wall, we performed SPR-based experiments as previously described[12]. In our SPR experiments, the LPS from bacterial *K. pneumoniae* O1 pathogens, which are involved in severe hospital-acquired infections (HAIs) and are clinically relevant to infections beyond those of the airways[13, 14], were immobilized through hydrophobic interactions between the lipid A portion and the SPR sensor chip, and they were treated with HL (Figure S1 in Supplementary Information) to clearly demonstrate the interaction between HL and the immobilized LPSs. To assess whether the O-chains of these LPSs were involved in the observed interactions, we combined NMR,

molecular modeling, data mining and X-ray crystallography techniques to investigate HL binding to synthetic disaccharide 1[15] and tetrasaccharide 2 (Figure 1C), which represented one and two repeating units of the O-chain of *K. pneumoniae* O1, respectively, at the sub-molecular level.

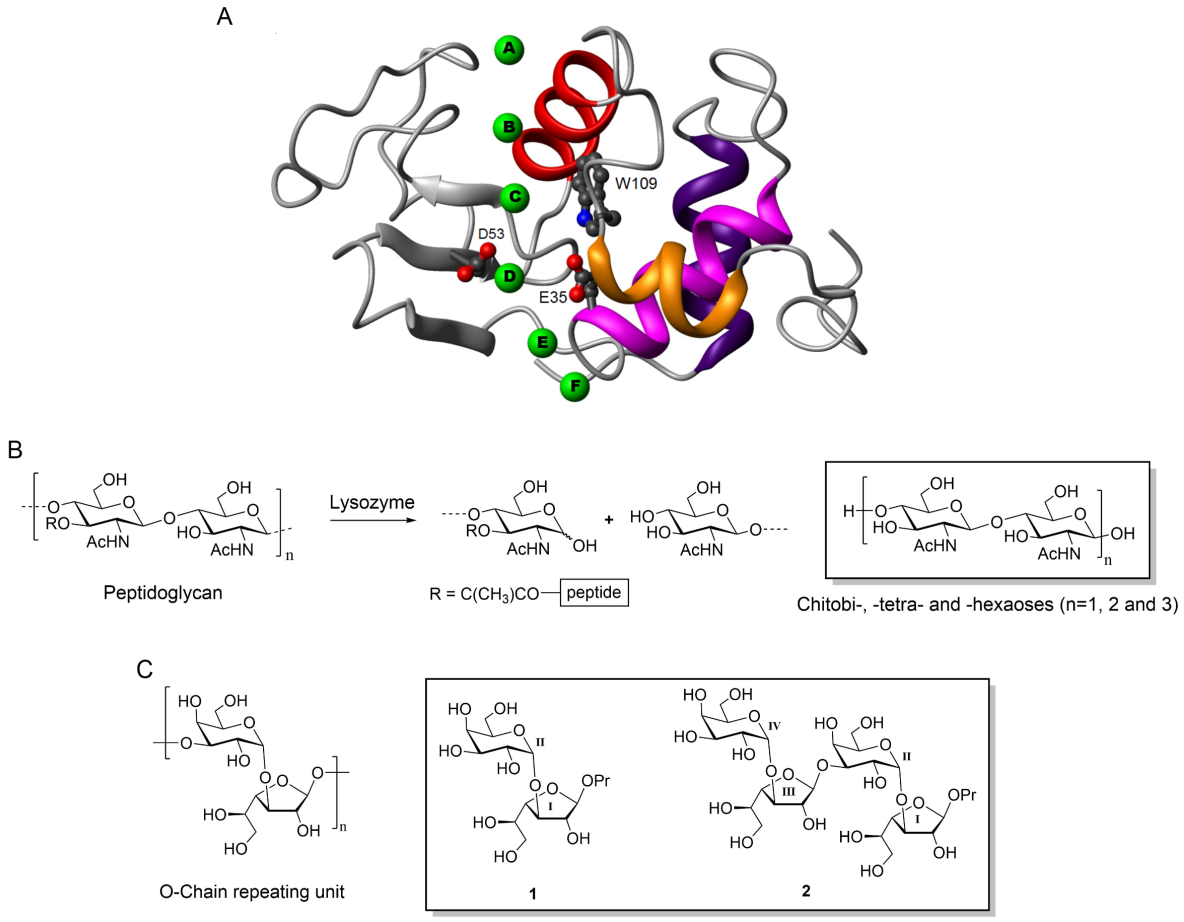

Figure 1. Lysozyme and its carbohydrate ligands A: Structure of HL (PDB code 1LZS[5]) with selected residues (Glu35, Asp53, and Trp109). Binding sites A-F are indicated by letters in green circles. Helices are colored as follows: a, violet; b, magenta; c, red; d, orange. In the orientation shown, the α-domain is to the right of the binding cleft and the β-domain is to the left. **B:** Hydrolysis of the (1→4)-glycosidic bond between N-acetyl muramic acid and N-acetyl glucosamine in the peptidoglycan. **C:** Structures of the repeating unit of the O-chain of the *K. pneumoniae* O1 lipopolysaccharide and the structurally related synthetic disaccharide 1 and tetrasaccharide 2. Monosaccharide units are numbered with Roman numerals.

RESULTS

NMR observations of structural rearrangements of the binding site of HL

The lysozyme enzymatic reaction requires an initial protonated form of the highly conserved Glu35, which exhibits a high pKa of 6.8[16]. A pH-based NMR titration of lysozyme with the weakly binding disaccharide 1 was used to provide atomistic insights into the relationship between the (de)protonation of Glu35 and its associated structural rearrangements in the surrounding helices, which were suspected to control the continuation of the catalysis reaction and hence influence specificity.

The pH dependence of the lysozyme binding site modulations was analyzed for free lysozyme and lysozyme in the presence of the weakly binding disaccharide 1 (Figure 1C), and conclusions regarding the interactions between lysozyme and disaccharide 1 were made on the basis of chemical shift changes. However, intermolecular NOEs between these two molecules were undetectable, thus suggesting the existence of only dynamic binding modes for which no stable structure could be determined. The results were therefore compared with the stable complex of lysozyme with tetrasaccharide 2 (Figure 1C), which occupies four binding sites (A, B, C and D) (Figure 1A).

NMR-based investigation of free human lysozyme

Titrations in the 3.8-8.5 pH range were observed for free HL by 1D and 2D NMR (Table S1, Supplementary Information). Figure 2A shows 1D spectra for different pH values, illustrating that the indole ring proton (Hε1) of residues Trp34, Trp109, Trp112, and the amide protons of Cys77 and Ala111 are strongly affected by pH. The most pronounced change was observed for Trp109, with a shift to lower field by 0.43 ppm, whereas Trp64 and the overlapping Trp28 (at 9.13 ppm, not shown) did not titrate in the 3.8-8.5 pH range. 2D NOESY spectra complemented the 1D titrations and provided a comprehensive picture of the chemical and structural changes in the enzyme (Figure 2B). Again, large changes were observed for the HN of Ala111 (around pH 6.8) and for various side-chain atoms of Trp109. Additional chemical shift perturbations were also observed in large portions of helices b and d

(Figure 1A). The observed effects outside of these two helices included Gln58, Ile59, Val100 and Ala108 (Table S1, Supplementary Information).

The strongest shift changes in the spatial neighborhood of the catalytic residue Glu35 were revealed by mapping of these shift changes onto the 3D structure of HL; they affect most of the b and d helices, and the loop between the second and third β-strands from the β-domain (Figure 2C). Changes involving the HNs of residues Gln58, Ile59, Val100 and Ala108, were located in the plane of the Trp109 ring, thus indicating rotation of this ring. The common pKa value (within the measurement error) of all these resonances, about pH 6.8, coincided with the reported (and unusually high) pKa value of the catalytic Glu35 protonation site[16], and furthermore identical pKa strongly indicated that all of these events are coupled (Table S1, Supplementary Information). The large shift variation of ~0.84 ppm for the HN of Ala111 is probably the result of an adjacent charge change, and the obvious cause of this shift variation is the Glu35 side chain, whose carboxyl group is nearby at 3.4 Å[17]. The remarkable behavior of the HN of Ala111 was an important observation that demonstrated a direct coupling between helices b and d. The next largest shift changes concerned the Trp109 side chain, which is an important component of the binding site surface and exhibited direct interactions with Glu35; the shortest distance between these side chains is 2.2 Å.

In addition to the well-known relative motions of the two domains required for ligand binding, human lysozyme undergoes a series of specific processes, both chemical and structural, when the pH is varied near 6.8. These processes include large parts of the α-domain with the catalytic Glu35, the side chain of Trp109, most of the b and d helices, and the loop between the second and third β-strands from the β-domain (Figure 2C). The identical pKa (within the measurement error) of all relevant resonances strongly indicated that all of these events are coupled (Table S1, Supplementary Information). Although some strong interactions with Glu35 have been previously reported (e.g., with Trp109[16]) or can be assumed on the basis of their proximities (e.g., to the amide of Ala 111), other titrating residues appeared to be too far away from Glu35 to show direct effects due to the charge change upon (de)protonation; reports have instead focused on a higher flexibility of the α-domain that involves

mutual rearrangements between helices b and d, which mirrors similar observations regarding factors such as ligand binding, temperature or pressure variations[18, 19]. The relative position of helices b and d within the α-domain modulated by the hydrogen bonding network with Glu35, Trp109 and Ala111 is further defined by the previously described interaction between Arg115 and Trp34, and the Arg115Glu mutation has been reported to modify both the position of helix d and the enzyme activity[17]. Thus, (de)protonation of Glu35 appears to trigger processes that spread over most of the α-domain.

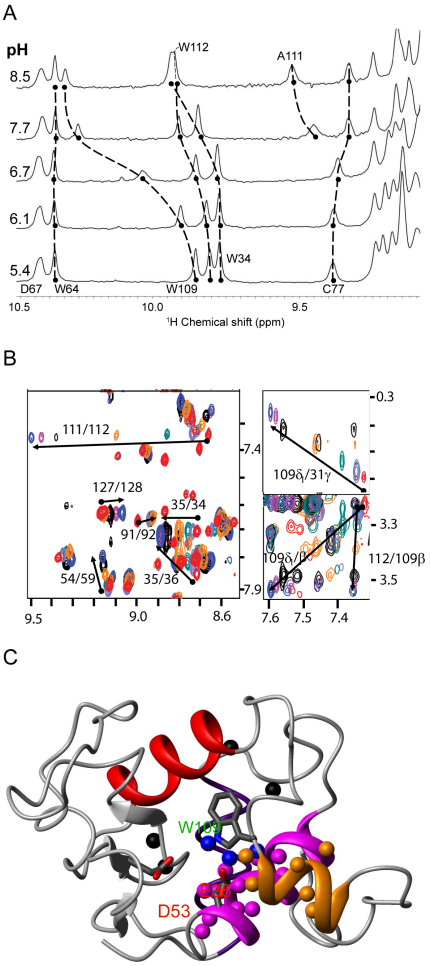

Figure 2. NMR-based investigation of free human lysozyme A: 1D spectra of pure HL at various pH values (indicated on the left border). For clarity, we show the residues, indole ring proton of Trp (Trp109, Trp112, and Trp34) and the HN of Cys77 and Ala111 (shown in top two traces), which show strong chemical shift perturbation. B: Selected 2D NOESY regions for HL at various pH values. Spectra for the different pH values are colored as follows: 3.8, red; 5.0, light blue; 5.5, green; 6.8, orange; 7.4, black; 7.7, purple; 8.1, dark blue. Chemical shifts that varied with pH are indicated by arrows on or beside the corresponding peaks with different

colors. Peak contours are calibrated such that the intensities of the HN-HN cross-peaks for helix c are constant across all pH values. C: Epitope mapping of HL from the pH titration. Spheres are color-coded as follows: atoms on helix b are magenta, atoms on helix d are orange, and Trp109 side-chain atoms are blue. Additionally, black spheres mark the HN positions from the following residues: 58 and 59 (near D53), 100 (at the end of the red helix c), and HN 108 (before Trp109). The structure is rotated by 30° around a vertical axis with respect to Figure 1A; the helix coloring is the same, and helix a is presented as a thin violet curve for clarity.

Interaction between human lysozyme and disaccharide 1, observed by NMR

The binding sites of the c-type lysozyme include six individual subsites (labeled A-F, Figure 1A) for specific interactions with multiple saccharide rings[4]. Mixtures of HL and disaccharide 1 (Figure 1C) yield observable chemical shift value changes at only pH 5.5; effects caused by intermolecular interactions were undetectable at pH 3.8. At pH 5.5, the nuclei in the residues surrounding the D-F subsites that show changes were Glu35 HN and Hγ, Asn44 H, Trp109 Hδ1 and Hε1, and Arg113 HN (Figure 3A).

The affected residues were mapped onto the 3D structure of HL in Figure 3B and demonstrated transient binding at subsites D and E (Figure 1A). Helices b and d and the catalytic Glu35 in particular responded to the addition of disaccharide 1. Furthermore, a chemical shift change was observed on the β-domain in the center of the first strand (Asn44). Since Trp109 is part of the binding cleft (Figure 1A), it is unsurprising that the aforementioned structural changes mediated by this tryptophan were affected by ligand binding. The observations of chemical shift changes for Arg113, whose location was distal to all binding sites and buried behind the preceding helix loop (residues 110-111), were in agreement with a coupling between the ligand-binding and conformational effects.

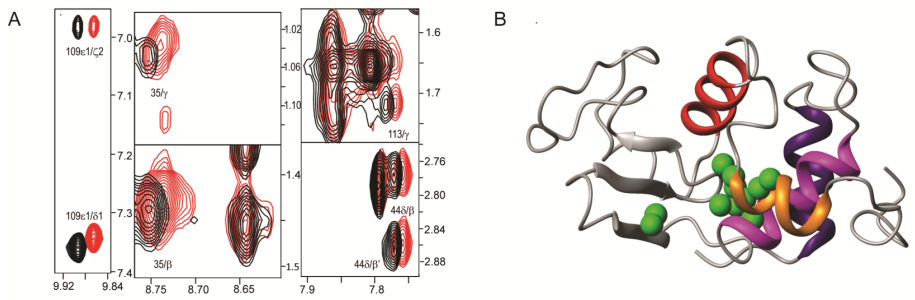

Figure 3. Interaction between human lysozyme and disaccharide 1, observed by NMR. A: Selected regions from the 2D NOESY spectra of pure human lysozyme (red) and a 1:1 mixture with disaccharide 1 (black) demonstrate some of the shift changes observed after the addition of disaccharide 1. Peak labeling is as described in Figure 2B. B: Mapping of resonances with chemical shift changes after the addition of disaccharide 1 onto the 3D structure of lysozyme; the atoms are indicated as green spheres. The structure has an identical orientation and helix coloring to that described in Figure 1A.

Molecular modeling of the interaction between human lysozyme and disaccharide 1

Molecular modeling[20, 21] and data mining[22, 23] tools are necessary for general discussions of the principles of carbohydrate-protein interactions. In order to gain some kind of insight into the binding mode for disaccharide, molecular modelling is a rational tool to use. During the docking, each simulation includes 100 runs which generate 100 conformers for the ligand. The top 10 conformers with low energy was selected for further analysis. For this step, both energy and ligand binding were considered. In fact, in the end, only the conformer with the lowest energy was selected for interaction description, which also shows a rational binding conformation. Figure 4A displays the most favorable energetic structure of HL and disaccharide 1. A close-up view of the basic pocket with the LPS-interacting side chains is presented in Figure 4B. Red dashed lines indicate the hydrogen bonds. The simulation of the binding for disaccharide indicated binding near the substrate binding sites C and D. This observation is in agreement with the analysis based on the crystal structure of HL with the tetrasaccharide since the binding sites C and especially D provided most of the interactions between sugar and protein. Comparisons of this specific result with similar cases in the Protein Data Bank (PDB) uncovered numerous meaningful agreements. The protein-carbohydrate interaction analysis in the PDB

revealed that Trp, Tyr, Asp, Asn and His were the most overrepresented amino acids in the vicinity of α-D-Gal*p* residues (Figure 4C). The previously described data mining approach[23, 24] provided important information regarding the amino acid residues that typically occur in the vicinity of α-D-Gal*p*. Using our data mining protocols, we performed an overview of the molecular interactions between α-D-Gal*p* and the functional groups of certain amino acid residues (Figure 4C) in relation to the general structural aspects of lysozyme-carbohydrate interactions.

Molecular modeling calculations with respect to the electrostatic surface potentials and hydrophobic patches were also performed (Figure S2). The differences in the patterns of the electrostatic surface potentials suggest variations in ligand binding and deviations in the aggregation/fibrillation behavior between human and avian lysozyme.

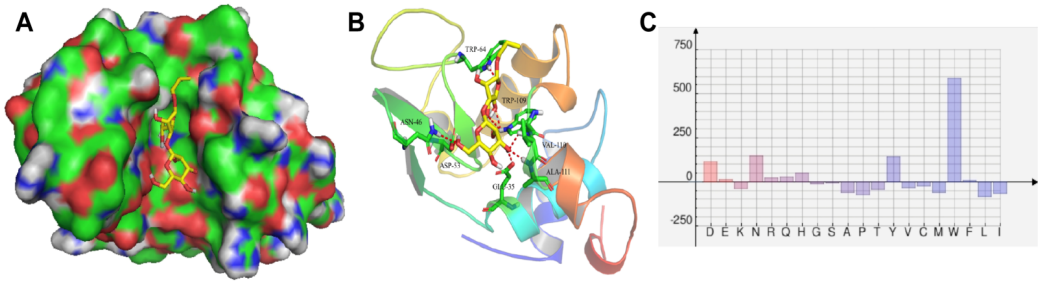

Figure 4. Molecular modeling of the interaction between human lysozyme and disaccharide 1. A: Molecular surface of lysozyme with carbons (green), oxygens (red), nitrogens (blue) and hydrogens (gray). B: Close-up view of the basic pocket with disaccharide 1 shown in stick rendering and with hydrogen bonds indicated by red dashed lines. C: Amino acid residues in the vicinity of α-Gal in the protein-carbohydrate complexes deposited in the Protein Data Bank (PDB), which indicates the deviation from natural abundance. Trp, Tyr, Asp, and His are overrepresented by greater than 100% (i.e., they are observed twice as often or more in a 4 Å radius of α-Gal compared with an average protein).

X-ray crystallography-based study of the interaction between HL and disaccharide **1**

To provide data that are independent of the results of the NMR measurements and molecular modeling calculations, X-ray crystallographic experiments were performed for human lysozyme. Extensive experiments to co-crystallize HL with bound disaccharide 1 (Figure 1C) at different pH values failed.

We did not observe a convincing electron density for bound disaccharide, even after the crystals were soaked with high disaccharide concentrations. We assume that the disaccharide was too short to provide sufficient interaction opportunities with the protein to form a stable complex. Therefore, the study of a longer oligosaccharide ligand representing a larger polysaccharide fragment was initiated.

Overall structure of the HL-tetrasaccharide 2 complex

The crystal complex of HL with tetrasaccharide 2 was successfully obtained by co-crystallization of 1.9 mM HL in the presence of 20 mM tetrasaccharide 2. The X-ray diffraction resolution of the crystals was approximately 1.0 Å. A summary of the data collection and structure refinement is presented in Table 1. For details regarding the definitions of the individual parameters, see Table S2 in the Supplementary Information.

Binding sites in the HL-tetrasaccharide 2 complex

The refined structure of human lysozyme in complex with tetrasaccharide 2 reveals the binding of tetrasaccharide 2 near the A, B, C, and D substrate-binding sites of the enzyme (Figure 5). The Gal*f*–I furanoside unit of tetrasaccharide 2 is located near site A, and the Gal*p*-II pyranoside unit is located near site B. The second repeating unit (Gal*f*-III)-(Gal*p*-IV) is in proximity to sites C and D. Both Gal*p* units of tetrasaccharide 2 adopt a chair conformation. Overall, there are eight direct hydrogen bonds between tetrasaccharide 2 and the amino acid residues of HL. Seven residues (Ile59, Asn60, Tyr63, Trp64, Ala76, Asp102, and Trp109) form hydrophobic interactions. Through comparison with tetra N-acetyl-D-glucosamine, it is clear that the sugar ring systems of tetrasaccharide 2 are not identically positioned. However, a similar number of direct hydrogen bonds, hydrophobic interactions and water-mediated bridged hydrogen bonds jointly contribute to the overall binding affinity.

A major contribution to the overall binding affinity for tetrasaccharide 2 is provided by bridged hydrogen bonds that are mediated by approximately 20 water molecules within the binding pocket toward the following lysozyme residues: Glu35, Asp49, Asp53, Asn60, Tyr63, Val99, Arg98, Gly105,

Ala108, Val110, and Ala111 (Figure 6 and Table S3, Supplementary Information). This ratio and mix of interactions is similar to those observed for $(GlcNAc)_4$ (PDB entry 1LZR) and $(GlcNAc)_4/(GlcNAc)_2$ (PDB entry 1LZS)[5] bound to HL. The superposition of HL-2 with HL-$(GlcNAc)_4$ and with HL-$(GlcNAc)_4/(GlcNAc)_2$ resulted in RMSD values of 0.23 Å and 0.46 Å, respectively (based on 130 C-alpha positions), thus indicating that the three-dimensional structures of the protein-ligand complexes are similar in all three complexes.

The binding modes of tetrasaccharides 2 and $(GlcNAc)_4$ in the A, B, C, and D sites display small but significant differences. Specifically, Arg98 forms a direct hydrogen bond between its side-chain atom, Nε2, and the O1 atom of the Gal*f*-I unit in site A of the HL-2 complex. Additionally, water molecules mediate a bridged hydrogen bond between the NH group of Arg98 and the OH group of Gal*f*-I. Arg98 is not involved in the binding of $(GlcNAc)_4$ or $(GlcNAc)_2$ to HL.

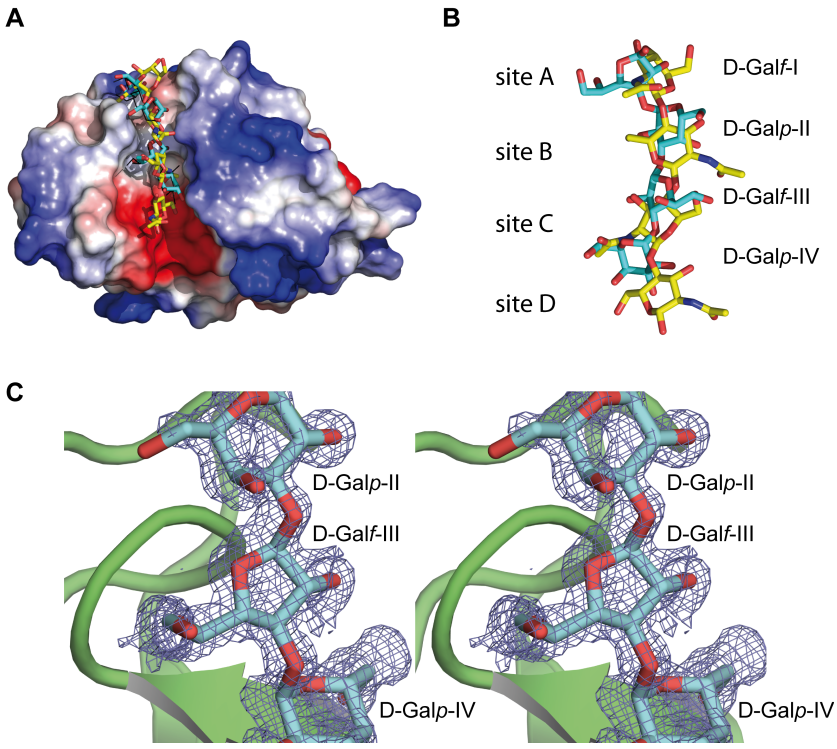

Figure 5. Molecular surface of HL in the complex with tetrasaccharide 2. A: Representation of the molecular surface of HL is colored according to the electrostatic potential. Tetrasaccharide 2 is represented by sticks for one conformation (carbon atoms in cyan and oxygen atoms in red) and by black lines for an alternative conformation. The HL (PDB-entry 1LZR[5])-bound chitotetraose $(GlcNAc)_4$ ligand is superimposed and represented by sticks

(carbon atoms in yellow). B: Close-up view of the superimposed ligands, tetrasaccharide 2 (carbon atoms in cyan) and $(GlcNAc)_4$ (carbon atoms in yellow, oxygen atoms in red and nitrogen atoms in blue. C: Representation in stereo of the electron density $2F_{obs}$-$1F_{calc}$ omit map defining bound tetrasaccharide 2. The Gal*p*-II, Gal*f*-III and Gal*p*-IV units are represented by sticks (carbon atoms in cyan and oxygen atoms in red). The protein backbone is indicated by a ribbon representation in green. The representation was generated using PyMOL v.1.6[27].

The major interactions of the Gal*p*-II unit in site B of HL are managed by direct hydrogen bonds with the surrounding amino acid residues Tyr63, Asp102, and Gln104. In addition to the hydrogen bond between atom O7 and the OH group of Tyr63, the aromatic plane of Tyr63 provides a strong hydrophobic interaction with the Gal*p*-II moiety. A similar interaction of Tyr63 with the second GlcNAc residue is present within the HL-$(GlcNAc)_4$ complex. Notably, the orientation of the Tyr63 side chain in the HL-2 complex is rotated by ca. 10° for an optimal interaction with the shifted sugar position in comparison with the GlcNAc unit. The Oδ2 side-chain atom of the Asp102 residue contributes two hydrogen bonds to the binding of the first two sugar units of 2, but only one direct hydrogen bond to the first GlcNAc unit is observed in $(GlcNAc)_4$. In the HL-$(GlcNAc)_4$/$(GlcNAc)_2$ complex, atom Oδ1 forms two hydrogen bonds with atoms N and O6 of the first GlcNAc moiety of $(GlcNAc)_4$/$(GlcNAc)_2$. As a consequence of these differences, tetrasaccharide 2 adopts a closer binding orientation toward the 'bottom' of the binding pocket, as compared with $(GlcNAc)_4$ and $(GlcNAc)_4$/$(GlcNAc)_2$.

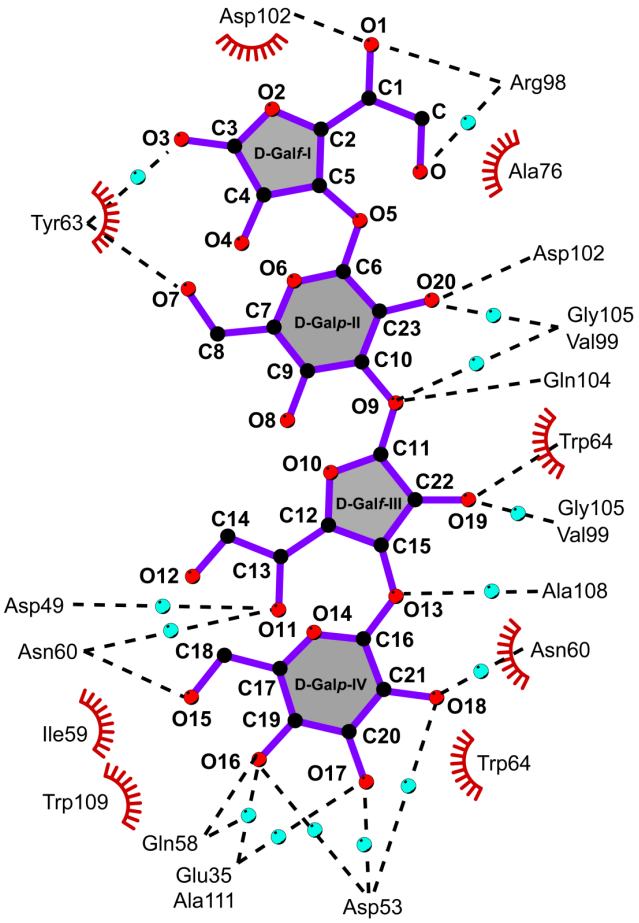

Figure 6. Binding site of human lysozyme with bound tetrasaccharide 2. The ligand is shown as a ball-and-stick representation; the bonds are indicated in purple. The protein residues are represented without side chains. Hydrogen bonds are shown as black dashed lines, and the spoked arcs represent protein residues that form hydrophobic interactions with the ligand. The cyan spheres indicate water molecules, which provide bridged hydrogen bonds between the ligand atoms and amino acid residues. The individual interactions are provided in Table S3 of the Supplementary Information. The representation was derived from an analysis with LigPlot+[28].

The Gal*f*-III unit is located near the C substrate-binding site. Two hydrogen bonds are formed: one occurs between the Trp64 atom Nε1 and atom O19, and the other occurs between atom O15 and the main-chain atom N of Asn60. Similar hydrogen bonds are contributed by these two residues for sugar binding in the HL complex to produce HL-$(GlcNAc)_4$ and HL-$(GlcNAc)_4$/$(GlcNAc)_2$. The unit Gal*p*-IV is located between the two substrate-binding sites, C and D. The only two direct hydrogen bonds are formed between atom O16 and the main-chain atom O of Gln58 and between atom O15 and the main-chain atom N of Asn60. Within the HL-$(GlcNAc)_4$ complex, a similar hydrogen bond is contributed by

Gln58 to the fourth GlcNAc moiety. Additionally, two residues, Asn46 and Asp53, form direct hydrogen bonds with GlcNAc atom O1 in the HL-$(GlcNAc)_4$ complex. Interestingly, in the HL-$(GlcNAc)_4$/$(GlcNAc)_2$ complex, Gln58 is not involved in the interaction with the fourth GlcNAc moiety; instead, it is involved in the interaction with the Asn46 side chain and the main-chain atoms of Ala108 and Val110. Notably, approximately 10 water molecules play an important role in mediating interactions between unit Gal*p*-IV of tetrasaccharide 2 and the Glu35, Asp49, Ser51, Asp53, Gln58, Gln104, Ala108, and Ala111 residues near the D and E substrate-binding sites. It is possible that a fifth sugar moiety may be adopted within this interaction network, which would contribute to a further gain in binding affinity.

Table 1. Data collection and refinement statistics.

PDB entry	5LSH
Data collection	
Temperature (K)	100
Resolution range (Å) [a]	29.05-1.061 (1.099-1.061)
Space group	P 2(1)2(1)2(1)
Unit cell a, b, c (Å)	33.1, 56.0, 60.5
Multiplicity [a]	11.9 (9.8)
Completeness (%) [a]	92 (69)
Mean (I)/σ(I) [a]	17.06 (1.52)
$R_{p.i.m.}$ (%) [a, b]	7.6 (108.8)
CC(1/2) (%) [a, b]	100 (63.3)
Refinement	
R-work (%) [a, b]	18.1 (32.4)
R-free (%) [a, b]	20.4 (33.6)
B-factors (Å^2) (No. of non-hydrogen atoms)	
All	11.4 (1414)
Ligand KTS	16.6 (90)
Water molecules	20.9 (160)
rmsd (bonds) (Å)	0.013
rmsd (angle) (°)	1.58
Rotamer outliers (%)	1.7
Ramachandran plot statistics (%)	
Favored	97.0
Allowed	2.8
Outliers	0.0

[a] Values in parentheses are for the high-resolution shell.
[b] For details regarding the definitions of the individual parameters, see Table S2 in the Supplementary Information.

DISCUSSION

This study is the first to indicate that tetrasaccharide 2, which represents part of the O-chain of the *K. pneumoniae* O1 LPS, binds to HL at its conserved sites (A, B, C and D) within the substrate binding pocket; this binding occurs mainly through direct hydrogen bonds and indirect hydrogen bonds that are mediated by water molecules. Our titrations provide a detailed picture of how the active site and the overall structure are related to each other. At pH 6.8, deprotonation of Glu35 occurs, which inactivates the enzyme at this unusually high pKa value, and helices b (with Glu35) and d undergo a substantial repositioning. Because one of the first catalysis steps also involves the deprotonation of Glu35, these domain-wide structural changes are likely to modulate the continuation of the catalysis reaction. Together with earlier studies[18, 19], our study indicates a general flexibility and lower stability of helix d,

which can be affected by numerous factors, including sugar binding and temperature changes. The ability of lysozyme to exhibit complex responses to environmental changes is evidenced by the following observations: the titration effects observed for the proton probes on Glu35, Trp109 and Ala111; the line broadening of local motions that involve Trp109 and Ala111; the spatial neighborhood of these three residues, which allows for direct interactions; and the wide range of titrating resonances on helices b and d. These structural rearrangements appear to be strongly coupled to enzyme activation by the (de)protonation of Glu35.

The carbohydrate binding site of HL displays a strong structural plasticity. Only a few amino acid residues are in direct hydrogen-bonding contact with the oligosaccharide chain. Most interactions are formed by hydrophobic contacts and particularly by water-mediated bridged hydrogen bonds. These latter two modes of interaction are less constraining and can be used to adopt binding environments for various ligands. The lectin-like ability of HL to interact with the O-chain of bacterial LPS highlights the strong possibility of a new role of HL in immune defense functions. This study may enable future developments of new and important therapeutic approaches to prevent and treat bacterial infections.

METHODS

Methods and any associated references are available in the online version of the paper.

Accession codes. Coordinates for of human lysozyme in complex with tetrasaccharide 2 representing two repeating units of the O-chain of *K. pneumoniae* have been deposited in the Protein Data Bank under accession code PDB 5LSH.

Acknowledgements

The Swedish NMR Centre is acknowledged for supplying instrument time and support. This work was supported by the King Abdullah University of Science and Technology (grant KUK-11-008-23 awarded to B.N. with a Ph.D. position for L.W.) and the European Research Council (ERC-2008-AdG 227700 to

B.N.). Diffraction data were collected on a P14 operated by EMBL at the PETRAIII storage ring (Hamburg, Germany). We are grateful to the beamline staff for providing assistance in using the beamline. Beamtime on the P14 at the EMBL outstation in Hamburg was funded by a BioStruct-X grant. We thank the Sialic Acids Society for financial support. The synthetic portion of the work was supported by the RSF (grant 14-23-00199 to N.E.N.).

Author contributions

….. V. B. K. and D. A. A. - synthesis of oligosaccharide ligands.

….. M. B.-R. - SPR measurements.

….. T. E., T. L., M. A. R.-M. - molecular modeling and data mining.

….. R. Z., A. J. S. - X-ray crystallography.

….. L. W., R. Z., M. B., B. N., A. B. - NMR spectroscopy.

….. P. M., A. G., M. A. E. - clinical advice in relation to the study design.

….. H.-C. S., N. E. N., R. S., M. B., B. N., R. Z., A. B., A. J. S. - general study design.

…. A. D., H.-C.S., V. B. K., N. E. N., A. J. S, M. B., A. B. –wrote the manuscript.

Competing financial interests

The authors declare no competing financial interests.

Note: Any Supplementary Information and Source Data files are available in the online version of the paper.

References

1. Travis, S.M.*, et al.* Activity of abundant antimicrobials of the human airway. *Am. J. Respir. Cell. Mol. Biol.* 20, 872-879 (1999).
2. Gupta, A. Hospital-acquired infections in the neonatal intensive care unit--Klebsiella pneumoniae. *Semin. Perinatol.* 26, 340-345 (2002).
3. Markart, P., Korfhagen, T.R., Weaver, T.E. & Akinbi, H.T. Mouse lysozyme M is important in pulmonary host defense against Klebsiella pneumoniae infection. *Am. J. Resp. Crit. Care* 169, 454-458 (2004).
4. Chipman, D.M. & Sharon, N. Mechanism of lysozyme in action. *Science* **165**, 454-465 (1969).
5. Song, H., Inaka, K., Maenaka, K. & Matsushima, M. Structural changes of active site cleft and different saccharide binding modes in human lysozyme co-crystallized with hexa-N-acetyl-chitohexaose at pH 4.0. *J. Mol. Biol.* 244, 522-540 (1994).
6. Masschalck, B. & Michiels, C.W. Antimicrobial properties of lysozyme in relation to foodborne vegetative bacteria. *Crit. Rev. Microbiol.* 29, 191-214 (2003).
7. Lee-Huang, S.*, et al.* Structural and functional modeling of human lysozyme reveals a unique nonapeptide, HL9, with anti-HIV activity. *Biochemistry* 44, 4648-4655 (2005).
8. Osserman, E.F., Klockars, M., Halper, J., & Fischel, R. E. Effects of lysozyme on normal and transformed mammalian cells, *Nature* **243**, 331-335 (1973).
9. Siwicki, A.K., Klein, P., Morand, M., Kiczka, W. & Studnicka, M. Immunostimulatory effects of dimerized lysozyme (KLP-602) on the nonspecific defense mechanisms and protection against furunculosis in salmonids. *Vet. Immunol. Immunopathol.* 61, 369-378 (1998).
10. Ohno, N. & Morrison, D.C. Lipopolysaccharide interactions with lysozyme differentially affect lipopolysaccharide immunostimulatory activity. *Eur. J. Biochem.* 186, 629-636 (1989).

11. Ohno, N. & Morrison, D.C. Lipopolysaccharide interaction with lysozyme. Binding of lipopolysaccharide to lysozyme and inhibition of lysozyme enzymatic activity. *J. Biol. Chem.* 264, 4434-4441 (1989).

12. Tsvetkov, Y.E.*, et al.* Synthesis and Molecular Recognition Studies of the HNK-1 Trisaccharide and Related Oligosaccharides. The Specificity of Monoclonal Anti-HNK-1 Antibodies as Assessed by Surface Plasmon Resonance and STD NMR. *J. Am. Chem. Soc.* 134, 426-435 (2012).

13. Enani, M.A. & El-Khizzi, N.A. Community acquired Klebsiella pneumoniae, K1 serotype. Invasive liver abscess with bacteremia and endophthalmitis. *Saudi Med. J.* 33, 782-786 (2012).

14. Enani, M.A. Antimicrobial resistance. Insights from the declaration of World Alliance Against Antibiotic Resistance. *Saudi Med. J.* 36, 11-12 (2015).

15. Krylov, V.B.*, et al.* Pyranoside-into-furanoside rearrangement: new reaction in carbohydrate chemistry and its application in oligosaccharide synthesis. *Chem. Eur. J.* 20, 16516-16522 (2014).

16. Kuramitsu, S., Ikeda, K., Hamaguchi, K., Fujio, H. & Amano, T. Ionization constants of Glu 35 and Asp 52 in hen, turkey, and human lysozymes. *J. Biochem.* 76, 671-683 (1974).

17. Harata, K., Abe, Y. & Muraki, M. Full-matrix least-squares refinement of lysozymes and analysis of anisotropic thermal motion. *Proteins* 30, 232-243 (1998).

18. Young, A.C., Tilton, R.F. & Dewan, J.C. Thermal expansion of hen egg-white lysozyme. Comparison of the 1.9 A resolution structures of the tetragonal form of the enzyme at 100 K and 298 K. *J. Mol. Biol.* 235, 302-317 (1994).

19. Refaee, M., Tezuka, T., Akasaka, K. & Williamson, M.P. Pressure-dependent changes in the solution structure of hen egg-white lysozyme. *J. Mol. Biol.* 327, 857-865 (2003).

20. Zhang, R.*, et al.* Structure-Function Relationships of Antimicrobial Peptides and Proteins with Respect to Contact Molecules on Pathogen Surfaces. *Curr. Top. Med. Chem.* 16, 89-98 (2016).

21. Kar, R.K.*, et al.* Evidence for Inhibition of Lysozyme Amyloid Fibrillization by Peptide Fragments from Human Lysozyme: A Combined Spectroscopy, Microscopy, and Docking Study. *Biomacromolecules* (2016).

22. Rojas-Macias, M.A. & Lutteke, T. Statistical analysis of amino acids in the vicinity of carbohydrate residues performed by GlyVicinity. *Methods Mol. Biol.* 1273, 215-226 (2015).

23. Lutteke, T., Frank, M. & von der Lieth, C.W. Carbohydrate Structure Suite (CSS): analysis of carbohydrate 3D structures derived from the PDB. *Nucleic Acids Res.* 33, D242-246 (2005).

24. Bhunia, A.*, et al.* Why Structurally Different Cyclic Peptides Can Be Glycomimetics of the HNK-1 Carbohydrate Antigen (vol 132, pg 96, 2010). *J. Am. Chem. Soc.* 132, 3636-3636 (2010).

25. Akinbi, H.T., Epaud, R., Bhatt, H. & Weaver, T.E. Bacterial killing is enhanced by expression of lysozyme in the lungs of transgenic mice. *J. Immunol.* 165, 5760-5766 (2000).

26. Krylov, V.B.,*et al.* The Pyranoside-into-Furanoside Rearrangement of Alkyl Glycosides: Scope and Limitations. *SynLett*, **27**, 1659-1664 (2016).

27. DeLano, W.L. The PyMOL Molecular Graphics System. (DeLano Scientific, San Carlos, California, USA, 2002) <http://www.pymol.org>.

28. Laskowski, R.A. & Swindells, M.B. LigPlot+: multiple ligand-protein interaction diagrams for drug discovery. *J. Chem. Inf. Model* 51, 2778-2786 (2011).

ONLINE METHODS

Lysozyme. Recombinant HL was provided by T. E. Weaver. The HL was purified as previously described for other lysozymes[3, 25].

Oligosaccharides. The synthesis of disaccharide **1** was performed[15] using the recently discovered pyranoside-*into*-furanoside rearrangement[15, 26]. The synthesis of tetrasaccharide **2** was based on similar approaches and is described in the supplementary information (Scheme S1).

SPR analysis was performed on a protein interaction array system (ProteOn XPR36, Bio-Rad, Munich, Germany). LPS from *Klebsiella pneumoniae* O1 (SIGMA) was immobilized onto flow cells of a GLM sensor chip (25 μg in 250 μL Protein acetate buffer, flow rate 30 μL/min until saturation). Lysozyme has been diluted 1:4 in buffer, final volume 250 μL) and injected at a flow rate 30 μL/min over flow cells coated with LPS. Analyses included an association step (lysozyme injection) of 350 sec (B350), followed by a dissociation step (only buffer) for 700 seconds (B700). A regeneration of the sensor surface was performed before each testing by injecting 25 mmol/L sodium hydroxide solution (100 μL/min for 18 sec). Data were analysed with the computer software (ProteOn manager software, Bio-Rad). A B700/B350 ratio was used to differentiate the LPS-to-lysozyme binding processes. Data were analysed with computer (ProteOn manager software, Bio-Rad).

NMR sample preparation. All samples were prepared by dissolving lyophilized human lysozyme (HL) in 0.3 ml H_2O containing 20 mM sodium phosphate buffer and 10% D_2O. Final concentrations of all samples were 0.5 mM protein as determined by measurement of the molar extinction coefficient, using E1%= 25.5 for HL. For mixtures of lysozyme with disaccharide**1**, a 40mM stock solution was prepared. The following samples were prepared: pure HL as well as 1:1 mixtures of these proteins with

disaccharide**1** at pH 3.8 and 5.5. Additional samples for HL were prepared in a similar manner for the pH titrations described below.

NMR measurements. All NMR spectra were recorded on a Varian Unity INOVA 800 MHz spectrometer at 35 ^{o}C using 3 mm Shigemi tubes. The ^{1}H chemical shifts were referenced to DSS. For disaccharide-lysozyme interaction measurements, equivalent amounts of disaccharide**1** were added to the enzymes. Homonuclear 2D NOESY (mixing time 150 ms) and TOCSY (mixing time 50 ms) with spectral width 11204 Hz for both dimensions were acquired with 512 increments in the indirect dimension and 4096 data points in the direct dimension, using Watergate solvent suppression and a pulse sequence repetition delay of 1.5 s. All data were processed with the NMRPipe software package[29] by zero–filling to 1024 points in the indirect dimension and ending with either a Gaussian or a shifted sine-bell function. After zero-filling the digital resolution was 0.0015 ppm for the direct dimension and 0.014 ppm for the indirect dimension. For pKa determinations of HL, ten NOESY spectra were recorded in the pH range 3.8-8.1 (3.8, 4.2, 4.6, 5.0, 5.5, 6.2, 6.8, 7.4, 7.7 and 8.1). A separate sample of HL was prepared for recording of 22 1D spectra covering the pH range of 3.17-8.13 in steps of ~0.2 units. All 1D data sets were defined by 4096 complex points and consisted of 256 transients. The digital resolution of the 1D spectra was 0.0024 ppm after zero-filling. Xeasy[30], Mnova[31], and CCPNmr[32] were used for analysis and resonance assignment. Line widths are defined as half-width at half-height of a peak; for most peaks the line width was estimated to be 0.01 ppm.

All pH adjustments were made by addition of small aliquots of either H_3PO_4 or NaOH. The pH meter was calibrated with standard solutions (from Sigma) at pH 4 and 7. The temperature dependence of the pH reading for HL was checked by recalibrating the pH meter at 35 °C: the difference between an incubated lysozyme sample at 35 °C and at room temperature was less than 0.1 pH unit. The pH for each sample was measured before and after each experiment to warrant constant conditions.

Signal assignments. ^{1}H resonance assignments at pH 3.8 and pH 5.5, both at 35 °C, were obtained for human lysozyme (HL) by transferring chemical shifts from the Biological Magnetic Resonance Bank

(BMRB, http://www.bmrb.wisc.edu/)[33] entries 5130 and 1093, respectively, to the NOESY and TOCSY spectra. Based on chemical shift changes, conclusions about interactions between lysozymes and disaccharide **1** could be made in several cases as described in the main text. However, no intermolecular NOEs were detectable, suggesting dynamic binding modes only.

Molecular modeling and data mining. Docking studies were performed with the AutoDock 4.2 software, which uses the Lamarckian Genetic Algorithm (LGA) implemented therein. For the docking of the LPS disaccharide fragment **1** with human or chicken lysozyme, the required file for the ligand was created by combining the Gaussian and AutoDock 4.2 software packages. The grid size was set to 126, 126, and 126 Å along the X-, Y-, and Z-axis, in order to recognize the LPS glycan binding site of human or chicken, the blind docking simulation was adopted. The docking parameters used were the following: LGA population size = 150; maximum number of energy evaluations = 250000. The lowest binding energy conformer was taken from 10 different conformations for each docking simulation and the resultant minimum energy conformation was applied for further analysis. The MOLMOL[34] and PyMOL[27] software packages were applied for visualisation and analysis of the docked complex. Data mining of protein-carbohydrate interactions in the PDB was performed with GlyVicinity at a redundancy level of 70% (www.glycosciences.de/tools/glyvicinity/). Only non-covalently bound ligands in structures with a resolution of at least 3Å have been considered. The analysed dataset comprised 498 amino acids that have been found within a 4Å radius of 73 alpha-galactose residues in 73 different PDB entries.

X-ray. For crystallization, the hanging-drop vapor-diffusion method was performed in 24-well plates. Single crystals of the human lysozyme were obtained by mixture of 2 µl of the reservoir solution (0.8 M NaCl, 25 mM NaOAc, pH 4.4-5.6) with 2 µl of the protein solution (50 mg/ml in 100 mM NaCl, 10 mM phosphate buffer, pH 6.0). These drops were equilibrated against 1 ml of the reservoir solution at 291 K. For co-crystallization, the protein solution was mixed with a 10-fold excess of tetrasaccharide 2

and incubated for 30 min at room temperature prior to setting up the crystallization drop. Data collection for X-ray diffraction was performed at 100 K. The crystals were transferred into liquid nitrogen for flash-cooling without the prior addition of cryoprotectants. All data processing was performed using the XDS/XSCALE[35] program package. Molecular replacement was carried out using the MOLREP[36] program with the human lysozyme structure (PDB id: 1REX)[37] as the search model. Model building and refinement were performed with the Refmac5 program as implemented in the CCP4 suite[38, 39] and PHENIX[40]. The COOT[41] graphics program was used to interpret the electron density maps and to rebuild the structure.

29. Delaglio, F., *et al.* NMRPipe: a multidimensional spectral processing system based on UNIX pipes. *J. Biomol. NMR* **6**, 277-293 (1995).
30. Bartels, C., Xia, T.H., Billeter, M., Guntert, P. & Wuthrich, K. The program XEASY for computer-supported NMR spectral analysis of biological macromolecules. *J. Biomol. NMR* **6**, 1-10 (1995).
31. Claridge, T. MNova: NMR data processing, analysis, and prediction software. *J. Chem. Inf. Model* **49**, 1136-1137 (2009).
32. Vranken, W.F., *et al.* The CCPN data model for NMR spectroscopy: development of a software pipeline. *Proteins* **59**, 687-696 (2005).
33. Ulrich, E.L., *et al.* BioMagResBank. *Nucleic Acids Res.* **36**, D402-408 (2008).
34. Koradi, R., Billeter, M. & Wuthrich, K. MOLMOL: a program for display and analysis of macromolecular structures. *J. Mol. Graph.* **14**, 51-55, 29-32 (1996).
35. Kabsch, W. Integration, scaling, space-group assignment and post-refinement. *Acta Crystallogr. Sect. D* 66, 133-144 (2010).
36. Vagin, A. & Teplyakov, A. MOLREP: an automated program for molecular replacement. *J Appl. Crystallogr.* 30, 1022-1025 (1997).
37 Muraki, M., Harata, K., Sugita, N. & Sato, K. Origin of carbohydrate recognition specificity of human lysozyme revealed by affinity labeling. *Biochemistry* 35, 13562-13567 (1996).

38. Winn, M.D., *et al.* Overview of the CCP4 suite and current developments. *Acta Crystallogr. Sect. D* 67, 235-242 (2011).

39. Murshudov, G.N., *et al.* REFMAC5 for the refinement of macromolecular crystal structures. *Acta Crystallogr. Sect. D* 67, 355-367 (2011).

40. Adams, P.D., *et al.* PHENIX: a comprehensive Python-based system for macromolecular structure solution. *Acta Crystallogr. Sect. D* 66, 213-221 (2010).

41. Emsley, P., Lohkamp, B., Scott, W.G. & Cowtan, K. Features and development of Coot. *Acta Crystallogr. Sect. D* 66, 486-501 (2010).

Supplementary information

Lysozyme's Lectin-like Characteristics Facilitates its Immune Defense Function

Ruiyan Zhang[1,2], Lisha Wu[3], Thomas Eckert[4,5], Monika Burg-Roderfeld[5], Miguel A. Rojas-Macias[5], Thomas Lütteke[5], Vadim B. Krylov[6], Dmitry A. Argunov[6], Aritreyee Datta[7], Philipp Markart[8,9], Andreas Günther[10], Bengt Norden[3], Roland Schauer[9], Anirban Bhunia[7], Mushira Abdelaziz Enani[11], Martin Billeter[12*], Axel J. Scheidig[2]*, Nikolay E. Nifantiev[6]*, Hans-Christian Siebert[1]*

[1]RI-B-NT Research Institute of Bioinformatics and Nanotechnology, Franziusallee 177, 24148 Kiel, Germany. [2]Institute of Zoology, Department of Structural Biology, Christian-Albrechts-University, Am Botanischen Garten 1-9, 24118 Kiel, Germany. [3]Department of Chemical and Biological Engineering, Chalmers University of Technology, 41296 Gothenburg, Sweden. [4]Clinic of Obstetrics, Gynecology and Andrology for Small and Large Animals, Justus-Liebig-University, Justus-Liebig-University Giessen, Frankfurter Str. 106, 35392 Giessen, Germany. [5]Institute for Veterinary Physiology and Biochemistry, Justus-Liebig-University, Frankfurter Str.100, 35392 Giessen, Germany. [6]Laboratory of Glycoconjugate Chemistry, N.D. Zelinsky Institute of Organic Chemistry, Russian Academy of Sciences, Leninsky prospect 47, 119991 Moscow, Russian Federation. [7]Department of Biophysics, Bose Institute, P-1/12 CIT Scheme VII (M), Kolkata 700054, India. [8]Pneumology, Heart-Thorax-Center Fulda, Pacelliallee 4 - 36043 Fulda, Germany. [9]Institute of Biochemistry, Christian-Albrechts-University, Olshausenstrasse 40, 24098 Kiel, Germany. [10]Medical Clinic II, Justus-Liebig-University, Klinikstraße 33, 35392 Giessen, Germany. [11]Infectious Diseases Division, Department of Medicine, King Fahad Medical City, PO Box 59046, Riyadh 11525, Kingdom of Saudi Arabia. [12]Department of Chemistry and Molecular Biology, University of Gothenburg, 40530 Gothenburg, Sweden. *e-mail: martin.billeter@chem.gu.se; axel.scheidig@strubio.uni-kiel.de; nen@ioc.ac.ru; hcsiebert@aol.com

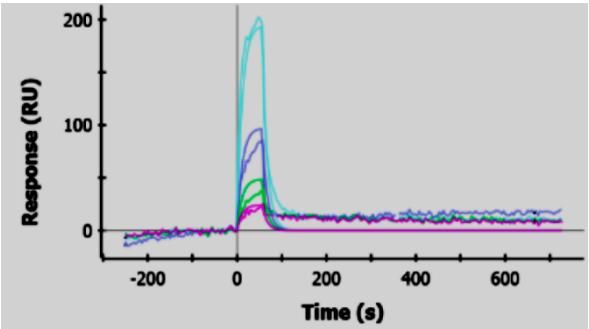

k_a (M^{-1} s^{-1}) = 2.16×10^{2}
k_d (s^{-1}) = 8.86×10^{-2}
K_D (M) = 3.98×10^{-4}

Figure S1. SPR data of human lysozyme interacting with LPS from *K. pneumoniae*O1. Five channels (A1 - A5) are used with different concentrations of LPS. Channel six was used for the running buffer only. The *K. pneumoniae* LPS concentrations are as follows: A1: 100 µl, A2: 80 µl, A3: 40 µl, A4: 20 µl, A5: 10 µl (k_a - association constant, k_d – dissociation constants).

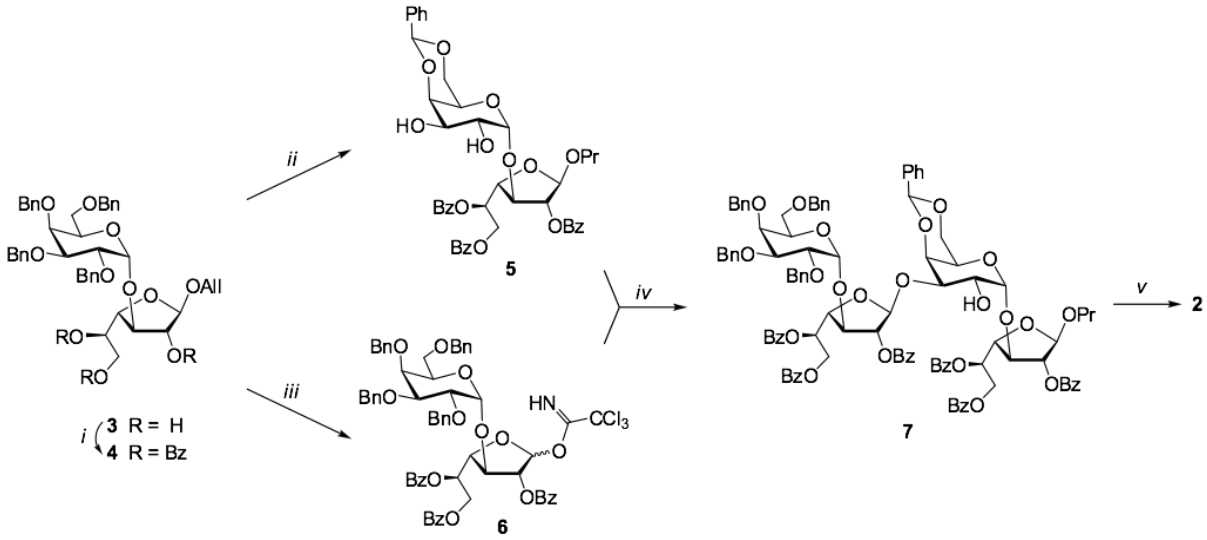

Scheme S1. The synthesis of disaccharide 1[1] was performed with the use of described[1] synthetic block 3 (scheme 1) which was prepared with the use of recently discovered pyranoside-*into*-furanoside rearrangement[1, 2]. Thus, the benzoylation of 3 (→4) and subsequent O-debenzylation, reduction of allyl group and 4',6'-O-benzylidenation produced diol 5. On the other hand, removal of allyl-aglycon in 3 and further introduction of imidate group gave the glycosyl donor 6. TMSOTf promoted coupling of disaccharide derivatives 5 and 6 proceeded with regioselective (1→3)-bond formation to give tetrasaccharide product 7. Its deblocking afforded to the desire tetrasaccharide 2. Its structure, and particularly β-(1→3)-structure of newly formed bond was determined on the basis of characteristic[3] values of $J_{H1",H2"}$ coupling constant (<2.0 Hz) in ^{1}H NMR spectrum and characteristic low-field chemical shift of C3' (77.52 ppm) in ^{13}C NMR spectrum. Reagents and conditions: i. BzCl, Py, rt, 90%; ii. 1) H_2, Pd/C, EtOAc, rt, 2) $PhCH(OMe)_2$, CSA, CH_3CN, rt, 70% (2 steps); iii. 1) $PdCl_2$, MeOH, rt, 2) CCl_3CN, DBU, CH_2Cl_2, -30 ^{o}C, 59% (2 steps); iv. TMSOTf, CH_2Cl_2, -40 ^{o}C, 68%; v. 1) H_2, $Pd(OH)_2/C$, EtOAc-MeOH, rt, 2) NaOH, MeOH-H_2O, rt, 85% (2 steps).

Table S1. Titrating resonances in HL upon pH variation in the range 3.8-8.5.

Residue	Atom	Shift change	Comment
Titrations with pKa 6.8 near Glu 35 and/or on helices b or d			
Leu31	HN	0.09	helix b
Leu31	Hβ	0.13	helix b
Leu31	Hγ	0.12	helix b
Lys33	HN	0.10	helix b
Glu35	HN	0.17	catalytic residue
Glu35	Hβ	0.21	catalytic residue
Glu35	Hβ'	0.14	catalytic residue
Glu35	Hγ	0.08	catalytic residue
Ser36	HN	0.13	helix b
Tyr38	HN	0.08	helix b
Gln58	HN	0.08	on β-domain, in Trp 109 plane
Ile59	HN	0.12	on β-domain, in Trp 109 plane
Val100	HN	0.10	in Trp 109 plane
Ala108	HN	0.07	in Trp 109 plane
Trp109	Hβ	0.32	Trp side chain in binding cleft
Trp109	H1	0.28	Trp side chain in binding cleft
Trp109	Hε1	0.48	Trp side chain in binding cleft
Val110	HN	0.12	helix d, shift change also at pH 3.8
Ala111	HN	0.84	helix d
Trp112	Hε1	0.13	helix d
Arg113	HN	0.21	helix d
Asn114	HN	0.13	helix d
Arg115	HN	0.11	helix d, interacts with helix b
Other titrations			
Leu79	HN	0.08	pKa 7.1
Asn75	Hδ	0.08	pKa 7.1
Trp34	Hε1	-	pKa >7.5
Asn39	Hα	-	pKa >7.5
Thr40	HN	-	pKa >7.5
Gly127	HN	-	pKa >7.5
Asp91	HN	-	pKa <4.0

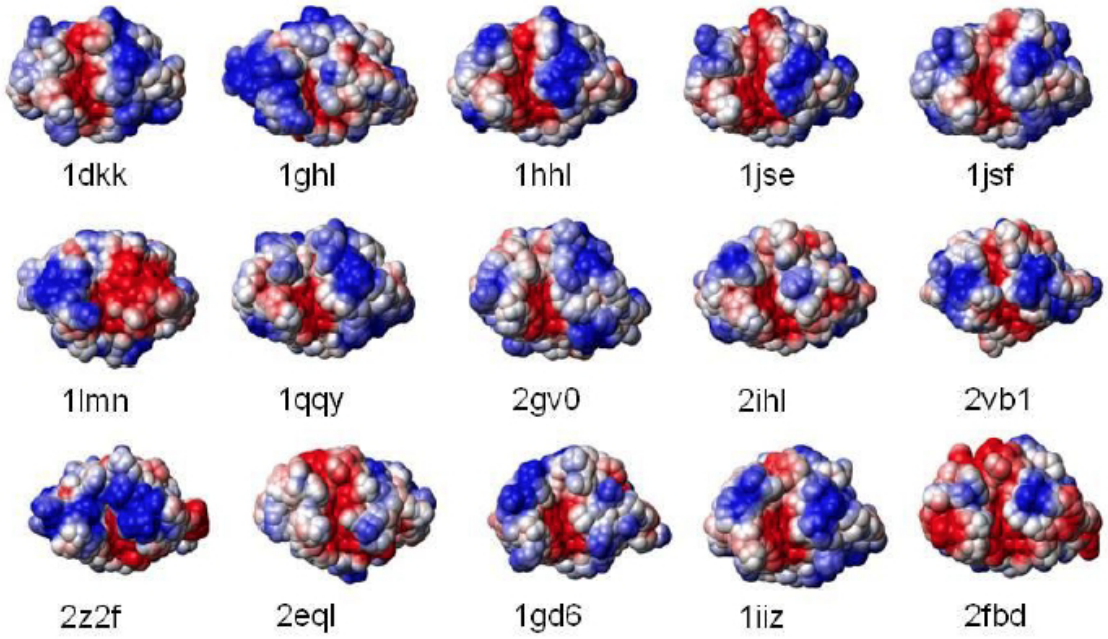

Figure S2. Electrostatic surface potentials for 15 c-type lysozyme. Electrostatic potentials where calculated with MOLMOL using charged Asp, Glu, Arg, Lys and uncharged His residues; the surfaces represent the centre positions of a solvent molecule rolling on the protein atoms. Below every figure, the PDB code is given. The different lysozymes are: 1dkk, bobwhite quail; 1ghl, pheasant egg white, 1hhl, guinea fowl; 1jse, turkey; 1jsf, human; 1lmn, rainbow trout; 1qqy, canine milk; 2gv0, soft shell turtle; 2ihl, Japanese quail egg white; 2vb1, hen egg white; 2z2f, bovine stomach; 2eql, equine milk; 1gd6, bombyx mori; 1iiz, tasar silkworm; 2fbd, musca domestica.

Table S2. Data collection and refinement statistics.

PDB entry	5LSH
Data collection	
Synchrotron X-ray source	PETRAIII (DESY)
Detector	Pilatus
Wave length (Å)	0.9762
Temperature (K)	100
Resolution range (Å)	29.05 - 1.061 (1.099 - 1.061)
Space group	P 2(1)2(1)2(1)
Unit cell a, b, c (Å)	33.1, 56.0, 60.5
Total reflections [a]	567827 (34483)
Unique reflections [a]	47721 (3498)
Multiplicity [a]	11.9 (9.8)
Completeness (%) [a]	92 (69)
Mean(I)/σ(I) [a]	17.06 (1.52)
$R_{p.i.m.}$(%) [a, b]	7.6 (108.8)
CC(1/2) (%) [a, c]	100 (63.3)
CC* (%) [a, c]	100 (88.0)
Wilson *B*-factor (Å^2)	9.80
Refinement	
Reflections used in refinement	47429 (3498)
Reflections used for R-free	2372 (175)
R-work (%) [d]	18.1 (32.4)
R-free (%) [e]	20.4 (33.6)

CC-work(%) [a, c]	96.9 (69.4)
CC-free (%) [a, c]	95.2 (70.1)
B-factors (Å^2) (No. of nonhydrogen atoms)	
All	11.4 (1414)
Main chain	9.3
Side chain	11.4
Sodium ion	17.3 (1)
Chlorid ion	13.2 (3)
Ligand KTS	16.6 (90)
Water molecules	20.9 (160)
Estimated coordinate error (Å) [f]	0.007
rmsd (bonds) (Å)	0.013
rmsd (angle) (°)	1.58
Molprobity all-atom clashscore	7,47
Rotamer outliers (%)	1.7
Ramachandran plot statistics (%)	
Favoured	97.0
Allowed	2.8
Outliers	0.0

[a] Values in parentheses are for the high-resolution bin.

[b]
$$R_{p.i.m} = 100 \times \sum_{hkl} \sqrt{\frac{1}{N-1}} \sum_i \left| I_i(hkl) - \langle I_i(hkl) \rangle \right| / \sum_{hkl} \sum_i I_i(hkl)$$

where $I_i(hkl)$ is the intensity of the *i*th individual measurement of the reflection with Miller indices *hkl* and $\langle I_i(hkl) \rangle$ is the mean intensity of all measurements of $I(hkl)$, calculated for $I \geq 3\sigma(I)$; N is the redundancy or multiplicity of the observed reflection[4,5].

[c] CC(1/2), percentage of correlation between intensities from random half datasets. Correlation significant at the 0.1 % level. CC*, the CC of the full dataset against the true intensities[6].

[d] $$R_{cryst} = 100 \times \sum \left(\left| F_{obs} \right| - k \left| F_{calc} \right| \right) / \sum \left| F_{obs} \right|$$

where F_{obs} and F_{calc} are the observed and calculated structure-factor amplitudes, respectively.

[e] R_{free} is equivalent to R_{cryst} but calculated with reflections (5 %) omitted from the refinement process[7, 8].

[f] Calculated based on a Luzzati plot using the program *SFCHECK*[9].

Table S3. Interactions of tetrasaccharide 2 (KTS) within the binding cleft of human lysozyme.

Residue-Atom	Atom (KTS)	Ring	Distance (Å)	Type of bond
D-Gal*f*-I				
Ala76-CB	C	1	3.8	Hydrophobic
Arg98-NH2	O1	1	3.1	Hydrogen Bond
Arg98-NH2:HOH-O	O	1	2.9	Bridged H-Bond [a]
Asp102-OD2	O1	1	2.8	Hydrogen Bond
Tyr63-OH:HOH-O	O3	1	3.3	Bridged H-Bond [a]
D-Gal*p*-II				
Asp102-OD2	O20	2	2.6	Hydrogen Bond
Tyr63-OH	O7	2	2.5	Hydrogen Bond
Gly105-O/N/Val99-O:HOH-O	O20	2	2.7	Bridged H-Bond [a]
Gln104-NE2	O9	2	3.3	Hydrogen Bond
Gly105-O/N/Val99-O:HOH-O	O9	2	2.8	Bridged H-Bond [a]
D-Gal*f*-III				
Trp64-NE1	O19	3	2.9	Hydrogen Bond
Ala108-O:HOH-O	O13	3	3.3	Bridged H-Bond [a]
Asn60-OD1/O:HOH-O	O11	3	2.8	Bridged H-Bond [a]
Asp49-OD2:HOH-O	O11	3	3.2	Bridged H-Bond [a]
Gly105-O/N/Val99-O:HOH-O	O19	3	2.7	Bridged H-Bond [a]
Asn60-OD1/Asp49-OD2:HOH-O	O11	3	3.2	Bridged H-Bond [a]
D-Gal*p*-IV				
Trp109-CA	C20	4	3.9	Hydrophobic
Trp109-CD1	C19	4	3.3	Hydrophobic
Trp109-CE2	C18	4	3.7	Hydrophobic
Trp109-CG	C19	4	3.7	Hydrophobic
Gln58-O	O16	4	3.1	Hydrogen Bond
Asn60-CB	C16	4	3.8	Hydrophobic
Asn60-N	O15	4	2.8	Hydrogen Bond
Trp64-CD1	C18	4	3.9	Hydrophobic
Asp53-OD2:HOH-O	O16	4	2.6	Bridged H-Bond [a]
Asp53-OD2:HOH-O	O17	4	2.6	Bridged H-Bond [a]
Asp53-OD2:HOH-O	O18	4	3.5	Bridged H-Bond [a]
Glu35-OE2/Val110-N/Ala111-N:HOH-O	O17	4	2.6	Bridged H-Bond [a]
Glu35-OE1:HOH-O	O16	4	2.6	Bridged H-Bond [a]
Asn60-OD1:HOH-O	O18	4	3.1	Bridged H-Bond [a]

a) The given distance for bridged hydrogen bonds is the distance of the bridging water oxygen to the next atom of the tetrasaccharide 2.

References

1. Krylov, V.B., *et al.* Pyranoside-into-furanoside rearrangement: new reaction in carbohydrate chemistry and its application in oligosaccharide synthesis. *Chem. Eur. J.* 20, 16516-16522 (2014).
2. Krylov, V.B., *et al.* The Pyranoside-into-Furanoside Rearrangement of Alkyl Glycosides: Scope and Limitations. *Synlett* 27, 1659-1664 (2016).
3. Gerbst, A.G., *et al.* C-13-NMR glycosylation effects in (1 -> 3)-linked furanosyl-pyranosides. *Carbohyd. Res.* 417, 1-10 (2015).
4. Weiss, M.S. Global indicators of X-ray data quality. *J. Appl. Crystallogr.* 34, 130-135 (2001).
5. Diederichs, K. & Karplus, P.A. Improved R-factors for diffraction data analysis in macromolecular crystallography. *Nat. Struct. Biol.* 4, 269-275 (1997).
6. Karplus, P.A. & Diederichs, K. Linking crystallographic model and data quality. *Science* 336, 1030-1033 (2012).
7. Brunger, A.T. Free R value: a novel statistical quantity for assessing the accuracy of crystal structures. *Nature* 355, 472-475 (1992).
8. Tickle, I.J., Laskowski, R.A. & Moss, D.S. Rfree and the rfree ratio. II. Calculation Of the expected values and variances of cross-validation statistics in macromolecular least-squares refinement. *Acta Crystallogr. Sect. D* 56, 442-450 (2000).
9. Vaguine, A.A., Richelle, J. & Wodak, S.J. SFCHECK: a unified set of procedures for evaluating the quality of macromolecular structure-factor data and their agreement with the atomic model. *Acta Crystallogr. Sect. D* 55, 191-205 (1999).

Chapter II: Molecular and medical basis of protein – carbohydrate interactions under special consideration of sialic acids

1. Introduction

1.1 Sialic acids

Sialic acids (Sia), are a group of derivatives of acidic nine carbon monosaccharides, which are frequently located at the end of glycan chains and as major components of glycoproteins, glycolipids and mucins. In 1952, in an article to present galactosamine existing in brain gangliosides and which acts as the main carbohydrate of submaxillary mucin, Gunnar Blix and his colleagues first used the term “sialic acid“ to describe the partially characterized structure[42]. The biosynthesis of sialic acids starting from glucose in the cytosol, then Neu5Ac-9-phosphate is activated in the nucleus by a cytidine monophosphate (CMP) residue through CMP-Neu5Ac synthase. Then CMP-Neu5Ac is transferred onto glycoconjugates in Golgi apparatus, followed by the vesicular transport of sialylated glycoconjugates to the plasma membrane. In the sialic acids catabolism process, the sialidases play a very important role. It can cause the removal of sialic acid residues from the cell surface or serum sialoglycoconjugates[43]. So far, more than 50 Sia naturally occurring members have been identified in this large family, which mainly derives from multiple substituents at C-4, C-5, C-7, C-8 and C-9 positions (Fig. 5). Among these diversities, C-5 decorated with acetamido (Neu5Ac) and, hydroxyacetamido (Neu5Gc) and hydroxyl group contribute much to Sia structural variations. These decorations may combine with the substituents of any of the hydroxyl groups positioned at C-4, C-7, C-8 and C-9, such as, the modifications of C-8 with methyl or sulfate moieties and C-9 with lactyl or phosphoryl residues etc[43-46]. Neu5Ac is the most widely distributed and the best-researched molecule of the Sia family, while Neu5Gc, and N-acetyl-9-O-acetylneuraminic acid (Neu5, 9Ac2) are the following most frequently occurring sialic acids in nature. Sia are found at all cell surfaces of vertebrates and some invertebrates, and are also widely reported in other organisms, ranging from plants, insects and microorganisms[47,48]. The diversity of Sia structures and its wide distributed closely link with its variety of biological functions, e.g. biological recognition processes, fertilization (egg-sperm interaction), development (brain, nervous system) and immune regulation as well as cancer and infections (virus, bacterium, protozoa and fungi

infection)[44,49], Fig. 6.

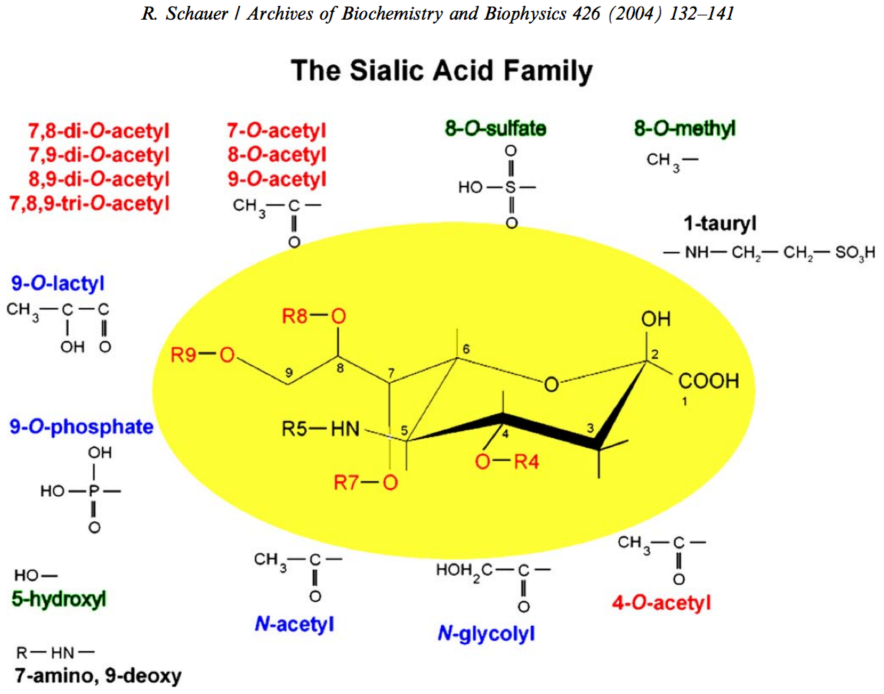

Fig. 5. The family of naturally occurring Sia[44].

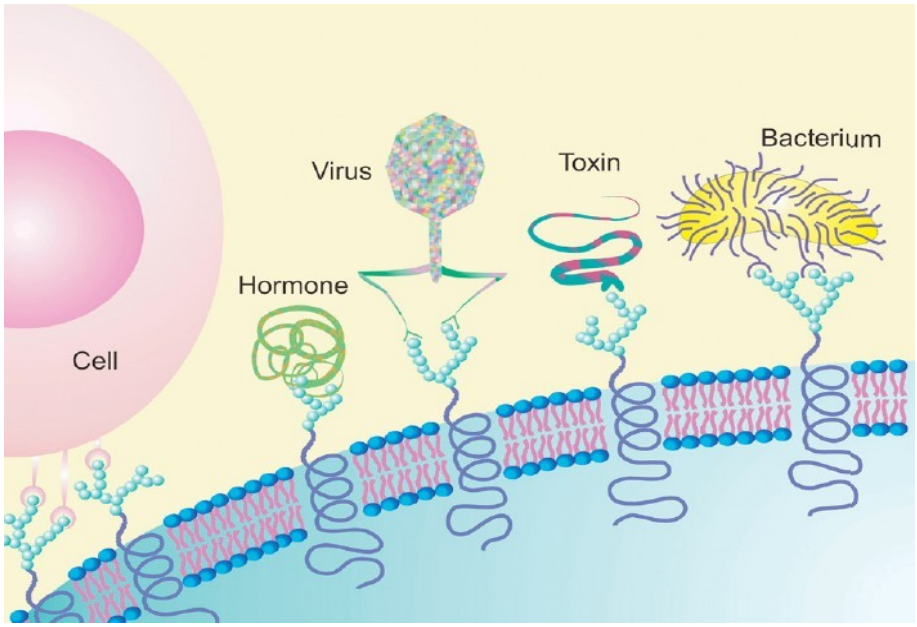

Fig. 6. Sia frequently occurring at the end of glycan chains as major compositions of glycoproteins and glycolipids, take part in many biological recognition processes[49].

1.2 Polysialic acid

Polysialic acid (polySia, PSA) is a homopolymer of sialic acid in α-2,8 or α-2,9 linkages or a combination of α-2,8 and α-2,9. It was first identified in *E. coli* (*Escherichia coli*) K-1 and K-235 by Barry[49]. Subsequent studies have discovered that PSA is predominantly attached to the protein backbone of the neural cell adhesion molecule (NCAM) of vertebrates[51]. Since polySia are located at cell surfaces, they have evolved dual functions, 'protector' and 'counter-receptor' or ligand. On the one hand, they mask cells or recognition sites to protect cells from attacking, e.g. the overexpression of polySia on the cell surfaces of many tumors like malignant gliomas, small cell lung cancer and neuroblastomas enables tumor cells to keep an undifferentiated state and therefore to exist outside of the cellular "social network" and grow irrespective of regulating factors expressed by the neighbouring cells[52-59]. On the other hand, they act as biological ligand and are recognized by numerous receptor proteins or lectins from different origin[48]. In addition, Sia interacting with the same binding partners at different organs may play different biological functions. For example, in the respiratory and reproductive systems, polySia attached to NCAM is discussed to counteract the cytotoxic characteristics of extracellular histones, which are generated during inflammation[60,61]. In contrast, in the neuronal system the interaction of polySia with histone H1 seems to be important for regeneration phenomena. Histone H1 directly binds to polySia at an extracellular position as shown for cultured cerebellar neurons. Immunostaining of live cerebellar neurons and Schwann cells confirmed that an extracellular pool of histone H1 colocalises with polySia at the cell surface and stimulates neuritogenesis and process formation as well as proliferation of Schwann cells *in vitro*. Furthermore, migration of neural precursor cells via a polySia-dependent mechanism also indicates that histone H1 is active extracellularly. These *in vitro* observations suggest an important functional role for the interaction between histone H1 and polySia not only for nervous system development but also for regeneration in the adult. Indeed, histone H1 improved functional recovery, axon regrowth, and precision of reinnervation of the motor branch in adult mice with femoral nerve injury[62].

1.3 Sialic acid binding partners

The most well-known Sia binding partners are viral capsid proteins, siglecs, selectins, sialidases and sialyl-transferases. These naturally occurring sialic-acid-binding lectins are widely found in virus, bacteria, protozoa, fungi, plant, as well as invertebrate and vertebrate[63,64]. Sialic acid receptors of diverse origin belong to different sequence families and fold classes. However, when focused on the binding site level, these lectins share structural similarities in

the architecture and geometry of the carbohydrate recognition domains (CRDs). This binding property of Sia is the same as binding behaviors of other saccharide ligand, e.g. mannose, glucose and galactose[65,66]. Utilizing the bioinformatics methods, Raghu Bhagavat and Nagasuma Chandra recently analyzed the common recognition principles of sialic acid binding proteins in the Protein Data Bank. The results indicated that the Sia binding sites of proteins with diverse amino acid sequences and structural features could be classified into only six structural clusterings, which are composed of one or more different combinations of the basic structural features over a common scaffold (Fig. 7). Moreover, among all these Sia interacting amino acid residues, tyrosine, arginine and aspartic acid were frequently found to be present in most binding architectures[67].

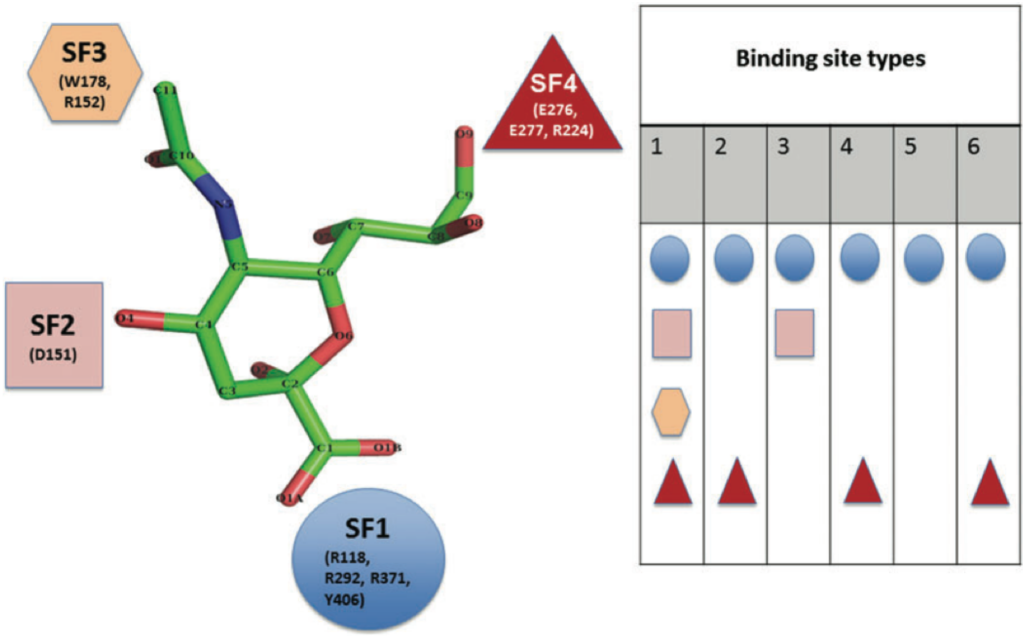

Fig. 7. Key binding site features existing in different combinations for the six site types identified are shown. Residues that belong to each feature are mentioned with their residue numbers (as in the reference site)[67].

2. Experimental research

2.1 Research proposals and methods

Sialic acids and especially the α2, 8-linked Neu5Ac residues (scheme 1) are involved in

diverse cell differentiation processes depending on the organ, the cell type and the stage of maturation[68-73]. When the impact of certain epitopes on these processes is analyzed with the aim of therapeutical improvements it is essential to describe the glycan-receptor interaction at atomic level. Therefore, it is important to determine the crucial functional groups on the ligand and on the receptor side as well as the positions of these functional groups located to each other. Since drug analysis and drug design are our goals we have looked for common principles, which are characteristic for these ligand - receptor interactions under study.

Here we applied a combination of NMR, molecular modelling (including docking algorithms as well as quantum chemical calculations) strategy to examine the interaction of polySia and sulfated polysaccharides with their cognate receptors on a sub-molecular level. In our study we are focusing on the polySia receptors, the myristoylated alanine-rich C kinase substrate (MARCKS), the α-defensins HNP1,2,3 and HD5 as well as the lectin from the Chinese bird hunting spider, SHL-1 (*Selenocosmia huwena* Lectin-I) to describe the molecular basis of polySia – protein interaction.

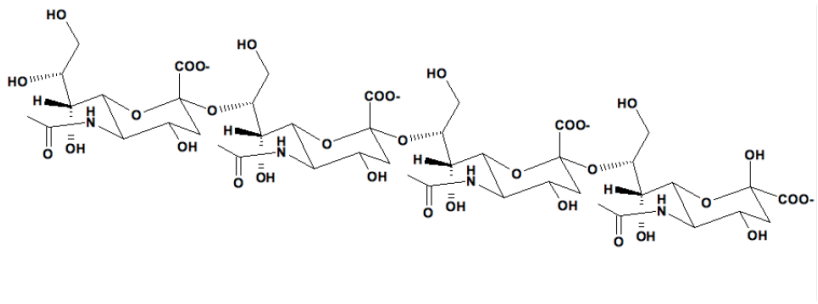

Scheme 1: Illustration of a sialic acid tetramer consisting of four α2, 8-linked Neu5Ac residues.

2.2 Main experimental results

1) Data mining approaches for a general analysis of all protein - sialic acid complexes in the Protein Data Bank (PDB) show that Arg (R), Tyr (Y) and Trp (W) residues are the most frequently occurring amino acid residues in the vicinity of bound sialic acids.

2) Our NMR results clearly indicate that the addition of polySia to the MARCKS-ED peptide causes spectral changes, suggesting that protons from the MARCKS-ED peptide are involved in binding with polySia.

3) When focusing on sulfate groups of glycan, the data mining approach shows that Lys (K) is

overrepresented in the vicinity of this functional group. Besides Lys (K) residues, Arg (R) residues are likely to primarily bind due to their vicinity preferably to sulfate groups and uronic acid.

4) Arg (R) and Asn (N) are overrepresented as well as the aromatic amino acid residues Tyr (Y) and Trp (W) when uronic acids are bound to the carbohydrate recognition domain (CRD) of their respective receptors.

5) NMR experiments using SHL-1 or the human α-defensins HNP1,2,3 as receptors and polySia fragments from colominic acid as ligands revealed that three aromatic amino acid residues and one Arg residue play a major role in carbohydrate binding.

6) Compared to a control group (poly-L-lysine), the sulfated polysaccharides from algae show a statistically significant enhancement of neurite outgrowth at concentrations from 0.0001 to 0.1 mg/ml. However, at concentrations that were higher than 1 mg/ml, the sulfated polysaccharides exhibit inhibitory effects on neurite outgrowth.

My major contribution to this study was to carry out the NMR experiments, molecular modelling analysis and testing the influence of sulfated polysaccharides from algae origin on neurite outgrowth as well as the analyses of the related results of these studies.

3. Research manuscripts

The detailed experimental methods, material, results as well as conclusion are presented in our following three manuscripts.

3.1 Molecular basis of the receptor interactions of polysialic acid (polySia), polySia mimetics, and sulfated polysaccharides (Published in *ChemMedChem*, 2016; DOI: 10.1002/cmdc.201500609)

3.2 Structure-function relationships of antimicrobial peptides and proteins with respect to contact molecules on pathogen surfaces (Published in *Current Topics in Medicinal Chemistry*, 2015; DOI: 10.2174/1568026615666150703120753)

3.3 Interaction studies of sialic acids with model receptors contribute to nanomedical therapies (Published in *Journal of Neurological Disorders*, 2015; DOI: 10.4172/2329-6895.1000212)

3.1 Molecular basis of the receptor interactions of polysialic acid (polySia), polySia mimetics, and sulfated polysaccharides

My contribution for this publication was to carry out the NMR, Molecular modelling experiments and analyse the related results, as well as test the impact of sulfated polysaccharides on the migration of primary neurons from cerebellar explants.

ChemPubSoc Europe

DOI: 10.1002/cmdc.201500609

CHEMMEDCHEM Full Papers

Molecular Basis of the Receptor Interactions of Polysialic Acid (polySia), polySia Mimetics, and Sulfated Polysaccharides

Ruiyan Zhang,[a, b] Gabriele Loers,[c] Melitta Schachner,[c, d] Rolf Boelens,[e] Hans Wienk,[e] Simone Siebert,[a] Thomas Eckert,[f, g] Stefan Kraan,[h] Miguel A. Rojas-Macias,[f] Thomas Lütteke,[f] Sebastian P. Galuska,[i] Axel Scheidig,[b] Athanasios K. Petridis,[j] Songping Liang,[k] Martin Billeter,[l] Roland Schauer,[m] Jürgen Steinmeyer,[n] Jens-Michael Schröder,[o] and Hans-Christian Siebert*[a]

Polysialic acid (polySia) and polySia glycomimetic molecules support nerve cell regeneration, differentiation, and neuronal plasticity. With a combination of biophysical and biochemical methods, as well as data mining and molecular modeling techniques, it is possible to correlate specific ligand–receptor interactions with biochemical processes and in vivo studies that focus on the potential therapeutic impact of polySia, polySia glycomimetics, and sulfated polysaccharides in neuronal diseases. With this strategy, the receptor interactions of polySia and polySia mimetics can be understood on a submolecular level. As the HNK-1 glycan also enhances neuronal functions, we tested whether similar sulfated oligo- and polysaccharides from seaweed could be suitable, in addition to polySia, for finding potential new routes into patient care focusing on an improved cure for various neuronal diseases. The knowledge obtained here on the structural interplay between polySia or sulfated polysaccharides and their receptors can be exploited to develop new drugs and application routes for the treatment of neurological diseases and dysfunctions.

Introduction

A deeper insight into the biological role of polysialic acid (polySia) and sulfated polysaccharides is possible when we understand more details about the complementarity of structure and function on a submolecular level by combining cell biological, biochemical, and biophysical methods. The correlations between neuro-oncological mechanisms and nerve cell regen-

[a] R. Zhang, S. Siebert, Prof. Dr. H.-C. Siebert
RI-B-NT: Research Institute of Bioinformatics and Nanotechnology, Franziusallee 177, 24148 Kiel (Germany)
E-mail: hcsiebert@aol.com

[b] R. Zhang, Prof. Dr. A. Scheidig
Zoological Institute, Department of Structural Biology, Kiel University, Am Botanischen Garten 1–9, 24118 Kiel (Germany)

[c] Dr. G. Loers, Prof. Dr. M. Schachner
Center for Molecular Neurobiology Hamburg, University Medical Center Hamburg-Eppendorf, University of Hamburg, Falkenried 94, 20251 Hamburg (Germany)

[d] Prof. Dr. M. Schachner
Center for Neuroscience, Shantou University Medical College, 22 Xin Ling Road, Shantou, Guangdong 515041 (China)

[e] Prof. Dr. R. Boelens, Dr. H. Wienk
Bijvoet Center for Biomolecular Research, NMR Spectroscopy, Utrecht University, Padualaan 8, 3584 CH Utrecht (The Netherlands)

[f] Dr. T. Eckert, M. A. Rojas-Macias, Dr. T. Lütteke
Institute of Veterinary Physiology and Biochemistry, Fachbereich Veterinärmedizin, Justus-Liebig-Universität Gießen, Frankfurter Str. 100, 35392 Gießen (Germany)

[g] Dr. T. Eckert
Clinic for Obstetrics, Gynecology and Andrology of Large and Small Animals, Justus-Liebig-Universität Gießen, Frankfurter Str. 106, 35392 Gießen (Germany)

[h] Dr. S. Kraan
Ocean Harvest Technology Ltd., N17 Business Park, Milltown, County Galway, (Ireland)

[i] Dr. S. P. Galuska
Institute of Biochemistry, Faculty of Medicine, Justus-Liebig-Universität Gießen Friedrichstr. 24, 35392 Gießen (Germany)

[j] Dr. A. K. Petridis
Department of Neurosurgery, Klinikum Duisburg GmbH, Zu den Rehwiesen 9, 47055 Duisburg (Germany)

[k] Prof. Dr. S. Liang
College of Life Sciences, Hunan Normal University, 410081 Changsha (China)

[l] Prof. Dr. M. Billeter
Department of Chemistry and Molecular Biology, University of Gothenburg, Box 100, 40530 Gothenburg (Sweden)

[m] Prof. Dr. R. Schauer
Institute of Biochemistry, Kiel University, Olshausenstr. 40, 24098 Kiel (Germany)

[n] Prof. Dr. J. Steinmeyer
Orthopaedic Research Laboratories, Department of Orthopaedic Surgery, University Hospital Giessen and Marburg GmbH, Paul-Meimberg-Str. 3, 35392 Gießen (Germany)

[o] Prof. Dr. J.-M. Schröder
Department of Dermatology, University Hospital Schleswig-Holstein, Campus Kiel, 24105 Kiel (Germany)

Supporting information for this article can be found under http://dx.doi.org/10.1002/cmdc.201500609.

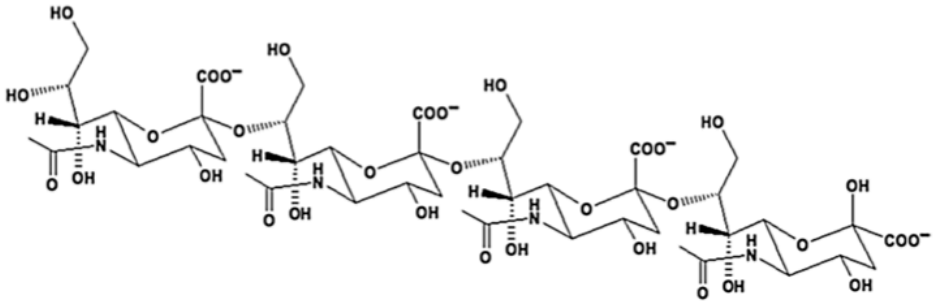

Figure 1. Illustration of a sialic acid tetramer consisting of four α2,8-linked Neu5Ac residues.

eration processes on a nanoscale size need to be determined for glycans, because sialic acids, and especially the α2,8-linked polysialic acid molecules (Figure 1), are involved in diverse cell differentiation processes depending on the organ, cell type, and stage of maturation.[1–7] When the impact of certain glycan epitopes on these processes is analyzed with the aim of improving therapeutic strategies, it is essential to describe the glycan–receptor interactions at atomic resolution. Therefore, it is important to determine the crucial functional groups on the ligand and on the receptor side, as well as the positions of these functional groups in relation to each other. As drug analysis and drug design are our goals, we looked for common principles that are characteristic of these ligand–receptor interactions. For example, in the respiratory and reproductive systems, polySia attached to neural cell adhesion molecule (NCAM) is believed to counteract the cytotoxic characteristics of extracellular histones, which are generated during inflammation.[8,9a] In contrast, in the neuronal system, the interaction of polySia with histone H1 seems to be important for regeneration phenomena.[10] Histone H1 directly binds to polySia in the extracellular space and at the plasma membrane, as shown for cultured cerebellar neurons. Immunostaining of live cerebellar neurons and Schwann cells confirmed that an extracellular pool of histone H1 co-localizes with polySia at the cell surface and stimulates neuritogenesis and process formation as well as proliferation of Schwann cells in vitro. Furthermore, migration of neural precursor cells by a polySia-dependent mechanism also indicates that histone H1 is active extracellularly. These in vitro observations suggest an important functional role for the interaction between histone H1 and polySia, not only for nervous system development, but also for regeneration in adults. Indeed, histone H1 improved functional recovery, axon regrowth, and precision of reinnervation of the motor branch in adult mice with femoral nerve injury.[10] In contrast to histone H1, the myristoylated alanine-rich C kinase substrate (MARCKS) does not interact with polySia extracellularly but within the plasma membrane.[11] We especially focused on the polySia receptor MARCKS in this study in order to find out whether this receptor binds polySia glycomimetic molecules in a similar way as it does polySia fragments. The highly basic effector domain of MARCKS (MARCKS-ED) that we analyzed here interacts with polySia at the cell membrane and mediates the membrane insertion of MARCKS.

In addition to the family of negatively charged sialic acids and their polymers or mimicking molecules, sulfated carbohydrates like the HNK-1 epitope play important roles as contact points on neuronal cells. In addition, the HNK-1 carbohydrate regulates migration of neural crest cells, synaptic plasticity, learning and memory, and preferential motor reinnervation.[12] When sulfated carbohydrates from marine organisms (e.g., algae) that express many different sulfated glycans can be identified which act in a similar manner to the HNK-1 glycan, this may identify an important source from which such bioactive molecules can be obtained. These sulfated polysaccharides can be used for the development of novel therapeutic drugs complementary to those generated on the basis of polySia and polySia mimicking molecules. Only the strategic combination of biochemical and biophysical methods allows a clear interpretation of how glycans influence and regulate the corresponding biochemical processes in different biological systems. Surface plasmon resonance (SPR) techniques, for instance, estimate how strongly carbohydrate self-recognition, which mediates marine sponge cellular adhesion, depends on the occurrence of sulfate groups on the carbohydrate residues.[13] Other biophysical devices, like quartz crystal microbalances (QCMs) or microarrays, are helpful tools to correlate physical–chemical parameters with neurobiological functions.[14,15] Here, a combination of NMR, molecular modeling (including docking algorithms and quantum chemical calculations), and data mining tools was identified as a suitable strategy to examine the interaction of polySia and sulfated carbohydrates with their cognate receptors on a submolecular level. Due to their important role in nervous system regeneration and neuro-oncological processes, polySia receptors (e.g., lectins) are of the highest clinical importance.[16–19] The involvement of polySia and sulfated oligosaccharides, such as the HNK-1 epitope, in neurite outgrowth allows development of new therapeutic strategies with strong supportive impact on nervous system regeneration in mammals.[7,20–24] NCAM, as well as other polySia-carrying proteins, which are neuropilin-2 and the synaptic cell adhesion molecule SynCAM1, interact with these receptors through a repeating unit, the disaccharide α2,8-linked sialic acid building block. In our study, we focused on the polySia receptors MARCKS, α-defensins HNP 1, 2, 3 and HD5, and a lectin from the Chinese bird-hunting spider, SHL-1, to describe the molecular basis of polySia–protein interactions. In combination with

our data on sulfated polysaccharides, we were able to define the functional groups that are responsible for the specific interactions between polySia receptors and their ligands. The *N*-acetyl and carboxyl groups of the Neu5Ac residue are of importance for ligand recognition, similar to the way in which the sulfate groups from algae polysaccharides or the HNK-1 glycan determine their biological function. As the α2,8 linkage between two Neu5Ac residues defines the minimum building unit of polySia, we also have to consider the conformational dynamics of these linkages. As we can learn from the ligand–receptor interactions in which polySia glycomimetics are involved, the shape of the molecule is not the only property that is responsible for initiating a specific binding process. Dynamic aspects that are correlated to the structural flexibility or rigidity of the molecules under study must be considered as well.

Results and Discussion

Molecular modeling and data mining

Sialic acid receptors of different origin have structural similarities in the architecture of their carbohydrate recognition domains (CRDs), pertaining, for instance, to the three-dimensional (3D) arrangement of certain amino acid residues.[19,24–27,28] In addition to arginine residues, aromatic amino acids, such as tryptophan and tyrosine are often involved in these interactions, leading to a stable complex formation. Due to its involvement in neuronal processes, MARCKS-ED was chosen as paradigmatic polySia mini-receptor. Lysine is the most frequently occurring amino acid residue (12 times) in the sequence. However, arginine, serine, and asparagine residues, which frequently occur in the vicinity of receptor-bound sialic acids (Figure 3) are also present in the MARCKS-ED sequence (Figure 2) and must be considered as important contributors

MARCKS-ED: KKKKKRFSFKKSFKLSGFSFKKNKK
MARCKS-ED control: KKKKKR**A**S**A**KKS**A**KLSG**A**S**A**KKNKK

Figure 2. Amino acid sequence of the effector domain of the myristoylated alanine-rich kinase C substrate (MARCKS-ED, top) and the MARCKS-ED control peptide (bottom). Phenylalanines that were changed to alanines in the control peptide are highlighted in bold.

for the specific binding process.

No tryptophan or tyrosine residues exist in the MARCKS-ED sequence. The phenylalanine residues in the sequence are of special interest with respect to polySia binding specificity mediated by aromatic residues. Five phenylalanine residues in the MARCKS-ED sequence are responsible for the nonpolar aromatic interactions with the carbohydrate moieties and support the four serine and the single arginine and asparagine residues to bind polySia in a specific way. Bioinformatic tools, such as data mining approaches for a general analysis of all protein–sialic acid complexes in the RCSB Protein Data Bank (PDB), show that arginine, serine, tyrosine, and tryptophan residues are the most frequently occurring amino acid residues in

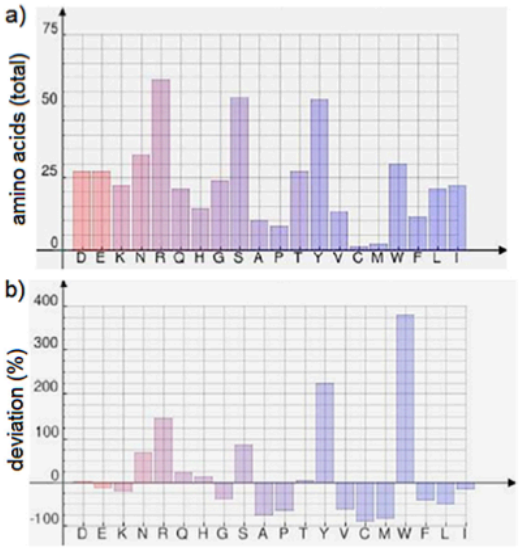

Figure 3. Data mining results with respect to sialic acid–protein complexes. Amino acid residues in the vicinity of sialic acid (basic form: Neu5Ac) according to their occurrence in the PDB (www.rcsb.org/pdb/). A dataset of glycan-binding proteins was analyzed with GlyVicinity (www.glycosciences.de/tools/glyvicinity/)[24] at a redundancy level of 70%. a) Total number of amino acids that are in the vicinity of sialic acid residues. b) Deviation (as a percentage) from the natural abundance of the corresponding amino acid residues; negative values signify that these amino acids are less frequently found in close contact with the sialic acid residues than in an average protein, whereas positive values indicate overrepresentation of amino acids in the vicinity of sialic acid residues.

the vicinity of bound sialic acids (Figure 3). Different amino acids occur in sialic acid receptors with variable abundance; therefore, their absolute values are not well suited to characterize residue binding sites (Figure 3a). Instead, the percentage deviation from their natural abundance is more appropriate for this purpose (Figure 3b). The most prominent binding partners that stabilize sialic acid–protein complexes are tryptophan, tyrosine, and arginine residues. Lysine residues are underrepresented when sialic acids are involved in binding. This means they show a negative deviation from the natural abundance, indicating that they are less frequently found in the vicinity of sialic acids than in the average of all proteins. As described in detail below, our NMR results clearly indicate that specific interactions between the lysine-rich MARCKS-ED peptide and sialic acid residues exist. Although tyrosine and tryptophan do not occur in the MARCKS-ED, arginine, asparagine, and serine are present and overrepresented in other sialic acid receptors (Figure 3b).

The picture becomes clearer when other negatively charged saccharides besides sialic acid are analyzed. Focusing on sulfate groups, the data mining approach shows that lysine is overrepresented in the vicinity of this functional group (Figure 4a). In addition to lysine residues, arginine residues are likely to primarily bind, due to their preferred vicinity to sulfate groups and uronic acid. Sulfate groups occur in different glycans, such as in the sulfated form of the HNK-1 epitope, where

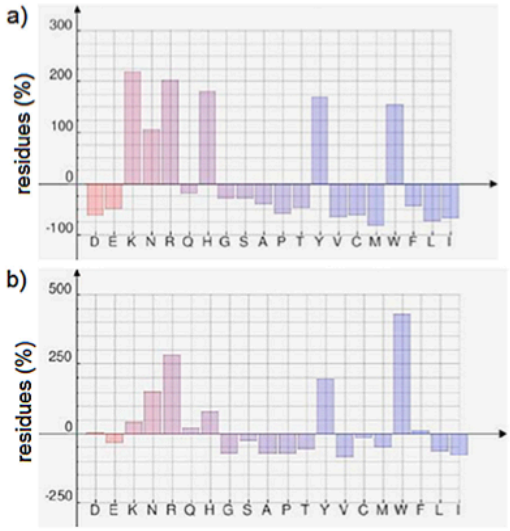

Figure 4. Data mining results with respect to carbohydrate–protein complexes in which sulfated carbohydrates and/or uronic acids occur as ligands. Amino acid residues in the vicinity of a) sulfated carbohydrates and b) uronic acids, according to their occurrence in the PDB. A dataset of glycan-binding proteins was analyzed using GlyVicinity at a redundancy level of 70%. The diagrams provide information about the deviation (as a percentage, please compare with Figure 3b) from the natural abundance for amino acid residues in the vicinity of sulfated ligands.

the sulfate group is linked to uronic acid.[29,30] Uronic acid is also present in various algae saccharides (e.g. in the brown algae *Saccharina latissima*, previously described as *Laminaria saccharina*).[31] Especially in algae saccharides, we find uronic acids and sulfated saccharides as building blocks and functional groups.[31,32] Arginine and asparagine are overrepresented, as well as the aromatic residues tyrosine and tryptophan, when uronic acids are bound to the carbohydrate recognition domain (CRD) of their respective receptors (Figure 4b). Our data mining approach, applied to all sialic acid receptors and receptors of uronic acid and sulfated saccharides in the PDB, showed that the amino acid residues discussed here are essential for the specificity of receptor binding. When polySia receptors are discriminated from those with specificity for sulfated saccharides, crucial amino acid residues are determined.

Biophysical and biochemical experiments

When looking at characteristic regions of the two-dimensional (2D) NMR spectra in Figure 5 (F2 between 9 and 7 ppm, and F1 between 3 and 1.5 ppm), it is clear that the addition of polySia to the MARCKS-ED peptide causes spectral changes, suggesting that protons from the MARCKS-ED peptide are involved in binding with polySia. As shown in Figure 5a, interaction of MARCKS-ED with polySia led to disappearance of the amide signals in the 2D NMR spectrum of the complex (yellow) at 7.54 ppm. This result was accompanied by the emergence of a new set of peaks at 7.95 ppm, as well as a change in chemical shifts between the amide signals at 8.12 ppm and

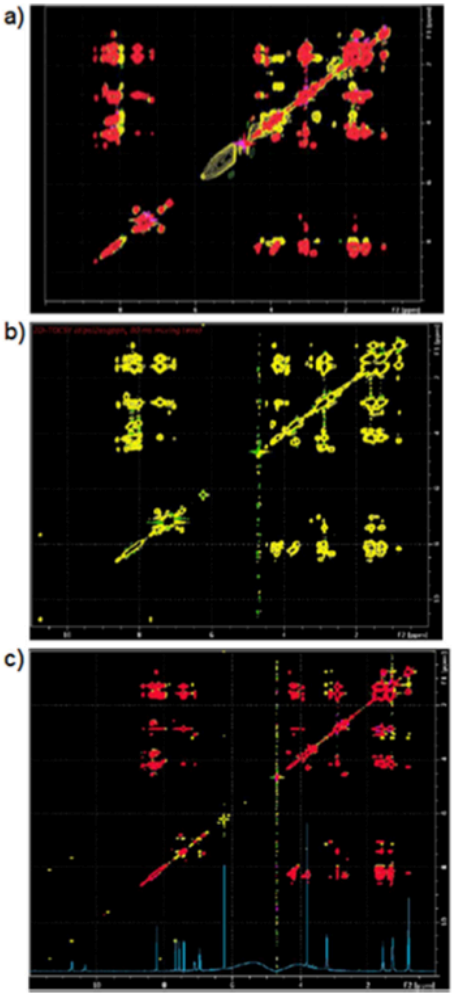

Figure 5. a) Overlay of the characteristic regions of two total correlation spectroscopy (TOCSY) spectra, indicating the interaction between polySia and the effector domain of the MARCKS-ED (KKKKKRFSFKKSFKLSGFSFKKNKK) peptide by alterations of specific ^{1}H NMR signals of amino acid residues from the MARCKS-ED. Red signals indicate the free, non-ligand-bound state, and yellow signals indicate the polySia-bound state of the MARCKS-ED. The disappearance and shifting of characteristic (yellow) cross-peaks in the bound state argues in favor of a strong participation of specific amino acid residues in ligand binding. b) MARCKS-ED in complex with tegaserod. c) MARCKS-ED control peptide (KKKKKRASAKKSAKLSGASAKKNKK) in complex with tegaserod. Red signals indicate the free, non-ligand-bound state, and yellow signals indicate the tegaserod-bound state of the MARCKS-ED control peptide. The 1D NMR spectrum on the bottom of the 2D TOCSY spectrum shows tegaserod in its free state. The strongest binding effects were detected for MARCKS-ED interacting with polySia (panel a).

8.31 ppm. Due to intermolecular exchange processes, characteristic cross-peaks disappeared in total correlation spectroscopy (TOCSY) spectra of the MARCKS-ED–polySia complex. Interaction of MARCKS-ED with the polySia mimicking compound tegaserod ((*Z*)-but-2-enedioic acid; 1-[[(*Z*)-(5-methoxyindol-3-ylidene)methyl]amino]-2-pentylguanidine)[33] led to only minor changes at these ppm values. These results argue in favor of

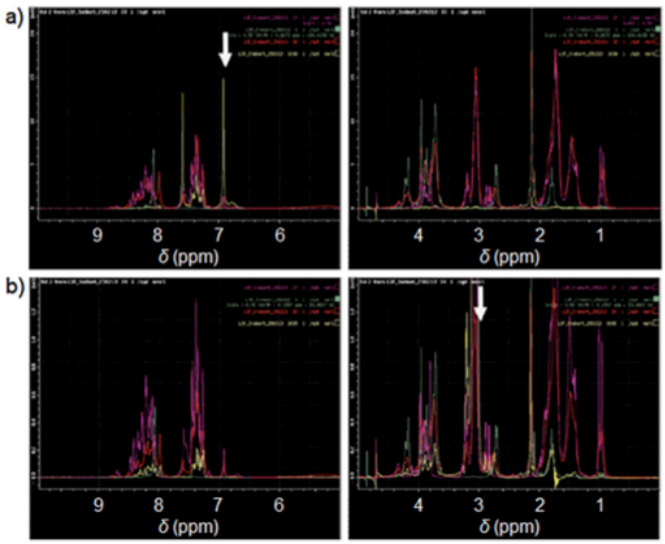

Figure 6. Saturation transfer difference (STD) NMR experiment with MARCKS-ED and polySia. a) Irradiation of a proton signal at 6.9 ppm (from protein Phe/Asn side chains). Irradiation is indicated by white arrows. Yellow: STD, red: MARCKS-ED–polySia (colominic acid) complex, green: free polySia (colominic acid), purple: free MARCKS-ED. b) Irradiation at 3.1 ppm (MARCKS-ED Lys side chain). Yellow: STD, red: MARCKS-ED–polySia (colominic acid) complex, green: free polySia (colominic acid), purple: free MARCKS-ED. The data suggest that irradiation of MARCKS-ED signals at 6.9 ppm influences the intensities of the peptide and all polySia signals at 8.0, 4.0, 3.9, 3.7, 2.1 ppm. Also, irradiation at 3.1 ppm results in an STD response to both polySia and MARCKS-ED signals, in this case predominantly, but not exclusively, to the peptide.

a weaker specific binding of the polySia mimicking molecule (Figure 5b) in comparison with the interaction with polySia fragments from colominic acid (CA). Data suggest that irradiation of MARCKS-ED signals at 6.9 ppm influenced the intensities of the peptide and all polySia signals at 8.0, 4.0, 3.9, 3.7, and 2.1 ppm (Figure 6a). Also, irradiation at 3.1 ppm resulted in a saturation transfer difference (STD) response to both polySia and MARCKS-ED signals, in this case predominantly, but not exclusively, to the peptide (Figure 6b and Supporting Information, Figure S4). These STD NMR results can therefore be used to establish a proper reference system for determining the impact of serine, arginine, and aromatic amino acid residues on binding to polySia fragments. Receptor binding of tegaserod with the control peptide did not lead to any spectral changes in these areas (no shifting or disappearing cross-peaks were observed; Figure 5c).

To further understand molecular details of the polySia receptor interaction processes, additional nuclear Overhauser effect spectroscopy (NOESY), TOCSY, and STD NMR experiments needed to be carried out for other sialic acid receptors with potential polySia affinity. Toward this aim, we also performed NMR experiments with lectin SHL-1 from the venom of the Chinese bird hunting spider *Selenocosmia huwena* Wang and with a mixture of the defensins HNP 1, 2 and 3. These data were used as a further reference to evaluate our NMR data of the linear 25-mer peptide MARCKS-ED in the absence and presence of polySia. The results of TOCSY (Figure 7) and STD (Figure 8) NMR experiments of polySia fragments with the spider lectin SHL-1 argue in favor of specific carbohydrate–protein interactions, as distinct SHL-1 NMR signals were affected. There were only a few signal alterations detected when comparing the SHL-1 TOCSY spectrum in the free state with that of the polySia-bound state (Figure 7).

To further evaluate these findings, we also performed STD NMR experiments that document an involvement of tryptophan residues in the binding process. The NMR results for the spider lectin SHL-1 in its ligand-free state, in comparison with SHL-1 interacting with a dimeric polySia fragment, were in agreement with the model description displayed in Figure 9a, which highlights three tryptophan residues (Trp23, Trp25, and Trp32) critical for binding. Another suitable sialic acid mini-receptor is the human neutrophil α-defensin HNP 2.

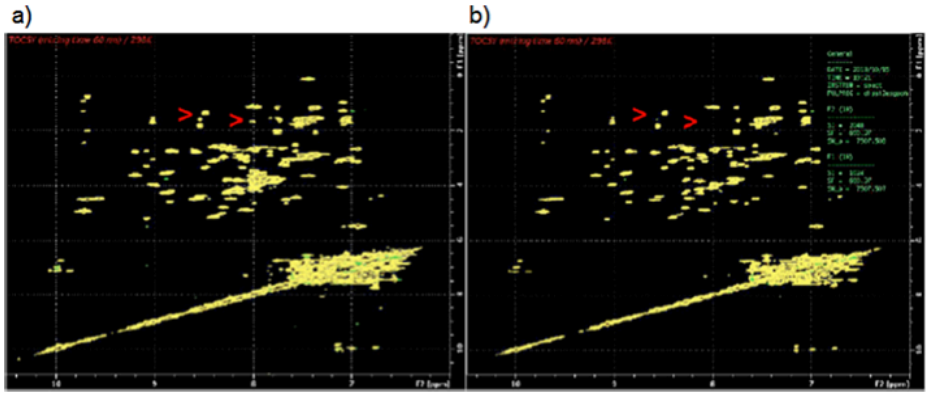

Figure 7. Two TOCSY NMR spectra indicating the interaction between polySia and the lectin from the venom of the Chinese bird-hunting spider *Selenocosmia huwena* Wang (SHL-1) by alterations of specific ^{1}H NMR signals of amino acid residues from SHL-1. a) Free, non-ligand-bound state and b) polySia-bound state of SHL-1. Signal alterations are highlighted by red arrowheads.

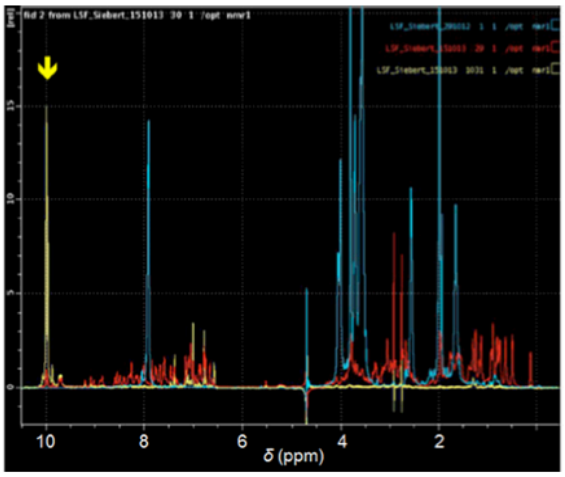

Figure 8. STD NMR experiments of SHL-1 and polySia. Yellow: STD spectrum of the lectin from the venom of the Chinese bird-hunting spider *S. huwena* Wang (SHL-1) in complex with polySia fragments; (red: free SHL-1, blue: free polySia fragments from colominic acid; yellow: SHL-1–polySia (colominic acid) complex). Irradiation is indicated by a yellow arrow at 10 ppm.

Defensins are small (18- to 45-residue) cationic peptides that are carbohydrate-binding lectins and possess antimicrobial properties. As displayed in Figure 9b, the amino acid residues relevant for binding were Tyr2, Arg4, Tyr20, and Trp25. Finally, as is also the case for the human α-defensins under study, a number of distinct signal alterations of characteristic amino acid residues were detected in a similar way as was possible when MARCKS-ED spectra were compared in the absence and presence of polySia fragments. NMR experiments using SHL-1 or the human α-defensins HNP 1, 2, or 3 as receptors and polySia fragments from CA as ligands revealed that three aromatic amino acid residues and an arginine residue play a major role in carbohydrate binding (Figure 9). As the MARCKS-ED also comprises the aromatic amino acid (Phe), we turned our attention to the interaction of polySia with arginine, phenylalanine, and serine in the MARCKS-ED. In this context, the strategic combination of methods led to new insight into molecular neurosciences, providing data that explained why bioactive compounds like cyclic and linear peptides or small organic molecules, especially polar molecules with partially equalized single and double bonds, can act as glycomimetics.[29,35–37] The polySia mini-receptors used in this study were derived from structural models of SHL-1,[25] as well as NMR and X-ray models from α-defensins HD5 and HNP 1, 2, and 3.[38–42] A combination of molecular dynamics docking simulations with ab initio calculations of the small organic glycomimetic molecules provided detailed information about the fine-tuning of such binding processes.

For example, it was possible to determine stable binding modes of the sialic acid mini-receptor HD5 with *cis*- as well as with *trans*-tegaserod (Figure 10a). Four low-energy states (I–IV)

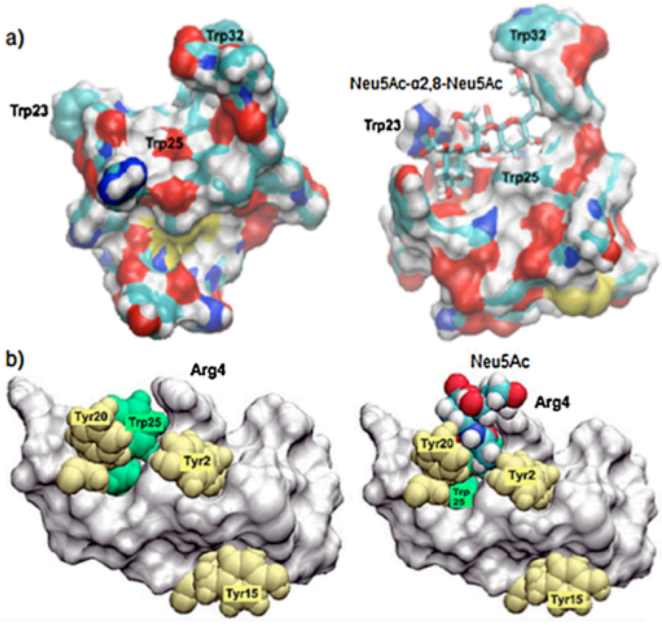

Figure 9. a) Surface representation of the lectin SHL-1 from the Chinese bird-hunting spider *S. huwena* Wang in the ligand-free state (left) and in complex with a polySia disaccharide fragment (right). Three tryptophan residues (Trp 23, Trp 25, and Trp 32) are indicated, all of which are involved in ligand binding. The images show the shape of a sialic acid binding pocket that is the length of two disaccharide units. In contrast to residues Trp 23 and Trp 25, which are essential for complex formation, the Trp 32 residue stabilizes the complex, but is not essential for specific ligand binding. b) Surface representation of the human α-defensin HNP2 in the absence (left) and presence (right) of a sialic acid ligand. The amino acids relevant to binding are: Tyr 2, Arg 4, Tyr 20, and Trp 25. The ligand-free state corresponds to the NMR structure (PDB ID: 1QK7) published in 1999.[81]

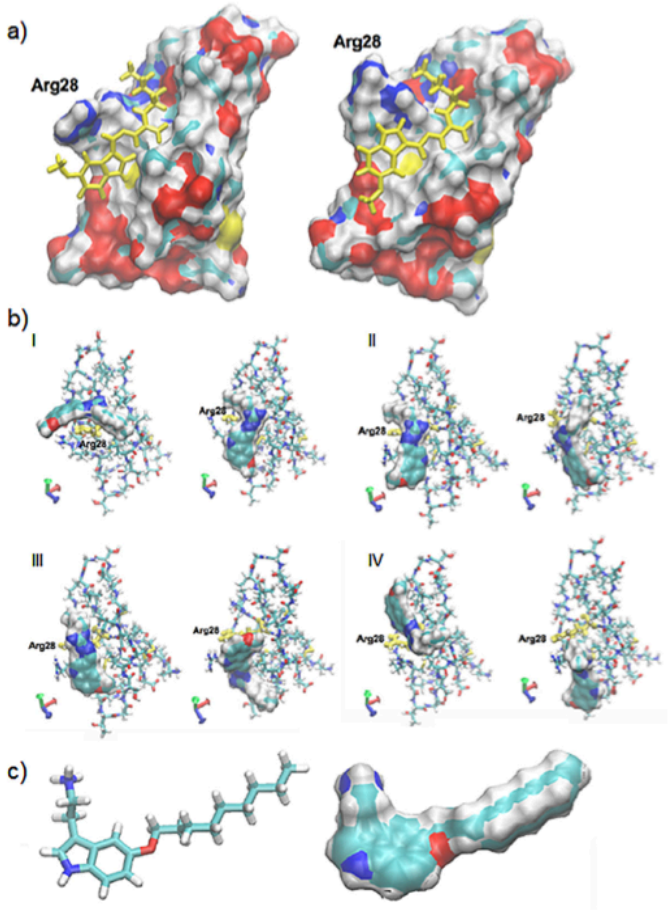

Figure 10. a) *cis*-Tegaserod (left) and *trans*-tegaserod (right) in complex with a sialic acid specific mini-receptor, the α-defensin HD5. b) Lowest energy states (I–IV) of *cis*-tegaserod (left) and *trans*-tegaserod (right) in complex with α-defensin HD5. Four low-energy complexes with *cis*-tegaserod are presented at left. Four corresponding low-energy complexes with *trans*-tegaserod are shown at right. Both configurations started at the lowest energy state (I). The maximum energy difference between *cis*-tegaserod–HD5 complexes I and IV is 7.2 kcal mol^{-1}. The maximum energy difference between *trans*-tegaserod–HD5 complexes I and IV is 5.6 kcal mol^{-1}. At least one arginine residue (Arg 28) in all energy-minimum conformations is involved in complex stabilization. c) Density functional theory (DFT) calculation of nonyloxytryptamine in water; presentation of the energy minimum conformation in the free state. Stick model is shown at left; space-filling surface low-energy structure is presented at right.

of *cis*-tegaserod and *trans*-tegaserod, each in complex with the α-defensin HD5, are displayed in Figure 10b. As defensins are cationic antimicrobial peptides, arginine residues are important contact points to initiate ligand binding. At least one arginine residue stabilizes the receptor–ligand complex, and in all cases, Arg 28 is involved as a crucial residue. The maximum energy difference between the *cis*-tegaserod–HD5 complex states I–IV was 7.2 kcal mol^{-1}, as revealed by molecular docking simulations. The maximum energy difference between the *trans*-tegaserod–HD5 complex states I–IV was 5.6 kcal mol^{-1}, according to the corresponding calculations.

These values can be used for the determination of a statistical abundance distribution of the adopted HD5–tegaserod complexes. α-Defensins such as HD5 and HNP 1, 2, and 3 bind to sialic acids, as indicated by the results from NMR and SPR experiments carried out during this study with these α-defensins, derived from psoriatic skin cells and various sialic acids. The crucial amino acid residue for Neu5Ac, as well as for tegaserod binding, was Arg 28 of HD5, as highlighted in Figure 10b (see also higher-magnification images in the Supporting Information). When determining the dissociation constant (K_D) values for HD5 and the ligands Neu5Ac or *N*-acetylmuramic acid (Mur2Ac) with SPR methods, we observed that the corresponding K_D value increased by more than 100% when the Arg 28 residue was replaced by alanine (Supporting Information, Figure S3). However, the replacement of Arg 32 by an alanine residue also led to a significant decrease in the K_D (unpublished observations). *Cis*- and *trans*-tegaserod molecules were bound by the sialic-acid-specific α-defensin HD5 with similar affinities for different orientations of the molecules. Therefore, we concluded that the overall shape of tegaserod is not the only binding criterion. Other physical parameters, such as the vibrational states of certain functional groups, which we also calculated using an ab initio approach, may be important for the creation of low energy ligand–receptor complexes. Sialic acid receptor interactions of molecules similar to tegaserod, like nonyloxytryptamine, have also been studied.[43] An energy minimized structure of this ligand, as derived from density functional theory (DFT) calculations in the framework of a molecular modeling study, is shown in Figure 10c. The shapes of nonyloxytryptamine and tegaserod are similar and differ significantly from that of polySia fragments. When comparing the structures of nonyloxytryptamine and tegaserod (Figure 10a,b vs. Figure 10c), the side chain of the pyrrole ring of the indole ring system, which influences the vibrational states of the two molecules, is the most obvious difference. It is remarkable that, in the case of nonyloxytryptamine (Figure 10c), an oxygen atom is present instead of a carbon atom, which is also responsible for remarkable differences in structural dynamics, as analyzed previously for other examples and described in the literature.[36] The deviations between these polySia mimetics and polySia itself are similar to those between HNK-1 and certain cyclic peptides, as described.[29] Therefore, we can conclude that, in addition to structural criteria, additional dynamic parameters are crucial for receptor binding, such as vibrational states,[44] which can be determined with the help of quantum chemical ab initio calculations.

The findings outlined above are of importance for therapeutic improvements in the field of nerve cell regeneration, as we provide here a submolecular description of why *cis*- and *trans*-tegaserod, or similar molecules like nonyloxytryptamine, can

act as polySia glycomimetic molecules, similar to polySia fragments of various lengths. Previously, evidence was found that tegaserod treatment enhances regeneration after femoral nerve injury and spinal cord injury in mice.[33,34] We will use these results for new clinical strategies to solve medical problems related to nerve cell regeneration processes as well as the problem of malignancy of neuronal tumors, as described in detail below. Our NMR and molecular modeling studies have also proven to be extremely helpful when sulfated polysaccharides need to be analyzed in molecular detail. These polysaccharides might be an important addition in the fine-tuning of new therapeutic approaches related to polySia or polySia mimetics because they are able to block migration of tumor cells.

As the analyzed sulfated polysaccharides from algae were mixtures of saccharides of different sizes, it was necessary that, in addition to the TOCSY and NOESY experiments, diffusion-ordered spectroscopy (DOSY) measurements were also carried out. DOSY spectra of two different polysaccharide samples from brown and green algae, as well as of CA (*E. coli*-derived polySia fragments) are shown in the Supporting Information (Figure S1 a,b,c). The polysaccharides studied can contain up to 100 monosaccharide residues. However, shorter fragments are preferable in solution. In all cases, linear polysaccharide fragments were only two to three residues in length, due to the sizes of the receptor binding pockets. Green algae contain sulfuric acid polysaccharides, sulfated galactans, and xylans. Brown algae incorporate alginic acid, fucoidan (sulfated fucose), laminarin (β-1,3 glucan), and sargassan (a sulfated heteropolysaccharide comprising D-glucuronic acid, D-mannose, D-galactose, D-xylose, and L-fucose residues).[31] DOSY experiments are suitable to determine the size distribution of compounds in a complex mixture. Values concerning the size distribution and the diffusion constants, which we obtained from the DOSY NMR experiments, indicated that these two algae polysaccharide mixtures were nearly identical (Supporting Information, Figure S1). The structural role of sulfation in saccharides has already been analyzed with molecular modeling tools, including ab initio calculations, in a previous study.[38] It was shown that sulfate groups are special contact points for a receptor but can also influence the conformation of the polysaccharide.

PolySia cleavage and tumor cell differentiation

A number of studies have shown that polySia is overexpressed in many tumors, such as malignant gliomas, small cell lung cancer, and neuroblastomas, to name a few.[18,45–52] It has been postulated that polySia enables tumor cells to remain in an undifferentiated state and therefore to exist outside of the cellular "social network" and grow irrespective of regulating factors expressed by the neighboring cells. Also, the characteristic polySia function, to accelerate migration of stem cells,[18,46–51] is used by tumor cells to infiltrate normal tissue and metastasize.[18] PolySia can act as ligand for certain receptors or as an NCAM interaction inhibitor.[11,20] The second scenario means that different pathways induced by NCAM activation can be blocked by the expression of polySia on NCAM. A model of

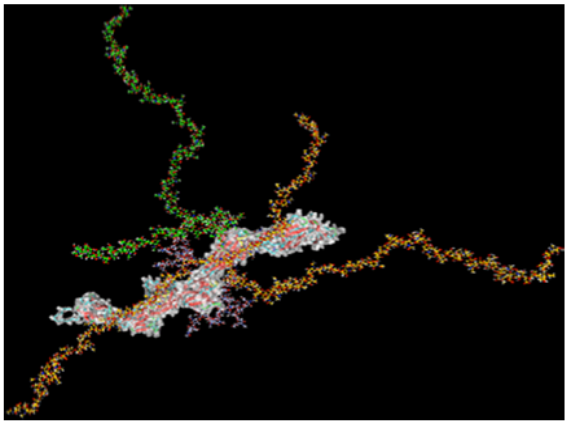

Figure 11. PolySia–NCAM-140 model generated from a published in silico dataset.[9a] A homology model of NCAM-140 was calculated with Modeller.[9b] Complex-type glycan chains were added with GlyProt[9c] to N-glycosylation sites N222, N315, N347, N423, N449, and N478. Based on characterization of the polysialylation status of NCAM in postnatal mouse brains, the glycan chain at position N449 (green) contains two polySia chains consisting of 38 and 20 sialic acid residues. The *N*-glycan chain at position N478 (orange) carries three polySia chains of 38, 30, and 20 sialic acid residues. No polySia residues were added to the remaining *N*-glycans (purple). The image was created with YASARA.[9d]

NCAM with its polySia chains is shown in Figure 11. For example, NCAM interacting with integrin on the cell surface initiates the differentiation of neuroblastoma cells. The presence of polySia on NCAM inhibits this interaction[53–56] and prevents tumor cells from differentiating. Pax3, which is a transcription factor involved in tumorigenesis, seems to induce NCAM polysialylation on medulloblastoma cells.[57] PolySia inhibits cell–cell interactions through its ability to bind a significant amount of water and therefore keeps receptors away from their ligand or other receptors. Some studies postulate that polySia expression on tumor cells can be used as a prognostic factor for tumor malignancy and severity of the disease outcome. Wilms tumor patients with increased polySia expression, for example, have a shorter survival time; therefore, polySia was claimed to be an oncodevelopmental antigen.[58,59] It should be considered here that such alterations at the glycocalix may have a significant impact on the physical properties of a cell, which are related to their motility.[60]

In addition to using polySia as a prognostic marker in tumors, there is also a therapeutic approach with respect to tumors through cleavage of polySia from the surface of polySia-expressing tumor cells. Endo N is a selective polySia-cleaving enzyme. PolySia cleavage on the surface of human SH-SY5Y neuroblastoma cells with the nontoxic endo N induced differentiation of these cells and led to development of axons and expression of neurofilaments (Figure 12). Additionally, the migration capacity of these cells was shown to be significantly decreased when they were treated with endo N.[61,62] Unfortunately, in vivo experiments with intravenous application of endo N in animals with polySia-rich tumors failed to remove

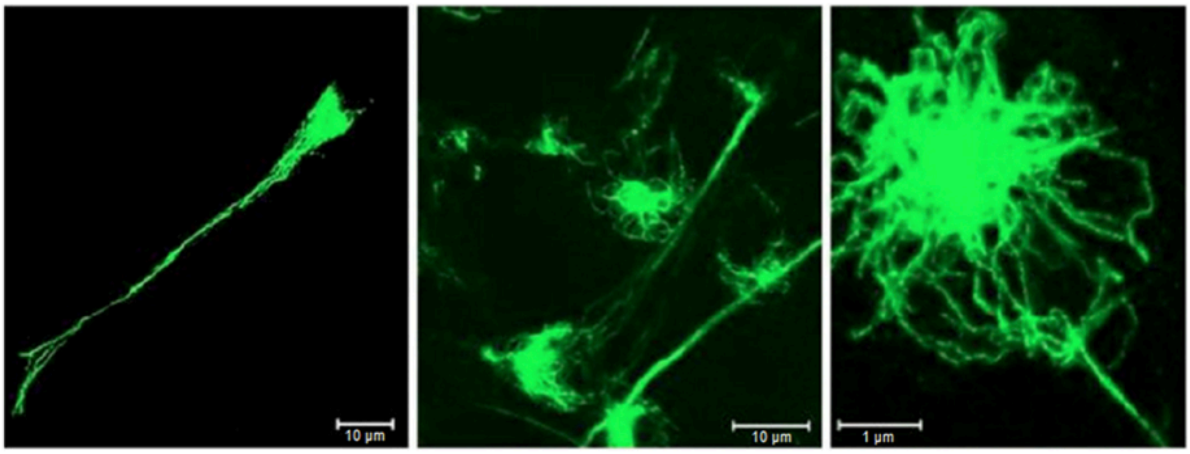

Figure 12. Intermediate neurofilament (NF-M) expression in human SH-SY5Y cells treated with endoneuraminidase N. The neuroblastoma cells which were treated with endoneuraminidase N not only phenotypically developed axons, but also expressed neurofilament M (intermediate). The green staining of neurofilament M indicates that cells differentiate into neuronal cells when observing and documenting this process after certain time steps. The neuroblastoma cells shown in this figure belong to the same cell cluster. Scale bars: 1 µm (right image) and 10 µm (middle and left image). The magnification was (from left to right) 1200×, 2000×, 5000× using a Zeiss confocal microscope.

polySia from the tumor cells, due to serum factors that inactivated endo N (unpublished observations). Therefore, alternative delivery methods for endo N to tumors have to be evaluated. However, the cleavage of polySia from tumor cells could be a promising tool in the treatment of cancer.

As we have found that sulfated polysaccharides of algae origin are able to block neuronal cell migration (Figure 13), the application of these molecules could also support an antitumor therapy and will be analyzed in a follow-up study. Furthermore, the sulfated polysaccharides studied have a concentration-dependent influence on neurite outgrowth, which we have tested also in combination with certain collagen fragments (Supporting Information, Figure S2). Compared with control cells grown on the neutral substrate poly-L-lysine, the sulfated polysaccharides from algae show a statistically significant enhancement of neurite outgrowth at concentrations from 0.0001 to 0.1 mg mL^{-1}. However, at concentrations that were higher than 1 mg mL^{-1}, the sulfated polysaccharides exhibited inhibitory effects on neurite outgrowth. Therefore, the sulfated polysaccharides from mixtures of brown and green algae, with or without bioactive collagen fragments, can also be applied in addition to polySia or polySia mimicking molecules when lesions in neuronal tissues need to be cured.[63–66]

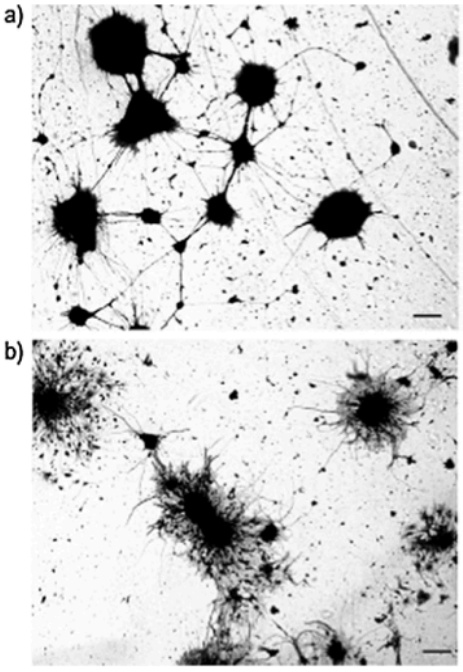

Figure 13. Impact of sulfated polysaccharides from brown and green algae[31] on the migration of primary neurons from cerebellar explants. Representative images show explants cultured on a) sulfated polysaccharides from brown and green algae, or b) control substrate poly-L-lysine. Sulfated polysaccharides strongly inhibited cerebellar neuron migration. The scale bars at the lower right of each image correspond to 100 µm. Various concentrations (1 µg mL^{-1} to 5 mg mL^{-1}) were used, as was the case for testing neurite outgrowth (see Supporting Information, Figure S2a).[82] The migration of neurons from the explant core was analyzed 48 h after seeding. An exemplary figure documenting neurite outgrowth in the presence and absence of collagen fragments is given in the Supporting Information (Figure S2b).

Induced polySia expression in glial scar tissue after spinal cord lesion

In addition to an important biomedical role in neurooncology, polySia–receptor interactions, as described here for various model systems, are also of particular clinical interest when neuronal regeneration processes have to be supported by innovative drugs for therapeutic reasons. In both cases (tumor growth and scar development after injuries in which nerve cells are involved), a high concentration of polySia on the cell

surfaces corresponds to de-differentiation processes that must be considered in each therapeutic approach. These findings are independent of the lengths of the various glycan chains that are occurring on the cell surfaces. The ability of polySia expressing cells to maintain their distance from other cells inspired work on a cell regeneration experiment in which polySia expression in astroglia was induced to inhibit the barrier of scar tissue after spinal cord lesions.[61] It was shown that retrovirally induced polySia overexpression in astroglia, which formed the spinal cord scar, rendered the glial scar permeable for regrowing spinal cord axons.[61] Furthermore, application of polySia mimicking peptides led to better functional recovery after spinal cord injury and to decreased reactive gliosis.[67,68] These are important experiments, demonstrating that spinal cord axons have the ability to grow but cannot pass the glial scar unless the scar tissue is made permeable. For the first time, penetration of the scar tissue and growth of a satisfactory number of axons distal to the scar could be observed in these studies.[61]

Conclusions

Although the results presented here are very promising, there is a major obstacle that has to be solved with the support of nanomedical techniques in near future. Previous studies using polySia-overexpressing cells or virally induced polySia expression proved that the gliosis is not a barrier that will never be broken, as Cajal stated in 1928.[69] However, the induced overexpression of polySia through retroviral delivery of this macromolecule in humans is not free of risk and could possibly have adverse effects. Other methods of polySia expression in a glial scar have to be developed which are safer for use in human beings. In this case, the expression of polySia in glial scars could become a milestone in the central nervous regeneration of spinal cord injuries when all interactions are understood on a submolecular level. Fragments of polySia, as well as polySia mimetics like tegaserod and nonyloxytryptamine, could also play a crucial role in this context,[33,34,67,68,70] due to their strong impact on neuronal outgrowth and migration. It is important to mention that polySia is not oncogenic. It is expressed by tumor cells, but there are no observations that it induces cancer.

The high clinical relevance with respect to the therapy of diseases associated with neuronal regeneration, tumor spread, and infection[71] opens a wide field for medical and pharmacological research projects related to polySia and polySia glycomimetic molecules. Sulfated polysaccharides of different origins (e.g., from green and brown algae) are well-suited to support these new therapeutic approaches. Sulfated polysaccharides mainly interact with arginine and tyrosine residues in the receptor binding pocket in a similar way to sialic acids. The most prominent binding partners that stabilize sialic acid–protein complexes are tryptophan, tyrosine, and arginine residues. This is also the case for polySia glycomimetics. Sulfated polysaccharides of algae origin are able to block neuronal cell migration. It is now possible to identify certain functional groups and correlate their interactions with biological effects. Sulfate groups of algae polysaccharides, as well as the *N*-acetyl group and the carboxyl group, together with hydroxy groups of sialic acid residues, are essential for stable binding with crucial amino acids (e.g., arginine, tyrosine, and tryptophan) on the receptor side. As shown in Figure S3 a–d (Supporting Information), when using the α-defensins HNP 2 and HD5 as sialic acid mini-receptor models, the carboxylic group is particularly essential for a specific and stable ligand–receptor interaction. Tegaserod and 5-nonyloxytryptamine, as polySia glycomimetic molecules, fit their aromatic ring systems in the corresponding binding pockets of sialic acid receptors. In Figure S4 a and b (Supporting Information), it is shown that the involvement of the aromatic ring system of tegaserod can already be documented by one-dimensional (1D) ^{1}H NMR experiments. The interactions between the MARCKS-ED peptide and SHL-1 with polySia were confirmed and explained on a submolecular level by combining NMR and in silico studies. We identified general binding principles for the interactions of MARCKS-ED peptide, SHL-1, and α-defensin with their respective carbohydrate or glycomimetic binding partners.

It should not be surprising that various diseases of different origin can be treated with drugs based on such insight, because these saccharides or their glycomimetics have to be considered as the essential contact structures on the cell surface.[72] We conclude that polySia, polySia glycomimetic molecules, and sulfated polysaccharides are feasible for clinical applications but need to be further analyzed on a nanoscale level, as described herein, in order to understand their interactions with other molecules in detail for optimal application in the corresponding therapies. Particularly when these molecules interact with certain receptors and impact nerve cell differentiation as well as tumor spread, the interactions must be fully describable in relation to various cell biological processes in order to improve such therapies.

Experimental Section

Materials: KKKKKRFSFKKSFKLSGFSFKKNKK and the corresponding control peptide KKKKKR**A**SAKKS**A**KLSG**A**S**A**KKNKK; (sequence differences are in bold) were purchased from Schafer-N (Copenhagen, Denmark). The polySia probes originated from colominic acid (CA). The α-defensins HNP 1, 2, and 3 were derived from psoriatic skin cells and isolated as published.[73]

Cell culture and treatment of SH-SY5Y neuroblastoma cells: SH-SY5Y neuroblastoma cells (ATCC, Rockville, MD, USA), which are rich in polySia expression, were plated on glass coverslips and cultivated in Dulbecco's modified Eagle's medium (DMEM)/Ham's F12 (1:1; Fisher Scientific) on a nanoscale level, as previously described.[47] When cells reached a confluency of ~60% (change of medium every 3 days), 6–8 U mL^{-1} of endoneuraminidase N (endo N; gift from Dr. Urs Rutishauser, Memorial Sloan Kettering Cancer Center [MSKCC], NY, USA) were added, and 24–48 h after addition of endo N, cells were fixed and prepared for immunostaining.[47] The complete removal of polySia was verified as described using polySia-specific antibodies.[47]

Staining of SH-SY5Y cells: Cells were fixed in 4% paraformaldehyde at 2 h and 4 °C as described, permeabilized, and stained for polySia using mouse monoclonal polySia-specific antibody 5A5

(1:1000; gift from Dr. Urs Rutishauser) or stained for neurofilament expression using a primary mouse antibody directed against neurofilament M (1:200; Sigma–Aldrich, St. Louis, MO, USA). Cells were incubated with primary antibody overnight at 4 °C, and after several washes with phosphate-buffered saline (PBS) solution, Cy3-conjugated secondary antibody (1:100; Jackson ImmunoResearch, West Grove, PA, USA) was applied for 1 h at room temperature. Coverslips were washed again and mounted using an anti-fading mounting solution (gift from Dr. El-Maarouf, MSKCC, NY, USA).[47]

NMR methods: NMR spectra were recorded on a Bruker Avance III 600 MHz UltraShield spectrometer at 298 K in 10% D_2O. TOCSY and NOESY spectra were recorded using standard pulse programs,[74,75] with mixing times of 80 ms and 200 ms, respectively. The molar ratio of polySia to the receptor peptides was 5:1 for these NMR experiments. The STD NMR experiments were performed as described[28,76] using a 10:1 ligand/receptor molar ratio for the interaction experiments, with 0.5, 1, and 2 s saturation times (by concatenation of 50 ms Gaussian pulses separated by 1 ms).

Molecular modeling / docking study: The 3D structure of *Selenocosmia huwena* Lectin-I (SHL-1) from the venom of the spider *S. huwena* Wang was taken from the PDB (PDB ID: 1QK7).[81] Docking studies were performed with the AutoDock 4.2 software, which uses the Lamarckian genetic algorithm (LGA). For docking of the polySia disaccharide fragment with SHL-1, the required file for the ligand was created by the AutoDock 4.2 software package. The grid size was set to 126, 126, and 126 Å along the *x*-, *y*-, and *z*-axes. In order to recognize the binding site of the polySia disaccharide in SHL-1, a blind docking simulation was adopted. The docking parameters used were as follows: GA population size = 150; maximum number of energy evaluations = 250000. The lowest binding energy conformer was taken from 10 different conformations for each docking simulation, and the resulting minimum energy conformation was applied for further analysis. The PyMOL software package was used for visualization of the docked complex.[77]

Mouse studies: C57BL/6J mice of either sex were used as wild-type mice. Mice were kept under standard laboratory conditions with food and water supply ad libitum and with an artificial 12 h light/dark cycle. All experiments were conducted in accordance with the German and European Community laws on protection of experimental animals, and all procedures used were approved by the responsible committee of the State of Hamburg. This paper was written in compliance with the ARRIVE guidelines for reports on animal research.

Neuronal culture and neurite outgrowth: Cerebellar granule neurons were used as archetype neurons and prepared from the cerebella of six- to eight-day-old wild-type mice and cultured in defined serum-free medium composed of Neurobasal A medium (Invitrogen, Thermo Fisher Scientific), supplemented with 1 mM L-glutamine (Invitrogen), 0.5% (*v/v*) B27 (Invitrogen), 100 $\mu g\,mL^{-1}$ holotransferrin (Merck Chemicals, Darmstadt), 10 $\mu g\,mL^{-1}$ insulin (Sigma–Aldrich), 30 nM sodium selenite (Sigma–Aldrich), and 4 nM L-thyroxine (Sigma–Aldrich), as previously described.[76] Neurons were seeded at a density of 2.5×10^4 cells per well in 48-well plates (Sarstedt, Numbrecht, Germany) coated with poly-L-lysine (PLL; Sigma–Aldrich) or with varying concentrations of glycans (special mixture from Ocean Harvest Ltd., 1 $\mu g\,mL^{-1}$ to 5 $mg\,mL^{-1}$), alone or in combination with collagen hydrolysates of fish or pig origin. Neurite length was measured after 24 h, as previously described, using an Axiovert 135 microscope equipped with AxioVision 4.6 software (Carl Zeiss, Oberkochen).[78] In each experiment, at least 50 cells on each of two coverslips were analyzed, and the total neurite length was determined by measuring the length of all neurites per cell that were longer than the cell body. The results of three independent experiments were averaged.

Microexplant culture and neuronal migration: Microexplant cultures from cerebella of six- or seven-day-old wild-type mice were prepared as described.[79,80] Cerebellar explants were cultured on PLL or glycans at 1 $\mu g\,mL^{-1}$ to 5 $mg\,mL^{-1}$ concentration in the same medium stated above, supplemented with 10% horse serum and 10% fetal calf serum. After 16 h in culture, the medium was changed to serum-free medium, and the explants were cultured for an additional 32 h. After 48 h, in vitro explants were fixed with glutaraldehyde, stained with toluidine blue/trypan blue, and imaged using an Axiovert 135 microscope equipped with AxioVision software 4.6 (Carl Zeiss).

Statistics: Differences between groups in the neurite outgrowth assay were determined by the two-tailed *t*-test. Results are expressed as mean ± SEM; $p<0.05$: statistically significant for all statistical tests.

Acknowledgements

The authors thank Philipp Siebert for technical assistance and Eva Kronberg for the excellent care of animals. Elements of the project were financed by the European Commission's Framework Program 7 (Bio-NMR; project number 261863). The authors also thank their colleagues, H. Maximilian Mehdorn, Robert I. Lehrer, and Wuyuan Lu for many fruitful discussions, and the Sialic Acids Society of Kiel for financial support.

Keywords: molecular interactions · polysia mimetics · polysialic acid · sulfated polysaccharides

[1] R. Schauer, *Curr. Opin. Struct. Biol.* **2009**, *19*, 507–514.
[2] M. D. Battistel, M. Shangold, L. Trinh, J. Shiloach, D. I. Freedberg, *J. Am. Chem. Soc.* **2012**, *134*, 10717–10720.
[3] C. Sato, K. Kitajima, *Front. Cell. Neurosci.* **2013**, *7*, 61.
[4] M. Rollenhagen, S. Kuckuck, C. Ulm, M. Hartmann, S. P. Galuska, R. Geyer, H. Geyer, M. Mühlenhoff, *J. Biol. Chem.* **2012**, *287*, 35170–35180.
[5] H. Hildebrandt, A. Dityatev, *Top. Curr. Chem.* **2013**, *366*, 55-96.
[6] *Sialobiology: Structure, Biosynthesis, and Function* (Eds.: J. Tiralongo, I. Martinez-Duncker), Bentham Science, Oak Park, **2013**.
[7] R. Schauer, *Zoology* **2004**, *107*, 49–64.
[8] P. Simon, S. Bäumner, O. Busch, R. Röhrich, M. Kaese, P. Richterich, A. Wehrend, K. Müller, R. Gerardy-Schahn, M. Mühlenhoff, H. Geyer, R. Geyer, R. Middendorff, S. P. Galuska, *J. Biol. Chem.* **2013**, *288*, 18825–18833.
[9] a) C. Ulm, M. Saffarzadeh, P. Mahavadi, S. Müller, G. Prem, F. Saboor, P. Simon, R. Middendorff, H. Geyer, I. Henneke, N. Bayer, S. Rinné, T. Lütteke, E. Böttcher-Friebertshäuser, R. Gerardy-Schahn, D. Schwarzer, M. Mühlenhoff, K. T. Preissner, A. Günther, R. Geyer, S. P. Galuska, *Cell. Mol. Life Sci.* **2013**, *70*, 3695–3708; b) N. Eswar, B. Webb, M. A. Marti-Renom, M. S. Madhusudhan, D. Eramian, M. Y. Shen, U. Pieper, A. Sali, *Curr. Protoc. Bioinformatics* **2006**, Ch. 5, Unit 5.6, DOI: 10.1002/0471250953.bi0506s15; c) A. Bohne-Lang, C. W. von der Lieth, *Nucleic Acids Res.* **2005**, *33*, W214–W219; d) E. Krieger, K. Joo, J. Lee, J. Lee, S. Raman, J. Thompson, M. Tyka, D. Baker, K. Karplus, *Proteins: Struct. Funct. Bioinf.* **2009**, *77*, 114–122.
[10] B. Mishra, M. von der Ohe, C. Schulze, S. Bian, T. Makhina, G. Loers, R. Kleene, M. Schachner, *J. Neurosci.* **2010**, *30*, 12400–12413.

[11] T. Theis, B. Mishra, M. von der Ohe, G. Loers, M. Prondzynski, O. Pless, P. J. Blackshear, M. Schachner, R. Kleene, *J. Biol. Chem.* **2013**, *288*, 6726–6742.
[12] Y. Kizuka, S. Oka, *Cell. Mol. Life Sci.* **2012**, *69*, 4135–4147.
[13] S. R. Haseley, H. J. Vermeer, J. P. Kamerling, J. F. G. Vliegenthart, *Proc. Natl. Acad. Sci. USA* **2001**, *98*, 9419–9424.
[14] K. Nishiyama, Y. Takakusagi, T. Kusayanagi, Y. Matsumoto, S. Habu, K. Kuramochi, F. Sugawara, K. Sakaguchi, H. Takahashi, H. Natsugari, S. Bioorg, *Med. Chem.* **2009**, *17*, 195–202.
[15] M. Kilcoyne, J. Q. Gerlach, R. Gough, M. E. Gallagher, M. Kane, S. D. Carrington, L. Joshi, *Anal. Chem.* **2012**, *84*, 3330–3338.
[16] U. Rutishauser, *Nat. Rev. Neurosci.* **2008**, *9*, 26–35.
[17] O. Senkov, M. Sun, B. Weinhold, R. Gerardy-Schahn, M. Schachner, A. Dityatev, *J. Neurosci.* **2006**, *26*, 10888–109898.
[18] A. K. Petridis, H. Wedderkopp, H. H. Hugo, H. M. Mehdorn, *Acta Neurochir.* **2009**, *151*, 601–603.
[19] H.-C. Siebert, K. Born, S. André, M. Frank, H. Kaltner, C. W. von der Lieth, A. J. Heck, J. Jiménez-Barbero, J. Kopitz, H. J. Gabius, *Chem. Eur. J.* **2006**, *12*, 388–402.
[20] R. Kleene, M. Schachner, *Nat. Rev. Neurosci.* **2004**, *5*, 195–208.
[21] S. N. Masand, J. Chen, I. J. Perron, B. C. Hammerling, G. Loers, M. Schachner, D. I. Shreiber, *Biomaterials* **2012**, *33*, 8353–8362.
[22] A. Mehanna, B. Mishra, N. Kurschat, C. Schulze, S. Bian, G. Loers, A. Irintchev, M. Schachner, *Brain* **2009**, *132*, 1449–1462.
[23] S. Liang, *Toxicon* **2004**, *43*, 575–585.
[24] M. A. Rojas-Macias, T. Lütteke, *Methods Mol. Biol.* **2015**, *1273*, 215–226.
[25] H.-C. Siebert, S. Y. Lu, R. Wechselberger, K. Born, T. Eckert, S. P. Liang, C. W. von der Lieth, J. Jiménez-Barbero, R. Schauer, J. F. G. Vliegenthart, T. Lütteke, S. André, H. Kaltner, H. J. Gabius, T. Kozár, *Carbohydr. Res.* **2009**, *344*, 1515–1525.
[26] H.-C. Siebert, S. Y. Lü, M. Frank, J. Kramer, R. Wechselberger, J. Joosten, S. André, K. Rittenhouse-Olson, R. Roy, C. W. von der Lieth, R. Kaptein, J. F. Vliegenthart, A. J. Heck, H. J. Gabius, *Biochemistry* **2002**, *41*, 9707–9717.
[27] H.-C. Siebert, S. André, S. Y. Lu, M. Frank, H. Kaltner, J. A. van Kuik, E. Y. Korchagina, N. Bovin, E. Tajkhorshid, R. Kaptein, J. F. G. Vliegenthart, C. W. von der Lieth, J. Jiménez-Barbero, J. Kopitz, H. J. Gabius, *Biochemistry* **2003**, *42*, 14762–14773.
[28] V. Roldós, F. J. Cañada, J. Jiménez-Barbero, *ChemBioChem* **2011**, *12*, 990–1005.
[29] A. Bhunia, S. Vivekanandan, T. Eckert, M. Burg-Roderfeld, R. Wechselberger, J. Romanuka, D. Bächle, A. V. Kornilov, C. W. von der Lieth, J. Jiménez-Barbero, N. E. Nifantiev, M. Schachner, N. Sewald, T. Lütteke, G. Hans-Joachim, H.-C. Siebert, *J. Am. Chem. Soc.* **2010**, *132*, 96–105.
[30] Y. E. Tsvetkov, M. Burg-Roderfeld, G. Loers, A. Ardá, E. V. Sukhova, E. A. Khatuntseva, A. A. Grachev, A. O. Chizhov, H.-C. Siebert, M. Schachner, J. Jiménez-Barbero, N. E. Nifantiev, *J. Am. Chem. Soc.* **2012**, *134*, 426–435.
[31] S. L. Holdt, S. Kraan, *J. Appl. Phycol.* **2011**, *23*, 543–597.
[32] D. O. Croci, A. Cumashi, N. A. Ushakova, M. E. Preobrazhenskaya, A. Piccoli, L. Totani, N. E. Ustyuzhanina, M. I. Bilan, A. I. Usov, A. A. Grachev, G. E. Morozevich, A. E. Berman, C. J. Sanderson, M. Kelly, P. Di Gregorio, C. Rossi, N. Tinari, S. Iacobelli, G. A. Rabinovich, N. E. Nifantiev, *PLoS One* **2011**, *6*, e17283.
[33] J. Bushman, B. Mishra, M. Ezra, S. Gul, C. Schulze, S. Chaudhury, D. Ripoll, A. Wallqvist, J. Kohn, M. Schachner, G. Loers, *Neuropharmacology* **2014**, *79*, 456–466.
[34] H. C. Pan, Y. G. Shen, G. Loers, I. Jakovcevski, M. Schachner, *Neuroscience* **2014**, *277*, 356–366.
[35] J. H. van Lenthe, D. H. W. van Boer, R. W. A. den Havenith, R. Schauer, H.-C. Siebert, *J. Mol. Struct.* **2004**, *677*, 29–37.
[36] H.-C. Siebert, E. Tajkhorshid, J. Dabrowski, *J. Phys. Chem. A* **2001**, *105*, 8488–8494.
[37] T. Eckert, S. Stötzel, M. Burg-Roderfeld, J. Sewing, T. Lütteke, N. E. Nifantiev, J. F. G. Vliegenthart, H.-C. Siebert, *Open J. Phys. Chem.* **2011**, *2*, 123–133.
[38] A. Szyk, Z. Wu, K. Tucker, D. Yang, W. Lu, J. Lubkowski, *Protein Sci.* **2006**, *15*, 2749–2760.
[39] R. I. Lehrer, G. Jung, P. Ruchala, S. Andre, H. J. Gabius, W. Lu, *J. Immunol.* **2009**, *183*, 480–490.
[40] J. M. Schröder, *Immunity* **2014**, *41*, 671–673.
[41] J. M. Schröder, *Cell. Mol. Life Sci.* **2006**, *63*, 469–486.
[42] R. I. Lehrer, W. Lu, *Immunol. Rev.* **2012**, *245*, 84–112.
[43] G. Loers, V. Saini, B. Mishra, F. Papastefanaki, D. Lutz, S. Chaudhury, D. R. Ripoll, A. Wallqvist, S. Gul, M. Schachner, G. Kaur, *J. Neurochem.* **2014**, *128*, 88–100.
[44] M. I. Franco, L. Turin, A. Mershin, E. M. C. Skoulakis, *Proc. Natl. Acad. Sci. USA* **2011**, *108*, 3797–3802.
[45] A. Seifert, D. Glanz, N. Glaubitz, R. Horstkorte, K. Bork, *Arch. Biochem. Biophys.* **2012**, *524*, 56–63.
[46] A. K. Petridis in *Recent Advances in Adhesion Research* (Eds.: A. McFarland, M. Akins), Nova Science, Hauppauge, **2013**, 115–122.
[47] A. K. Petridis, A. El Maarouf, U. Rutishauser, *Dev. Dyn.* **2004**, *230*, 675–684.
[48] R. Miyahara, F. Tanaka, T. Nakagawa, K. Matsuoka, K. Isii, H. Wada, *J. Surg. Oncol.* **2001**, *77*, 49–54.
[49] S. Glüer, C. Schelp, R. Gerardy-Schahn, D. von Schweinitz, *J. Pediatr. Surg.* **1998**, *33*, 1516–1520.
[50] S. Glüer, C. Schelp, N. Madry, D. von Schweinitz, M. Eckhardt, R. Gerardy-Schahn, *British J. Cancer* **1998**, *78*, 106–110.
[51] M. Suzuki, M. Suzuki, J. Nakayama, A. Suzuki, K. Angata, S. Chen, K. Sakai, K. Hagihara, Y. Yamaguchi, M. Fukuda, *Glycobiology* **2005**, *15*, 887–894.
[52] M. C. Amoureux, B. Coulibaly, O. Chinot, A. Loundou, P. Metellus, G. Rougon, D. Figarella-Branger, *BMC Cancer* **2010**, *10*, 91.
[53] H. Cremer, R. Lange, A. Christoph, M. Plomann, G. Vopper, J. Roes, R. Brown, S. Baldwin, P. Kraemer, S. Scheff, *Nature* **1994**, *367*, 455–459.
[54] K. Ono, H. Tomasiewicz, T. Magnuson, U. Rutishauser, *Neuron* **1994**, *13*, 595–609.
[55] H. Tomasiewicz, K. Ono, D. Yee, C. Thompson, C. Goridis, U. Rutishauser, T. Magnuson, *Neuron* **1993**, *11*, 1163–1174.
[56] A. K. Petridis, S. N. Nikolopoulos, A. El-Maarouf, *J. Clin. Neurosci.* **2011**, *18*, 1109–1113.
[57] C. S. K. Mayanil, D. George, B. Mania-Farnell, C. L. Bremer, D. McLone, E. G. Bremer, *J. Biol. Chem.* **2000**, *275*, 23259–23266.
[58] F. Tanaka, Y. Otake, T. Nakagawa, Y. Kawano, R. Miyahara, M. Li, K. Yanagihara, K. Inui, H. Oyanagi, T. Yamada, J. Nakayama, I. Fujimoto, K. Ikenaka, H. Wada, *Cancer Res.* **2001**, *61*, 1666–1670.
[59] J. Roth, C. Zuber, P. Wagner, D. J. Taatjes, C. Weisgerber, P. U. Heitz, C. Goridis, D. Bitter-Suermann, *Proc. Natl. Acad. Sci. USA* **1988**, *85*, 2999–3003.
[60] E. Sackmann, F. Keber, D. Heinrich, *Annu. Rev. Condens. Matter Phys.* **2010**, *1*, 257–276.
[61] A. El Maarouf, A. K. Petridis, U. Rutishauser, *Proc. Natl. Acad. Sci. USA* **2006**, *103*, 16989–16994.
[62] R. Seidenfaden, A. Krauter, F. Schertzinger, R. Gerardy-Schahn, H. Hildebrandt, *Mol. Cell. Biol.* **2003**, *23*, 5908–5918.
[63] V. B. Krylov, A. A. Grachev., N. E. Ustyuzhanina, N. A. Ushakova, M. E. Preobrazhenskaya, N. I. Kozlova, M. N. Portsel, I. N. Konovalova, V. Y. Novikov, H.-C. Siebert, A. S. Shashkov, N. E. Nifantiev, *Russian Chem. Bull. (Med. Chem. Issue) Int. Ed.* **2011**, *60*, 746–753.
[64] H.-C. Siebert, M. Burg-Roderfeld, T. Eckert, S. Stötzel, U. Kirch, T. Diercks, M. J. Humphries, M. Frank, R. Wechselberger, E. Tajkhorshid, S. Oesser, *Protein Cell* **2010**, *1*, 393–405.
[65] O. Raabe, C. Reich, S. Wenisch, A. Hild, M. Burg-Roderfeld, H.-C. Siebert, S. Arnhold, *Histochem. Cell Biol.* **2010**, *134*, 545–554.
[66] S. Schadow, H.-C. Siebert, G. Lochnit, J. Kordelle, M. Rickert, J. Steinmeyer, *PLoS One* **2013**, *8*, e53955.
[67] A. Mehanna, I. Jakovcevski, A. Acar, M. Xiao, G. Loers, G. Rougon, A. Irintchev, M. Schachner, *Mol. Ther.* **2010**, *18*, 34–43.
[68] P. Marino, J. C. Norreel, M. Schachner, G. Rougon, M. C. Amoureux, *Exp. Neurol.* **2009**, *219*, 163–174.
[69] S. G. Cajal, *Histology of the Nervous System of Man and Vertebrates*, Vol. 1 and 2, Oxford University Press, London, **1928**.
[70] G. Loers, T. Makhina, U. Bork, A. Dörner, M. Schachner, R. Kleene, *J. Neurosci.* **2012**, *32*, 3917–3930.
[71] M. Sumida, M. Hane, U. Yabe, Y. Shimoda, O. M. T. Pearce, M. Kiso, T. Miyagi, M. Sawada, A. Varki, K. Kitajima, C. Sato, *J. Biol. Chem.* **2015**, *290*, 13202–13214..
[72] H.-C. Siebert, R. Zhang, A. Scheidig, T. Eckert, H. Wienk, R. Boelens, M. Mahvash, A. K. Petridis, R. Schauer, *J. Neurol. Disord.* **2015**, *3*, 212.
[73] J. Harder, J. M. Schröder, *J. Leukocyte Biol.* **2005**, *77*, 476–486.

[74] J. Jeener, B. H. Meier, P. Bachmann, R. R. Ernst, *J. Chem. Phys.* **1979**, *71*, 4546 – 4553.
[75] L. Braunschweiler, R. R. Ernst, *J. Magn. Reson.* **1983**, *53*, 521 – 528.
[76] A. Bernardi, D. Potenza, A. M. Capelli, A. García-Herrero, F. J. Canada, J. Jiménez-Barbero, *Chem. Eur. J.* **2002**, *8*, 4598 – 4612.
[77] W. L. De Lano, De Lano Scientific, San Carlos, CA (USA), **2002**.
[78] G. Loers, S. Chen, M. Grumet, M. Schachner, *J. Neurochem.* **2005**, *92*, 1463 – 1476.
[79] I. Jakovcevski, J. Siering, G. Hargus, N. Karl, L. Hoelters, N. Djogo, S. Yin, N. Zecevic, M. Schachner, A. Irintchev, *J. Comp. Neurol.* **2009**, *513*, 496 – 510.
[80] I. Kalus, B. Schnegelsberg, N. G. Seidah, R. Kleene, M. Schachner, *J. Biol. Chem.* **2003**, *278*, 10381 – 10388.
[81] S. Lü, S. Liang, X. Gu, *J. Protein Chem.* **1999**, *18*, 609 – 617.
[82] J. Schindelin, I. Arganda-Carreras, E. Frise, V. Kaynig, M. Longair, T. Pietzsch, S. Preibisch, C. Rueden, S. Saalfeld, B. Schmid, J. Y. Tinevez, D. J. White, V. Hartenstein, K. Eliceiri, P. Tomancak, A. Cardona, *Nat. Methods* **2012**, *9*, 676 – 682.

Received: December 30, 2015
Revised: March 1, 2016
Published online on ■■ ▮▮, 0000

FULL PAPERS

*R. Zhang, G. Loers, M. Schachner, R. Boelens, H. Wienk, S. Siebert, T. Eckert, S. Kraan, M. A. Rojas-Macias, T. Lütteke, S. P. Galuska, A. Scheidig, A. K. Petridis, S. Liang, M. Billeter, R. Schauer, J. Steinmeyer, J.-M. Schröder, H.-C. Siebert**

■■ – ■■

Molecular Basis of the Receptor Interactions of Polysialic Acid (polySia), polySia Mimetics, and Sulfated Polysaccharides

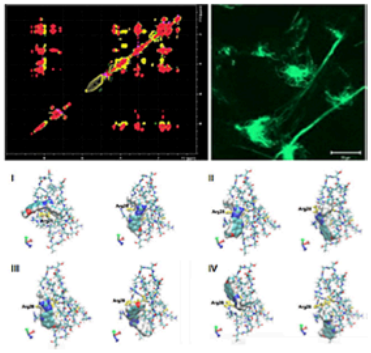

Submolecular polySia interactions: Specific interactions of polysialic acid (polySia) and polySia glycomimetic molecules were studied at the submolecular level using a combination of NMR and molecular modeling. The structure–function interplay between polySia or sulfated polysaccharides and their receptors can be exploited to develop new drugs and application routes for the treatment of neurological diseases and dysfunctions.

Submolecular polysialic acid studies: #DrugDevelopment for #NeurologicalDisease @KielUni SPACE RESERVED FOR IMAGE AND LINK

Share your work on social media! *ChemMedChem* has added Twitter as a means to promote your article. Twitter is an online microblogging service that enables its users to send and read text-based messages of up to 140 characters, known as "tweets". Please check the pre-written tweet in the galley proofs for accuracy. Should you or your institute have a Twitter account, please let us know the appropriate username (i.e., @accountname), and we will do our best to include this information in the tweet. This tweet will be posted to the journal's Twitter account @ChemMedChem (follow us!) upon online publication of your article, and we recommended you to repost ("retweet") it to alert other researchers about your publication.

Please check that the ORCID identifiers listed below are correct. We encourage all authors to provide an ORCID identifier for each coauthor. ORCID is a registry that provides researchers with a unique digital identifier. Some funding agencies recommend or even require the inclusion of ORCID IDs in all published articles, and authors should consult their funding agency guidelines for details. Registration is easy and free; for further information, see http://orcid.org/.

Ruiyan Zhang
Dr. Gabriele Loers
Prof. Dr. Melitta Schachner
Prof. Dr. Rolf Boelens
Dr. Hans Wienk
Simone Siebert
Dr. Thomas Eckert
Dr. Stefan Kraan
Miguel A. Rojas-Macias
Dr. Thomas Lütteke http://orcid.org/0000-0002-7140-9933
Dr. Sebastian P. Galuska
Prof. Dr. Axel Scheidig
Dr. Athanasios K. Petridis
Prof. Dr. Songping Liang
Prof. Dr. Martin Billeter
Prof. Dr. Roland Schauer
Prof. Dr. Jürgen Steinmeyer
Prof. Dr. Jens-Michael Schröder
Prof. Dr. Hans-Christian Siebert

3.2 Structure-function relationships of antimicrobial peptides and proteins with respect to contact molecules on pathogen surfaces

My contribution for this publication was to carry out Molecular modelling experiments and to analyse the related results.

Send Orders for Reprints to reprints@benthamscience.ae

Current Topics in Medicinal Chemistry, 2016, *16*, 89-98

Structure-Function Relationships of Antimicrobial Peptides and Proteins with Respect to Contact Molecules on Pathogen Surfaces

Ruiyan Zhang[1,2], Thomas Eckert[3,4], Thomas Lütteke[3], Stefan Hanstein[5], Axel Scheidig[1], Alexandre M. J. J. Bonvin[6], Nikolay E. Nifantiev[7], Tibor Kožár[8], Roland Schauer[9], Mushira Abdulaziz Enani[10] and Hans-Christian Siebert[2,*]

H.-C. Siebert

[1]Zoologisches Institut - Strukturbiologie, Zentrum für Biochemie und Molekularbiologie, Christian-Albrechts-Universität Kiel, Kiel, Germany; [2]RI-B-NT - Research Institute of Bioinformatics and Nanotechnology, Kiel, Germany; [3]Institut fur Veterinärphysiolgie und -Biochemie, Fachbereich Veterinärmedizin, Justus-Liebig-Universität Gießen, Gießen, Germany; [4]Klinik fur Geburtshilfe, Gynäkologie und Andrologie der Groß- und Kleintiere mit Tierärztlicher Ambulanz, Fachbereich Veterinärmedizin, Justus-Liebig-Universität Gießen, Gießen, Germany; [5]Geschäftsfeldleitung Biowerkstoffe, Lebensmittel, Fraunhofer-Institut fur Silicatforschung ISC, Projektgruppe fur Wertstoffkreisläufe und Ressourcenstrategie IWKS, Alzenau, Germany; [6]Bijvoet Center for Biomolecular Research, NMR Spectroscopy, Utrecht University, Utrecht, The Netherlands; [7]Laboratory of Glycoconjugate Chemistry, Zelinsky Institute of Organic Chemistry, Russian Academy of Sciences, Moscow, Russian Federation; [8]Centre of Interdisciplinary Biosciences, Pavol Jozef Safarik University in Kosice, Kosice, Slovakia; [9]Biochemisches Institut, Universitat Kiel, Kiel, Germany; [10]Infectious Diseases Division, Department of Medicine, King Fahad Medical City, Kingdom of Saudi Arabia

Abstract: The Antimicrobial peptides (e.g. defensins, hevein-like molecules and food-protecting peptides like nisin) are able to interact specifically with contact structures on pathogen surfaces. Besides protein receptors, important recognition points for such contacts are provided by pathogen glycan chains or surface lipids. Therefore, structural data concerning surface exposed glycans and lipids are of the highest clinical interest since these recognition functions play a key role when optimising anti-infection therapies. Approaches in nanomedicine and nanopharmacology in which various biophysical techniques such as NMR (Nuclear Magnetic Resonance), AFM (Atomic Force Microscopy), SPR (Surface Plasmon Resonance) and X-ray crystallography can be combined with biochemical and cell-biological methods will lead to improved antimicrobial peptides by this rational drug design approach. Such a strategy is extremely well suited to support clinical studies focussing on an effective fight against multiresistant pathogens. The data sets which are described here can be considered as universal for the design of various antimicrobial drugs against certain pathogens (bacteria, viruses and fungi) which cause severe diseases in humans and animals. Furthermore, these insights are also helpful for progressing developments in the field of food conservation and food preservation. A detailed analysis of the structure-function relationships between antimicrobial peptides and contact molecules on pathogen surfaces at the sub-molecular level will lead to a higher degree of specificity of antimicrobial peptides.

Keywords: Biophysical methods, Nanomedicine, Nanopharmacology, Structure-function relationship.

1. INTRODUCTION

Antimicrobial peptides by a strict definition are regarded as small peptides of up to ten amino acid residues with the property of attacking single-cell organisms with pathogenic potential. In a broader definition, peptides/proteins of up to 100 amino acid residues which are able to destroy the pathogenicity of microbes such as bacteria, viruses and fungi can also be included.

Independent of such definitions, the complementarity of structure and function has to be analysed on a nanoscale level with a strategic combination of various biophysical methods in order to obtain detailed information regarding the role of antimicrobial peptides in various diseases. A significant improvement in drug design in different medical fields is an important outcome of such an approach. Furthermore, antimicrobial peptides also play a key role in relation to food preservation and conservation. We will discuss in this article whether certain patterns in the arrangement of amino acids which determine the structural architecture of antimicrobial peptides are characteristic for specific interactions with contact structures (proteins, glycans or lipids) on pathogen surfaces. These recognition molecules are determined by certain functional groups which establish specific interaction processes. Very often the arrangements of functional groups of the contact structures on the pathogen surfaces which are recognised by antimicrobial peptides show a high degree of

*Address correspondence to this author at the RI-B-NT - Research Institute of Bioinformatics and Nanotechnology, Franziusallee 177, 24148 Kiel, Germany; Tel: +49 431 880 4353; Fax: +49 431 880 4929;
E-mail: hcsiebert@aol.com

1873-5294/16 $58.00+.00

similarity or are even identical with those structures which enable the pathogen to dock to a host cell and spread the infection.

2. VARIOUS ASPECTS AND CONCLUSIONS

2.1. Medical Aspects

In the study of antimicrobials sialic acids play a prominent role as potential interaction partners since they are the terminal carbohydrate residues of many glycolipids (in this case called gangliosides) and glycan chains from glycoproteins [1, 2]. N-acetyl neuraminic acid (Neu5Ac) and related molecules (e.g. O-acetylated Neu5Ac moieties) constitute the large family of sialic acids [1]. These molecules are specific and clinically important contact structures for antimicrobial proteins and peptides. Sialic acids on pathogens are therefore a suitable target for a number of antimicrobial peptides. Sialic acids interact e.g. with a small lectin from the Chinese bird hunting spider *Selenocosmia huwena* Wang (Wang: Chinese expression for King) [3, 4] but are also specific interaction partners for α-defensins. The three classes of defensins, α-, β- and θ-defensins are antimicrobial peptides with three characteristic disulphide bridges and have to be considered as an important part of the innate immune system [5-16]. It can be shown with NMR, SPR and molecular modelling methods that sialic acid residues form stable complexes with HNP1, 2, or 3 (derived from psoriatic skin cells) in a specific way (Fig. **1**). For the molecular recognition process, it is very important to which other carbohydrate moiety in a saccharide chain the sialic acid residue is linked and which atoms are involved in the glycosidic linkage. Very often the sialic acid molecule Neu5Ac is alpha 2-3 linked to

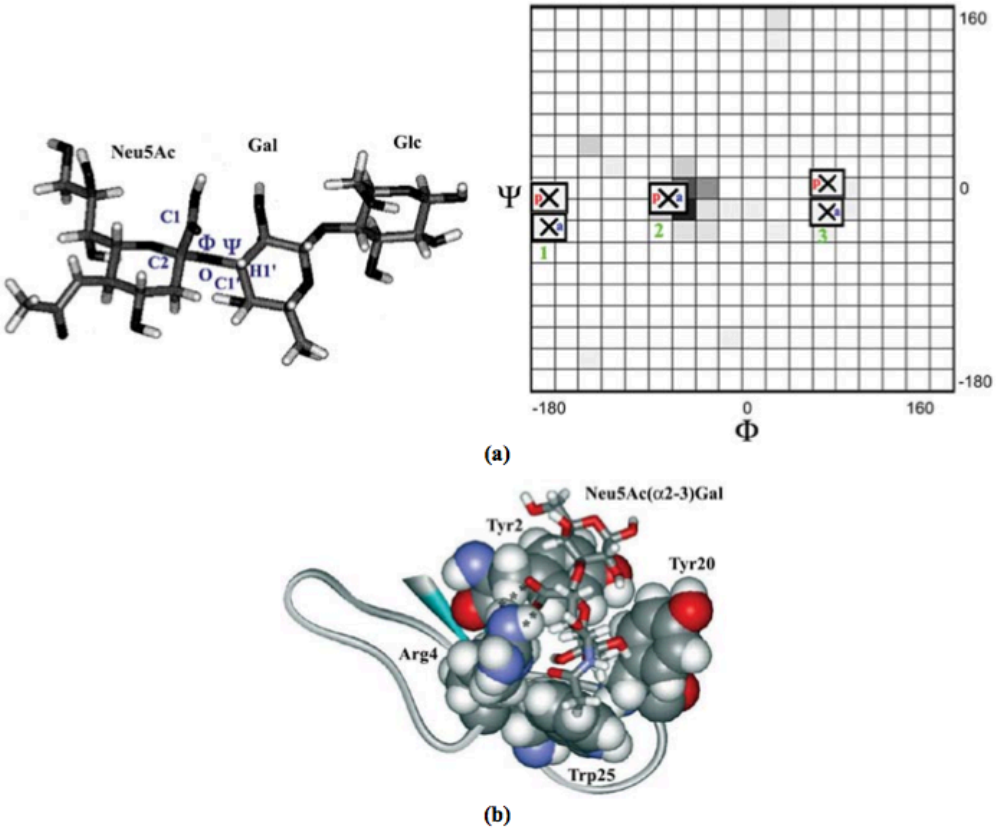

Fig. (1). a: Quantum chemical calculations of the preferred conformations of the Neu5Ac(α2-3)Gal linkage using the B3LYB/6-31G* method. The calculations were carried out in the protonated and in the anionic state in order to perform energy minimization under various physical-chemical conditions. In the anionic state the carboxylic groups are calculated without the hydrogen ions. Instead of hydrogen two water molecules have been added. The results from the quantum chemical calculations are combined with data from a Φ/ Ψ - map of this linkage generated with GlyTorsion: www.glycosciences.de/tools/glytorsion/ to compare the calculated values with experimental data.The definition of the glycosidic angles is as follows Φ: C1-C2-O-C1', Ψ: C2-O-C1'-H1' (C1'and H1'are galactose atoms). The three different energetic local minima of the Neu5Ac(α2-3)Gal linkage delivered from the data bank are derived from Neu5Ac(α2-3)Gal linkages in PDB entries. At the positions of minima 1 and 3 we have obtained small differences between the protonated and anionic state concerning the values of the glycosidic angles Φ and Ψ determined with our quantum chemical methods. The protonated state refers to the crosses with the red letter "p" and the anionic state to the crosses with the blue letter "a". The values of the glycosidic Φ and Ψ - angle referring to the protonated and to the anionic state only match exactly in the case of minimum 2. The conformational flexibility of the Gal(β1-4)Glc linkage between galactose and glucose is not considered here. b: HNP2 in complex with a Neu5Ac(α2-3)Gal fragment at the energy minimum conformation 2. The glycosidic angles of the Neu5Ac(α2-3)Gal linkage are Φ: -64° and Ψ: 0° (conformation 2). The important binding-stabilising contact between the carboxylic group of Neu5Ac and Arg4 is highlighted by asterisks. Tyr2, Tyr20 and Trp25 are responsible for stabilisation of the complex mainly by π-interactions.

galactose (Gal) (Fig. **1a**, top). In this case, the carbon atom 2 of Neu5Ac in its alpha configuration is connected by an oxygen atom with the carbon atom 3 of galactose (Gal). It should be emphasised that this linkage has rotational degrees of freedom and energy minimum conformations (defined by the glycosidic angles Φ and Ψ) which can be determined by the biophysical methods described here. These energy minimum conformations of the free state (Fig. **1a**, bottom) are selected by receptors as bound state conformations [17-21], for example, as shown for the α-defensin HNP1 (Fig. **1b**). As demonstrated in Fig. (**2a, b, c**), atoms of Trp (a), Tyr (b) and Arg (c) residues which occur in the vicinity of Neu5Ac residues (according to Protein Data Bank (PDB) entries at www.pdb.org) are monitored respective to their positions in relation to Neu5Ac and allow a statistical overview (www.glycosciences.de/tools/glytorsion/). For example, it is of special interest which atoms are mainly involved in sialic acid binding. As Fig. (**2c**) demonstrates, in the case of Arg the interactions with sialic acids are dominated by nitrogen atoms of the amino acid side chain. The α-defensins HNP2 and HD5 are canonical examples for sialic acid binding mini-lectins. In order to visualise their binding modes the free and bound state conformations of these antimicrobial peptides are presented in Fig. (**3a** and **b**). The HNP2 conformations in the ligand free and in the sialic acid bound state are shown in the three model pictures presented in Fig. (**3a**). In particular, the comparison between the HNP2 conformation in the ligand-free (Fig. **3a**, left, middle) and the sialic acid bound state (Fig. **3a**, right) reveals clear differences when focussing on the orientations of the binding relevant amino acid residues Tyr2 Arg4, Tyr20 and Trp25. Conformational differences between the bound state conformations of the human α -defensin HD5 in complex with the sialic acid mimicking the tegaserod molecule in its cis- (Fig. **3b**, left) or in its trans- (Fig. **3b**, right) configuration are also observable. The tegaserod molecules are not displayed in order to visualise their impact on the overall shape of HD5 more clearly. Only the binding-relevant Arg28 residue is marked. Tegaserod is discussed as a polySia glycomimicking molecule with an impact on nerve cell regeneration [22]. Therefore, the conformations of the sialic acid mini-receptor HD5 in its cis- as well as in its trans-tegaserod bound state have been calculated by molecular docking routines within molecular dynamics simulations, and are presented in Fig. (**3b**). Also in the case of small glycomimicking molecules in their cis- and trans-configurations, a significant conformational impact on HD5 could be calculated with our molecular docking approaches (our own unpublished results, data not shown). When studying lectin SHL-1 from the Chinese bird-hunting spider *Selenocosmia huwena* Wang it turned out that sialic acid specificity is dominated by aromatic amino acid residues as shown in Fig. (**3c**) [3]. The three tryptophan residues (Trp23, Trp25, Trp32) which are all involved in binding with the polySia disaccharide fragment are labelled. For comparison, a snapshot of a molecular docking study of the α-defensin HD5-double mutant (A13R, A32R) with N-acetyl muramic acid (MurNAc), where Arg residues play a crucial role, is presented in Fig. (**4**). Our molecular docking calculations indicate that the replacement of Ala13 by Arg and Ala 32 by Arg alters the affinity to muramic acid (MurNAc) according to the calculated energy values, which will be published elsewhere. MurNAc is, like Neu5Ac, an acid and N-acetylated carbohydrate. It is part of a biopolymer in the bacterial cell wall, built from alternating units of N-acetylglucosamine (GlcNAc) and N-acetylmuramic acid (MurNAc), cross-linked with oligopeptides at the lactic acid residue of MurNAc. This layered structure is called peptidoglycan murein.

2.2. Nutritional Aspects

Antimicrobial peptides are also of highest importance when new concepts in the field of food preservation are needed. The molecular interplay of certain peptides already serve as such agents, can be taken as starting point for these concepts. The N-terminal part of nisin (Fig. **5**, crucial residues between 1-12 are shown in a surface representation) encages the pyrophosphate moiety of the pathogen surface lipid 3LII, e.g. the gram-positive methicillin-resistant *Staphylococcus aureus* (MRSA) [23, 24]. The side chains of these nisin residues are labelled in different colours. The N-acetyl muramic acid (MurNAc) moiety, which occurs on the surface on many bacteria forms stable complexes with nisin. This moiety, the pyrophosphate part, and the first isoprene unit of 3LII fit in the binding pocket of nisin (Fig. **5**). In this case the carbohydrate and the fatty part of the pathogen lipid 3LII both contribute to the stable 3LII - nisin complex. The antimicrobial activity of nisin against the pathogen depends therefore on the specific contact with the surface lipid 3LII. Other instructive examples of food-

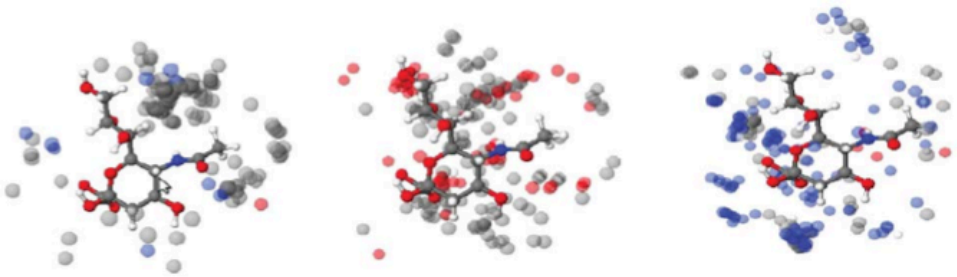

Fig. (2). Atoms of Trp (left), Tyr (middle) and Arg (right) residues occurring around Neu5Ac residues according to pdb-entries and an evaluation with the GlyVicinity program [82]. In order to avoid redundancies in respect of similar structures in the protein data bank a 90% clustering filter was used [82]. This presentation allows a statistical evaluation to figure out which functional groups of Neu5Ac and Trp (**a**), Tyr (**b**) or Arg (**c**) residues are interacting with each other. The atoms of these three amino acid residues which occur in the vicinity of Neu5Ac can be discriminated by their colour: carbon: grey, nitrogen: blue, oxygen: red, hydrogen: white.

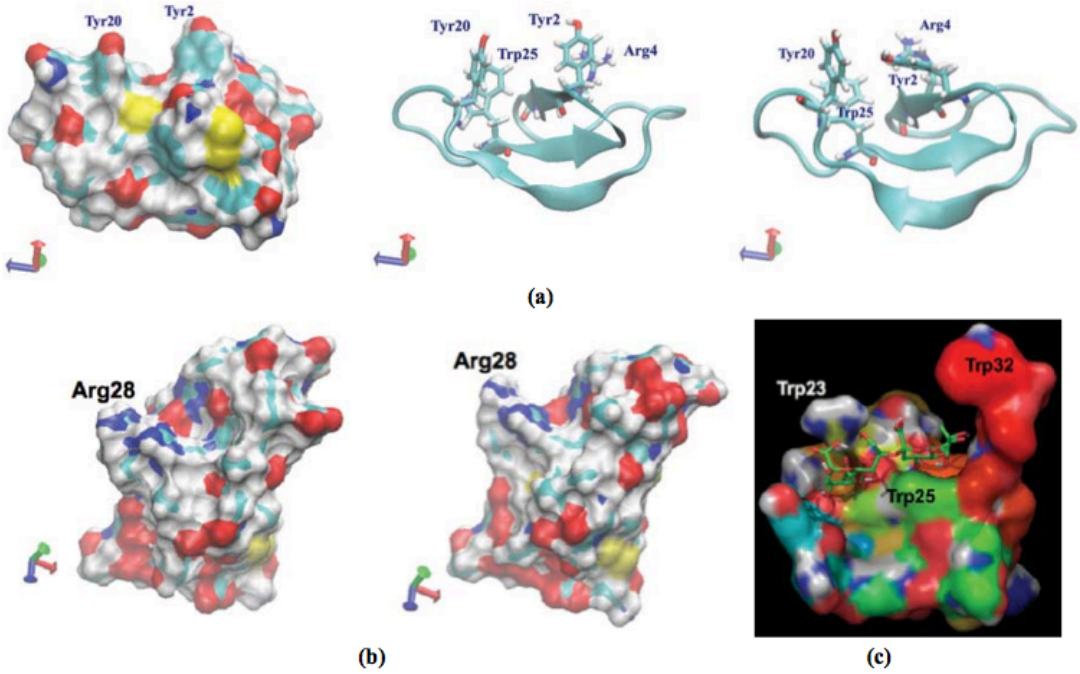

Fig. (3). a: HNP2 conformations in the ligand-free (left, middle) and in the sialic acid bound state (right). The conformational differences can clearly be observed when the orientations of the relevant binding amino acid residues Tyr2, Arg4, Tyr20 and Trp25 are compared. Especially, when comparing the orientations of Tyr2 and Arg4 (middle *vs*. right picture) their turns to the carbohydrate binding pocket in the ligand-bound state are obvious. **b**: HD5 conformations (based on X-ray crystallographic data [15]) in the bound state of the sialic acid mimicking molecule tegaserod in its cis (left) or in its trans (right) configuration. The tegaserod molecules are not displayed in order to visualise their impact on the overall shape of HD5 more clearly. The binding-relevant Arg28 residue of HD5 is marked. **c**: Surface representation of the lectin SHL-1 from the Chinese bird-hunting spider *Selenocosmia huwena* Wang in complex with a polySia disaccharide fragment. Three tryptophan residues (Trp23, Trp25, Trp32) are labelled, which all are involved in ligand binding. The image shows the shape of a sialic acid binding pocket in the length of two disaccharide units. In contrast to tryptophan residues Trp23 and Trp25, which are essential for complex formation, the Trp32 residue stabilises the complex, but is not essential for specific ligand binding.

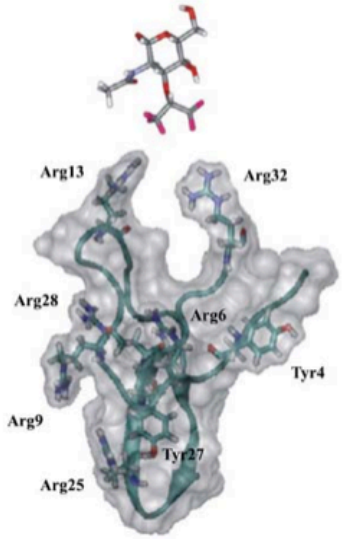

Fig. (4). Docking study of the defensin HD5-double mutant (A13R, A32R) and N-acetyl muramic acid (MurNAc). The replacement of Ala13 by Arg and Ala 32 by Arg lowers the affinity to MurNAc according to the docking simulation. Such exchanges of amino acids have led to the conclusion that Arg28 is an essential residue for specific carbohydrate interaction processes.

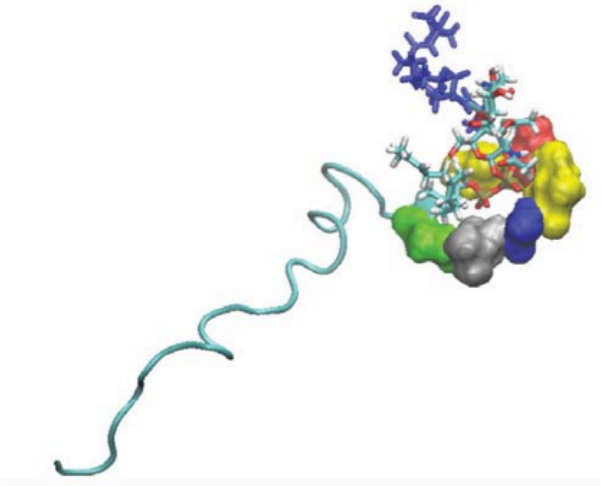

Fig. (5). Nisin structure (1WCO.pdb). The amino acid residues which are essential for carbohydrate (MurNAc) binding are shown in the surface representation. Ile1 and Ile4: yellow, Dhb2: red, Dha5: blue, Leu6: silver, Pro9: green, (Dha: Dehydroalanine, Dhb: Dehydrobutyrine). The blue stick model consists of five residues with a Lys in the middle.

protecting peptides are lactoferrin fragments. Lactoferrin is a carbohydrate binding glycoprotein and an effective antimicrobial peptide in milk. The X-ray derived structure of this glycoprotein in complex with a trisaccharide (2DP8.pdb) is shown in Fig. (**6**), top. A structural model of bovine lactoferrin (1BLF.pdb) with the highlighted ferrampin sequence is displayed in Fig. (**6**), bottom. Besides lactoferrampin, the peptide lactoferricin is a further lactoferrin-derived antimicrobial peptide. Lactoferricin is an amphipathic, cationic peptide with antimicrobial and anti-cancer properties. It can be generated by a pepsin-mediated digestion of lactoferrin. Lactoferricin is the most studied antimicrobial peptide derived from milk proteins. The complete sequence of lactoferricin (FKCRRWQWRMKKLGAPSITCVRRAF) corresponds to the lactoferrin fragment of residues 17-41. The sequence of lactoferricin is present in the antimicrobial lactoferrin fragment (1LFC.pdb) shown in Fig. (**7**) as stick (top) and space filling (bottom) models. This peptide interacts with the lipid part of the pathogen, e.g. MRSA [25, 26]. Furthermore, the already mentioned defensins also play a crucial role in food preservation and are in some cases important for the survival of certain animals. For example, for male king penguins (*Aptenodytes patagonicus*) it is feasible to preserve undigested food in their stomach for several weeks during the last part of egg incubation. This ensures survival of the newly hatched chick, in cases where the return of the female penguin from the sea is delayed. It is described in the literature that a 38-residue antimicrobial peptide named spheniscin which belongs to the β -defensin subfamily is mainly responsible for the food preservation properties in the stomach of male king penguins [12, 27]. The spheniscin concentration was found to strongly increase during the period of food storage. It could be shown that this peptide has a broad antimicrobial activity spectrum, affecting the growth of both pathogenic bacteria and fungi. When highlighting the two aromatic residues Phe19 and Trp38 it is obvious how the positions of the two contact residues alter when comparing four NMR minimum conformations with each other (Fig. **8a-d**). These observations are of special interest when potential target structures have to be analysed aiming at new strategies in food protection.

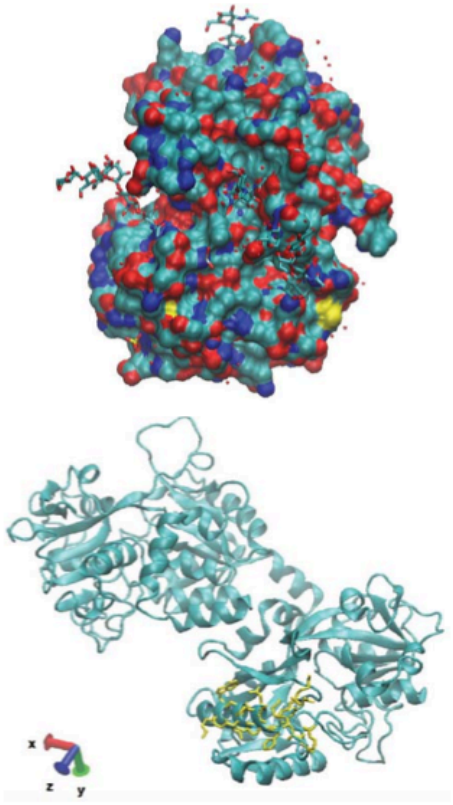

Fig. (6). Surface presentation of the glycoprotein lactoferrin from *Bos taurus* in complex with a trisaccharide (2DP8.pdb) - top [PDB: Singh N.; Sharma S.; Singh T. P. - to be published]. The covalently bound glycochain fragments and the trisaccharide ligand are displayed as stick models. Backbone representation of *Bos taurus* lactoferrin (1BLF.pdb) - bottom [25]. The ferrampin sequence is highlighted in yellow: WKLLSKAQEKFGKNKSR (W268 to R284) [26]. This lactoferrin fragment permeabilises the outer membrane of gram-negative bacteria and neutralises endotoxins. The three perpendicular oriented arrows are stretching the x, y, z coordinate system [80, 81].

2.3. Animal Health Care-Medical and Nutritional Aspects

An actual example in respect of the need for new potent antimicrobial peptides is respiratory infection caused by

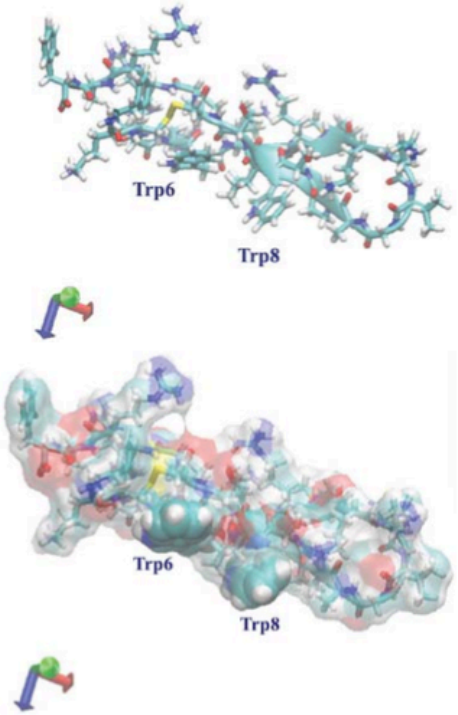

Fig. (7). Lactoferricin (1LFC.pdb) [83] in a stick (top) and in a space-filling surface (bottom) representation. The Trp residues 6 and 8 of this membrane interacting peptide are labelled. Lactoferricin consists in total of 25 amino acid residues: FKCRRWQWRMKKLGAPSITCVRRAF. The three perpendicular oriented arrows which are stretching the x, y, z coordinate system are orientated identically in respect to the model representations at the top and at the bottom.

Middle East Respiratory Syndrome corona viruses (MERS-CoV). The viral spike S glycoprotein is responsible for mediating receptor binding and membrane fusion. Recent studies have proposed that the carboxyl terminal portion (S2 subunit) of the S protein is a class I viral fusion protein (Fig. **9**). This structure (2RUM.pdb) of the related Severe Acute Respiratory Syndrome corona viruses (SARS-CoV) [28] interacts with the lipid part of the host cell membranes. Potential strategies against SARS-CoV and MERS-CoV, as well as the inhibition of the carbohydrate-protein-interaction, also include blocking-strategies which prevent a docking of the virus to lipid parts of the host cell membranes. In this context the lipid fusion peptide is of special interest. Biophysical methods such as Nuclear Magnetic Resonance (NMR) and Atomic Force Microscopy (AFM) as well as molecular modelling can be used to improve antiviral strategies. A sophisticated NMR technique which is known as the laser photo Chemically Induced Nuclear Polarisaton (CIDNP) method can be applied for a receptor - ligand analysis [29-31] if Tyr- and Trp-residues are surface exposed. The virus fusion peptide shown in five energy minimum conformations in Fig. (**9**) has two CIDNP sensitive amino acid residues which are always surface-exposed in the receptor-unbound state: Trp2 and Tyr9. It is therefore possible to establish these two residues as special sensors when specially designed fusion peptides are tested to block the contact with the virus. These interaction studies can be carried out with model membranes in NMR tubes. Possible modifications of these fusion peptides are the addition of certain amino acid residues and/or the introduction of special functional groups. Beside structural properties, the interaction dynamics have to be taken under account. As the flexibility of the CIDNP sensitive Trp38 residue in the β-defensin spheniscin suggests (Fig. **8**) this special NMR method is also extremely suitable when the surface accessibilities of α- and β-defensins, hevein-like molecules or other mini-lectins are analysed in the absence and in the presence of various ligands [3, 12, 15, 28, 29]. In the case where potent new antimicrobial peptides have to be designed it is also important to focus on low mammalian cell toxicity and suitable model membrane systems [32, 33]. Nature itself provides a number of blueprints for this purpose. Cyclic defensins can be considered as such examples. Theta-defensins (θ-defensins) also called retrocyclins are a family of mammalian antimicrobial cyclic peptides which are found in „old world" primates, but not in humans, gorillas, bonobos, or chimpanzees. This defensin sub-family consists of a pair of antiparallel β-sheets linked by three disulphide bonds arranged as a ladder along the sheets to form an extremely stable structure. Depending on the pH value, θ -defensins have a tendency to self-associate into trimers. In contrast to α- and β-defensins the θ-defensins have no aromatic amino acid residues, which are important for carbohydrate interactions. However, these cyclic antimicrobial peptides are rich in arginine (Arg) residues, which are also crucial moieties when specific peptide/protein - carbohydrate interactions are taking place (Fig. **1b**, Fig. **2c**, Fig. **4**). Therefore, the antimicrobial θ -defensins should not be underestimated as proper scaffolds for peptide-based drug design [34].

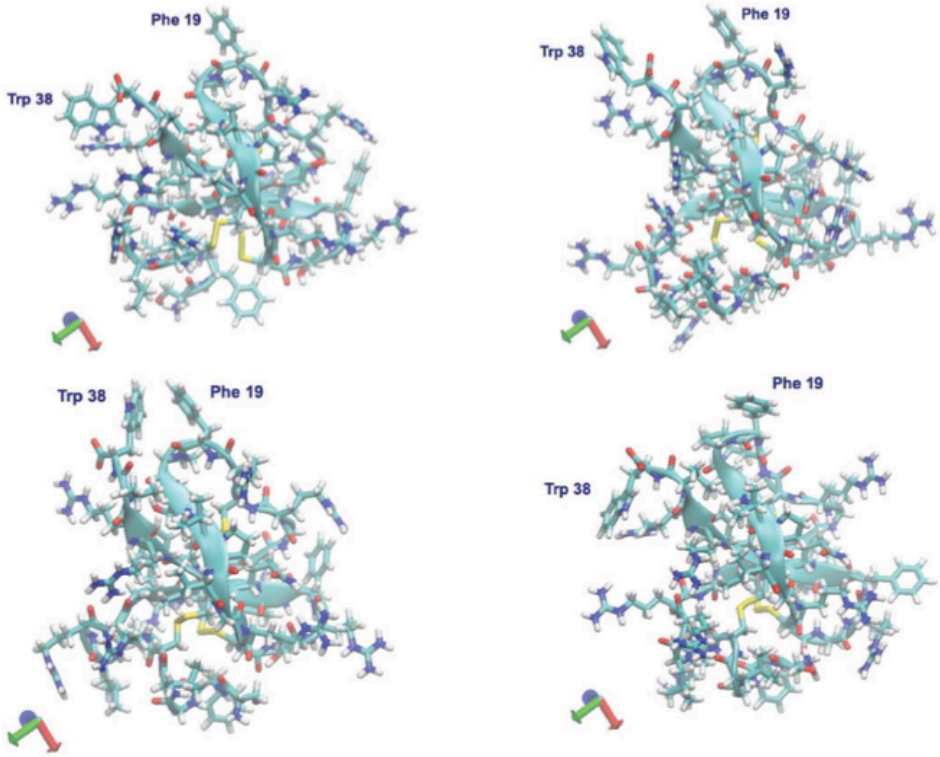

Fig. (8). Four NMR energy minimum structures of spheniscin (1UT3.pdb) [12], a β-defensin from the stomach of male king penguins (*Aptenodytes patagonicus*). The aromatic amino acids Phe19 and Trp38 with potential pathogen specificity are highlighted. A comparison with chicken ovodefensin has recently been described in the literature [84].

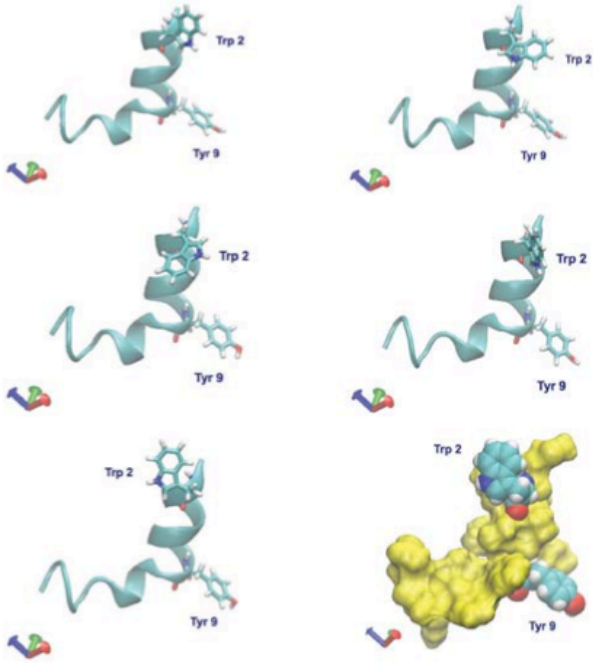

Fig. (9). SARS-CoV fusion peptide (2RUM.pdb) [PDB: Mahajan M.; Bhattacharjya S. - to be published]. Five NMR structures in which the backbone and the amino acid residues Trp2 and Tyr9 are shown, thereby focussing on the different conformations of the aromatic amino acid residues. The space-filling structure corresponds to the fifth NMR structure shown as stick model at the bottom on the left side. In this picture six at the bottom on the right side, the residues 1, 3-8 and 9-17 are displayed in the yellow surface representation. Residues 2 and 9 are shown in a van-der-Waals representation. This antimicrobial peptide which interacts directly with membrane lipids can be studied with laser photo CIDNP NMR methods in the absence and in the presence of membrane fragments.

CONCLUSION

Significant advances in the design of antimicrobial peptides can be expected when suitable model systems are analysed with state-of-the-art biophysical techniques. When studying hevein-domains [35-39] and their interactions with ligand structures on the nanoscale level, it turned out that certain amino acid residues play a dominant role if carbohydrates are bound in a specific way to the receptor structure. Besides the aromatic Tyr and Trp residues, Arg is a crucial building brick which stabilises glycan-protein complexes. However, the optimal strategy to hinder the pathogen attack, strongly depends on the particular disease [40-45]. Mini-lectins such as the sialic acid binding spider lectin SHL-1 and several defensins are able to interact specifically with sialic acid containing carbohydrate chains, which are characteristic for various infections. In the case of antimicrobial peptides which target contact structures on pathogen surfaces (e.g. Neu5Ac), further improvements are especially needed, because several multiresistant bacterial strains exist. The necessary therapeutic improvements concerning the antimicrobial effects of peptides will be provided by rational modifications of structural properties in respect to binding strength and specificity. This will support anti-infective therapies against bacteria, viruses and fungi significantly, including the important aspect of anti-inflammation. A combination of biophysical techniques and bioinformatics-derived tools with biochemical and cell biological methods allows the generation of new drugs which are effective against dangerous pathogens, e.g. gram-negative *Klebsiella pneumoniae* [46-48]. Beside viral and bacterial infections, fungi as severe pathogens should not be forgotten [49]. Defensins are also described in respect of their antifungal properties [50] and are therefore proper candidates for such therapeutic approaches. As well as sialic acids being crucial contact structures in bacteria or virus - host cell interaction processes they also play a similar important role when fungi cause health problems as pathogens [51, 52]. Therefore, antimicrobial peptides with a specificity for sialic acids are of great relevance in clinical approaches directed against fungal diseases. When studying the interactions between pathogens and host cells intensely on a nanoscale level not only the specific binding processes between antimicrobial peptides and carbohydrate chains have to be considered. Also protein- and lipid-contact structures are crucial interaction partners for antimicrobial peptides. Since all three classes of biomolecules have to be taken into account, being the Achilles heel of a pathogen, nanomedical and nanopharmacological approaches must focus on characteristic molecular recognition points including conformational aspects on the ligand and on the receptor side [53-60]. Such recognition points are, for example, distinct functional groups of carbohydrate residues (such as O-acetyl groups) or sulphate groups interacting with certain amino acid residues of antimicrobial peptides. Both cyclic and linear peptides [54, 55] have to be taken into account as antimicrobial molecules. Taking these approaches, improved strategies for food preservation in the field of applied health care will also be achieved. Further developments in the field of antimicrobial peptide design can be expected when these molecules are analysed in a similar way as for the structure-function relationships of bio-active

collagen-fragments [61-65]. From a purely structural point of view, antimicrobial peptides are diverse, however, when suitable model systems [66-73] are analysed with nanomedical and nanopharmacological emphasis, results of general validity can be expected. Addressing the question whether antimicrobial peptides can interact with carbohydrate or lipid components on pathogen surfaces [74-79] it is possible to optimise drug design approaches against multiresistant pathogens (e.g. against vancomycin resistant *Staphylococcus aureus* strains). Such promising nanomedical and nanopharmacological developments can also be expected in other clinical fields such as oncology and neuronal regeneration, thereby, shortening the route from "bench to clinical bedside".

CONFLICT OF INTEREST

The authors confirm that this article content has no conflict of interest.

ACKNOWLEDGEMENTS

We thank our colleagues Jens-Michael Schröder, Daron Freedberg, Bob Lehrer and Wuyuan Lu for many fruitful discussions about antimicrobial peptides and their contact structures on pathogen surfaces. NEN is supported by RSF grant 14-23-00199.

REFERENCES

[1] Schauer, R. Sialic acids: fascinating sugars in higher animals and man. *Zoology (Jena),* **2004**, *107*, 49-64.

[2] Severi, E.; Hood, D. W.; Thomas, G. H. Sialic acid utilization by bacterial pathogens. *Microbiology,* **2007,** *153*, 2817-2822.

[3] Siebert, H.-C.; Lu, S.-Y.; Wechselberger, R.; Born, K.; Eckert, T.; Liang, S.; von der Lieth, C.-W.; Jiménez-Barbero, J.; Schauer, R.; Vliegenthart, J. F. G.; Lütteke, T.; André, S.; Kaltner, H.; Gabius, H.-J.; Kožár, T. A lectin from the Chinese bird-hunting spider binds sialic acids. *Carbohydr. Res.,* **2009,** *344,* 1515-1525.

[4] Liang, S. An overview of peptide toxins from the venom of the Chinese bird spider *Selenocosmia huwena* Wang [= Ornithoctonus huwena (Wang)]. *Toxicon,* **2004,** *43,* 575-585.

[5] Ding, L.; Yang, L.; Weiss, T. M.; Waring, A. J.; Lehrer, R. I.; Huang, H. W. Interaction of antimicrobial peptides with lipopolysaccharides. *Biochemistry,* **2003,** *42,* 12251-12259.

[6] Wei, G.; de Leeuw, E.; Pazgier, M.; Yuan, W.; Zou, G.; Wang, J.; Ericksen, B.; Lu, W.-Y.; Lehrer, R. I.; Lu, W. Through the looking glass, mechanistic insights from enantiomeric human defensins. *J. Biol. Chem.,* **2009,** *284,* 29180-29192.

[7] Nguyen, T. X.; Cole, A. M.; Lehrer, R. I. Evolution of primate θ-defensins: a serpentine path to a sweet tooth. *Peptides,* **2003,** *24,* 1647-1654.

[8] Cole, A. M.; Hong, T.; Boo, L. M.; Nguyen, T.; Zhao, C.; Bristol, G.; Zack, J. A.; Waring, A. J.; Yang, O. O.; Lehrer, R. I. Retrocyclin: a primate peptide that protects cells from infection by T- and M-tropic strains of HIV-1. *Proc. Natl. Acad. Sci. USA,* **2002,** *99,* 1813-1818.

[9] Lehrer, R. I. Primate defensins. *Nat. Rev. Microbiol.,* **2004,** *2,* 727-738.

[10] Ganz, T. Defensins: antimicrobial peptides of innate immunity. *Nat. Rev. Immunol.,* **2003,** *3,* 710-720.

[11] Zasloff, M. Antimicrobial peptides of multicellular organisms. *Nature,* **2002,** *415,* 389-395.

[12] Landon, C.; Thouzeau, C.; Labbé, H.; Bulet, P.; Vovelle, F. Solution structure of spheniscin, a â-defensin from the penguin stomach. **2004,** *279,* 30433-30439.

[13] Lehrer, R. I.; Lu, W. α-Defensins in human innate immunity. *Immunol Rev.,* **2012,** *245,* 84-112.

[14] Lehrer, R. I.; Jung, G.; Ruchala, P.; Wang, W.; Micewicz, E. D.; Waring, A. J.; Gillespie, E. J.; Bradley, K. A.; Ratner, A. J.; Rest, R. F.; Lu, W. Human α-defensins inhibit hemolysis mediated by cholesterol-dependent cytolysins *Infect. Immun.,* **2009,** *77,* 4028-4040.

[15] Szyk, A.; Wu, Z.; Tucker, K.; Yang, D.; Lu, W.; Lubkowski, J. Crystal structures of human α- defensins HNP4. HD5, and HD6. *Protein Sci.,* **2006,** *15,* 2749-2760.

[16] Lehrer, R. I.; Jung, G.; Ruchala, P.: André, S.; Gabius, H.-J.; Lu, W. Multivalent binding of carbohydrates by the human α-defensin, HD5. *J. Immunol.,* **2009,** *183,* 480-490.

[17] Siebert, H.-C.; Reuter, G.; Schauer, R.; von der Lieth, C. W.; Dabrowski, J. Solution conformation of GM_3 gangliosides containing different sialic acid residues as revealed by NOE based distance mapping, molecular mechanics, and molecular dynamics calculations. *Biochemistry,* **1992,** *31,* 6962-6971.

[18] Siebert, H.-C.; André, S.; Lu, S.-Y.; Frank, M.; Kaltner, H.; van Kuik, J. A.; Korchagina, E. Y.; Bovin, N.; Tajkhorshid, E.; Kaptein, R.; Vliegenthart, J. F. G.; von der Lieth, C.-W.; Jiménez-Barbero, J.; Kopitz, J.; Gabius, H.-J. Unique conformer selection of the human growth-regulatory lectin galectin-1 for ganglioside GM_1 versus bacterial toxins. *Biochemistry,* **2003,** *42,* 14762-14773.

[19] André, S.; Kaltner, H.; Lensch, M.; Russwurm, R.; Siebert, H.-C.; Tajkhorshid, E.; Heck, A. J. R. M.; von Knebel-Doeberitz, Gabius, H.-J.; Kopitz, J. Determination of structural and functional overlap/divergence of five proto-type galectins by analysis of the growth-regulatory interaction with ganglioside GM_1 in silico and *in vitro* human neuroblastoma cells. *Int. J. Cancer,* **2005,** *114,* 46-57.

[20] Siebert, H.-C.; Rosen, J.; Seyrek, K.; Kaltner, H.; André, S.; Bovin, N. V.; Nyholm, P.-G.; Sinowatz, F.; Gabius, H.-J. alpha2,3/alpha2,6-Sialylation of N-glycans: non-synonymous signals with marked developmental regulation in bovine reproductive tracts. *Biochimie,* **2006,** *88,* 399-410.

[21] Siebert, H.-C.; Born, K.; André, S.; Frank, M.; Kaltner, H.; von der Lieth, C.-W.; Heck, A. J. R.; Jiménez-Barbero, J.; Kopitz, J.; Gabius H.-J.; Carbohydrate chain of ganglioside GM_1 as a ligand: identification of the binding strategies of three 15mer peptides and their divergence from the binding modes of growth-regulatory galectin-1 and cholera toxin. *Chem. Eur. J.,* **2006,** *12,* 388-402.

[22] Bushman, J.; Mishra, B.; Ezra, M. M.; Gul, S.; Schulze, C.; Chaudhury, S.; Ripoll, D.; Wallqvist, A.; Kohn, J.; Schachner, M.; Loers, G. Tegaserod mimics the neurostimulatory glycan polysialic acid and promotes nervous system repair. *Neuropharmacology,* **2014,** *79,* 456-466.

[23] Hsu, S.-T.D.; Breukink, E.; Tischenko, E.; Lutters, M. A. G.; De Kruijff, B.; Kaptein, R.; Bonvin, A. M. J. J.; van Nuland, N. A. J. The nisin-lipid II complex reveals a pyrophosphate cage that provides a blueprint for novel antibiotics. *Nat. Struct. Mol. Biol.,* **2004,** *11,* 963-967.

[24] Hsu S. T.; Breukink E.; de Kruijff B.; Kaptein R.; Bonvin A. M. J. J.; van Nuland, N. A. J. Mapping the targeted membrane pore formation mechanism by solution NMR: the nisin Z and lipid II interaction in SDS micelles. *Biochemistry,* **2002,** *41,* 7670-7676.

[25] Moore, S. A.; Anderson, B. F., Groom, C. R.; Haridas, M.; Baker, E. N. Three-dimensional structure of diferric bovine lactoferrin at 2.8 Å resolution. *J. Mol. Biol.,* **1997,** *274,* 222-236.

[26] Ghosh, A.; Datta, A.; Jana, J.; Kar, R. K.; Chatterjee, C.; Chatterjee, S.; Bhunia, A. Sequence context induced antimicrobial activity: insight into lipopolysaccharide permeabilization. *Mol. BioSyst.,* **2014,** *10,* 1596-1612.

[27] Thouzeau, C.; Le Maho, Y.; Froget, G.; Sabatier, L.; Le Bohec, C.; Hoffmann, J. A.; Bulet, P. Spheniscins, avian β-defensins in preserved stomach contents of the king penguin, Aptenodytes patagonicus. *J. Biol. Chem.,* **2003,** *278,* 51053-51058.

[28] Mahajan, M.; Bhattacharjya, S. NMR structures and localization of the potential fusion peptides and the pre-transmembrane region of SARS-CoV: Implications in membrane fusion. Biochim. *Biophys. Acta,* **2015,** *1848,* 721-730.

[29] Siebert, H.-C.; von der Lieth, C.-W.; Kaptein, R.; Beintema, J. J.; Dijkstra, K.; Nuland, N.; Soedjanaatmadja, U. M. S.; Rice, A.; Vliegenthart, J. F. G.; Wright, C. S.; Gabius, H.-J. Role of aromatic amino acids in carbohydrate binding of plant lectins. Laser photo CIDNP (chemically induced dynamic nuclear polarization) study of hevein domain-containing lectins. *Proteins,* **1997,** *28,* 268-284.

[30] Siebert, H.-C.; Adar, R.; Arango, R.; Burchert, M.; Kaltner, H.; Kayser, G.; Tajkhorshid, E.; von der Lieth, C.-W.; Kaptein, R.; Sharon, N.; Vliegenthart, J. F. G.; Gabius, H.-J. Involvement of laser photo CIDNP (chemically induced dynamic nuclear polariza-

tion) - reactive amino acid side chains in ligand binding by galactoside-specific lectins in solution. Similarities in the role of tryptophan/ tyrosine residues for ligand binding between a plant agglutinin and mammalian/avian galectins and the detection of an influence of single-site mutagenesis on surface presentation of spatially separated residues. *Eur. J. Biochem.,* **1997,** *249,* 27-38.

[31] Gabius, H.-J.; Siebert, H.-C.; André, S.; Jiménez-Barbero, J.; Rü diger, H. Chemical biology of the sugar code. *ChemBioChem,* **2004,** *5,* 740-764.

[32] Chai, H.; Allen, W. E.; Hicks, R. P. Spectroscopic investigations of the binding mechanisms between antimicrobial peptides and membrane models of Pseudomonas aeruginosa and Klebsiella pneumoniae. *Bioorg. Med. Chem.,* **2014,** *22,* 4210-4222.

[33] Javadpour, M. M.; Juban, M. M.; J. Lo, W.-C.; Bishop, S. M.; Alberty, J. B.; Cowell, S. M.; Becker, C. L.; McLaughlin, M. L. *De novo* antimicrobial peptides with low mammalian cell toxicity. *J. Med. Chem.,* **1996,** *39,* 3107-3113.

[34] Conibear, A.; Craik, D. The chemistry and biology of theta defensins. *Angew. Chem., (Intern. ed.),* **2014,** *53,* 10612-10623.

[35] Jiménez-Barbero, J.; Cañada, F. J.; Asensio, J. L.; Aboitz, N.; Vidal, P.; Canales, M. A.; Gabius, H.-J.; Siebert, H.-C. Hevein-domains: an attractive model to study carbohydrate-protein interactions at atomic resolution. *Adv. Carbohydr. Chem. Biochem.,* **2006,** *60,* 303-354.

[36] Asensio, J. L.; Cañada, F. J.; Siebert, H.-C.; Laynez, J.; Poveda, A.; Nieto, P. M.; Soedjanaatmadja, U. M.; Gabius, H.-J.; Jiménez-Barbero, J. Structural basis for chitin recognition by defense proteins of plants: GlcNAc residues are bound in a multivalent fashion by extended binding sites in hevein domains. *Chem. Biol.,* **2000,** *7,* 529-543.

[37] Asensio, J. L.; Siebert, H-C.; Cañada, F. J.; von der Lieth, C.-W.; Laynez, J.; Menéndez, M.; Bruix, M.; Soedjanaatmadja, U. M. S.; Beintema, J. J.; Gabius, H.-J.; Jiménez-Barbero, J. NMR investigation of protein-carbohydrate interactions. Structure determination of the complex between pseudohevein and N,N',N''-triacetylchitotriose and delineation of two different binding modes. *Proteins,* **2000,** *40,* 218-236.

[38] Espinosa, J. F.; Asensio, J. L.; García, J.-L.; Laynez, J.; Bruix, M.; Wright, C.; Siebert, H-C.; Gabius, H.-J.; Cañada, F. J.; Jiménez-Barbero, J. NMR investigation of protein-carbohydrate interactions. Binding studies and refined three dimensional solution structure of the complex between the B domain of wheat germ agglutinin and N,N',N''-triacetylchitotriose. *Eur. J. Biochem.,* **2000,** *267,* 3965-3978.

[39] Koppisetty, C. A. K.; Frank, M.; Lyubartsev, A. P.; Nyholm, P.-G. Binding energy calculations for hevein-carbohydrate interactions using expanded ensemble molecular dynamics simulations. *J. Comput. Aided Mol. Des.,* **2015,** *29,* 13-21.

[40] Battistel, M. D.; Shangold, M.; Trinh, L.; Shiloach, J.; Freedberg, D. I. Evidence for helical structure in a tetramer of alpha2-8 sialic acid: unveiling a structural antigen. *J. Am. Chem. Soc.,* **2012,** *134,* 10717-10720.

[41] Schröder, J. M. Revealing the achilles heel of bacterial toxins. *Immunity,* **2014,** *41,* 671-673.

[42] Schröder, J. M.; Harder, J. Antimicrobial skin peptides and proteins. *Cell. Mol. Life Sci.,* **2006,** *63,* 469-486.

[43] Böhling, A.; Hagge, S. O.; Roes, S.; Podschun, R.; Sahly, H.; Harder, J.; Schröder, J.-M.; Grötzinger, J.; Seydel, U.; Gutsmann, T. Lipid-specific membrane activity of human β-defensin-3. *Biochemistry,* **2006,** *45,* 5663-5670.

[44] Kudryashova, E.; Quintyn, R.; Seveau, S.; Lu, W.; Wysocki, V. H.; Kudryashov, D. S. Human defensins facilitate local unfolding of thermodynamically unstable regions of bacterial protein toxins. *Immunity,* **2014,** *41,* 709-721.

[45] Kudryashova, E.; Heisler, D.; Zywiec, A.; Kudryashov, D. S. Thermodynamic properties of the effector domains of MARTX toxins suggest their unfolding for translocation across the host membrane. *Mol. Microbiol.,* **2014,** *92,* 1056-1071.

[46] Enani, M. A., El-Khizzi, N. A. Community acquired *Klebsiella pneumoniae*, K1 serotype. Invasive liver abscess with bacteremia and endophthalmitis. *Saudi Med. J.,* **2012,** *33,* 782-786.

[47] Al-Saadi, M. A. K.; Al-Charrakh, A. H.; Al-Greti, S. H. H. Prevalence of bacteremia in patients with diabetes mellitus in Karbala, *Iraq. J. Bacteriol.,* **2011,** *3,* 108-116.

[48] Krylov, V. B.; Argunov, D. A.; Vinnitskiy, D. Z.; Verkhnyatskaya, S. A.; Gerbst, A. G.; Ustyuzhanina, N. E.; Dmitrenok, A. S.; Huebner, J.; Holst, O.; Siebert, H.-C.; Nifantiev, N. E. Pyranoside into furanoside rearrangement: new reaction in carbohydrate chemistry and its application in oligosaccharide synthesis. *Chem. Eur. J.,* **2014,** *20,* 16516-16522.

[49] Enani, M. A.; Alharthi, B. N.; Dewanjee, N.; Bhat, N. A.; Fagih, M. Spontaneous gastric ulcer perforation and acute spleen infarction caused by invasive gastric and splenic mucormycosis. *J. Glob. Infect. Dis.,* **2014,** *6,* 122-124.

[50] Silva, P. M.; Gonçalves, S.; Santos, N. C. Defensins: antifungal lessons from eukaryotes *Front. Microbiol.,* **2014,** *5,* 1-17.

[51] Alviano, C. S.; Travassos, L. R.; Schauer, R. Sialic acids in fungi: a minireview. *Glycoconj. J.,* **1999,** *6,* 545-554.

[52] Almeida, C. A.; de Campos-Takaki, G. M.; Portela, M. B.; Travassos, L. R.; Alviano, C. S.; Alviano, D. S. Sialoglycoproteins in morphological distinct stages of mucor polymorphosporus and their influence on phagocytosis by human blood phagocytes. *Mycopathologia,* **2013,** *176,* 183-189.

[53] Tsvetkov, Y. E.; Burg-Roderfeld, M.; Loers, G.; Ard., A.; Sukhova, E. V.; Khatuntseva, E. A.; Grachev, A. A.; Chizhov, A. O.; Siebert, H.-C.; Schachner, M.; Jiménez-Barbero, J.; Nifantiev, N. E. Synthesis and molecular recognition studies of the HNK-1 trisaccharide and related oligosaccharides. The specificity of monoclonal anti-HNK-1 antibodies as assessed by surface plasmon resonance and STD NMR. *J. Am. Chem. Soc.* **2012,** *134,* 426-435.

[54] Bhunia, A.; Vivekanandan, S.; Eckert, T.; Burg-Roderfeld, M.; Wechselberger, R.; Romanuka, J.; Bächle, D.; Kornilov, A. V.; von der Lieth, C.-W.; Barbero, J. J.; Nifantiev, N. E.; Schachner, M.; Sewald, N.; Lütteke, T.; Gabius, H.-J.; Siebert, H.-C. Why structurally different cyclic peptides can be glycomimetics of HNK-1. *J. Am. Chem. Soc.,* **2010,** *132,* 96-105.

[55] Siebert, H.-C.; Lu, S.-Y.; Frank, M.; Kramer, J.; Wechselberger, R.; Joosten, J.; André, S.; Rittenhouse-Olson, K.; Roy, R., von der Lieth, C.-W.; Kaptein, R.; Vliegenthart, J. F. G.; Heck, A. J. R.; Gabius, H.-J. Analysis of protein-carbohydrate interaction at the lower size limit of the protein part (15-mer peptide) by NMR spectroscopy, electrospray ionization mass spectrometry and molecular modeling. *Biochemistry,* **2002,** *41,* 9707-9717.

[56] Siebert, H-C.; André, S.; Asensio, J. L.; Cañada, F. J.; Dong, X.; Espinosa, J. F.; Frank, M.; Gilleron, M.; Kaltner, H.; Kožár, T.; Bovin, N. V.; von der Lieth, C.-W.; Vliegenthart, J. F. G.; Jiménez-Barbero, J.; Gabius, H.-J. A new combined computational and NMR-spectroscopical strategy for the identification of additional conformational constraints of the bound ligand in an aprotic solvent. *ChemBioChem,* **2000,** *1,* 181-195.

[57] von der Lieth, C. W.; Siebert, H.-C.; Kožár, T.; Burchert, M.; Frank, M.; Gilleron, M.; Kaltner, H.; Kayser, G.; Tajkhorshid, E.; Bovin, N. V.; Vliegenthart, J. F. G.; Gabius, H.-J. Lectin ligands: new insights into their conformations and their dynamic behavior and the discovery of conformer selection by lectins. *Acta Anat.,* **1998,** *161,* 91-109.

[58] Gilleron, M.; Siebert, H.-C.; Kaltner, H.; von der Lieth, C. W.; Kožár, T.; Halkes, K. M.; Korchagina, E. Y.; Bovin, N. V.; Gabius, H.-J.; Vliegenthart, J. F. G. Conformer selection and differential restriction of ligand mobility by a plant lectin. Conformational behaviour of Galβ1- 3GlcNAcβ1-R, Galβ1-3GalNAcβ1-R and Galβ1-2Galβ1-R' in the free state and complexed with galactoside-specific mistletoe lectin as revealed by random walk and conformational clustering molecular mechanics calculations, molecular dynamics simulations and nuclear Overhauser experiments. *Eur. J. Biochem.,* **1998,** *252,* 416-427.

[59] Wu, A. M.; Singh, T.; Liu, J.-H.; Krzeminski, M.; Russwurm, R.; Siebert, H.-C.; Bonvin, A. M. J. J.; André, S.; Gabius, H.-J. Activity-structure correlations in divergent lectin-evolution: fine specificity of chicken galectin CG-14 and computational analysis of flexible ligand docking for CG- 14 and the closely related CG-16. *Glycobiology,* **2007,** *17,* 165-184.

[60] Wu, A. M.; Singh, T.; Liu, J.-H.; André, S.; Lensch, M.; Siebert, H.-C.; Krzeminski, M.; Bonvin, A. M. J. J.; Kaltner, H.; Wu, J. H.; Gabius, H.-J. Adhesion/growth-regulatory galectins: Insights into their ligand selectivity using natural glyco-proteins and glycotopes. *Adv. Exp. Med. Biol.,* **2011,** *705,* 117-141.

[61] Schadow, S.; Siebert, H.-C.; Lochnit, G.; Kordelle, J.; Rickert, M.; Steinmeyer, J. Collagen metabolism of human osteoarthritic articular cartilage as modulated by bovine collagen hydrolysates. *PLOS ONE,* **2013,** *8,* e53955.

[62] Stötzel, S.; Schurink, M.; Wienk, H.; Siebler, U.; Burg-Roderfeld, M.; Eckert, T.; Kulik, B.; Wechselberger, R.; Sewing, J.; Steinmeyer, J.; Oesser, S.; Boelens, R.; Siebert, H.-C. Molecular organization of various collagen fragments as revealed by atomic force microscopy and diffusion ordered NMR spectroscopy. *ChemPhysChem,* **2012,** *13,* 3117-3125.

[63] Eckert, T.; Stötzel, S.; Burg-Roderfeld, M.; Sewing, J.; Lütteke, T.; Nifantiev, N. E.; Vliegenthart, J. F. G.; Siebert, H.-C. In silico study on sulfated and non-sulfated carbohydrate chains from proteoglycans in *Cnidaria* and their interaction with collagen. *O. J. Phys. Chem.,* **2012,** *2,* 123-133.

[64] Raabe, O.; Reich, C.; Wenisch, S.; Hild, A.; Burg-Roderfeld, M.; Siebert, H.-C.; Arnhold, S. Hydrolyzed fish collagen induced chondrogenic differentiation of equine adipose tissue-derived stromal cells. *Histochem. Cell Biol.,* **2010,** *134,* 545-554.

[65] Siebert, H.-C.; Burg-Roderfeld, M., Eckert, T.; Stötzel, S.; Kirch, U.; Diercks, T.; Humphries, M. J.; Frank, M.; Wechselberger, R.; Tajkhorshid, E.; Oesser, S. Interaction of the α2A domain of integrin with small collagen fragments. *Protein Cell,* **2010,** *1,* 393-405.

[66] Sudheendra, U. S.; Dhople, V.; Datta, A.; Kar, R. K.; Shelburne, C. E.; Bhunia, A.; Ramamoorthy, A. Membrane disruptive antimicrobial activities of human β-defensin-3 analogs. *Eur. J. Med. Chem.,* **2015,** *91,* 91-99.

[67] Santra, A.; Si, A.; Kar, R. K.; Bhunia, A.; Misra, A. K. Linear synthesis and conformational analysis of the pentasaccharide repeating unit of the cell wall O-antigen of Escherichia coli O13. *Carbohydr. Res.,* **2014,** *391,* 9-15.

[68] Saravanan, R.; Joshi, M., Mohanram, H.; Bhunia, A.; Mangoni, M. L., Bhattacharjya, S. NMR structure of temporin-1 ta in lipopolysaccharide micelles: Mechanistic insight into inactivation by outer membrane. *PLoS ONE,* **2013,** *8,* e72718.

[69] Mohanran, H.; Nip, A.; Domadia, P. N.; Bhunia, A.; Bhattacharjya, S. NMR structure, localization, and vesicle fusion of Chikungunya virus fusion peptide. *Biochemistry,* **2012,** *51,* 7863-7872.

[70] Bhunia, A.; Saravanan, R.; Mohanram, H.; Mangoni, M. L.; Bhattacharjya, S. NMR structures and interactions of temporin-1Tl and temporin-1Tb with lipopolysaccharide micelles: mechanistic insights into outer membrane permeabilization and synergistic activity. *J. Biol. Chem.,* **2011,** *286,* 24394-24406.

[71] Bhunia, A.; Bhattacharjya, S. Mapping residue-specific contacts of polymyxin B with lipopolysaccharide by saturation transfer difference NMR: insights into outer-membrane disruption and endotoxin neutralization. *Biopolymers.,* **2011,** *96,* 273-287.

[72] Domadia, P. N.; Bhunia, A.; Ramamoorthy, A.; Bhattacharjya, S. Structure, interactions, and antibacterial activities of MSI-594 derived mutant peptide MSI-594F5A in lipopolysaccharide micelles: role of the helical hairpin conformation in outermembrane permeabilization. *J. Am. Chem. Soc.,* **2010,** *132,* 18417-18428.

[73] Bhunia, A.; Domadia, P. N.; Torres, J.; Hallock, K. J.; Ramamoorthy, A.; Bhattacharjya, S. NMR structure of pardaxin, a pore-forming antimicrobial peptide, in lipopolysaccharide micelles: mechanism of outer membrane permeabilization. *J. Biol. Chem.,* **2010,** *285,* 3883-3895.

[74] Konno, K.; Hisada, M.; Fontana, R.; Lorenzi, C. C. B.; Naoki, H.; Itagaki, Y.; Miwa, A.; Kawai, N.; Nakata, Y.; Yasuhara, T.; Neto, J. R.; de Azevedo, W. F.; Jr., Palma, M. S.; Nakajima, T. Anoplin, a novel antimicrobial peptide from the venom of the solitary wasp Anoplius samariensis. *Biochim. Biophys. Acta,* **2001,** *1550,* 70-80.

[75] Mannis, M. J. The use of antimicrobial peptides in ophthalmology: an experimental study in corneal preservation and the management of bacterial keratitis. *Tr. Am. Ophth. Soc.,* **2001,** *99,* 241-269.

[76] Peschel, A. How do bacteria resist human antimicrobial peptides? *Trends Microbiol.,* **2002,** *10,* 179-186.

[77] Shankaramma, S. C.; Athanassiou, Z.; Zerbe, O.; Moehle, K.; Mouton, C.; Bernardini, F.; Vrijbloed, J. W.; Obrecht, D.; Robinson, J. A. Macrocyclic hairpin mimetics of the cationic antimicrobial peptide protegrin I: A new family of broad-spectrum antibiotics. *ChemBioChem,* **2002,** *3,* 1126-1133.

[78] D. Scheglmann, K. Werner, G. Eiselt, R. Klinger Role of paired basic residues protein C-termini phospholipid binding. *Protein Eng.,* **2002,** *15,* 521-527.

[79] Asensio J. L.; Ardá A.; Cañada, F. J.; Jiménez-Barbero, J. Carbohydrate-aromatic interactions. *Acc. Chem. Res.*, **2013,** *46*(4), 946-954.

[80] Das, K. M.; Lee, E. Y.; Al Jawder, S. E.; Enani, M. A.; Singh, R.; Skakni, L.; Al-Nakshabandi, N.; Al-Dossari, K. S.; Larsson, G. Acute Middle East Respiratory Syndrome Coronavirus: Temporal lung changes observed on the chest radiographs of 55 patients. *Am. J. Roentgenol.* **2015**, *205,* W267-S274.

[81] Siebert, H.-C.; Zhang, R. Y.; Scheidig, A.; Eckert, T.; Wienk, H.; Boelens, R.; Mahvash, M.; Petridis, A. K.; Schauer, R. Interaction studies of sialic acids with model receptors contribute to nanomedical therapies. *J. Neurol. Disord.,* **2015,** in press.

[82] Rojas-Macias M. A.; Lütteke T. Statistical analysis of amino acids in the vicinity of carbohydrate residues performed by GlyVicinity. *Methods Mol. Biol.,* **2015,** *1273,* 215-226.

[83] Hwang P. M.; Zhou N.; Shan X.; Arrowsmith C. H.; Vogel H. J. Three-dimensional solution structure of lactoferricin B, an antimicrobial peptide derived from bovine lactoferrin. *Biochemistry,* **1998,** *37,* 4288-4298.

[84] Hervé V.; Meudal H.; Labas V.; Réhault-Godbert S.; Gautron J.; Berges M.; Guyot N.; Delmas A. F.; Nys Y.; Landon C. Three-dimensional NMR structure of hen egg gallin (chicken ovodefensin) reveals a new variation of the β-defensin fold. *J. Biol. Chem.* **2014,** *289,* 7211-7220.

Received: March 12, 2015 **Revised: April 29, 2015** **Accepted: May 05, 2015**

3.3 Interaction studies of sialic acids with model receptors contribute to nanomedical therapies

My contribution for this publication was to perform the NMR and Molecular modelling experiments and to analyse the related results.

Neurological Disorders

Siebert et al., et al., J Neurol Disord 2015, 3:2
http://dx.doi.org/10.4172/2329-6895.1000212

Review Article Open Access

Interaction Studies of Sialic Acids with Model Receptors Contribute to Nanomedical Therapies

Hans-Christian Siebert[1], Ruiyan Zhang[1,2], Axel Scheidig[2], Thomas Eckert[1,3], Hans Wienk[4], Rolf Boelens[4], Mehran Mahvash[5], Athanasios K. Petridis[6], Roland Schauer[7]

[1]*RI-B-NT – Research Institute of Bioinformatics and Nanotechnology, Schauenburgerstrasse 116, 24118 Kiel, Germany*
[2]*Zoologisches Institut – Strukturbiologie, Zentrum für Biochemie und Molekularbiologie, Christian-Albrechts-Universität Kiel, Am Botanischen Garten 1-9, 24118 Kiel, Germany*
[3]*Klinik für Geburtshilfe, Gynäkologie und Andrologie, Fachbereich Veterinärmedizin, Justus-Liebig-Universität Gießen, Frankfurter Str. 106, 35392 Gießen, Germany*
[4]*Bijvoet Center for Biomolecular Research, NMR Spectroscopy, Utrecht University, Padualaan 8, 3584 CH Utrecht, The Netherlands*
[5]*Neurochirurgische Abteilung, Klinikum Merheim, Köln, Germany*
[6]*Neurochirurgie, Klinikum Duisburg GmbH, Zu den Rehwiesen 9, 47055 Duisburg, Germany*
[7]*Biochemisches Institut, Universität Kiel, Olshausenstrasse 40, 24098 Kiel, Germany*

Abstract

Sialic acid supports nerve cell regeneration, differentiation and neuronal plasticity. Especially, polysialic acid (polySia) chains which are built up by α2,8-linked Neu5Ac Neu5Ac residues influence by their specific interactions with polySia receptors neuronal processes related to tumor spread and differentiation processes. With a combination of biophysical and biochemical methods including molecular modeling as described here it is possible to support cell biological experiments and *in vivo* studies on a nanoscale level. The submolecular analytical approaches which are directed to crucial functional groups focus on the potential therapeutic impact of sialic acids and in particular polySia. Such results are helpful for the development of new drugs which might have a high clinical relevance in respect to the therapy of various diseases correlated to neuronal regeneration, tumor spread and infections. It is not surprising that several diseases belonging to these different clinical fields (e.g. oncology, infection diseases, neuronal disorder) can be treated as indicated because sialic acids represent essential contact structures on numerous cell surfaces in dependence to their state of differentiation.

Keywords: Nanomedical therapies; Polysialic acid; Cell-cell interactions

Introduction

A deeper insight into the biological role of sialic acids particularly polysialic acid (polySia) is possible when we understand the complementarity between structure and function on a submolecular level using a strategic combination of biochemical and biophysical methods. Similarities between interactions with cell pathogens and cell surfaces, cell-cell interactions, neuro-oncological mechanisms and nerve cell regeneration processes are obvious since sialic acids and especially the α2,8-linked Neu5Ac residues which build up polySia chains (Scheme 1) are often involved in these molecular recognition processes. These characteristic recognition processes are strongly dependent on the organ, the cell type and the stage of differentiation [1-6]. For example, in the respiratory and reproductive systems polySia covalently conneted with NCAM is discussed to counteract the cytotoxic characteristics of extracellular histones, which are generated during inflammation [7,8]. In contrast, in the neuronal system the interaction of polySia with histone H1 seems to be important for regeneration processes [9]. Thereby, histone H1 directly binds to polySia at an extracellular position as shown for cultured cerebellar neurons. Immunostaining of living cerebellar neurons and Schwann cells confirmed that an extracellular pool of histone H1 colocalizes with polySia at the cell surface. Histone H1 stimulated neuritogenesis *in vitro*, process formation and proliferation of Schwann cells as well as migration of neural precursor cells via polySia-dependent mechanisms, further indicating that histone H1 is active extracellularly. These *in vitro* observations suggested an important functional role for the interaction between histone H1 and polySia not only for nervous system development but also for regeneration in the adult organism. Indeed, histone H1 improved glycan chain chafunctional recovery, axon regrowth, and precision of reinnervation of the motor branch in adult mice with femoral nerve injury [9]. Due to their important role in nervous system regeneration and neuro-oncological processes, polySia receptors (e.g. lectins) are of highest clinical importance [10-12]. The involvement of sialic acid in general and polySia in special as well as sulfated oligosaccharides (e.g. the HNK-1 epitope) in neurite outgrowth allows to develop new therapeutic strategies with strong supportive impact on nervous system regeneration in mammals [13-17]. The neural cell adhesion molecule NCAM as well as other polySia-carrying proteins, i.e. neuropilin and the synaptic cell adhesion molecule SynCAM1, interact with these receptors via the polySia

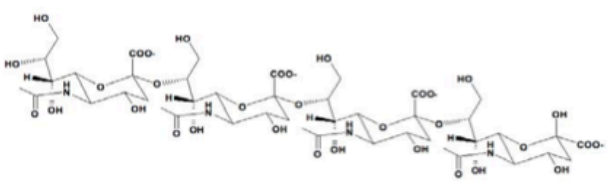

Scheme 1: Illustration of an α2,8-linked Neu5Ac tetramer.

***Corresponding author:** Athanasios K. Petridis, Neurochirurgie, Klinikum Duisburg GmbH, Zu den Rehwiesen 9,47055 Duisburg, Germany,, Tel: 004915123465406; E-mail: opticdisc@aol.com

Received February 05, 2015; **Accepted** February 26, 2015; **Published** February 28, 2015

Citation: Siebert HC, Zhang R, Scheidig A, Eckert T, Wienk H, et al. (2015) Interaction Studies of Sialic Acids with Model Receptors Contribute to Nanomedical Therapies. J Neurol Disord 3: 212. doi:10.4172/2329-6895.1000212

SHL-1 conf.	1	2	3	4	5	6	7	8	9	10	11	12	13	14	15	16	17	18	19	20
Trp32	No	No	Yes	Yes	Yes	No	Yes	Yes	No	Yes	No	No	No	Yes	No	Yes	Yes	No	No	No

Table 1: Three Trp residues are stabilizing in the SHL-1 – sialic acid complex: Trp23, Trp25 and in parts Trp32. Twenty energy minimum conformations based on the NMR conformations of the ligand-free SHL-1 structure 1QK7.pdb (59) are listed. A contribution of Trp32 in the initial part of complex formation has been detected in nearly half of the analyzed conformations. Nine-times "Yes" means participation in the sialic acid recognition process in respect to Trp32. Eleven-times "No" indicates a lack of involvement concerning Trp32 when the initial binding step with the carbohydrate-recognition region of SHL-1 is discussed.

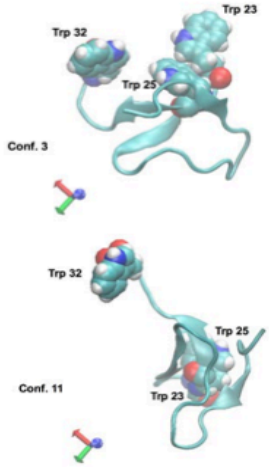

Figure 1: Conformation 3 (top) and conformation 11 (bottom) of the lectin SHL-1 from the Chinese bird-hunting spider *Selenocosmia huwena* Wang (Wang = King) are listed in Table 1. Three tryptophane residues (Trp23, Trp25, Trp32) are involved in ligand binding (18) and highlighted in a van-der-Waals presentation. The conformations 3 (top) and 11 (bottom) correspond to a ligand-free NMR structure of SHL-1 (59). In contrast to Trp23 and Trp25, which are essential for ligand binding, the Trp32 residue stabilizes the complex, but is not crucial for the initial specific ligand recognition step.

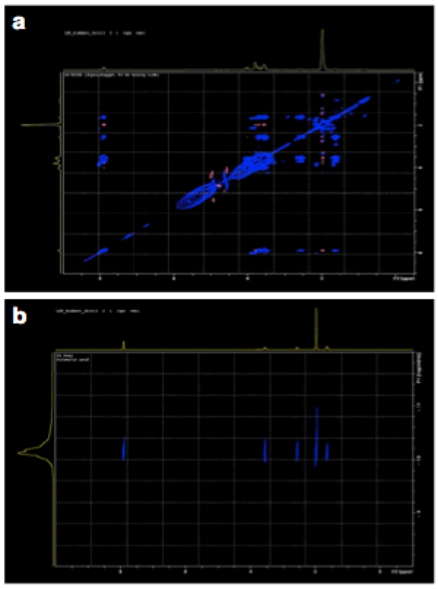

Figure 2: (a) TOCSY NMR spectrum of colominic acid (α2,8-linked Neu5Ac polysaccharide chains of different size). (b) DOSY (Diffusion Ordered SpectroscopY) NMR spectrum of colominic acid which can be used to determine the size distribution of the α2,8-linked Neu5Ac polysaccharide fragments.

glycan chain. The building block of the polySia glycan chain is the disaccharide repeating unit α2,8-linked sialic acid which interacts with the amino acid residues highlighted in Figure 1. In order to analyze the intermolecular processes between sialic acid molecules and their receptors on a nanoscale level suited model systems are needed. Such a suited model system is provided by the lectin SHL-1 from the Chinese bird hunting spider *Selenocosmia huwena* Wang. Sialic acid receptors of different origin have structural similarities in the architecture of their carbohydrate recognition domains (CRDs), pertaining, for instance, in the three-dimensional arrangement of crucial residues [18,19]. Beside arginine residues, aromatic amino acids, such as tryptophan and tyrosine (Figure 1) are often involved in sialic acid interaction processes [18-21]. However, as indicated by the different conformational states listed in Table 1 the structural dynamics of a sialic acid receptor is of highest relevance for the carbohydrate recognition process.

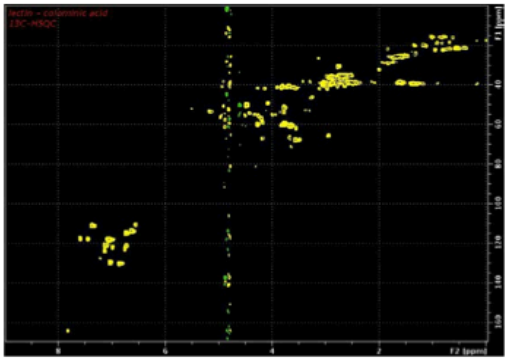

Figure 3: ^{13}C HSQC (Heteronuclear Single Quantum Coherence) NMR spectrum of the lectin SHL-1from the Chinese bird-hunting spider *Selenocosmia huwena* Wang in the presence of colominic acid.

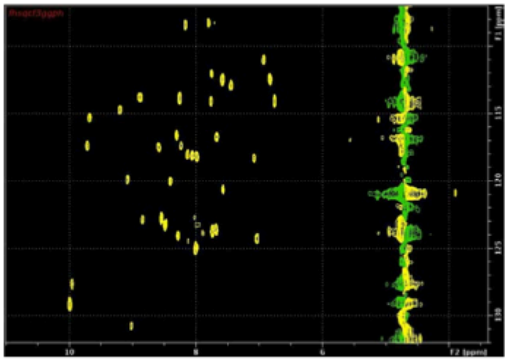

Figure 4: ^{15}N HSQC (Heteronuclear Single Quantum Coherence) NMR spectrum of the lectin SHL-1from the Chinese bird-hunting spider *Selenocosmia huwena* Wang in the presence of colominic acid.

Results and Discussion

Analytical approaches

To further validate these nanomedical role models, it is advisable, for instance, to make use of nuclear magnetic resonance (NMR) methods which monitor the interactions between polySia and its sialic acid receptors (Figures 2-4). NMR and molecular modeling studies can be further extended to define whether the ligand-binding results are in agreement with general binding principles and/or similarities in the CRD architectures of sialic acid receptors [18-21]. In this context the strategic combination of methods lead to a new nanomedical approach in neurosciences providing data that explain why bio-active molecules like cyclic and linear peptides or small organic molecules can act as glycomimetics [22-34]. Especially, polar molecules with partially equalized single and double bonds which can be analyzed with *ab initio* calculations are proper candidates for effective new drugs which can mimick sialic acid functions. O-acetylated sialic acids are suited blue-prints to identify further glycomimetic molecules since O-acetylation at various positions on Neu5NAc represents an important functional group [35]. In this context we have also refined our tools to understand the molecular interactions on a nanoscale level, thereby, we considered beside polySia the binding processes of HNK-1 and related sulfated saccharides. Furthermore, bio-active peptides and small organic molecules show specific interactions with receptors such as laminin, myristoylated alanine-rich C kinase substrate (MARCKS) and various integrins. Processes of neuronal regeneration and tumor growth are related to sialic acid concentrations as we have learned from stem cell studies. Therefore, it is feasible to invent new therapeutic strategies in these important field of neurological disorders with panels of suited molecules. The physiological role of polySia shall now be discussed in order to understand how inhibition of its expression or increasing of its expression can affect cancer growth as well as central nervous system cell regeneration.

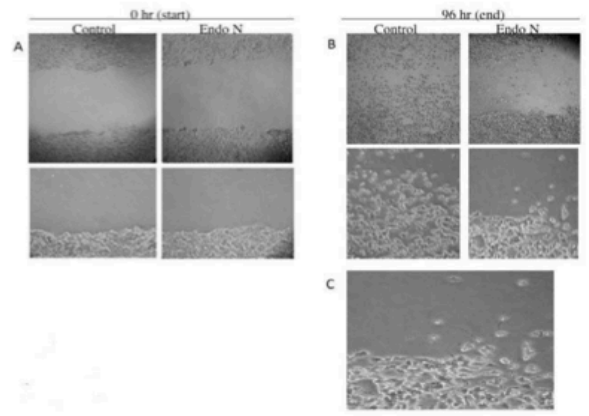

Figure 5: PolySia cleavage inhibits neuroblastoma cell migration. Wound scratch assay of neuroblastoma cell culture. A. Starting point (0 hr). In controls the cells (SY5Y neuroblastoma, which are polySia rich) were untreated and in the endo N group, enodneuraminidase (3 U / ml) was added into the culture medium. B. 96 hours after treatment the migration into the wound scratch in the endo N treated cultures was significantly reduced and in addition the cells started to build clusters (cell-cell interactions seem to be enabled). After endoneuraminidase N treatment neuroblastoma cells showed to establish an axonal growth, which can be seen in the magnified image in C.

Therapeutical and diagnostic consequences

PolySia cleavage and tumor cell differentiation are directly related to each other. A number of studies have shown that polySia is overexpressed in malignant tumors like malignant gliomas, small cell lung cancer, neuroblastomas to name a few [12,36-43]. It has been postulated that polySia enables tumor cells to keep an undifferentiated state and therefore to exist outside of the cellular "social network" and grow irrespective of regulating factors expressed by their neighbor cells. Also the characteristic polySia function, to accelerate migration of stem cells [44-46], is used by tumor cells to infiltrate normal tissue and metastasize [12]. As a logical consequence, polySia seems to act as NCAM interaction inhibitor. This means that different pathways induced by NCAM activation can be blocked by the expression of polySia on NCAM. The presence of polySia on NCAM inhibits this interaction [47] and keeps tumor cells away from differentiation back to normal cells. In relation to this it is of clinical interest that the transcription factor Pax3 involved in tumorigenesis seems to induce NCAM polysialylation on medulloblastoma cells [48]. Regarding these processes on a nanoscale level, polySia inhibits cell-cell interactions through its ability to bind significant amount of water and therefore

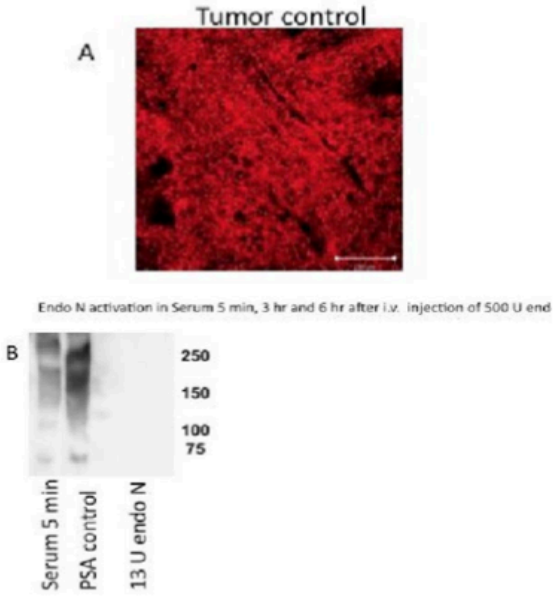

Figure 6: A: PolySia immunostainings expression in rhabdomyosarcoma cells. PolySia immunostainings of a rhabdomyosarcoma tumor induced into a Bulb C mouse. **B:** When endoneuraminidase N is applied intrathecally in animals, polySia in the subventricular zone stem cells is cleaved. However when endoneuraminidase N is applied intravenously to animals, polySia is not cleaved from tumor cells. It could be shown that the presence of serum inactivates endoneuraminidase N. When Serum was added in a cell culture and the polySia rich cells (SY5Y neuroblastoma cells) were treated with endoneuraminidase N the enzyme was inactive and failed to remove polySia from the cells. Serum 5 min: SY5Y cells treated with endo N for 5 min in the presence of serum. PolySia is present as a smear from 150-250 kDa. PolySia-control: SY5Y cultures not treated with endo N. 13 U endo N:SY5Y cells treated with endo N without the presence of Serum. No polySia can be seen. Western blot electrophoresis of SY5Y cell lysates stained with anti-polySia antibody 5A5.

keeping receptors away from their ligand or other receptors. Some studies are postulating that polySia expression of tumor cells can be used as a prognostic factor in different tumors. Wilms tumor patients with increased polySia expression for example have a shorter survival time, therefore, polySia was claimed to be an oncodevelopmental antigen [49,50].

Nanomedical improvements

Apart from using polySia as a prognostic marker in tumors there is also a therapeutic approach to tumors through cleavage of polySia from the surface of polySia expressing tumor cells.

Endoneuraminidase N is a polySia selective cleavage enzyme. A polySia cleavage in neuroblastoma cells with the non-toxic endoneuraminidase N induces differentiation of these cells with developing axons and expressing neurofilaments [38]. Additionally, the migration capacity of these cells was significantly reduced [38,51-53] (Figure 5). Unfortunatelly, *in vivo* experiments with intravenous application of endoneuraminidase N in animals with polySia-rich tumors failed to remove polySia from the tumor cells. Reason of this seemed to be factors in the serum, which inactivated endoneuraminidase N there (Figure 6). Therefore, different alternative delivery methods for endoneuramoinidase to tumors have to be evaluated. Since the cleavage of polySia from tumor cells is a promising tool in the treatment of cancer nanomedical tools for their delivery are now under construction. These tools can also be used as vessels for polySia fragments and other molecules with an impact on neuronal differentiation. It is important to mention that polySia is not oncogenic. This molecule is expressed by tumor cells but there are no observations that it is inducing cancer. It is indeed fascinating that new drugs can be developed by a precise knowledge of the structural and functional properties of polySia, HNK-1 and the corresponding glycomimetic molecules. The high clinical relevance in respect to the therapy of diseases correlated to neuronal regeneration, tumor spread and infection opens a wide field for medical and pharmacological research projects. It should not be surprising that various diseases of different origin can be treated with drugs based on polySia because this

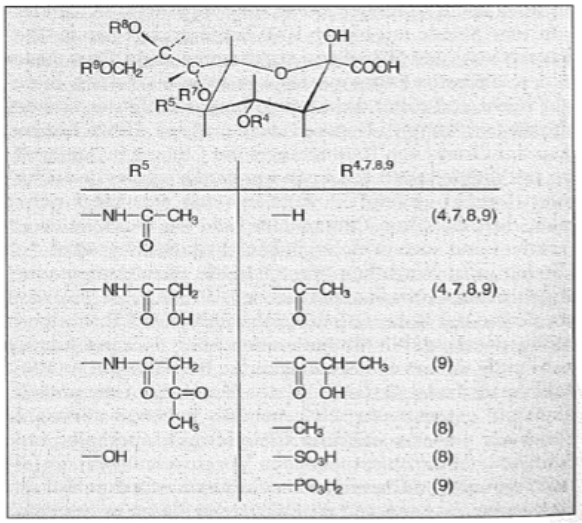

Figure 7: The carboxyl group (COOH). The N-acetyl group (left column) is always found at C-atom 5 whereas an O-acetyl group (right column) can be attached to the C-atoms 4, 7, 8 and 9 of a sialic acid residue.

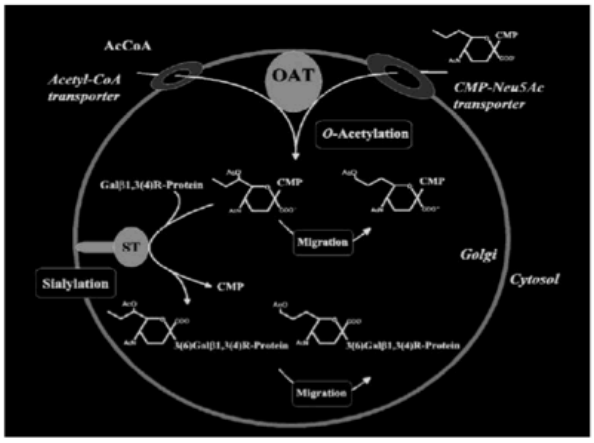

Figure 8: The postulated pathway for the incorporation of O-acetyl groups into sialic acids in human colon mucosa. ST, sialyltransferase; R, GlcNAc or GalNAc. The migration (or isomerisation) of acetyl groups from C-7 to C-9, as shown in the postulated pathway, can occur spontaneously under mild-alkaline conditions, or as postulated by Vandamme-Feldhaus and Schauer, 1998 (54), be catalyzed by a hypothetical 'migrase'. It is unclear whether isomerisation takes place at the nucleotide-sugar level or following sialic acid transfer to glycoprotein acceptors.

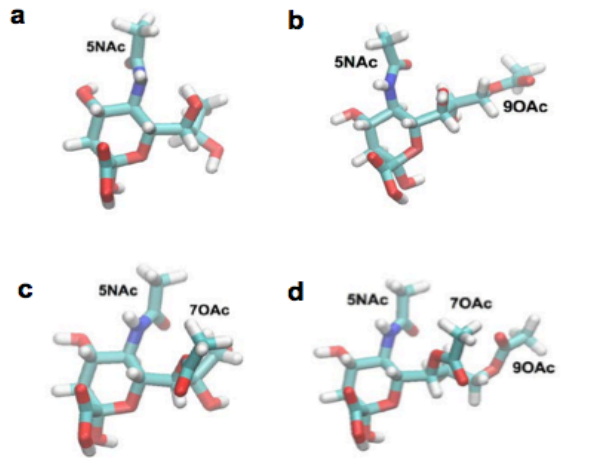

Figure 9: Quantum chemical calculations of (a) NeuN5Ac, (b) Neu5NAc9OAc, (c) Neu5NAc7OAc,(d) Neu5NAc7,9OAc were carried out with the DFT (Density Functional Theory) method (B3LYP/6-31G*) using the Gaussian03 program. Beside the 5-acetyl group also 9O-acetyl- and 7O-acetyl groups are important contact parts for the fine-tuning of ligand – receptor interactions when sialic acids are involved.

polysaccharide has to be considered as an essential contact structure on the cell surface related to many innovative clinical approaches in the field of nanomedicine. In particular, O-acetylation of sialic acids may play an important role in respect to a rational-based design of new drugs since the O-acetyl groups act as special recognition points (Figure 7). The postulated pathway for the incorporation of O-acetyl groups into sialic acids in human colon mucosa is described in the literature [54,55] and shown in (Figure 8). When the biological effects of sialic acid modifications caused by different functional groups have to

be understood completely it is essential to consider all their biophysical properties. As it is the case when studying olfaction processes beside the molecular shape and its dynamics also the vibrational states of certain functional groups have to be considered [56]. Quantum chemical calculations of (a) Neu5Ac, (b) Neu5Ac9OAc, (c) Neu5Ac7OAc, (d) Neu5Ac7,9OAc were carried out with the DFT (Density Functional Theory) method (B3LYP/6-31G*) using the Gaussian03 program in order to collect all these physical parameters. Pictures of the energy minimum conformations are displayed in (Figure 9) This knowledge opens new routes for a rational based drug design of molecules, since also the complete set of physical parameters including the vibrational states of these molecules are taken into account. In such a context therapeutical improvements could be expected in relation to sialic acid - receptor interactions especially when focusing on polySia with special patterns of O-acetyations. A combination of the biophysical methods described here with clinical studies could lead to neuro-oncological approaches related to applied patient-care [57,58].

Acknowledgement

We thank Philipp Siebert for technical assistance and Prof. Dr. Hubertus Maximilian Mehdorn (Department of Neurosurgery, Universitatsklinikum Schleswig-Holstein Campus Kiel, Kiel, Germany) for fruitful scientific discussions. Elements of the project are financed by the European Commission's Framework Program 7 (Bio-NMR; project number 261863).

References

1. Schauer R (2009) Sialic acids as regulators of molecular and cellular interactions. Curr Opin Struct Biol 19: 507-514.
2. Battistel MD, Shangold M, Trinh L, Shiloach J, Freedberg DI (2012) Evidence for helical structure in a tetramer of alpha2-8 sialic acid: unveiling a structural antigen. J Am Chem Soc 134: 10717-10720.
3. Sato C, Kitajima K (2013) Impact of structural aberrancy of polysialic acid and its synthetic enzyme ST8SIA2 in schizophrenia. Frontiers in cellular neuroscience 7: 61.
4. Rollenhagen M, Kuckuck S, Ulm C, Hartmann M, Galuska SP, et al. (2012) Polysialylation of the synaptic cell adhesion molecule 1 (SynCAM 1) depends exclusively on the polysialyltransferase ST8SiaII in vivo. J Biol Chem 287: 35170-35180.
5. Hildebrandt H, Dityatev A (2013) Polysialic acid in brain development and synaptic plasticity. Topics in current chemistry. Advance online publication.
6. Tiralongo J, Martinez-Duncker I (2013) Sialobiology: Structure, Biosynthesis and Function (eds J. T & I. M-D, Betham e Books).
7. Simon P, Bäumner S, Busch O, Röhrich R, Kaese M, et al. (2013) Polysialic acid is present in nammalian semen as a post-translational modification of the neural cell adhesion molecule NCAM and the polysialyltransferase ST8SiaII. J Biol Chem 288: 18825-18833.
8. Ulm C, Saffarzadeh M, Mahavadi P, Muller S, Prem G, et al. (2013) Soluble polysialylated NCAM: a novel player of the innate immune system in the lung. Cell Mol Life Sci 70: 3695-3708.
9. Mishra B, von der Ohe M, Schulze C, Bian S, Makhina T, et al. (2010) Functional role of the interaction between polysialic acid and extracellular histone H1. J Neurosci 30: 12400-12413.
10. Rutishauser U (2008) Polysialic acid in the plasticity of the developing and adult vertebrate nervous system. Nat Rev Neurosci 9: 26-35.
11. Senkov O, Sun M, Weinhold B, Gerardy-Schahn R, Schachner M, et al. (2006) Polysialylated neural cell adhesion molecule is involved in induction of long-term potentiation and memory acquisition and consolidation in a fear-conditioning paradigm. J Neurosci 26: 10888- 109898.
12. Petridis AK, Wedderkopp H, Hugo HH, Maximilian Mehdorn H (2009) Polysialic acid overexpression in malignant astrocytomas. Acta neurochirurgica 151: 601-603; discussion 603-604.
13. Siebert HC, Born K, André S, Frank M, Kaltner H, et al. (2006) Carbohydrate chain of ganglioside GM1 as a ligand: identification of the binding strategies of three 15 mer peptides and their divergence from the binding modes of growth-regulatory galectin-1 and cholera toxin. Chemistry – A European Journal 12: 388-402.
14. Kleene R, Schachner M (2004) Glycans and neural cell interactions. Nat Rev Neurosci 5: 195- 208.
15. Masand SN, Chen J, Perron IJ, Hammerling BC, Loers G, et al. (2012) The effect of glycomimetic functionalized collagen on peripheral nerve repair. Biomaterials 33: 8353-8362.
16. Mehanna A, Mishra B, Kurschat N, Schulze C, Bian S, et al. (2009) Polysialic acid glycomimetics promote myelination and functional recovery after peripheral nerve injury in mice. Brain 132: 1449-1462.
17. Schauer R (2004) Sialic acids: fascinating sugars in higher animals and man. Zoology (Jena) 107: 49-64.
18. Siebert HC, Lü SY, Wechselberger R, Born K, Eckert T, et al. (2009) A lectin from the Chinese bird-hunting spider binds sialic acids. Carbohydr Res 344: 1515-1525.
19. Siebert HC, Lu¨SY, Frank M, Kramer J, Wechselberger R, et al. (2002) Analysis of protein-carbohydrate interaction at the lower size limit of the protein part (15-mer peptide) by NMR spectroscopy, electrospray ionization mass spectrometry, and molecular modeling. Biochemistry 41: 9707-9717.
20. Siebert HC, André S, Lu SY, Frank M, Kaltner H, et al. (2003) Unique conformer selection of human growth-regulatory lectin galectin-1 for ganglioside GM1 versus bacterial toxins. Biochemistry 42:14762-14773.
21. André S, Kaltner H, Lensch M, Russwurm R, Siebert HC, et al. (2005) Determination of structural and functional overlap/divergence of five proto-type galectins by analysis of the growth-regulatory interaction with ganglioside GM1 in silico and in vitro on human neuroblastoma cells. Int J Cancer 114: 46-57.
22. Bhunia A, Vivekanandan S, Eckert T, Burg-Roderfeld M, Wechselberger R, et al. (2010) Why structurally different cyclic peptides can be glycomimetics of the HNK-1 carbohydrate antigen. J Am Chem Soc 132: 96-105.
23. Tsvetkov YE, Burg-Roderfeld M, Loers G, Ardá A, Sukhova EV, et al. (2012) Synthesis and molecular recognition studies of the HNK-1 trisaccharide and related oligosaccharides. The specificity of monoclonal anti-HNK-1 antibodies as assessed by surface plasmon resonance and STD NMR. J Am Chem Soc 134: 426-435.
24. Siebert HC, Burg-Roderfeld M, Eckert T, Stötzel S, Kirch U, et al. (2010) Interaction of the alpha2A domain of integrin with small collagen fragments. Protein and Cell 1: 393-405.
25. Stötzel S, Schurink M, Wienk H, Siebler U, Burg-Roderfeld M, et al. (2012) Molecular organization of various collagen fragments as revealed by atomic force microscopy and diffusionordered NMR spectroscopy. ChemPhysChem: a European journal of chemical physics and physical chemistry 13: 3117-3125.
26. Schadow S, Siebert HC, Lochnit G, Kordelle J, Rickert M, et al. (2013) Collagen metabolism of human osteoarthritic articular cartilage as modulated by bovine collagen hydrolysates. PLoS One 8: e53955.
27. Siebert HC, Rosen J, Seyrek K, Kaltner H, André S, et al. (2006) alpha2,3/alpha2,6-Sialylation of N-glycans: non-synonymous signals with marked developmental regulation in bovine reproductive tracts. Biochimie 88: 399-410.
28. Siebert HC, Tajkhorshid E, Dabrowski J (2001) Barrier to rotation around the Csp2-Csp2 bond of the ketoaldehyde enol ether MeC(O)CH=CH-OEt as determined by 13C NMR and ab initio calculations. J Phys Chem A: 8488-8494.
29. Lenthe JH, van Boer DHW, den Havenith RWA, Schauer R, Siebert HC (2004) Ab initio calculations on various sialic acids provide valuable information about sialic acid-specific enzymes. J. Mol. Struct. (THEOCHEM) 677: 29-37.
30. Eckert T, Stötzel S, Burg-Roderfeld M, Sewing J, Lutteke T, et al. (2012) In silico study on sulfated and non-sulfated carbohydrate chains from proteoglycans in Cnidaria and interaction with collagen. O J Phys Chem 2:123-133.
31. Krylov VB, Grachev AA, Ustyuzhanina NE, Ushakova NA, Preobrazhenskaya ME, et al. (2011) Preliminary structural characterization, anti-inflammatory and anticoagulant activities of chondroitin sulfates from marine fish cartilage. Russian Chem Bull (Med Chem Issue) Int Ed 60: 746-753.
32. Siebert S, Engelhard P, Kraan S, Schauer R, Siebert HC (2013) Gibt es die Apotheke aus dem Meer? Praxis der Naturwissenschaften. Praxis der Naturwissenschaften – Biologie 2 (63): 39-42.
33. Raabe O, Reich C, Wenisch S, Hild A, Burg-Roderfeld M, et al. (2010) Hydrolyzed fish collagen induced chondrogenic differentiation of equine adipose tissue-derived stromal cells. Histochemistry and cell biology 134: 545-554.

34. Jiménez-Barbero J, Javier Cañada F, Asensio JL, Aboitiz N, Vidal P, et al. (2006) Hevein domains: an attractive model to study carbohydrateprotein interactions at atomic resolution. Advances in carbohydrate chemistry and biochemistry 60: 303- 354.

35. Siebert HC, von der Lieth CW, Dong X, Reuter G, Schauer R, et al. (1996) Molecular dynamics-derived conformation and intramolecular interaction analysis of the Nacetyl- 9-O-acetylneuraminic acid-containing ganglioside GDIa and NMR-based analysis of its binding to a human polyclonal immunoglobulin G fraction with selectivity for O-acetylated sialic acids. Glycobiology 6 (6): 561-572.

36. Seifert A, Glanz D, Glaubitz N, Horstkorte R, Bork K (2012) Polysialylation of the neural cell adhesion molecule: Interfering with poly-sialylation and migration in neuroblastoma cells. Arch Bioch Biophys 524: 56-63.

37. Petridis AK (2013) Implication of polysialic acid overexpression on tumorigenesis of neuroectodermal and other tumors. Impairment of cell adhesion. Recent Advances in Adhesion Research Nova Publishers: 115-122.

38. Petridis AK, El Maarouf A, Rutishauser U (2004) Polysialic acid regulates cell contactdependent neuronal differentiation of progenitor cells from the subventricular zone. Develop Dyn 230: 675-684.

39. Miyahara R, Tanaka F, Nakagawa T, Matsuoka K, Isii K, et al. (2001) Expression of neural cell adhesion molecules (polysialylated form of neural cell adhesion molecule and L1-cell adhesion molecule) on resected small cell lung cancer specimens: in relation to proliferation state. J Surg Oncol 77: 49-54.

40. Glüer S, Schelp C, Gerardy-Schahn R, von Schweinitz D (1998) Polysialylated neural cell adhesion molecule as a marker for differential diagnosis in pediatric tumors. J Pediatr Surg 33: 1516-1520.

41. Glüer S, Schelp C, Madry N, von Schweinitz D, Eckhardt M, et al. (1998) Serum polysialylated neural cell adhesion molecule in childhood neuroblastoma. British J of Cancer 78: 106-110.

42. Suzuki M, Suzuki M, Nakayama J, Suzuki A, Angata K, et al. (2005) Polysialic acid facilitates tumor invasion by glioma cells. Glycobiology 15: 887-894.

43. Amoureux MC, Coulibaly B, Chinot O, Loundou A, Metellus P, et al. (2010) Poly sialic acid neural cell adhesion molecule (PSA-NCAM) is an adverse prognosis factor in glioblastoma, and regulates olig2 expression in glioma cell lines. BMC Cancer, 10: 91, 1-12.

44. Cremer H, Lange R, Christoph A, Plomann M, Vopper G, et al. (1994) Inactivation of the NCAM gene in mice results in size reduction of the olfactory bulb and deficits in spatial learning. Nature 367: 455-459.

45. Ono K, Tomasiewicz H, Magnuson T, Rutishauser U (1994) NCAM mutation inhibits tangential neuronal migartion and is phenocopied by enzymatic removal of polysialic acid. Neuron 13: 595-609.

46. Tomasiewicz H, Ono K, Yee D, Thompson C, Goridis C, et al. (1993) Genetic deletion of a neural cell adhesion molecule variant (NCAM-180) produces distinct defects in the central nervous system. Neuron 11: 1163-1174.

47. Petridis AK, Nikolopoulos SN, El-Maarouf A (2011). Physical and functional cooperation of neural cell adhesion molecule and beta1-integrin in neurite outgrowth induction. J Clin Neurosci 18: 1109-1113.

48. Mayanil CSK, George D, Mania-Farnell B, Bremer CL, McLone D, et al. (2000) Overexpression of murine Pax3 increases NCAM polysialylation in a human medulloblastoma cell line. J Biol Chem 275: 23259-23266.

49. Tanaka F, Otake Y, Nakagawa T, Kawano Y, Miyahara R, et al. (2001) Prognostic significance of polysialic acid expression in resected non-small cell lung cancer. Cancer Research 61: 1666-1670.

50. Roth J, Zuber C, Wagner P, Taatjes DJ, Weisgerber C, et al. (1988) Presence of long chain form of polysialic acid oft he neural adhesion molecule in Wilm´s tumor. Am J Pathol 133: 227-239.

51. Seidenfaden R, Krauter A, Schertzinger F, Gerardy-Schahn R, Hildebrandt H (2003) Polysialic acid directs tumor cell growth by controlling heterophilic neural cell adhesion molecule interactions. Mol Cell Biol 23: 5908-5918.

52. El Maarouf A, Petridis AK, Rutishauser U (2003) Use of polysialic acid in repair of the central nervous system. Proc Natl Acad Sci USA 103: 16989-94.

53. Cajal SG (1928). Degeneration and regeneration of the nervous system, vol. 1 and 2. Oxford University Press, London.

54. Vandamme-Feldhaus V, Schauer R (1998) Characterization of the enzymatic 7-O-acetylation of sialic acids and evidence for enzymatic O-acetyl migration from C-7 to C-9 in bovine submandibular gland. J Biochem (Tokyo) 124: 111–121.

55. Shen Y, Tiralongoa J, Kohla G, Roland Schauer R (2004) Regulation of sialic acid Oacetylation in human colon mucosa. Biol. Chem. 385: 145–152.

56. Franco MI, Turin L, Mershin A, Skoulakis EMC (2011) Molecular vibration-sensing component in Drosophila melanogaster olfaction. Proc Natl Acad Sci USA 108 (9): 3797–3802.

57. Mahvash M, Pechlivanis I, Charalampaki P, Jansen O, Mehdorn HM (2014) Visualization of small veins with susceptibility-weighted imaging for stereotactic trajectory planning in deep brain stimulation. Clinical Neurology and Neurosurgery 124: 151-155.

58. Fuster MM, Esko JD (2005) The sweet and sour of cancer: glycans as novel therapeutic targets. Nature Reviews Cancer 5: 526-542.

Citation: Siebert HC, Zhang R, Scheidig A, Eckert T, Wienk H, et al. (2015) Interaction Studies of Sialic Acids with Model Receptors Contribute to Nanomedical Therapies. J Neurol Disord 3: 212. doi:10.4172/23296895.1000212

Chapter III: The analysis of molecular weight distribution of hyaluronic acid with ImageJ

1. Introduction

1.1 Hyaluronic acid

Hyaluronic acid (HA), also named hyaluronan, is a long chain, non-sulfated glycosaminoglycan. It consists of the disaccharide repeating units, D-glucuronic acid and N-acetyl D-glucosamine (Fig. 8). HA is a major extracellular matrix component in cartilage, synovial fluid (SF), eye fluid, epithelial and vitreous humor, as well as various tissues, including brain, kidney, nerve and muscle[74-76]. Accompanied with its wide distribution, HA also plays a multiple role in different biological processes. For example, tissue hydration, lubrication, and interactions with proteins and proteoglycans, as well as mediating signaling pathways etc[76-79]. HA has a broad molecular weight (MW) distribution, in human SF, it ranges from 27 kDa to 10 MDa, with the average of 3 MDa - 4 MDa[80-83]. It was indicated that HA in SF from patient knee joints with advanced osteoarthritis degraded to the lower MW glycosaminoglycan, because of enzymatic cleavage of HA long chains[84].

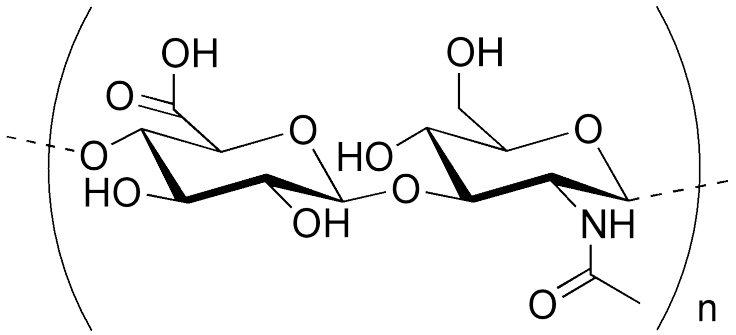

Fig. 8. Hyaluronic acid molecular formula. Picture derived from Wikipedia (https://en.wikipedia.org/wiki/Hyaluronic_acid).

1.2 ImageJ software program

ImageJ is a Java-based, freely accessible public domain software tool for image processing and analyzing (Fig. 9). It was initially called NIH Image, developed by Wayne Rasband at the

National Institutes of Health, in 1987. About 10 years later, when he decided to use Java as the programming language of NIH Image, he renamed the software as ImageJ, with a “J” to represent its Java property. ImageJ has many features that make it very popular and thrived during the last three decades[85,86]. Parts of these advantages are shown as following:

1) ImageJ is a public domain and open source program. Combined with its Java source code, macros and plugins, one can freely download the program from its official website (http://rsb.info.nih.gov/ij/download.html).

2) It is available for most operating systems, such as Macintosh, Linux, Windows, and PDA, in both, 32-bit and 64-bit architecture.

3) It can read, manipulate and analyze lots of different kind of image file formats, including GIF, JPEG, BMP, PNG, PGM, FITS, ASCII, TIFF, and raw data.

4) ImageJ has many image processing and analyzing functions, e.g. image enhancement, geometric transformations, color handling, measuring distances, angles, areas and pixel values etc. It has been widely used by researchers in life sciences.

5) In addition, ImageJ has an inter-disciplinary community worldwide. So far, there exist more than 1700 experts in the ImageJ mailing list. They contribute to knowledgeable discussions and solutions regarding the applications of ImageJ in various scientific fields.

   For more details concerning ImageJ software program, one can visit its official website (http://rsb.info.nih.gov/ij/index.html).

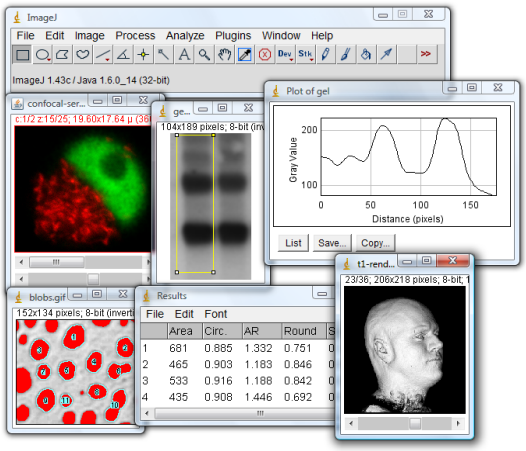

Fig. 9. ImageJ software interface and some of its function representations. The figure derived from ImageJ official website (http://rsb.info.nih.gov/ij/docs/concepts.html).

2. Analysis of hyaluronic acid molecular weight distribution with ImageJ

One of our experiments is focused on the testing of the collective levels of HA, in SF patients with common joint diseases (e.g. early-or late-stage osteoarthritis). Hyaluronic acids from these patients were purified and separated based on their molecular weight using agarose gel electrophoresis followed by staining (The gels were stained overnight using 0.005% Stains-All (Sigma-Aldrich, Taufkirchen, Germany) in 50% ethanol and destained with 10% ethanol for a minimum of 24 h.).

My contribution in this study project has been the development of a new ImageJ analyzing method, to determine the molecular weight distribution of HA.

The molecular weight distribution of HA forms according to its markers being commercially available (<0.5, 0.5–1.1, 1.1–3.1, 3.1–6.1, >6.1 MDa) was determined densitometrically. The detailed processing and analyzing steps of HA images from agarose gel electrophoresis are summerized below:

ImageJ analyzing protocol

Since its broad MW distribution, the continuous bands of HA were obtained from agarose gel electrophoresis. However, it is not available for ImageJ to analyze the corresponding images with the common methods that have been used for analyzing separated bands. Therefore, we developed a new method based on ImageJ functionality after a specific processing of the images.

1) Open the ImageJ software and load the raw HA image (Fig. a).
2) Use the **Image** → **Transform** → **Rotate 90 Degrees Right** tool to rotate the image (Fig. b).

Fig. a Raw HA image

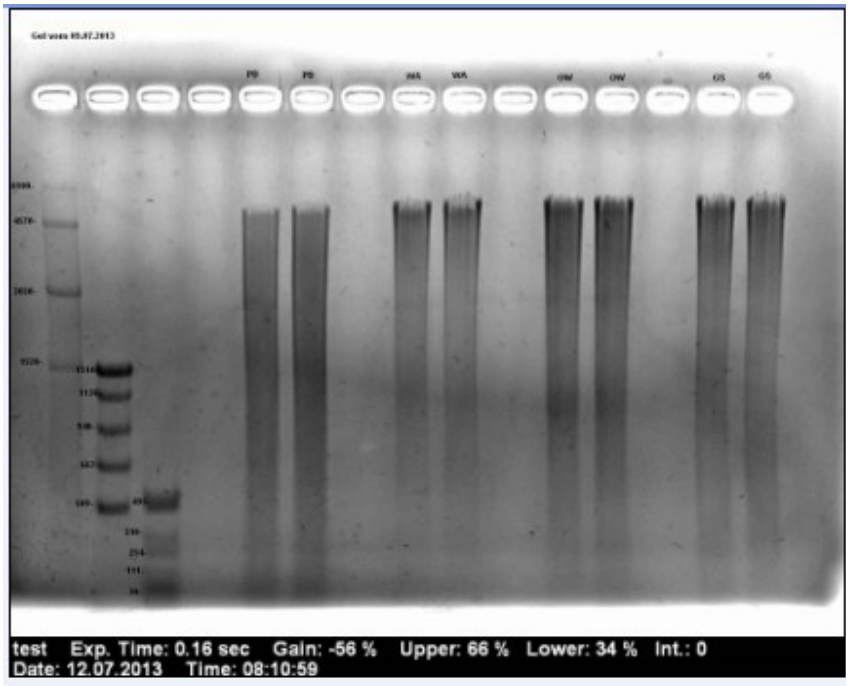

Fig. b After 90 degrees clockwise rotation.

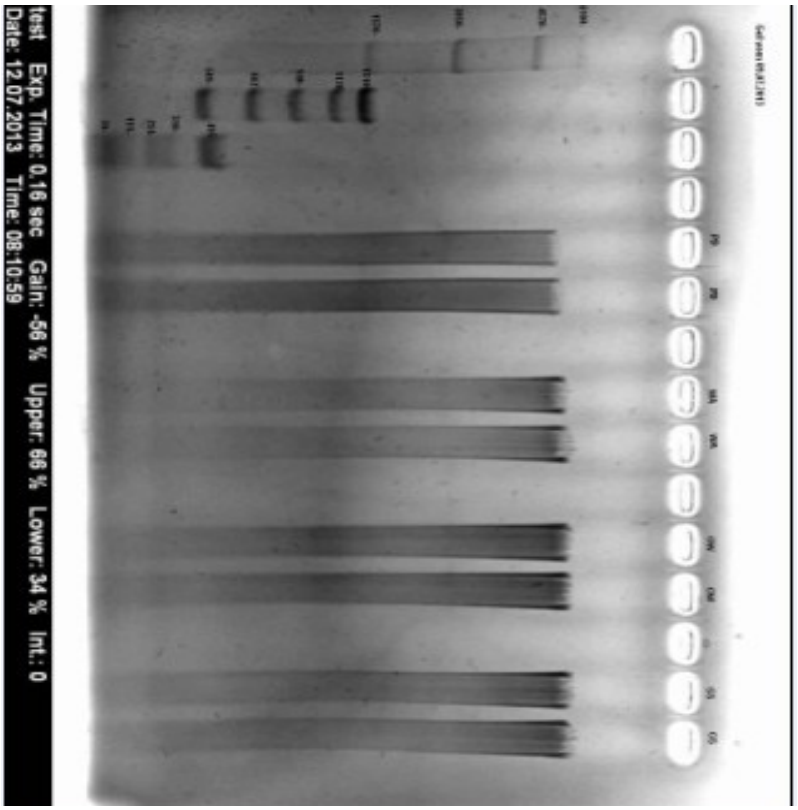

3) Select the **Edit** → **Invert** tool to invert the image.

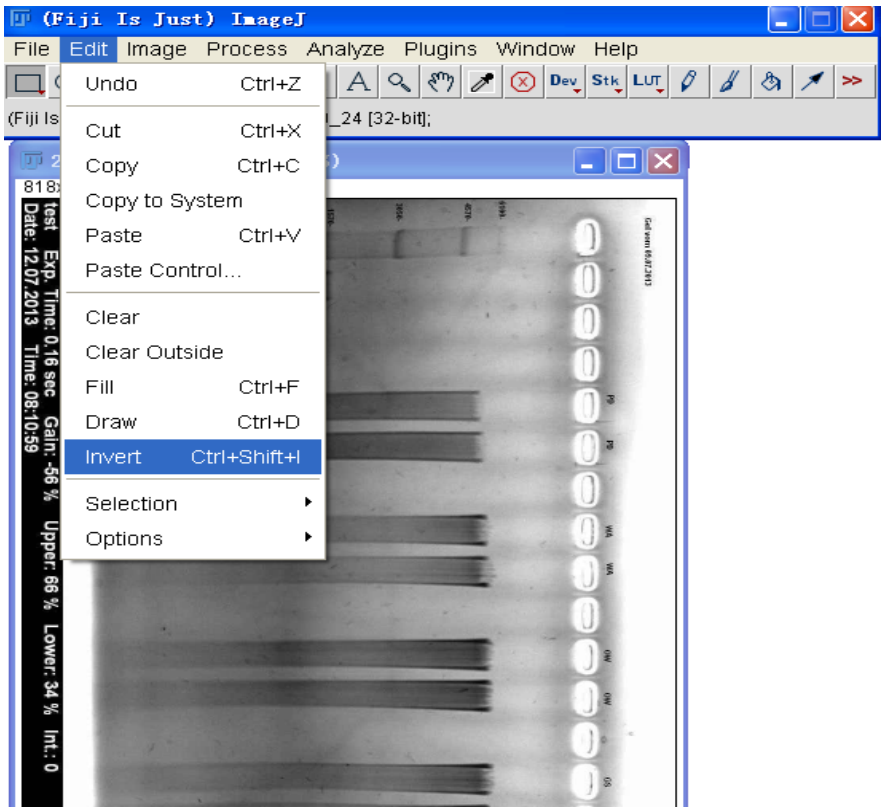

4) Select the **rectangular** selection tool on the left side of the tool menu.

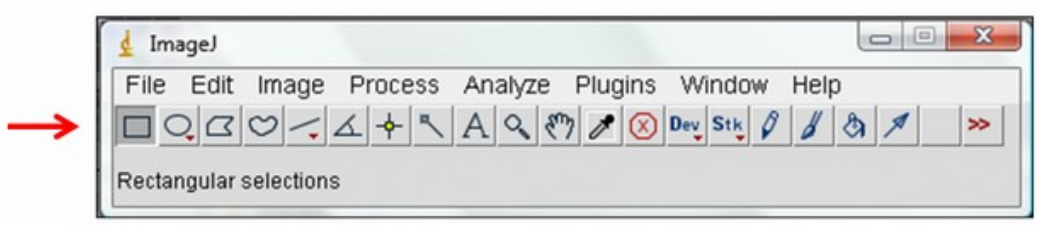

5) Draw the rectangle in the region where we want to measure (e.g. MW 3.1KDa-6.1KDa). Then click **Analyze** → **Gels** → **SelectFirst Lane** (or "**control+1**" in Windows).

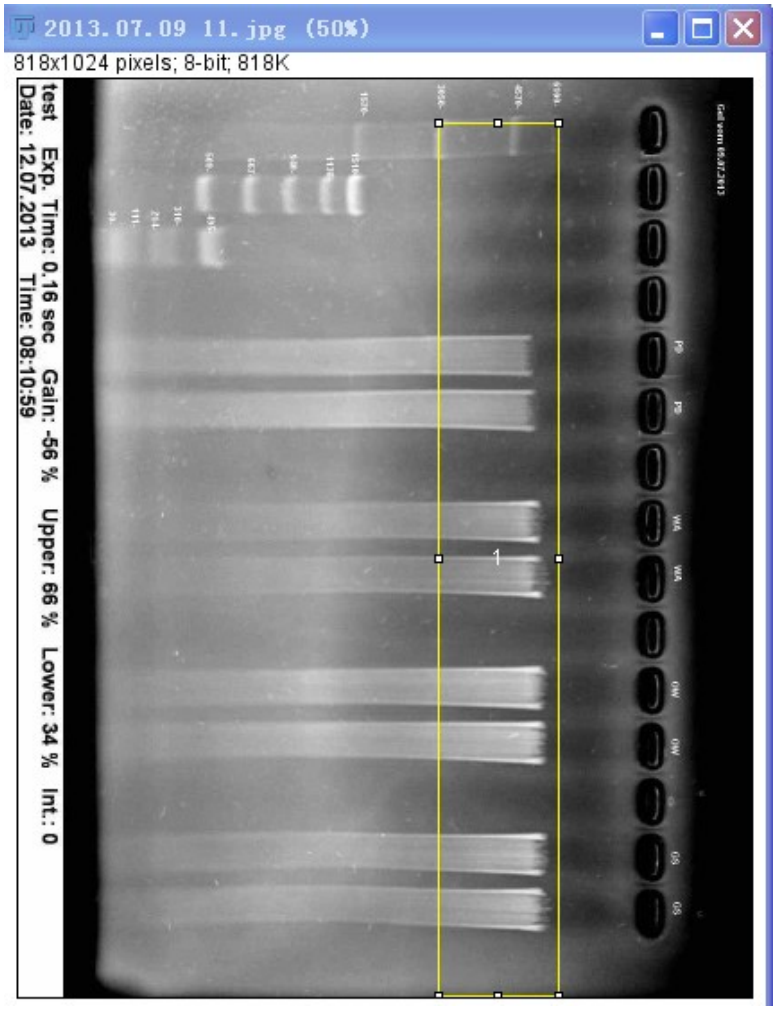

6) Choose **Analyze** → **Gels** → **Plot Lanes** (or "**control+3**" in Windows). A window will pop open. It is the densitometry measurements interface, which gives a graphical depiction of the average intensity of pixels from the top of the rectangle to the bottom.

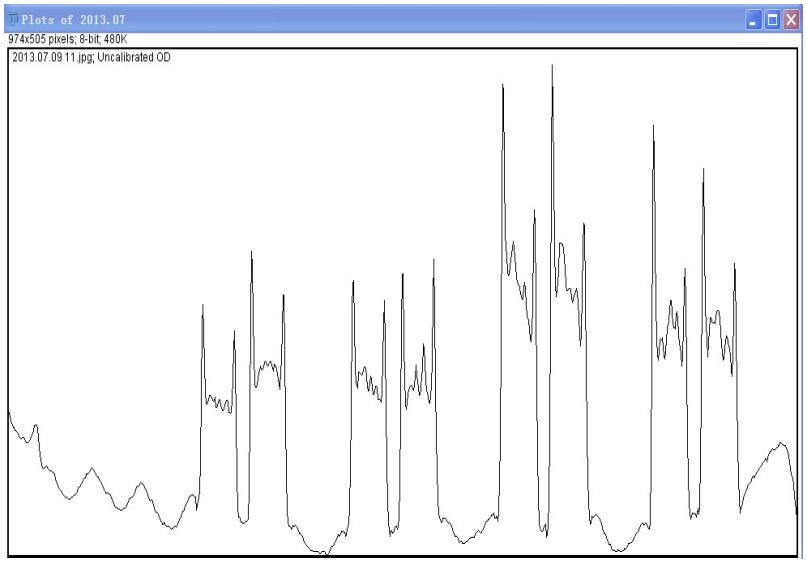

7) To measure the density of bands, one just needs to measure the area under the peak (subtracting the background noise) from this plot. To do so, select the **straight-line** tool from the main menu to close off all peaks.

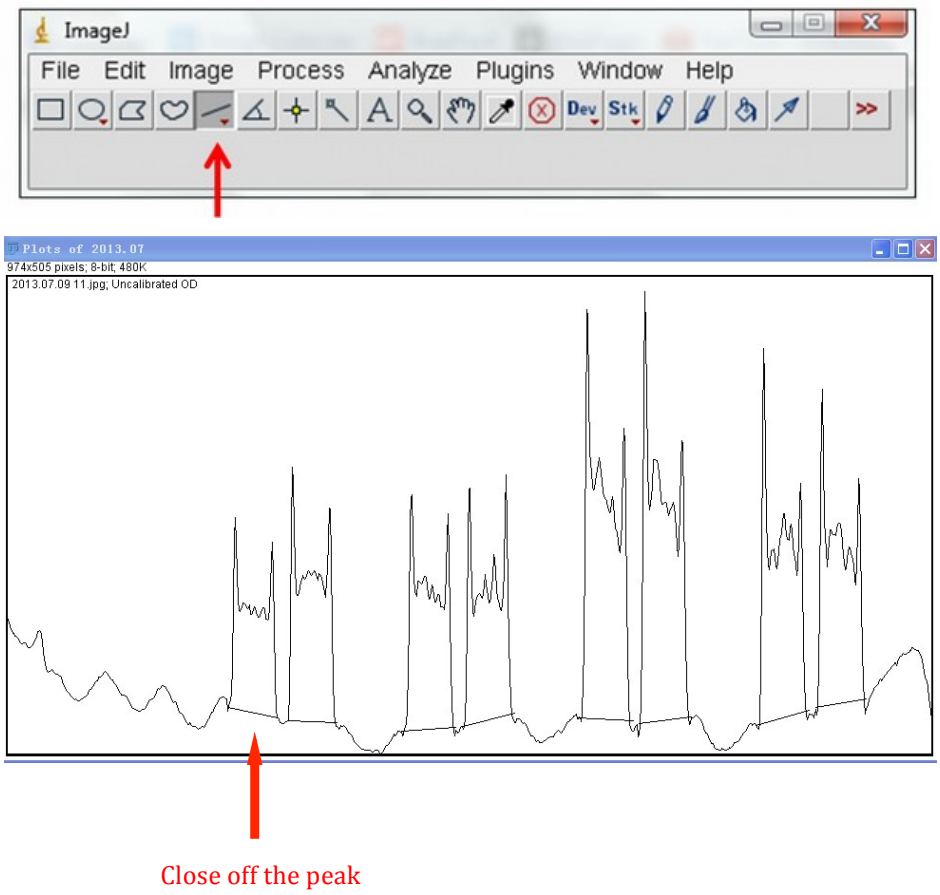

8) Using the **wand** (tracing) tool to click on each peak. The peaks will be yellow outlined. This step integrates the area under the curve of each peak. After that another "**Results**" window will be shown automatically.

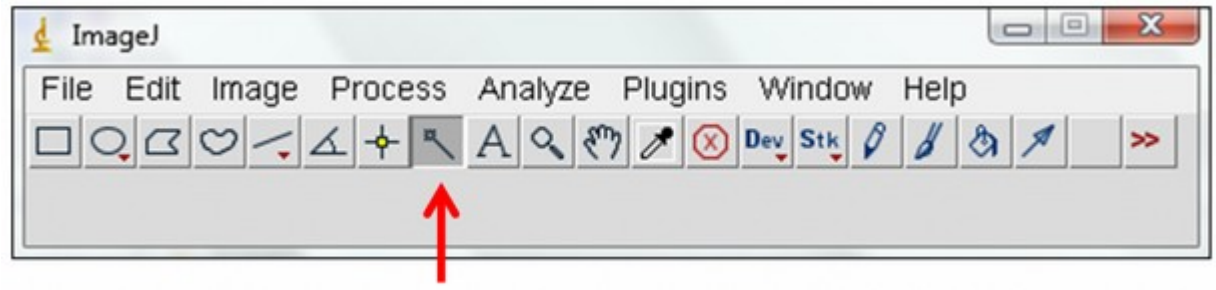

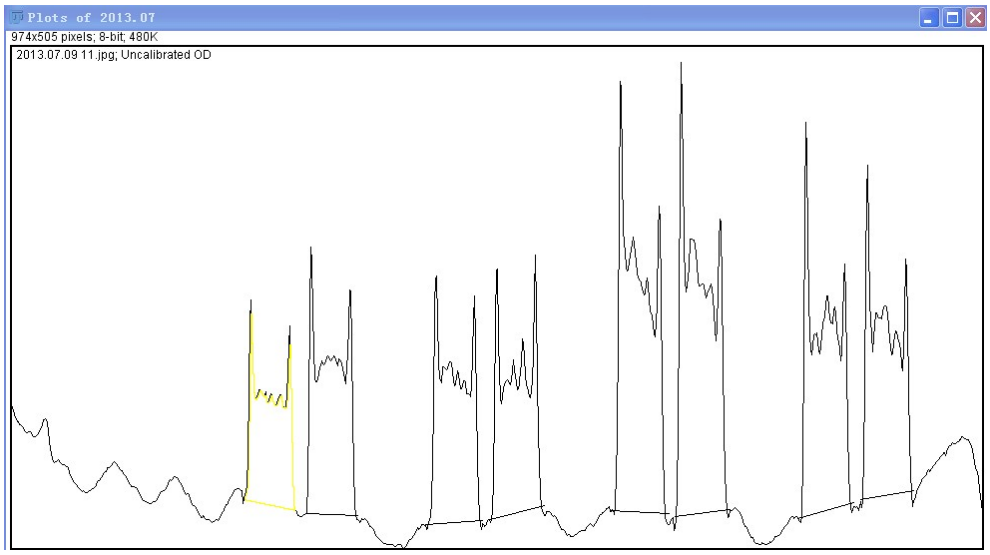

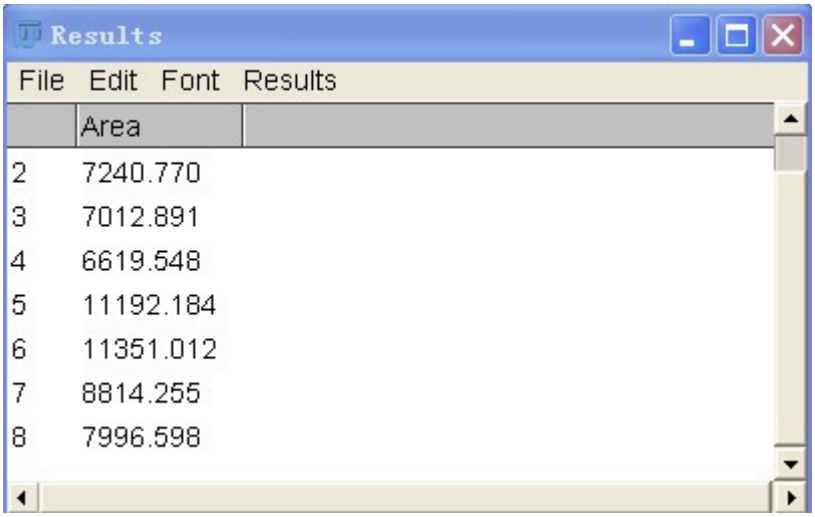

9) The values appearing in this **Results window** are the areas of peaks. These values are related to the band intensity of each lane, and could subsequently present the amounts of substance (e.g. HA) that were loaded into each well.

3. Research paper

We have applied this ImageJ protocol to analyze the MW distribution of HA in SF and published a paper as below:

3.1 Articular joint lubricants during osteoarthritis and rheumatoid arthritis display altered levels and molecular species

(Published in *PLoS One*, 2015; DOI: 10.1371/journal.pone.0125192)

PLOS | ONE

RESEARCH ARTICLE

Articular Joint Lubricants during Osteoarthritis and Rheumatoid Arthritis Display Altered Levels and Molecular Species

Marta Krystyna Kosinska[1☯], Taryn E. Ludwig[2☯], Gerhard Liebisch[3], Ruiyan Zhang[4,5], Hans-Christian Siebert[4], Jochen Wilhelm[6], Ulrich Kaesser[7], Reinhard B. Dettmeyer[8], Heiko Klein[1], Bernd Ishaque[1], Markus Rickert[1], Gerd Schmitz[3], Tannin A. Schmidt[2], Juergen Steinmeyer[1]*

1 Orthopedic Research Laboratories, Department of Orthopedics, Justus-Liebig-University, Giessen, Germany, **2** Faculty of Kinesiology & Biomedical Engineering Graduate Program, University of Calgary, Alberta, Canada, **3** Department of Clinical Chemistry and Laboratory Medicine, University Hospital, Regensburg, Germany, **4** RI-B-NT Research Institute of Bioinformatics and Nanotechnology, Kiel, Germany, **5** Zoological Institute, Structural Biology, Center for Biochemistry and Molecular Biology, Christian-Albrechts-University, Kiel, Germany, **6** Medical Clinic II/IV, Justus-Liebig-University, Giessen, Germany, **7** Internistisches Praxiszentrum am Krankenhaus Balserische Stiftung, Giessen, Germany, **8** Institute of Forensic Medicine, Justus-Liebig-University, Giessen, Germany

☯ These authors contributed equally to this work.
* juergen.steinmeyer@ortho.med.uni-giessen.de

OPEN ACCESS

Citation: Kosinska MK, Ludwig TE, Liebisch G, Zhang R, Siebert H-C, Wilhelm J, et al. (2015) Articular Joint Lubricants during Osteoarthritis and Rheumatoid Arthritis Display Altered Levels and Molecular Species. PLoS ONE 10(5): e0125192. doi:10.1371/journal.pone.0125192

Academic Editor: Oreste Gualillo, SERGAS (Servizo Galego de Saude) and IDIS (Instituto de Investigación Sanitaria de Santiago), the NEIRID Lab, Research Laboratory 9, Santiago University Clinical Hospital. Santiago de Compostela, SPAIN

Received: December 21, 2014

Accepted: March 11, 2015

Published: May 1, 2015

Data Availability Statement: All relevant data are within the paper and its Supporting Information files.

Funding: Supported in part by a grant of the DRB foundation, the Natural Sciences and Engineering Research Council of Canada, and Alberta Innovates Health Solutions, and by the "LipidomicNet" project, funded within the Seventh Framework Programme of the European Union (Grant agreement number 202272). The funders had no role in study design,

Abstract

Background

Hyaluronic acid (HA), lubricin, and phospholipid species (PLs) contribute independently or together to the boundary lubrication of articular joints that is provided by synovial fluid (SF). Our study is the first reporting quantitative data about the molecular weight (MW) forms of HA, lubricin, and PLs in SF from cohorts of healthy donors, patients with early (eOA)- or late (lOA)-stage osteoarthritis (OA), and patients with active rheumatoid arthritis (RA).

Methods

We used human SF from unaffected controls, eOA, lOA, and RA. HA and lubricin levels were measured by enzyme-linked immunosorbent assay. PLs was quantified by electrospray ionization tandem mass spectrometry. Fatty acids (FAs) were analyzed by gas chromatography, coupled with mass spectrometry. The MW distribution of HA was determined by agarose gel electrophoresis.

Results

Compared with control SF, the concentrations of HA and lubricin were lower in OA and RA SF, whereas those of PLs were higher in OA and RA SF. Moreover, the MW distribution of HA shifted toward the lower ranges in OA and RA SF. We noted distinct alterations between cohorts in the relative distribution of PLs and the degree of FA saturation and chain lengths of FAs.

data collection and analysis, decision to publish, or preparation of the manuscript.

Competing Interests: The authors have declared that no competing interests exist.

Conclusions

The levels, composition, and MW distribution of all currently known lubricants in SF—HA, lubricin, PLs—vary with joint disease and stage of OA. Our study is the first delivering a comprehensive view about all joint lubricants during health and widespread joint diseases. Thus, we provide the framework to develop new optimal compounded lubricants to reduce joint destruction.

Introduction

Lubrication of cartilage within synovial joints entails a complex interaction of several mechanical and molecular factors, resulting in decreased friction between opposing surfaces of articular cartilage. In healthy weight-bearing joints, a layer of lubricating molecules covers the surfaces of articular cartilage and acts as a boundary lubricant, effecting nearly frictionless motion of joints [1, 2]. The lubricant components of synovial fluid (SF), such as hyaluronic acid or hyaluronan (HA) [1], lubricin [3], and surface-active phospholipids [4], interact with and adsorb to the surface of articular cartilage and have been suggested, independently or in combination, to promote boundary lubrication [2]. Alterations in the composition and concentration of these molecules leads to insufficient boundary lubrication and thus might be associated with degenerative joint diseases, such as osteoarthritis (OA) [5–8].

HA is an extracellular matrix component in SF, cartilage, eye fluid, vitreous humor, and lung, kidney, brain, and muscle tissues [9–11]. This glycosaminoglycan has a high molecular weight (MW) distribution in human SF, ranging from 27 kDa to 10 MDa [12–14]. HA forms long nonsulfated chains of repeating disaccharides, comprising D-glucuronic acid and N-acetyl D-glucosamine, and provides SF with its high viscosity [9–12, 15, 16].

Several functions have been attributed to HA such as tissue hydration, lubrication, and interactions with proteins and proteoglycans of the extracellular matrix were found. Also, HA binds to the cell surface receptors CD44 and RHAMM, which mediate signaling pathways in inflammation, cell and tissue functions, and expression of catabolic enzymes, such as aggrecanases [11, 13, 16–18]. HA in the MW range of 0.5–1.0 x 10(6) Da partially restores SF rheological properties and fibroblast-like synoviocytes (FLSs) metabolism in animal models [13]. High-MW HA inhibits phospholipase A_2 activity and thus protects phospholipid integrity [19].

Notably, HA in SF from 24 human knee joints with advanced OA was found to be shifted toward the low-MW forms, due to enzymatic cleavage of HA chains [6, 20]. In contrast, the MW distribution of HA was unaltered in SF from 5 patients with advanced OA versus 5 patients who were undergoing meniscectomy or ligament reconstruction without any evident OA [12]. The concentration of HA in human OA SF was reported to be normal [12, 20] but declines in RA [6]. Although the specific contribution of HA to overall cartilage boundary lubrication remains a topic of debate, viscosupplementation with intra-articular HA is still used often to treat OA [21, 22].

Lubricin is a large mucin-like glycoprotein that comprises 3 domains: a cysteine-rich, somatomedin B-like N-terminal domain; a mucin-like *O*-linked oligosaccharide-rich domain; and a C-terminal domain [23]. Homologs of lubricin—superficial zone protein, proteoglycan 4 (PRG4), megakaryocyte-stimulating factor precursor, and arthritis-like camptodactyly-arthropathy-coxa vara-pericarditis syndrome protein—are all encoded by *PRG4* [24].

Lubricin is synthesized and secreted by chondrocytes from the superficial zone of articular cartilage, FLSs and cells in the meniscus [24, 25] and is present in SF, where it acts as a cartilage

boundary lubricant, alone or synergistically with HA [1, 26]. Lubricin is expressed in human SF as various isoforms [27], the form that provides better boundary lubrication is unknown. SF from human knee joints with advanced OA was reported to have markedly elevated lubricin concentrations compared with normal human SF [8, 20] and a similar friction-lowering lubricating function [8, 20]. However, compared to normal the levels of lubricin can also be low in some OA SF concomitant with a diminished cartilage boundary lubricating function [7]. Lubricin has been proposed to be chondroprotective, potentially protecting articular chondrocytes against apoptosis [28].

The surface of articular cartilage was described to be hydrophobic, most likely due to the hydrophobic hydrocarbon layer that is generated by surface-active phospholipids that have attached [29, 30]. Most phospholipid species possess a zwitterionic head group, harboring a negative charge on the phosphate group and a positive charge on the amine group. Water-insoluble phospholipids was reported to contribute to a small fraction (~11%) of lubricin in SF [4]. FLSs are believed to be a biosynthetic source of phospholipids [31]; other phospholipids can diffuse from the plasma to SF or be released during cell necrosis. Our recently published lipidomic study demonstrated significantly elevated concentrations of most phospholipid species in OA and RA SF [5]. Changes in the relative distribution and levels of certain phospholipids might alter the lubricating ability of SF and modulate synovial joint inflammation [5]. However, the paucity of detailed data on the biological functions of lipid species in RA and OA underscore the necessity for further studies.

HA, phospholipids, and lubricin have been examined *in vitro* individually and in combination, and all of them mediate boundary lubrication in SF [1, 2]. Nevertheless, the SF lubricant that contributes most to boundary lubrication in healthy, OA, and RA joints remains debated [32–35]. Individual differences in the level and composition of lubricants might cause patient-specific variability in joint lubrication and thus the speed of joint deterioration.

No data exist on the collective levels of HA, lubricin, and phospholipids in SF in patients with common joint diseases, such as OA and RA. Thus, the aim of our study was to quantify lubricin, the various molecular weight forms of HA, and all phospholipid species in parallel in SF from cohorts of healthy donors, patients with early- or late-stage OA, and patients with active RA.

Methods

Synovial fluid donors

SF samples were collected from knee joints of 16 postmortem donors, 20 patients with rheumatoid arthritis (RA), and 48 patients with OA. This study was approved by the ethical review committee of the Faculty of Medicine (Justus-Liebig-University of Giessen, Germany), and all patients provided written informed consent for their donor samples to be used for research. The ethical review committee waived the need for consent to be obtained from relatives of deceased donors, based on a judicial order that allowed an autopsy to be performed and to avoid additional emotional strain on relatives.

Detailed information about the SF donors is provided in Table 1. Based on the macroscopic appearance of the 6 cartilage surfaces—patella, trochlea, and femur and tibia from the medial and lateral sides—we used the Outerbridge classification (OU) [36] to subcategorize OA patients. To estimate OU scores for the entire knee joint, the 6 individual OU scores were added up and divided by 6 to generate an average score. OA joints were categorized as early (eOA; average OU $\leq$ 2; n = 26)- or late-stage OA (lOA; average OU > 2; n = 22). RA was diagnosed per the American College of Rheumatology [37]. Active arthritis in SF of RA patients was defined

Table 1. Demographic and disease characteristics of donors.

	Postmortem donors n = 16	Patients with eOA n = 26	Patients with lOA n = 22	Patients with RA n = 20
Age	22 (20–26)	38 (26–56)	69 (53–74)	56 (49–72)
female/male	2/14	9/17	8/14	15/5
BMI	23.2 (21.2–25.0)	24.9 (23.7–28.1)	27.6 (26.1–30.4)	22.9 (24.2–32.6)
CRP	nd	0.5 (0.5–1.0)	1.5 (0.65–2.1)	9.7 (3.5–33.4)
No. of cells	nd	nd	nd	5800 (3763–12,788) cells/μl SF
DAS28	nd	nd	nd	2.63 (3.12–4.79)
Outerbridge score	nd	1.16 (0.33–1.58)	3.5 (2.5–3.6)	nd
K/L-score	nd	0 (0–1)	3 (2.75–3)	nd

Inclusion criteria: both genders, age 18–85 years, BMI <40, CRP ≤ 3 mg/L, and all CRP levels for RA. Exclusion criteria: joint infection; severe liver or kidney disease; any surgery within the last 3 months; knee joint surgery within the last 6 months; diabetes mellitus (OA); drug abuse; intra-articular treatment with hyaluronate or corticosteroid treatment within the last 3 months; HIV infection; and tumor/cancer. BMI- body mass index, CRP- C-reactive protein, DAS28- disease activity score 28, K/L-score, Kellgren-Lawrence score, nd, not determined.

doi:10.1371/journal.pone.0125192.t001

by the cell count of granulocytes (>1500/μl SF) in absence of bacteria and crystals (polarization microscopy) to exclude other forms of arthritis.

Synovial fluid samples

SF was collected from knee joints by aspiration during arthroscopy (patients with early OA cartilage damages), knee replacement surgery of late OA patients or arthrocentesis during medical exam for RA [5, 38] All SF samples were first incubated for 15 min at 37°C, passed through a 1.2-μm filter to eliminated cells and cellular debris, and centrifuged at 16,100 x *g* for 45 min at RT [5, 38]. To quench protease and phospholipase activity, 10% (v/v) inhibitor cocktail was added (PPI) [5]. The supernatants were then collected and stored at -86°C until analysis.

Level and molecular weight distribution of HA in synovial fluid

To examine HA levels in SF, samples were initially diluted 1:40,000 in 5% Tween20 in PBS (pH 7.2–7.4) and serially diluted 1:4 three times. HA concentration in human SF was measured in triplicate per dilution by sandwich ELISA (DuoSet ELISA Development kit) according to the manufacturer's instructions (R&D Systems, Minneapolis, USA). This kit contained recombinant human aggrecan to capture HA and biotinylated recombinant human aggrecan to detect bound HA using streptavidin-conjugated horseradish peroxidase. According to the information provided by the manufacturer, the HA ELISA detects low molecular weight (15–40 kDa), medium molecular weight (75–350 kDa), and high molecular weight (>950 kDa) forms of HA.

The molecular weight distribution of HA forms in human SF was determined in duplicate by horizontal 1% agarose gel electrophoresis, as described previously [7, 14]. In brief, SF samples without PPI were first treated with proteinase K (Roche Applied Science, Mannheim, Germany) overnight. The Lo-Ladder (30–500 kDa), Hi-Ladder (0.5–1.5 MDa), and Mega-Ladder (1.5–6.1 MDa; Hyalose, Oklahoma City, USA) markers were loaded in separate lanes as references.

Electrophoresis was performed at 50 V for 3 h. The gels were stained overnight using 0.005% Stains-All (Sigma-Aldrich, Taufkirchen, Germany) in 50% ethanol and destained with 10% ethanol for a minimum of 24 h. To visualize the bands better, the staining and destaining were occasionally repeated. The molecular weight distribution of HA forms according to MW markers being commercially available (<0.5, 0.5–1.1, 1.1–3.1, 3.1–6.1, >6.1 MDa) was

determined densitometrically, with automatic subtraction of background noise, using ImageJ (National Institutes of Health).

Analysis of lubricin in human synovial fluid

Lubricin (PRG4) concentration was measured in triplicate in SF that was stored with PPI using a custom sandwich ELISA method [7]. Briefly, a capture antibody against AA1356-1373 at the C-terminus of full-length PRG4 [39] was used to coat high-binding ELISA plates, followed by incubation with SF or PRG4 standards and detection with horseradish peroxidase-conjugated peanut agglutinin, which recognizes glycosylation in the mucin domain [40]. Purified PRG4 for the standard curve was prepared from culture medium that was conditioned with bovine cartilage explants, as described [1]; purified by Superose 6 size exclusion chromatography; verified with regard to purity by western blot; and quantified by BCA protein assay.

SF was digested sequentially with S. hyaluronidase (1 U/mL, 3 h at 37°C) and sialidase A-66 (overnight at 37°C) prior to quantification. Purified PRG4 standards were also treated with sialidase. SF samples, diluted 1:4, and PRG4 standard (320 μg/mL) were loaded and serially diluted (2X). If SF was diluted during aspiration from the joint and could not be loaded at 1:4 dilution, a higher dilution—up to approximately 15X—was used.

Analysis of lipids in human synovial fluid

Lipids were extracted from SF samples in the presence of internal standards (Avanti Polar Lipids, Alabaster, AL, USA) [5]. Phospholipid and sphingolipid species were quantified by electrospray ionization mass spectrometry (ESI-MS/MS) as described [5]. Lipid species were annotated according to a recently proposed shorthand nomenclature [41].

Gas chromatography

Total fatty acids (FAs) were analyzed by gas chromatography, coupled with mass spectrometry (GC-MS), as described [42]. In brief, 50 μl of SF from lOA patients was derivatized to FA methyl esters (FAMEs) in the presence of internal standards. FAMEs were separated in a highly polar BPX70 column using a GC-2010 that was coupled to a GCMS-QP2010 detector (Shimadzu, Duisburg, Germany). Quantification was performed in the selected ion monitoring mode using calibration with authentic standards.

Statistical analysis

Analysis of variance (ANOVA) was used to assess statistically significant differences between cohorts. Subsequently, confidence intervals for pairwise differences between cohorts (control, eOA, lOA, RA) were adjusted by Tukey's honestly significant difference (HSD) procedure. The statistical analysis was performed with R, version 3.1.0 using linear models of the logarithm or the logits of the response. The data were expressed as medians with interquartile ranges for the box plots. The values in the text are the medians with interquartile ranges in brackets.

Results

Level and molecular weight distribution of HA in human SF

By sandwich ELISA, as shown in Fig 1A, the concentrations of HA were highest in control SF [2.2 mg/ml (1.6–3.7 mg/ml)], whereas the levels in eOA SF [1.7 mg/ml (1.1–1.9 mg/ml), $p = 0.004$] and lOA SF [1.9 mg/ml (1.5–2.3 mg/ml), n.s.] were lower by 23.7% and 14.0%, respectively. The lowest concentrations were observed in RA SF [1.0 mg/ml (0.8–1.2 mg/ml), $p<0.001$], representing 47.1% of HA in control SF (100%).

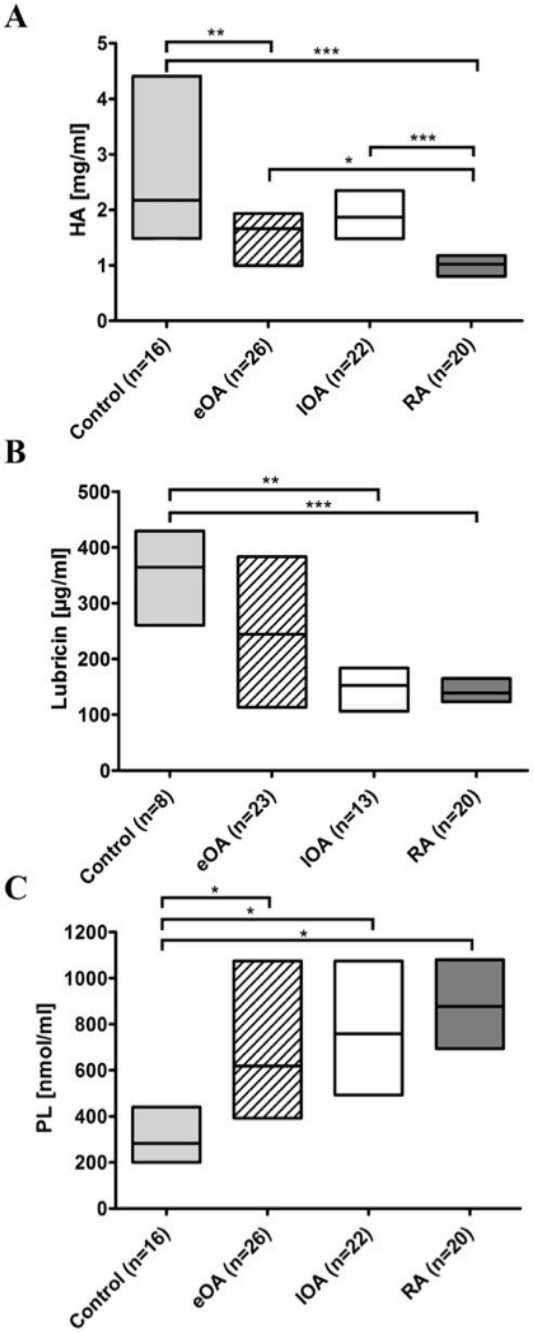

Fig 1. The concentrations of boundary lubricants in human SF. The content of HA (**A**) and lubricin (**B**) in SF were determined by ELISA, and ESI-MS/MS was used to quantify phospholipids (**C**) in 16 control SF (shaded bars), 27 eOA SF (hatched bars), 22 IOA SF (open bars), and 20 RA SF (grey bars) as described in Material and Methods. Data are presented as median with interquartile ranges. *P*-values less than 0.05 were considered statistically significant: *0.01< p≤0.05, **0.001<p≤0.01, ***p≤0.001.

doi:10.1371/journal.pone.0125192.g001

Relative HA concentration was calculated as the percentage of total HA, defined as 100%. By horizontal agarose gel electrophoresis [7, 14], compared with control SF, the MW of HA shifted toward the lower range in OA and RA SF (Fig 2A). The percentage of HA in the upper range of 3.1–6.1 MDa was highest in control SF [46.0% (39.6% to 51.2%)], followed by eOA [40.0% (28.5% to 52.7%)] and lOA SF [41.2% (32.9% to 50.7%)], and bottoming in RA SF [38.1% (21.8% to 41.8%), $p = 0.03$]. In the lower ranges of 0.5–1.1 MDa and <0.5 MDa, the relative HA concentrations were significantly higher in eOA, lOA, and RA SF versus control SF ($p<0.001$).

Lubricin content in human SF

By ELISA, the concentration of lubricin in control SF [364.4 μg/ml (305.0–404.8 μg/ml), $n = 8$)] was 1.5-fold higher than in eOA [244.5 μg/ml (119.6–381.7 μg/ml), $n = 23$] (Fig 1B). Notably, compared with control SF, the concentration of lubricin declined by 58.2% in lOA SF [152.3 μg/ml (108.2–183.9 μg/ml), $p = 0.005$] and by 61.7% in RA SF (139.4 μg/ml (124.6–162.4 μg/ml), $p<0.001$].

Levels of phospholipids in human SF

Lipids were extracted from cell- and cellular debris-free SF samples of 16 controls and 26 eOA, 22 lOA, and 20 active RA subjects and quantified by ESI-MS/MS. The content of total phospholipids in SF was calculated as the sum of the concentrations of all lipid species that contained a phosphate group. Compared with control SF [314.2 nmol/ml (247.3–487.1 nmol/ml)], the concentrations of phospholipids rose by 2.1-fold in eOA [643.8 nmol/ml (394.9–1106.5 nmol/ml), $p = 0.03$], 2.4-fold in lOA SF [758.8 nmol/ml (503.3–1009.7 nmol/ml), $p = 0.01$], and 2.8-fold in RA SF [877.7 nmol/ml (713.3–1065.0 nmol/ml), $p = 0.015$] (Fig 1C).

Correlation between lubricants

The concentrations of all lubricants were plotted against each other to examine their correlations (Fig 3); the data were analyzed by linear regression, and the slopes, 95% confidence intervals, and Pearson correlation coefficients (r) were calculated. In eOA SF, the concentrations of HA and lubricin correlated significantly ($r = 0.69$, Fig 3A, $p<0.001$). Further, in lOA SF, correlations between the levels of HA and lubricin ($r = 0.62$, Fig 3A, $p = 0.002$) and between HA and phospholipids ($r = 0.63$, Fig 3B, $p = 0.002$) were observed.

Notably, lubricin concentration and the MW distribution of HA were associated only in eOA SF [Fig 3C ($R = 0.590$, $p = 0.008$), Fig 3D ($R = 0.540$, $p = 0.02$, Fig 3E ($R = 0.486$, $p = 0.04$), and Fig 3F ($R = 0.656$, $p = 0.003$)]. Increasing percentage of degraded HA (Fig 3C–3E) corresponded to lower levels of lubricin, whereas higher percentages of high-molecular-weight HA were linked to greater concentrations of lubricin (Fig 3F).

Phospholipid classes and species in human SF

Seven lipid classes were identified in human SF: phosphatidylcholine (PC), lysophosphatidylcholine (LPC), phosphatidylethanolamine (PE), phosphatidylethanolamine-based plasmalogen (PE P), phosphatidylserine (PS), phosphatidylglycerol (PG), and sphingomyelin (SM) (Fig 2B). PC was the most predominant lipid class, constituting 52.7% to 80.8% of all lipids. The percentage of PC was lowest in SF from the control group [63.6% (60.7% to 64.7%)], increasing to 63.4% in eOA SF (61.6% to 66.9%), 69.0% in lOA SF (64.9% to 69.6%), and 72.9% in RA SF (71.9% to75.3%).

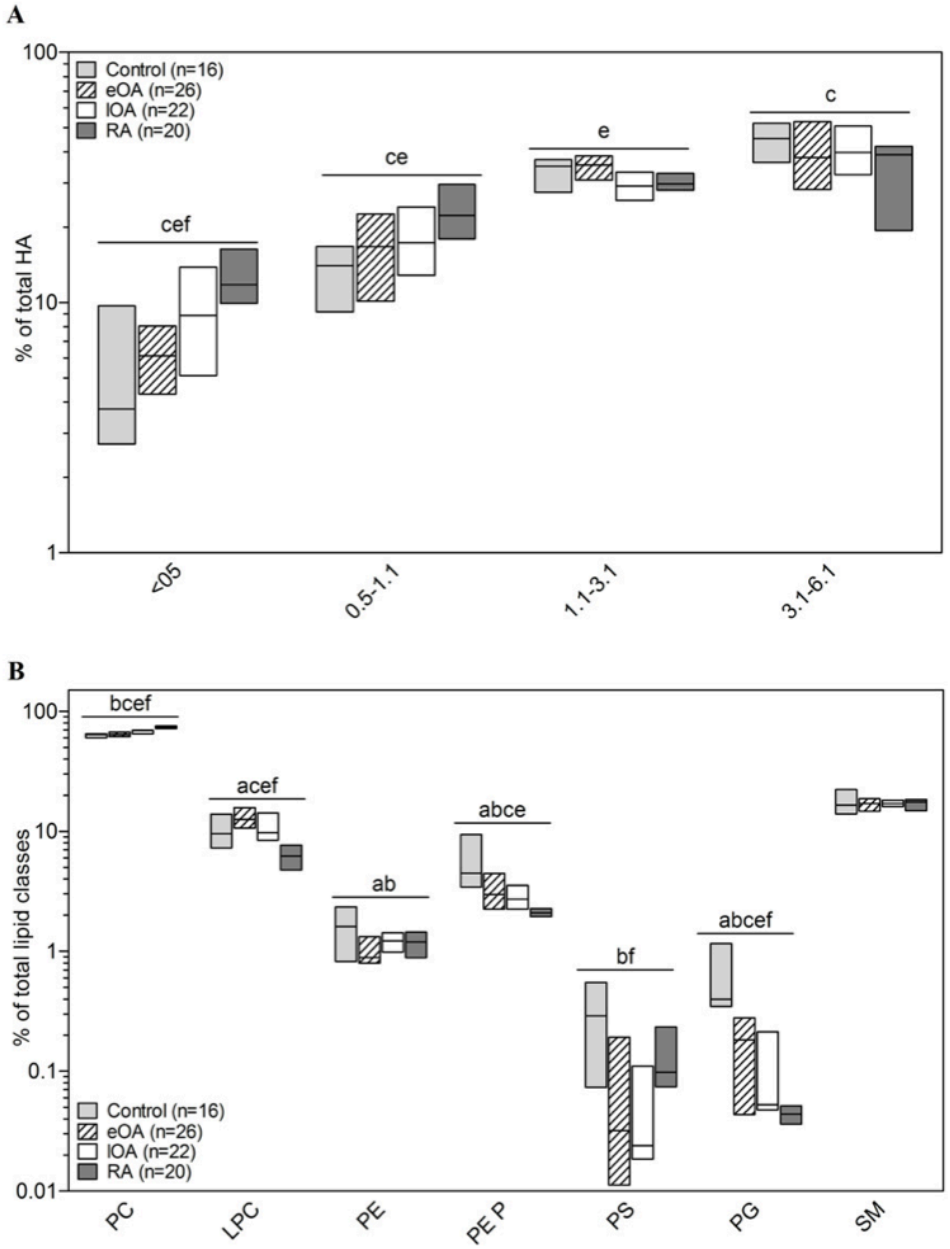

Fig 2. Characterization of hyaluronic acid (HA) and lipids in human SF. The molecular weight distribution of HA (**A**) was determined by horizontal agarose gel electrophoresis, and ESI-MS/MS was used to quantify phospholipid classes (**B**) in 16 control SF (shaded bars), 26 eOA SF (hatched bars), 22 lOA SF (open bars), and 20 RA SF (grey bars) as described in Methods. The molecular weight distribution of HA was calculated as the percentage of total HA (= 100%), whereas the relative distribution of phospholipid classes is shown as the percentage of total lipid content (= 100%). Data are presented as the median and interquartile ranges. Significance was defined as follows: a: $p \leq 0.05$: control vs. RA; b: $p \leq 0.05$: control vs. eOA; c: $p \leq 0.05$: eOA vs. late OA; and d: $p \leq 0.05$: eOA vs. RA, e: $p \leq 0.05$: eOA vs. RA; and f: $p \leq 0.05$: lOA vs. RA. The lipids that we measured were phosphatidylcholine (PC), lysophosphatidylcholine (LPC), phosphatidylethanolamine (PE), PE-based plasmalogens (PE P), phosphatidylserine (PS), phosphatidylglycerol (PG), and sphingomyelin (SM).

doi:10.1371/journal.pone.0125192.g002

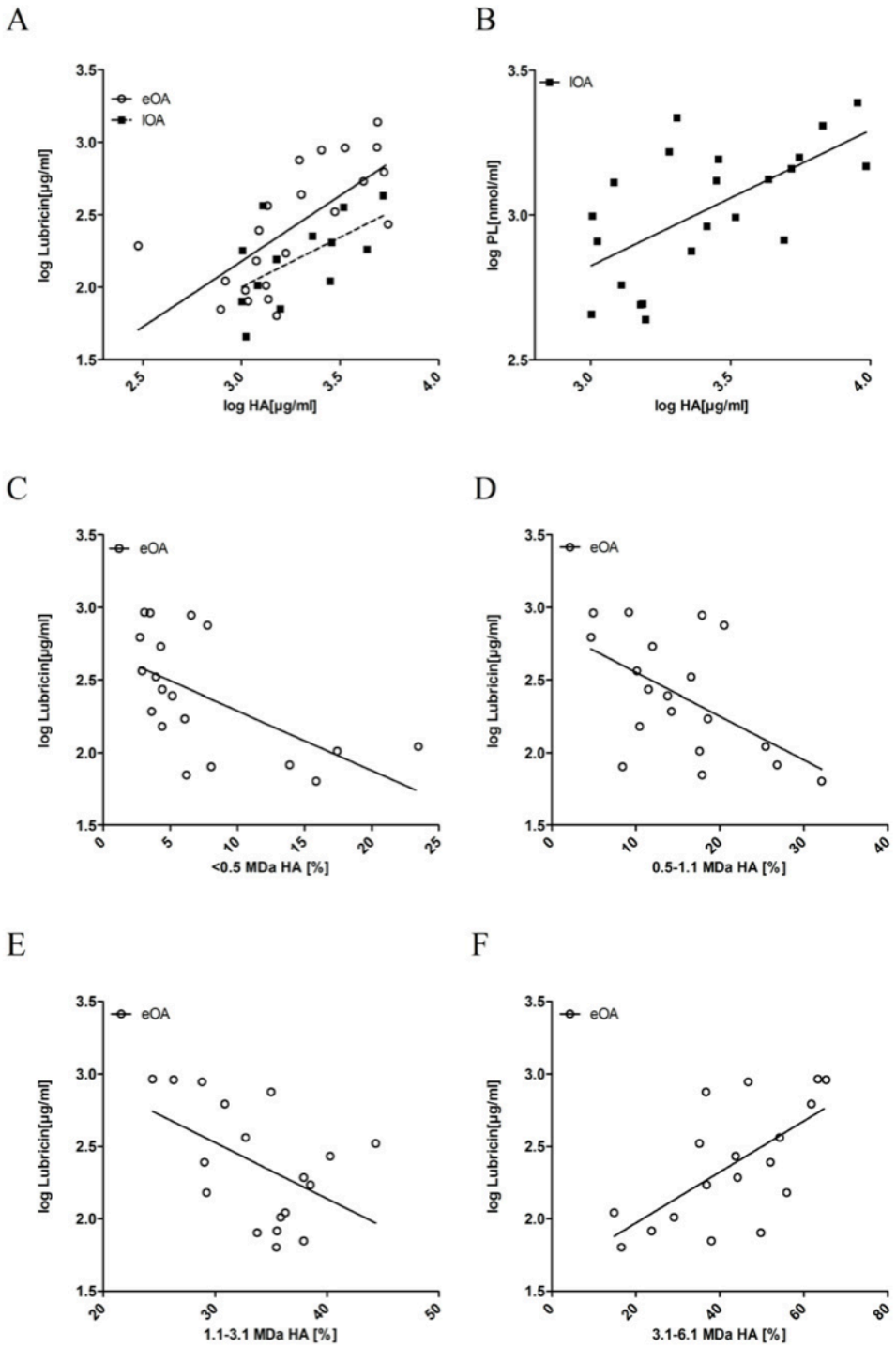
A
eOA
IOA
log Lubricin[µg/ml]
log HA[µg/ml]
B
IOA
log PL[nmol/ml]
log HA[µg/ml]
C
eOA
log Lubricin[µg/ml]
<0.5 MDa HA [%]
D
eOA
log Lubricin[µg/ml]
0.5-1.1 MDa HA [%]
E
eOA
log Lubricin[µg/ml]
1.1-3.1 MDa HA [%]
F
eOA
log Lubricin[µg/ml]
3.1-6.1 MDa HA [%]

Fig 3. Scatterplot of concentrations of hyaluronic acid (HA) by levels of lubricin (A) and phospholipids (PL) (B) and concentration of lubricin by MW distribution of HA (C-F). HA and lubricin content in SF was determined by ELISA, and ESI-MS/MS was used to quantify phospholipids in 16 control SF, 27 eOA SF, and 22 lOA SF samples as described in Methods. Molecular weight distribution of HA was calculated as the percentage of total HA (= 100%). Linear regression was performed, and Pearson correlation coefficients were calculated.

doi:10.1371/journal.pone.0125192.g003

In contrast, compared with control SF [4.8% (3.7% to 9.1%)], the percentage of PE P declined by 39.6% in eOA SF [2.9% (2.2% to 4.4%), p<0.001], 39.6% in lOA SF [2.9% (2.3% to 3.4%), p<0.001], and 56.3% in RA SF [2.1% (2.0% to 2.3%), p<0.001]. The lowest percentages of LPC were observed in control [9.0% (7.3% to 13.8%)] and RA SF [6.5 (4.8% to 7.5%)], whereas LPC percentage peaked in eOA SF [12.7% (11.1% to 15.6%) and lOA SF [10.3% (9.1% to 13.8%), p<0.001].

The 7 lipid classes in human SF comprise 124 lipid species. Figs 4 and 5 shows all 23 PC and 15 LPC species. Quantitatively, PC 34:2 was the main species in the PC class, constituting 18% to 22% of total PC. The species pattern of PC was similar between all cohorts, except for PC 30:0, PC 32:1, PC 34:1, PC 34:2 and PC 36:5. For instance, when compared with control SF [17.6% (16.3% to 19.9%)] the percentage of PC 34:1 decreased in eOA SF [15.8% (14.4% to 16.7%), p<0.001], lOA SF [14.7% (13.8% to 15.6%), p<0.001], and RA SF [13.3% (12.0% to 14.0%), p<0.001]. However, the percentage of PC 36:5 rose in eOA SF [0.72% (0.58% to 0.95%), p = 0.02], lOA [0.91% (0.83% to 1.15%), p = 0.001], and RA SF [1.01% (0.85% to 1.13%), p<0.001] versus control SF [0.62% (0.51–0.71%)] (Fig 4).

The predominant LPC species in SF was LPC 16:0, accounting for 42% to 49% of all LPCs (Fig 5). The percentages of most LPC species peaked in control SF compared with other cohorts, except for LPC 18:0, which was 1.5-fold higher in lOA SF [18.1% (17.3% to 19.7%], p<0.001] and 2-fold higher in RA SF [24.4% (23.9% to 26.1%), p<0.001] than in control SF [12.5% (11.6% to 13.0%)] (Fig 5).

The biophysical properties of lipid species depend on the fatty acid (FA) chain length and the degree of FA saturation. Thus, we calculated the relative contribution of PC and LPC species with various FA chain lengths and degrees of saturation to the total amount of PCs and LPCs (Fig 6). PC contains 2 FAs, but our mass spectrometry method only analyzed the sum of carbon atoms and double bonds in FAs.

In all cohorts, most PCs were unsaturated (Fig 6A)—7.2% of PC species in control SF, 5.1% in eOA SF, 4.1% in lOA SF, and 3.6% in RA SF were present in saturated form (p<0.001). In contrast, FAs were more saturated among LPCs (Fig 6B). Compared with control SF, [56.9% (53.4% to 58.3%)], more LPC species with saturated FAs were recorded in eOA [63.5% (59.0% to 70.7%), p<0.001], lOA [68.8% (65.3% to 70.6%), p<0.001], and RA SF [72.4% (70.2% to 75.4%), p<0.001].

Analysis of FA chain lengths revealed that more than 80% of PC species contained 36 C-atoms or less and that nearly 20% of PC species more than 36 C-atoms (Fig 6C), but these differences were not significant between cohorts. In all cohorts, approximately 90% of all LPC species had FA chain lengths with 18-C atoms or less. Moreover, versus control SF, [89.1% (86.2% to 91.5%)], the lengths of FA chains of LPC species were shorter in eOA [91.8% (90.7% to 94.0%), p<0.001], lOA [93.5% (90.3% to 94.4%), p<0.001], and RA SF [94.2% (93.2% to 94.8%), p<0.001] (Fig 6D).

In order to get an overview of the FAs in SF, total composition was determined by gas chromatography coupled to mass spectrometry (GS-MS) for 6 lOA SF samples (Fig 6E). The principal FAs were FA 16:0, FA 18:1, and FA 18:2, each of which accounted for 20–25% of total FAs. The polyunsaturated FAs constituted 13.5%. Medium long (<14 C-atoms) and very long (22–

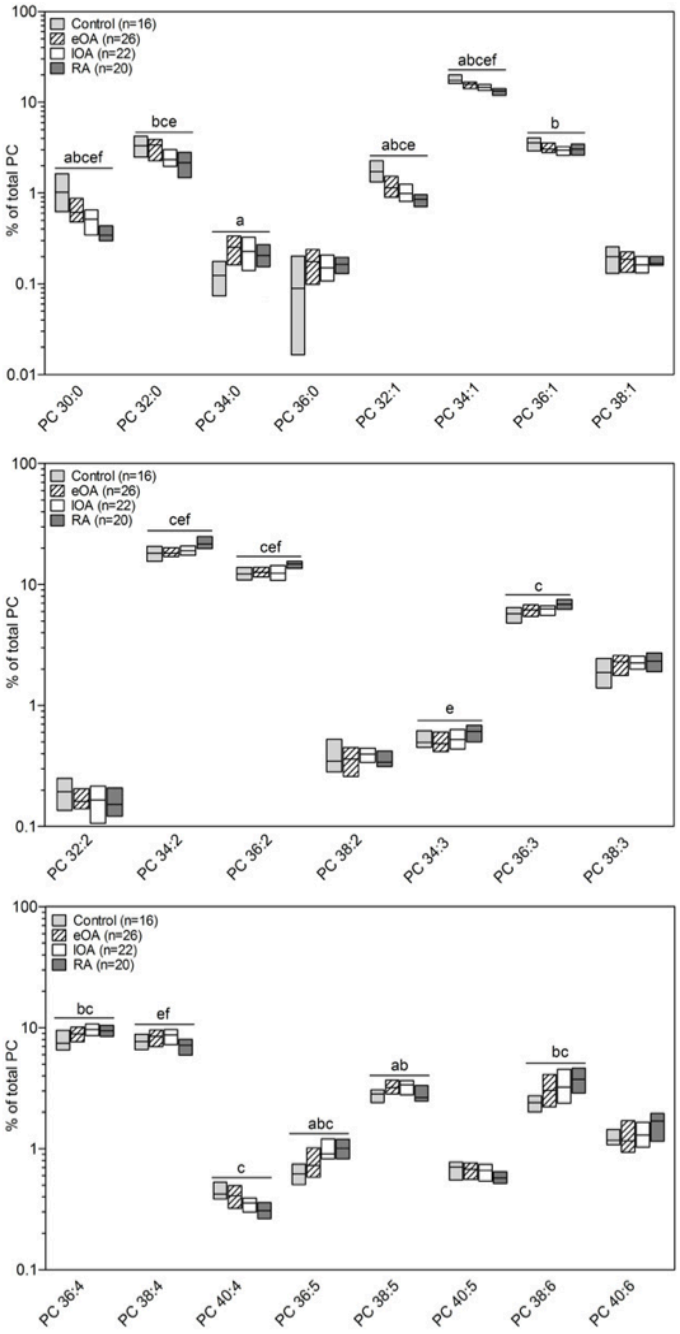

Fig 4. Percentage composition of phosphatidycholine (PC) species in human SF. PC species were quantified by ESI-MS/MS in 16 control SF (shaded bars), 27 eOA SF (hatched bars), 22 IOA SF (open bars), and 20 RA SF (grey bars) samples as described in Methods. Species were assigned based on the assumption that only FAs with an even number of carbon atoms are present. Subsequently, the percentage was calculated, defining total PC as 100%. Data are presented as the median and interquartile ranges.

Significance was defined as follows: a: $p \leq 0.05$: control vs. RA; b: $p \leq 0.05$: control vs. eOA; c: $p \leq 0.05$: eOA vs. late OA; d: $p \leq 0.05$: eOA vs. RA, e: $p \leq 0.05$: eOA vs. RA; and f: $p \leq 0.05$: lOA vs RA.

doi:10.1371/journal.pone.0125192.g004

24 C atoms) FA chains were minor FAs [1.72% (1.26% to 1.92%) and 1.69 (0.91% to 2.12%), respectively].

Lubricants and age dependency

Our cohorts differ with respect of their age (Table 1). Thus, the levels of lubricants were plotted against the age of each donor within each cohort (S1 Fig). Subsequently, linear regression was performed, and Pearson correlation coefficients were calculated. We did not find any age dependency on the levels of all three lubricants (S1 Fig, [43]). In addition, the HA MW distributions were plotted against the age. Again, our analysis revealed no correlation between the HA MW distribution in SF of our four cohorts and the age of donors (S2 Fig). We already reported that no correlation was found between the levels of PLs and the age of patients [5].

Discussion

HA, lubricin, and phospholipids contribute to cartilage boundary lubrication that is provided by SF [1, 3, 4]. However, the most important SF component in maintaining efficient joint lubrication has long been debated. This study is the first to measure the levels of HA, lubricin, and phospholipids in SF from the same cohorts of healthy donors, patients with early- and late-stage OA, and patients with active RA. Further, we have detailed the MW forms of HA, the relative distribution of phospholipid classes, the phospholipid species composition, and the degree of saturation and FA chain lengths.

OA and RA SF contained less HA and lubricin and are enriched with phospholipids. Also, the MW distribution of HA shifted toward the lower range in OA and RA SF. These results indicate that the catabolic activities in OA and RA SF are enhanced, leading to decreased levels of lubricin and high-MW HA.

The levels of lubricin vary in OA SF compared with control SF. Some studies have demonstrated lower levels of lubricin in OA and RA SF [1, 44–46], whereas others have reported opposite results [8, 20, 44]. In our study, the levels of lubricin are consistent with those of Ludwig et al., who observed that some OA SF is lubricin-deficient and has poor boundary-lubricating ability compared with healthy control SF [7]. Further, we confirmed our previous findings that phospholipid levels are elevated under pathological conditions, which might compensate for the decreased levels of HA and lubricin in SF to protect cartilage surfaces against wear [5, 43].

Several studies have attempted to characterize the components of SF, but none has determined which species is crucial for effective cartilage boundary lubrication. HA provides viscosity in SF and mediates the retention of water [9]. Lubricin has been suggested to be the most important component for cartilage boundary lubrication and has chondroprotective properties [3]. Phospholipids are believed to cover the surface of articular cartilage, where they generate a microscopically thick biofilm, contributing to cartilage boundary lubrication [4, 30]. However, the interaction between these components and their functions in cartilage boundary lubrication remain poorly understood.

Several models of cartilage boundary lubrication have been proposed. A model that was developed by Hills claims that a mono- to multilayered membrane-like structure adheres to the surface of articular cartilage, where HA and phospholipids interact and form stable complexes. HA molecules constitute a core filament that is surrounded by a bilayer of phospholipids, generating oligolamellar structures [30, 47]. Another model opines that a network of multilamellar

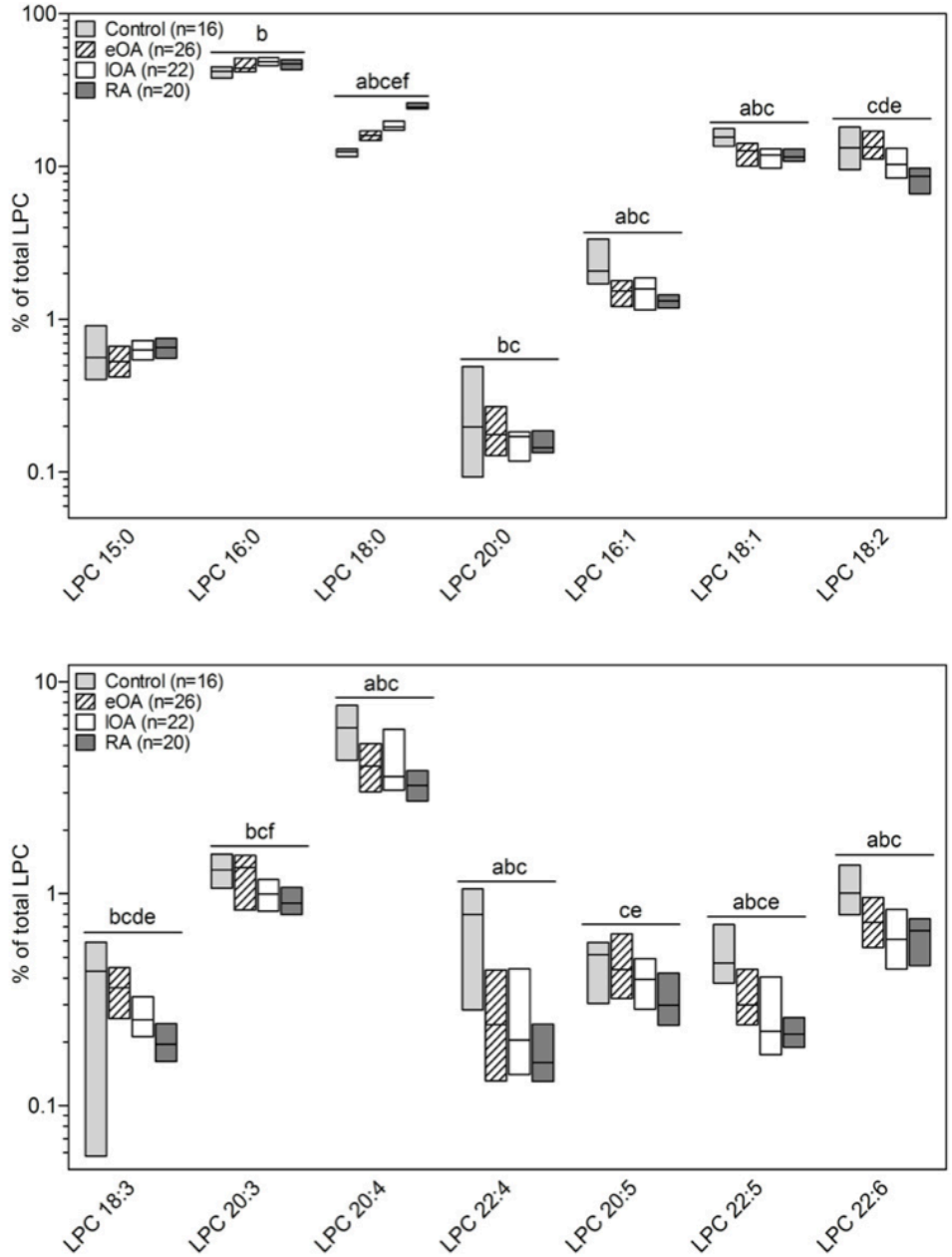

Fig 5. Percentage composition of lysophosphatidylcholine (LPC) species in human SF. PC species were quantified by ESI-MS/MS in 16 control SF (shaded bars), 27 eOA SF (hatched bars), 22 lOA SF (open bars), and 20 RA SF (grey bars) samples as described in Methods. Species were assigned based on the assumption that only FAs with an even number of carbon atoms are present. Subsequently, the percentage was calculated, defining total LPC as 100%. Data are presented as the median and interquartile ranges. Significance was defined as follows: a: $p \leq 0.05$: control vs. RA; b: $p \leq 0.05$: control vs. eOA; c: $p \leq 0.05$: eOA vs. late OA; d: $p \leq 0.05$: eOA vs. RA e: $p \leq 0.05$: eOA vs. RA; and f: $p \leq 0.05$: lOA vs RA.

doi:10.1371/journal.pone.0125192.g005

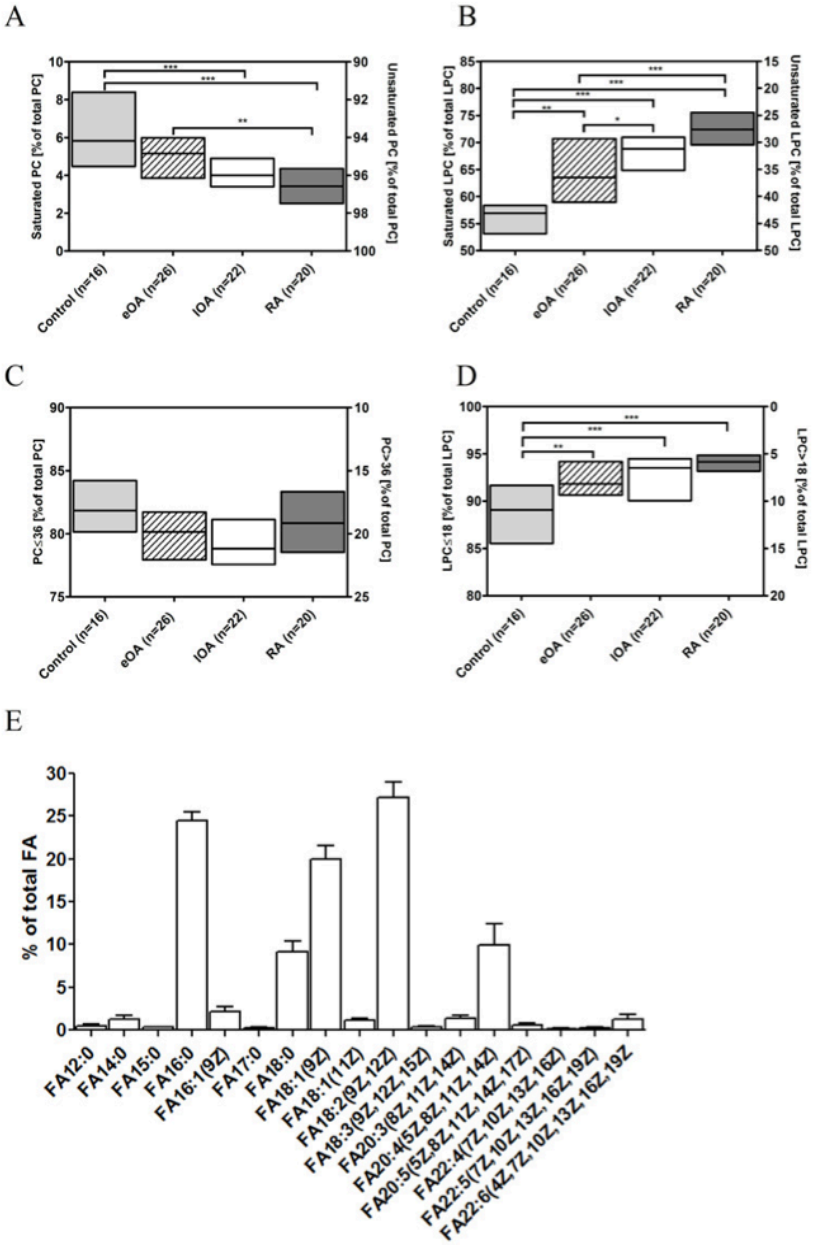

Fig 6. The degree of saturation and length of fatty acids from phosphatidylcholine (PC) and lysophosphatidylcholine (LPC). Phospholipid species were quantified by ESI-MS/MS in 16 control SF (shaded bars), 27 eOA SF (hatched bars), 22 IOA SF (open bars), and 20 RA SF (grey bars) samples as described in Methods. Subsequently, PC and LPC species were grouped by degree of saturation and number of carbon atoms in the FA chains, respectively, and calculated as a percentage of total PC and LPC, defined 100%. Composition of total FA was determined by gas chromatography for 6 IOA SF samples as described in Methods. Data are presented as median and interquartile ranges **(A-D)** or mean ± SD **(E)**. *P*-values less than 0.05 were considered statistically significant: *0.01< p≤0.05, **0.001<p≤0.01,

***p≤0.001. **A,** Relative distribution of PC species according to degree of FA saturation. **B,** Relative distribution of LPC species by degree of FA saturation. **C,** Relative distribution of PC species according to chain length of FAs. **D,** Relative distribution of LPC species by chain length of FAs. **E,** Degree of saturation and length of fatty acid of total FAs representing 100%.

doi:10.1371/journal.pone.0125192.g006

vesicles exists—by transmission electron microscopy and biotribological techniques, there are vesicular structures that comprise 3–7 lipid bilayers that encapsulated HA with seric proteins, such as albumin and y-globulin. Here lubricin functions solely to anchor this lipid layer to the articular surfaces [2]. We noted correlations between the concentrations of HA and lubricin, between the levels of HA and phospholipids, and between lubricin levels and the HA MW distribution in SF, supporting a model of tight interactions between these molecules.

The friction-reducing properties of HA at the cartilage-cartilage interface depend on the concentration and molecular weight of HA [6, 44]. High-MW HA has distinct cartilage lubricating abilities, and *in vitro* supplementation with high-MW HA is believed to partially restore the cartilage boundary lubricating function of SF [44]. We found that OA and RA SF contain significantly higher levels of small-MW HA, mitigating the impact of HA on lubrication. However, HA in the MW range of 0.5–1.1 x 10(6) Da was reported to restore SF rheological properties in animal models of OA (13).

The phospholipid organization on the surface of articular cartilage is thought to depend strictly on the MW of HA [47]. Throughout the enzymatic degradation of HA during joint inflammation and OA, a membrane-like sheet that is constructed from phospholipids is destroyed. Thus, altered MW distribution of HA can impair cartilage boundary lubrication and might also explain the elevated levels of phospholipids in OA and RA SF.

The lubricating properties of phospholipids remain poorly understood. However, the tribological properties of phospholipids depend on the molecular structure of the lipids—especially chain length and the number of double bounds. To better understand the molecular mechanisms of the lubricating abilities of phospholipids, the pattern of phospholipid species must be analyzed in details. Dipalmitoylphosphatidylcholine has been considered to be the chief phospholipid in SF, as it is in the lung [30]. However, we and other groups have shown that unsaturated forms of PC, such as dioleoylphosphatidylcholine, palmitoyloleoylphosphatidylcholine, and palmitoyllinoleoylphosphatidylcholine, are the predominant phospholipids in SF [5, 48].

Further, LPC chain length is significantly shorter in OA and RA SF compared with control SF. One study on boundary lubrication found that shorter FA chains increase the friction coefficient, whereas more extensive unsaturation reduces the friction [49]. Further studies are needed to elaborate the overall lubricating ability of these altered PC and LPC species in SF.

Conclusions

In conclusion, we have provided novel comprehensive measurements of HA, lubricin, and phospholipids levels in SF from the same cohorts of healthy donors, patients with early- and late-stage OA, and patients with RA. Our study provide insight into the detailed composition of SF, correlating the concentrations of lubricants and the alterations that occur during widespread joint diseases, which can impair the joint lubricating ability of SF. These results extend our current knowledge on cartilage boundary-lubricating molecules. Thus our study provides the framework to develop new optimal compounded lubricants able to reduce joint destruction by improved lubrication.

Supporting Information

S1 Fig. Scatterplot of lubricin and hyaluronic acid (HA) levels by the age of donors. HA and lubricin content in SF was determined by ELISA in 16 control SF **(A)**, 27 eOA SF **(B)**, 22 lOA SF **(C)**, and 20 RA SF samples **(D)** as described in Methods. Linear regression was performed, and Pearson correlation coefficients were calculated. The Pearson correlation coefficients (r) were as follow: r = -0.12 for HA and r = 0.33 for lubricin in control SF; r = -0.29 for HA and r = -0.19 for lubricin in eOA SF; r = -0.59 for HA and r = -0.45 for lubricin in lOA SF; r = 0.23 for HA and r = -0.01 for lubricin in RA SF.
(TIF)

S2 Fig. Scatterplot of the hyaluronic acid (HA) molecular weight distribution by the age of donors. HA content in SF was determined by ELISA in 16 control SF **(A)**, 27 eOA SF **(B)**, 22 lOA SF **(C)**, and 20 RA SF samples **(D)** as described in Methods. The molecular weight distribution of HA was calculated as the percentage of total HA (= 100%). Linear regression was performed, and Pearson correlation coefficients were calculated. The Pearson correlation coefficients range as follow: from -0.30 to 0.10 for control SF; from -0.10 to 0.07 for eOA SF; from -0.11 to 0.19 for lOA SF, and from -0.10 to 0.14 for RA SF.
(TIF)

Acknowledgments

The authors wish to express their sincere thanks to Anne Staubitz, Christiane Hild, and Simone Düchtel for their expert technical support and to Manuela Döller for her assistance with the study organization.

Author Contributions

Conceived and designed the experiments: TAS JS. Performed the experiments: MKK TEL GL RZ. Analyzed the data: MKK TEL GL RZ HCS JW BI TAS JS. Contributed reagents/materials/analysis tools: GL RZ HCS JW UK RBD HK BI MR GS TAS JS. Wrote the paper: MKK JS. Revised the manuscript: TEL GL RZ HCS JW UK RBD HK BI MR GS TAS.

References

1. Schmidt TA, Gastelum NS, Nguyen QT, Schumacher BL, Sah RL. Boundary lubrication of articular cartilage: role of synovial fluid constituents. Arthritis Rheum. 2007; 56: 882–891. PMID: 17328061
2. Mirea DA, Trunfio-Sfarghiu AM, Matei CI, Munteanu B, Piednoir A, Rieu JP, et al. Role of the biomolecular interactions in the structure and tribological properties of synovial fluid. Tribol Int. 2013; 16: 302–311.
3. Jay GD, Torres JR, Warman ML, Laderer MC, Breuer KS. The role of lubricin in the mechanical behavior of synovial fluid. Proc Natl Acad Sci U S A. 2007; 104: 6194–6199. PMID: 17404241
4. Schwarz IM, Hills BA. Surface-active phospholipid as the lubricating component of lubricin. Br J Rheumatol. 1998; 37: 21–26. PMID: 9487246
5. Kosinska MK, Liebisch G, Lochnit G, Wilhelm J, Klein H, Kaesser U, et al. A lipidomic study of phospholipid classes and species in human synovial fluid. Arthritis Rheum. 2013; 65: 2323–2333. doi: 10.1002/art.38053 PMID: 23784884
6. Dahl LB, Dahl IM, Engstrom-Laurent A, Granath K. Concentration and molecular weight of sodium hyaluronate in synovial fluid from patients with rheumatoid arthritis and other arthropathies. Ann Rheum Dis. 1985; 44: 817–822. PMID: 4083937
7. Ludwig TE, McAllister JR, Lun V, Wiley JP, Schmidt TA. Diminished cartilage-lubricating ability of human osteoarthritic synovial fluid deficient in proteoglycan 4: Restoration through proteoglycan 4 supplementation. Arthritis Rheum. 2012; 64: 3963–3971. doi: 10.1002/art.34674 PMID: 22933061

8. Neu CP, Reddi AH, Komvopoulos K, Schmid TM, Di Cesare PE. Increased friction coefficient and superficial zone protein expression in patients with advanced osteoarthritis. Arthritis Rheum. 2010; 62: 2680–2687. doi: 10.1002/art.27577 PMID: 20499384
9. Fraser JR, Laurent TC, Laurent UB. Hyaluronan: its nature, distribution, functions and turnover. J Intern Med. 1997; 242: 27–33. PMID: 9260563
10. Laurent TC, Laurent UB, Fraser JR. The structure and function of hyaluronan: An overview. Immunol Cell Biol. 1996; 74: A1–7. PMID: 8724014
11. Hui AY, McCarty WJ, Masuda K, Firestein GS, Sah RL. A systems biology approach to synovial joint lubrication in health, injury, and disease. Wiley Interdiscip Rev Syst Biol Med. 2012; 4: 15–37. doi: 10.1002/wsbm.157 PMID: 21826801
12. Dunn S, Kolomytkin OV, Marino AA. Pathophysiology of osteoarthritis: evidence against the viscoelastic theory. Pathobiology. 2009; 76: 322–328. doi: 10.1159/000245898 PMID: 19955844
13. Ghosh P, Guidolin D. Potential mechanism of action of intra-articular hyaluronan therapy in osteoarthritis: are the effects molecular weight dependent? Semin Arthritis Rheum. 2002; 32: 10–37. PMID: 12219318
14. Lee HG, Cowman MK. An agarose gel electrophoretic method for analysis of hyaluronan molecular weight distribution. Anal Biochem. 1994; 219: 278–287. PMID: 8080084
15. Murano E, Perin D, Khan R, Bergamin M. Hyaluronan: from biomimetic to industrial business strategy. Nat Prod Commun. 2011; 6: 555–572. PMID: 21560767
16. Dicker KT, Gurski LA, Pradhan-Bhatt S, Witt RL, Farach-Carson MC, Jia X. Hyaluronan: A simple polysaccharide with diverse biological functions. Acta Biomater. 2014; 10: 1558–1570. doi: 10.1016/j.actbio.2013.12.019 PMID: 24361428
17. Kataoka Y, Ariyoshi W, Okinaga T, Kaneuji T, Mitsugi S, Takahashi T, et al. Mechanisms involved in suppression of ADAMTS4 expression in synoviocytes by high molecular weight hyaluronic acid. Biochem Biophys Res Commun. 2013; 432: 580–585. doi: 10.1016/j.bbrc.2013.02.043 PMID: 23438438
18. Goldberg VM, Buckwalter JA. Hyaluronans in the treatment of osteoarthritis of the knee: evidence for disease-modifying activity. Osteoarthritis Cartilage. 2005; 13: 216–224. PMID: 15727888
19. Nitzan DW, Nitzan U, Dan P, Yedgar S. The role of hyaluronic acid in protecting surface-active phospholipids from lysis by exogenous phospholipase A(2). Rheumatology (Oxford). 2001; 40: 336–340. PMID: 11285383
20. Temple-Wong MM, Hansen BC, Grissom MJ. Effect of knee osteoarthritis on the boundary lubricating molecules and friction of human synovial fluid [abstract]. Trans Orthop Res Soc. 2010: 56:340.
21. Abate M, Pulcini D, Di Iorio A, Schiavone C. Viscosupplementation with intra-articular hyaluronic acid for treatment of osteoarthritis in the elderly. Curr Pharm Des. 2010; 16: 631–640. PMID: 20388073
22. Brockmeier SF, Shaffer BS. Viscosupplementation therapy for osteoarthritis. Sports Med Arthrosc. 2006; 14: 155–162. PMID: 17135962
23. Ikegawa S, Sano M, Koshizuka Y, Nakamura Y. Isolation, characterization and mapping of the mouse and human PRG4 (proteoglycan 4) genes. Cytogenet Cell Genet. 2000; 90: 291–297. PMID: 11124536
24. Jay GD, Britt DE, Cha CJ. Lubricin is a product of megakaryocyte stimulating factor gene expression by human synovial fibroblasts. J Rheumatol. 2000; 27: 594–600. PMID: 10743795
25. Schumacher BL, Block JA, Schmid TM, Aydelotte MB, Kuettner KE. A novel proteoglycan synthesized and secreted by chondrocytes of the superficial zone of articular cartilage. Arch Biochem Biophys. 1994; 311: 144–152. PMID: 8185311
26. Jay GD, Torres JR, Rhee DK, Helminen HJ, Hytinnen MM, Cha CJ, et al. Association between friction and wear in diarthrodial joints lacking lubricin. Arthritis Rheum. 2007; 56: 3662–3669. PMID: 17968947
27. Lord MS, Estrella RP, Chuang CY, Youssef P, Karlsson NG, Flannery CR, et al. Not all lubricin isoforms are substituted with a glycosaminoglycan chain. Connect Tissue Res. 2012; 53: 132–141. doi: 10.3109/03008207.2011.614364 PMID: 21966936
28. Waller KA, Zhang LX, Elsaid KA, Fleming BC, Warman ML, Jay GD. Role of lubricin and boundary lubrication in the prevention of chondrocyte apoptosis. Proc Natl Acad Sci U S A. 2013; 110: 5852–5857. doi: 10.1073/pnas.1219289110 PMID: 23530215
29. Sarma AV, Powell GL, LaBerge M. Phospholipid composition of articular cartilage boundary lubricant. J Orthop Res. 2001; 19: 671–676. PMID: 11518278
30. Hills BA, Crawford RW. Normal and prosthetic synovial joints are lubricated by surface-active phospholipid: a hypothesis. J Arthroplasty. 2003; 18: 499–505. PMID: 12820095
31. Schwarz IM, Hills BA. Synovial surfactant: lamellar bodies in type B synoviocytes and proteolipid in synovial fluid and the articular lining. Br J Rheumatol. 1996; 35: 821–827. PMID: 8810664

32. Sun Y, Chen MY, Zhao C, An KN, Amadio PC. The effect of hyaluronidase, phospholipase, lipid solvent and trypsin on the lubrication of canine flexor digitorum profundus tendon. J Orthop Res. 2008; 26: 1225–1229. doi: 10.1002/jor.20624 PMID: 18404658

33. Jay GD, Cha CJ. The effect of phospholipase digestion upon the boundary lubricating ability of synovial fluid. J Rheumatol. 1999; 26: 2454–2457. PMID: 10555909

34. Hills BA, Monds MK. Enzymatic identification of the load-bearing boundary lubricant in the joint. Br J Rheumatol. 1998; 37: 137–142. PMID: 9569067

35. Hills BA. Identity of the joint lubricant. J Rheumatol. 2002; 29: 200–201. PMID: 11824962

36. Outerbridge RE. The etiology of chondromalacia patellae. J Bone Joint Surg Br. 1961; 43-B: 752–757. PMID: 14038135

37. Arnett FC, Edworthy SM, Bloch DA, McShane DJ, Fries JF, Cooper NS, et al. The American Rheumatism Association 1987 revised criteria for the classification of rheumatoid arthritis. Arthritis Rheum. 1988; 31: 315–324. PMID: 3358796

38. Scanzello CR, Umoh E, Pessler F, Diaz-Torne C, Miles T, Dicarlo E, et al. Local cytokine profiles in knee osteoarthritis: elevated synovial fluid interleukin-15 differentiates early from end-stage disease. Osteoarthritis Cartilage. 2009; 17: 1040–1048. doi: 10.1016/j.joca.2009.02.011 PMID: 19289234

39. Schmidt TA, Plaas AH, Sandy JD. Disulfide-bonded multimers of proteoglycan 4 (PRG4) are present in normal synovial fluids. Biochim Biophys Acta. 2009; 1790: 375–384. doi: 10.1016/j.bbagen.2009.03.016 PMID: 19332105

40. Estrella RP WJ, Packer NH et al. The glycosylation of human synovial lubricin: implications for its role in inflammation. Biochem J. 2010; 429: 359–367. doi: 10.1042/BJ20100360 PMID: 20443780

41. Liebisch G, Vizcaino JA, Kofeler H, Trotzmuller M, Griffiths WJ, Schmitz G, et al. Shorthand notation for lipid structures derived from mass spectrometry. J Lipid Res. 2013; 54: 1523–1530. doi: 10.1194/jlr.M033506 PMID: 23549332

42. Ecker J, Scherer M, Schmitz G, Liebisch G. A rapid GC-MS method for quantification of positional and geometric isomers of fatty acid methyl esters. J Chromatogr B Analyt Technol Biomed Life Sci. 2012; 897: 98–104. doi: 10.1016/j.jchromb.2012.04.015 PMID: 22542399

43. Kosinska MK, Liebisch G, Lochnit G, Wilhelm J, Klein H, Kaesser U, et al. Sphingolipids in human synovial fluid-a lipidomic study. PloS One. 2014; 9: e91769. doi: 10.1371/journal.pone.0091769 PMID: 24646942

44. Antonacci JM, Schmidt TA, Serventi LA, Cai MZ, Shu YL, Schumacher BL, et al. Effects of equine joint injury on boundary lubrication of articular cartilage by synovial fluid: role of hyaluronan. Arthritis Rheum. 2012; 64: 2917–2926. doi: 10.1002/art.34520 PMID: 22605527

45. Elsaid KA, Jay GD, Chichester CO. Reduced expression and proteolytic susceptibility of lubricin/superficial zone protein may explain early elevation in the coefficient of friction in the joints of rats with antigen-induced arthritis. Arthritis Rheum. 2007; 56: 108–116. PMID: 17195213

46. Barton KI, Ludwig TE, Achari Y, Shrive NG, Frank CB, Schmidt TA. Characterization of proteoglycan 4 and hyaluronan composition and lubrication function of ovine synovial fluid following knee surgery. J Orthop Res. 2013; 31: 1549–1554. doi: 10.1002/jor.22399 PMID: 23722645

47. Pasquali-Ronchetti I, Quaglino D, Mori G, Bacchelli B, Ghosh P. Hyaluronan-phospholipid interactions. J Struct Biol. 1997; 120: 1–10. PMID: 9356287

48. Chen Y, Crawford RW, Oloyede A. Unsaturated phosphatidylcholines lining on the surface of cartilage and its possible physiological roles. J Orthop Surg Res. 2007; 2: 14. PMID: 17718898

49. Trunfio-Sfarghiu AM, Berthier Y, Meurisse MH, Rieu JP. Role of nanomechanical properties in the tribological performance of phospholipid biomimetic surfaces. Langmuir. 2008; 24: 8765–8771. doi: 10.1021/la8005234 PMID: 18620439

References

1 Varaldo, P. E., Biavasco, F., Mannelli, S., Pompei, R. & Proietti, A. Distribution and antibiotic susceptibility of extraintestinal clinical isolates of Klebsiella, Enterobacter and Serratia species. *European journal of clinical microbiology & infectious diseases : official publication of the European Society of Clinical Microbiology* **7**, 495-500 (1988).

2 Bagley, S. T. Habitat association of Klebsiella species. *Infection control : IC* **6**, 52-58 (1985).

3 Kohler, W. & Mochmann, H. [Carl Friedlander (1847-1887) and the discovery of the Pneumococcus--in memory of the centenary of his death]. *Zeitschrift fur arztliche Fortbildung* **81**, 615-618 (1987).

4 Podschun, R. & Ullmann, U. Klebsiella spp. as nosocomial pathogens: epidemiology, taxonomy, typing methods, and pathogenicity factors. *Clinical microbiology reviews* **11**, 589-603 (1998).

5 Broberg, C. A., Palacios, M. & Miller, V. L. Klebsiella: a long way to go towards understanding this enigmatic jet-setter. *F1000prime reports* **6**, 64, doi:10.12703/P6-64 (2014).

6 Carpenter, J. L. Klebsiella pulmonary infections: occurrence at one medical center and review. *Reviews of infectious diseases* **12**, 672-682 (1990).

7 Emori, T. G. & Gaynes, R. P. An overview of nosocomial infections, including the role of the microbiology laboratory. *Clinical microbiology reviews* **6**, 428-442 (1993).

8 Munoz-Price, L. S. *et al.* Clinical epidemiology of the global expansion of Klebsiella pneumoniae carbapenemases. *The Lancet. Infectious diseases* **13**, 785-796, doi:10.1016/S1473-3099(13)70190-7 (2013).

9 Yigit, H. *et al.* Novel carbapenem-hydrolyzing beta-lactamase, KPC-1, from a carbapenem-resistant strain of Klebsiella pneumoniae. *Antimicrobial agents and chemotherapy* **45**, 1151-1161, doi:10.1128/AAC.45.4.1151-1161.2001 (2001).

10 Borer, A. *et al.* Attributable mortality rate for carbapenem-resistant Klebsiella pneumoniae bacteremia. *Infection control and hospital epidemiology* **30**, 972-976, doi:10.1086/605922 (2009).

11 Patel, G., Huprikar, S., Factor, S. H., Jenkins, S. G. & Calfee, D. P. Outcomes of carbapenem-resistant Klebsiella pneumoniae infection and the impact of antimicrobial and adjunctive therapies. *Infection control and hospital epidemiology* **29**, 1099-1106, doi:10.1086/592412 (2008).

12 Wilson, J. W. *et al.* Mechanisms of bacterial pathogenicity. *Postgraduate medical journal* **78**, 216-224 (2002).

13 Rietschel, E. T. *et al.* Lipid A, the endotoxic center of bacterial lipopolysaccharides: relation of chemical structure to biological activity. *Progress in clinical and biological research* **231**, 25-53 (1987).

14 Cortes, G. *et al.* Molecular analysis of the contribution of the capsular polysaccharide and the lipopolysaccharide O side chain to the virulence of Klebsiella pneumoniae in a murine model of pneumonia. *Infection and immunity* **70**, 2583-2590 (2002).

15 Shankar-Sinha, S. *et al.* The Klebsiella pneumoniae O antigen contributes to bacteremia and lethality during murine pneumonia. *Infection and immunity* **72**, 1423-1430 (2004).

16 Lugo, J. Z. *et al.* Lipopolysaccharide O-antigen promotes persistent murine bacteremia. *Shock* **27**, 186-191, doi:10.1097/01.shk.0000238058.23837.21 (2007).

17 Alberti, S. *et al.* Development of an enzyme-linked immunosorbent assay method for typing and quantitation of Klebsiella pneumoniae lipopolysaccharide: application to serotype O1. *Journal of clinical microbiology* **31**, 1379-1381 (1993).

18 Hansen, D. S. *et al.* Klebsiella pneumoniae lipopolysaccharide O typing: revision of prototype strains and O-group distribution among clinical isolates from different sources and countries. *Journal of clinical microbiology* **37**, 56-62 (1999).

19 Tomas, J. M., Camprubi, S., Merino, S., Davey, M. R. & Williams, P. Surface exposure of O1 serotype lipopolysaccharide in Klebsiella pneumoniae strains expressing different K antigens. *Infection and immunity* **59**, 2006-2011 (1991).

20 Szabo, M., Bronner, D. & Whitfield, C. Relationships between rfb gene clusters required for biosynthesis of identical D-galactose-containing O antigens in Klebsiella pneumoniae serotype O1 and Serratia marcescens serotype O16. *Journal of bacteriology* **177**, 1544-1553 (1995).

21 Kelly, R. F. *et al.* Structural variation in the O-specific polysaccharides of Klebsiella pneumoniae serotype O1 and O8 lipopolysaccharide: evidence for clonal diversity in rfb genes. *Molecular microbiology* **10**, 615-625 (1993).

22 Whitfield, C., Richards, J. C., Perry, M. B., Clarke, B. R. & MacLean, L. L. Expression of two structurally distinct D-galactan O antigens in the lipopolysaccharide of Klebsiella pneumoniae serotype O1. *Journal of bacteriology* **173**, 1420-1431 (1991).

23 Krylov, V. B. *et al.* Pyranoside-into-furanoside rearrangement: new reaction in carbohydrate chemistry and its application in oligosaccharide synthesis. *Chemistry* **20**, 16516-16522, doi:10.1002/chem.201405083 (2014).

24 Poinsot, V., Carpéné, M. A. & Couderc, F. *Coupled Mass Spectrometric Strategies for the Determination of Carbohydrates at Very Low Concentrations: The Case of Polysaccharides Involved in the Molecular Dialogue Between Plants and Rhizobia*. (2012).

25 Proctor, V. A. & Cunningham, F. E. The chemistry of lysozyme and its use as a food preservative and a pharmaceutical. *Critical reviews in food science and nutrition* **26**, 359-395, doi:10.1080/10408398809527473 (1988).

26 Callewaert, L. & Michiels, C. W. Lysozymes in the animal kingdom. *Journal of biosciences* **35**, 127-160 (2010).

27 Song, H., Inaka, K., Maenaka, K. & Matsushima, M. Structural changes of active site cleft and different saccharide binding modes in human lysozyme co-crystallized with hexa-N-acetyl-chitohexaose at pH 4.0. *Journal of molecular biology* **244**, 522-540, doi:10.1006/jmbi.1994.1750 (1994).

28 Blake, C. C. *et al.* Structure of hen egg-white lysozyme. A three-dimensional Fourier synthesis at 2 Angstrom resolution. *Nature* **206**, 757-761 (1965).

29 Smith, L. J., Sutcliffe, M. J., Redfield, C. & Dobson, C. M. Structure of hen lysozyme in solution. *Journal of molecular biology* **229**, 930-944, doi:10.1006/jmbi.1993.1097 (1993).

30 Chipman, D. M. & Sharon, N. Mechanism of lysozyme action. *Science* **165**, 454-465 (1969).

31 Vocadlo, D. J., Davies, G. J., Laine, R. & Withers, S. G. Catalysis by hen egg-white lysozyme proceeds via a covalent intermediate. *Nature* **412**, 835-838, doi:10.1038/35090602 (2001).

32 Kuramitsu, S., Ikeda, K., Hamaguchi, K., Fujio, H. & Amano, T. Ionization constants of Glu 35 and Asp 52 in hen, turkey, and human lysozymes. *J Biochem* **76**, 671-683 (1974).

33 Velankar, S. *et al.* PDBe: Protein Data Bank in Europe. *Nucleic acids research* **40**, D445-452, doi:10.1093/nar/gkr998 (2012).

34 Wu, L. Unveiling biomacromolecule interactions, NMR and optical spectroscopy studies on ligand binding to DNA and lysozyme, Department of Chemical and Biological Engineering. Chalmers University of Technology. *Thesis for the degree of doctor of philosophy* (2013).

35 Young, A. C., Tilton, R. F. & Dewan, J. C. Thermal expansion of hen egg-white lysozyme. Comparison of the 1.9 A resolution structures of the tetragonal form of the enzyme at 100 K and 298 K. *Journal of molecular biology* **235**, 302-317 (1994).

36 Refaee, M., Tezuka, T., Akasaka, K. & Williamson, M. P. Pressure-dependent changes in the solution structure of hen egg-white lysozyme. *Journal of molecular biology* **327**, 857-865 (2003).

37 Mine, S., Ueda, T., Hashimoto, Y. & Imoto, T. Analysis of the internal motion of free and ligand-bound human lysozyme by use of 15N NMR relaxation measurement: a comparison with those of hen lysozyme. *Protein Sci* **9**, 1669-1684, doi:10.1110/ps.9.9.1669 (2000).

38 Kumeta, H. *et al.* Low-temperature-induced structural changes in human lysozyme elucidated by three-dimensional NMR spectroscopy. *Biochemistry* **42**, 1209-1216, doi:10.1021/bi026730w (2003).

39 Xue, M. & Findenegg, G. H. Lysozyme as a pH-responsive valve for the controlled release of guest molecules from mesoporous silica. *Langmuir : the ACS journal of surfaces and colloids* **28**, 17578-17584, doi:10.1021/la304152j (2012).

40 Markart, P., Korfhagen, T. R., Weaver, T. E. & Akinbi, H. T. Mouse lysozyme M is important in pulmonary host defense against Klebsiella pneumoniae infection. *American journal of respiratory and critical care medicine* **169**, 454-458, doi:10.1164/rccm.200305-669OC (2004).

41 Ivanovska, N., Georgieva, P. & Barot-Ciorbaru, R. Correlation between inhibited alternative complement activity and the protective effect induced by Nocardia lysozyme digest (NLD) during Klebsiella pneumoniae infection in mice. *International journal of immunopharmacology* **18**, 515-519 (1996).

42 Jolles, Z. E. & Morgan, W. T. The isolation of small quantities of glucosamine and chondrosamine. *The Biochemical journal* **34**, 1183-1190 (1940).

43 Schauer, R. Sialic acids: fascinating sugars in higher animals and man. *Zoology (Jena)* **107**, 49-64, doi:10.1016/j.zool.2003.10.002 (2004).

44 Schauer, R. Victor Ginsburg's influence on my research of the role of sialic acids in biological recognition. *Archives of biochemistry and biophysics* **426**, 132-141, doi:10.1016/j.abb.2004.03.008 (2004).

45 Angata, T. & Varki, A. Chemical diversity in the sialic acids and related alpha-keto acids: an evolutionary perspective. *Chemical reviews* **102**, 439-469 (2002).

46 Li, Y. T., Maskos, K., Chou, C. W., Cole, R. B. & Li, S. C. Presence of an unusual GM2 derivative, taurine-conjugated GM2, in Tay-Sachs brain. *The Journal of biological chemistry* **278**, 35286-35291, doi:10.1074/jbc.M306126200 (2003).

47 Wang, B. & Brand-Miller, J. The role and potential of sialic acid in human nutrition. *European journal of clinical nutrition* **57**, 1351-1369, doi:10.1038/sj.ejcn.1601704 (2003).

48 Mandal, C. Sialic acid binding lectins. *Experientia* **46**, 433-441 (1990).

49 Lehmann, F., Tiralongo, E. & Tiralongo, J. Sialic acid-specific lectins: occurrence, specificity and function. *Cellular and molecular life sciences : CMLS* **63**, 1331-1354, doi:10.1007/s00018-005-5589-y (2006).

50 Barry, G. T. & Goebel, W. F. Colominic acid, a substance of bacterial origin related to sialic acid. *Nature* **179**, 206 (1957).

51 Wallace, A. C., Laskowski, R. A. & Thornton, J. M. LIGPLOT: a program to generate schematic diagrams of protein-ligand interactions. *Protein engineering* **8**, 127-134 (1995).

52 Seifert, A., Glanz, D., Glaubitz, N., Horstkorte, R. & Bork, K. Polysialylation of the neural cell adhesion molecule: interfering with polysialylation and migration in neuroblastoma cells. *Archives of biochemistry and biophysics* **524**, 56-63, doi:10.1016/j.abb.2012.04.011 (2012).

53 Petridis, A. K., Wedderkopp, H., Hugo, H. H. & Maximilian Mehdorn, H. Polysialic acid overexpression in malignant astrocytomas. *Acta neurochirurgica* **151**, 601-603; discussion 603-604, doi:10.1007/s00701-009-0324-3 (2009).

54 Petridis, A. K., El-Maarouf, A. & Rutishauser, U. Polysialic acid regulates cell contact-dependent neuronal differentiation of progenitor cells from the subventricular zone. *Developmental dynamics : an official publication of the American Association of Anatomists* **230**, 675-684, doi:10.1002/dvdy.20094 (2004).

55 Miyahara, R. *et al.* Expression of neural cell adhesion molecules (polysialylated form of neural cell adhesion molecule and L1-cell adhesion molecule) on resected small cell lung cancer specimens: in relation to proliferation state. *Journal of surgical oncology* **77**, 49-54 (2001).

56 Gluer, S., Schelp, C., Gerardy-Schahn, R. & von Schweinitz, D. Polysialylated neural cell adhesion molecule as a marker for differential diagnosis in pediatric tumors. *Journal of pediatric surgery* **33**, 1516-1520 (1998).

57 Gluer, S. *et al.* Serum polysialylated neural cell adhesion molecule in childhood neuroblastoma. *British journal of cancer* **78**, 106-110 (1998).

58 Suzuki, M. *et al.* Polysialic acid facilitates tumor invasion by glioma cells. *Glycobiology* **15**, 887-894, doi:10.1093/glycob/cwi071 (2005).

59 Amoureux, M. C. *et al.* Polysialic acid neural cell adhesion molecule (PSA-NCAM) is an adverse prognosis factor in glioblastoma, and regulates olig2 expression in glioma cell lines. *BMC cancer* **10**, 91, doi:10.1186/1471-2407-10-91 (2010).

60 Simon, P. *et al.* Polysialic acid is present in mammalian semen as a post-translational modification of the neural cell adhesion molecule NCAM and the polysialyltransferase ST8SiaII. *The Journal of biological chemistry* **288**, 18825-18833, doi:10.1074/jbc.M113.451112 (2013).

61 Ulm, C. *et al.* Soluble polysialylated NCAM: a novel player of the innate immune system in the lung. *Cellular and molecular life sciences : CMLS* **70**, 3695-3708, doi:10.1007/s00018-013-1342-0 (2013).

62 Mishra, B. *et al.* Functional role of the interaction between polysialic acid and extracellular histone H1. *The Journal of neuroscience : the official journal of the Society for Neuroscience* **30**, 12400-12413, doi:10.1523/JNEUROSCI.6407-09.2010 (2010).

63 Chen, X. & Varki, A. Advances in the biology and chemistry of sialic acids. *ACS chemical biology* **5**, 163-176, doi:10.1021/cb900266r (2010).

64 Neu, U., Bauer, J. & Stehle, T. Viruses and sialic acids: rules of engagement. *Current opinion in structural biology* **21**, 610-618, doi:10.1016/j.sbi.2011.08.009 (2011).

65 Ramachandraiah, G. & Chandra, N. R. Sequence and structural determinants of mannose recognition. *Proteins* **39**, 358-364 (2000).

66 Gruner, S. A., Locardi, E., Lohof, E. & Kessler, H. Carbohydrate-based mimetics in drug design: sugar amino acids and carbohydrate scaffolds. *Chemical reviews* **102**, 491-514 (2002).

67 Bhagavat, R. & Chandra, N. Common recognition principles across diverse sequence and structural families of sialic acid binding proteins. *Glycobiology* **24**, 5-16, doi:10.1093/glycob/cwt063 (2014).

68 Schauer, R. Sialic acids as regulators of molecular and cellular interactions. *Current opinion in structural biology* **19**, 507-514, doi:10.1016/j.sbi.2009.06.003 (2009).

69 Battistel, M. D., Shangold, M., Trinh, L., Shiloach, J. & Freedberg, D. I. Evidence for helical structure in a tetramer of alpha2-8 sialic acid: unveiling a structural antigen. *Journal of the American Chemical Society* **134**, 10717-10720, doi:10.1021/ja300624j (2012).

70 Sato, C. & Kitajima, K. Impact of structural aberrancy of polysialic acid and its synthetic enzyme ST8SIA2 in schizophrenia. *Frontiers in cellular neuroscience* **7**, 61, doi:10.3389/fncel.2013.00061 (2013).

71 Rollenhagen, M. *et al.* Polysialylation of the synaptic cell adhesion molecule 1 (SynCAM 1) depends exclusively on the polysialyltransferase ST8SiaII in vivo. *The Journal of biological chemistry* **287**, 35170-35180, doi:10.1074/jbc.M112.375642 (2012).

72 Hildebrandt, H. & Dityatev, A. Polysialic Acid in Brain Development and Synaptic Plasticity. *Topics in current chemistry* **366**, 55-96, doi:10.1007/128_2013_446 (2015).

73 Suzuki, Y. Sialobiology of influenza: molecular mechanism of host range variation of influenza viruses. *Biological & pharmaceutical bulletin* **28**, 399-408 (2005).

74 Fraser, J. R., Laurent, T. C. & Laurent, U. B. Hyaluronan: its nature, distribution, functions and turnover. *Journal of internal medicine* **242**, 27-33 (1997).

75 Laurent, T. C., Laurent, U. B. & Fraser, J. R. The structure and function of hyaluronan: An overview. *Immunology and cell biology* **74**, A1-7, doi:10.1038/icb.1996.32 (1996).

76 Hui, A. Y., McCarty, W. J., Masuda, K., Firestein, G. S. & Sah, R. L. A systems biology approach to synovial joint lubrication in health, injury, and disease. *Wiley interdisciplinary reviews. Systems biology and medicine* **4**, 15-37, doi:10.1002/wsbm.157 (2012).

77 Dicker, K. T. *et al.* Hyaluronan: a simple polysaccharide with diverse biological functions. *Acta biomaterialia* **10**, 1558-1570, doi:10.1016/j.actbio.2013.12.019 (2014).

78 Kataoka, Y. *et al.* Mechanisms involved in suppression of ADAMTS4 expression in synoviocytes by high molecular weight hyaluronic acid. *Biochemical and biophysical research communications* **432**, 580-585, doi:10.1016/j.bbrc.2013.02.043 (2013).

79 Goldberg, V. M. & Buckwalter, J. A. Hyaluronans in the treatment of osteoarthritis of the knee: evidence for disease-modifying activity. *Osteoarthritis and cartilage / OARS, Osteoarthritis Research Society* **13**, 216-224, doi:10.1016/j.joca.2004.11.010 (2005).

80 Dunn, S., Kolomytkin, O. V. & Marino, A. A. Pathophysiology of osteoarthritis: evidence against the viscoelastic theory. *Pathobiology : journal of immunopathology, molecular and cellular biology* **76**, 322-328, doi:10.1159/000245898 (2009).

81 Ghosh, P. & Guidolin, D. Potential mechanism of action of intra-articular hyaluronan therapy in osteoarthritis: are the effects molecular weight dependent? *Seminars in arthritis and rheumatism* **32**, 10-37 (2002).

82 Lee, H. G. & Cowman, M. K. An agarose gel electrophoretic method for analysis of hyaluronan molecular weight distribution. *Analytical biochemistry* **219**, 278-287, doi:10.1006/abio.1994.1267 (1994).

83 Saari, H., Konttinen, Y. T., Friman, C. & Sorsa, T. Differential effects of reactive oxygen species on native synovial fluid and purified human umbilical cord hyaluronate. *Inflammation* **17**, 403-415 (1993).

84 Dahl, L. B., Dahl, I. M., Engstrom-Laurent, A. & Granath, K. Concentration and molecular weight of sodium hyaluronate in synovial fluid from patients with rheumatoid arthritis and other arthropathies. *Annals of the rheumatic diseases* **44**, 817-822 (1985).

85 Schneider, C. A., Rasband, W. S. & Eliceiri, K. W. NIH Image to ImageJ: 25 years of image analysis. *Nature methods* **9**, 671-675 (2012).

86 Collins, T. J. ImageJ for microscopy. *BioTechniques* **43**, 25-30 (2007).

Acknowledgements

First of all, I would like to express my sincere gratitude to my supervisor Prof. Dr. Axel Scheidig for his guidance and support during all my studies making the preparation and accomplishment of the present thesis possible.

I gratefully thank my co-supervisors Prof. Dr. Dr. habil. Hans-Christian Siebert and Prof. Dr. med. Dipl. Biochem. Roland Schauer for their understanding, patience, outstanding scientific support, as well as thoughtful discussions. I also appreciate their corrections of my manuscripts and work, most importantly, their invaluable help and advice in getting my PhD graduate career started and providing me with an excellent atmosphere for doing research. With their instruction, this project could have reached the present results.

I thank the Roland und Elfriede Schauer-Stiftung (Stifterverband für die Deutsche Wissenschaft e.V.) for providing me financial support during my study.

I thank the RI-B-NT Research Institute of Bioinformatics and Nanotechnology for giving me the opportunity to learn more professional knowledge and attend conferences. Thank the Kiel University for their good organization.

I thank all my colleagues from the Institute of Zoology, the Department of Structural Biology, of the Christian-Albrechts-University,who offered the pleasant working atmosphere.

I also thank my wife Ning Zhang for her constant help and encouragement.

Last but not least, a huge thank to my family for their love and continuous support.

Publications

R. K. Kar, Z. Gazova, Z. Bednarikova, K. H. Mroue, A. Ghosh, **R. Zhang,** K. Ulicna, H.-C. Siebert, N. E. Nifantiev, A. Bhutia (2016) Evidence for inhibition of lysozyme amyloid fibrillization by peptide fragments from human lysozyme: A combined spectroscopy, microscopy and docking study. ***Biomacromolecules***, 7(6), 1998-2009.

R. Zhang, G. Loers, M. Schachner, R. Boelens, H. Wienk, S. Siebert, T. Eckert, S. Kraan, M. A. Rojas-Macias, T. Lütteke, S. P. Galuska, A. Scheidig, A. K. Petridis, S. Liang, M. Billeter, R. Schauer, Jürgen Steinmeyer, J.-M. Schröder, H.-C. Siebert (2016) Molecular basis of the receptor interactions of polysialic acid (polySia), polySia mimetics and sulphated polysaccharides. ***ChemMedChem,*** 11(9), 990-1002.

M. K. Kosinska, T. E. Ludwig, G. Liebisch, **R. Zhang**, H.-C. Siebert, J. Wilhelm, U. Kaesser, R. B. Dettmeyer, H. Klein, B. Ishaque, M. Rickert, G. Schmitz, T. A. Schmidt, J. Steinmeyer (2015) Altered levels, composition, and molecular weight distribution of lubricin, phospholipids, and hyaluronan in synovial fluid during osteoarthritis and rheumatoid arthritis. ***PLOS ONE,*** 10(5): e0125192. doi:10.1371/journal.pone.0125192

R. Zhang, T. Eckert, T. Lütteke, S. Hanstein, A. Scheidig, A. M. J. J. Bonvin, N. E. Nifantiev, T. Kožár, R. Schauer, M. A. Enani, H.-C. Siebert (2015) Structure-function relationship of antimicrobial peptides and proteins in respect to contact-molecules on pathogen surfaces. ***Curr. Top. Med. Chem.***, 16, 89-98.

H.-C. Siebert, **R. Zhang**, A. Scheidig, T. Eckert, H. Wienk, R. Boelens, M. Mahvash, A. K. Petridis, R. Schauer (2015) Interaction studies of sialic acids with model receptors contribute to nanomedical therapies. ***J. Neurol. Disord.***, 3 (2), 1-6.

N. Zhang, **R. Zhang**, A. K. Petridis, T. Eckert, G. Scheiner-Bobis, A. Wehrend, M. Bergmann, A. Scheidig, R. Schauer, S. Fraune, T. C. G. Bosch, B. K. Chatterjee, H.-C. Siebert (2016) The nematocyst discharge process in relation to its physical-chemical properties as a role model for nanomedical tools. Ready for submission.

R. Zhang, L. Wu, T. Eckert, V. B. Krylov, A. Antosova, S. Ponikova, Z. Bednarikova, P. Markart, A. Günther, B. Norden, M. Billeter, R. Schauer, A. J. Scheidig, A. Bhunia, K. Hesse, M. A. Enani, Jürgen Steinmeyer, A. K. Petridis, Z. Gazova, N. E. Nifantiev, H.-C. Siebert (2016) New insights in the aggregation dynamic of lysozymes and insulins. Submitted.

R. Zhang, L. Wu, T. Eckert, M. Burg-Roderfeld, M. A. Rojas-Macias, T. Lütteke, V. B. Krylov, D. A. Argunov, P. Markart, A. Günther, B. Norden, R. Schauer, A. Bhunia, M. A. Enani, M. Billeter, A. J. Scheidig, N. E. Nifantiev, H.-C. Siebert (2016) Lysozyme's lectin-like characteristics facilitates its immune defense function. Ready for submission.

Declaration

I hereby declare that apart from the guidance from my supervisors, I have prepared this thesis autonomously according to the Rules of Good Scientific Practice of the German Research Foundation. It has not been submitted either partially or wholly as part of a doctoral degree to another examining body.
Parts of this thesis have been published in the articles as follows:

R. Zhang, G. Loers, M. Schachner, R. Boelens, H. Wienk, S. Siebert, T. Eckert, S. Kraan, M. A. Rojas-Macias, T. Lütteke, S. P. Galuska, A. Scheidig, A. K. Petridis, S. Liang, M. Billeter, R. Schauer, Jürgen Steinmeyer, J.-M. Schröder, H.-C. Siebert (2016) Molecular basis of the receptor interactions of polysialic acid (polySia), polySia mimetics and sulphated polysaccharides. ChemMedChem, 11(9), 990-1002.

M. K. Kosinska, T. E. Ludwig, G. Liebisch, **R. Zhang**, H.-C. Siebert, J. Wilhelm, U. Kaesser, R. B. Dettmeyer, H. Klein, B. Ishaque, M. Rickert, G. Schmitz, T. A. Schmidt, J. Steinmeyer (2015) Altered levels, composition, and molecular weight distribution of lubricin, phospholipids, and hyaluronan in synovial fluid during osteoarthritis and rheumatoid arthritis. PLOS ONE, 10(5): e0125192. doi:10.1371/journal.pone.0125192

R. Zhang, T. Eckert, T. Lütteke, S. Hanstein, A. Scheidig, A. M. J. J. Bonvin, N. E. Nifantiev, T. Kožár, R. Schauer, M. A. Enani, H.-C. Siebert (2015) Structure-function relationship of antimicrobial peptides and proteins in respect to contact-molecules on pathogen surfaces. Curr. Top. Med. Chem., 16, 89-98.

H.-C. Siebert, **R. Zhang**, A. Scheidig, T. Eckert, H. Wienk, R. Boelens, M. Mahvash, A. K. Petridis, R. Schauer (2015) Interaction studies of sialic acids with model receptors contribute to nanomedical therapies. J. Neurol. Disord., 3 (2), 1-6.

Additionally, parts of this thesis are prepared in a manuscript for scientific publication:

R. Zhang, L. Wu, T. Eckert, M. Burg-Roderfeld, M. A. Rojas-Macias, T. Lütteke, V. B. Krylov, D. A. Argunov, P. Markart, A. Günther, B. Norden, R. Schauer, A. Bhunia, M. A. Enani, M.

Billeter, A. J. Scheidig, N. E. Nifantiev, H.-C. Siebert (2016) Lysozyme's lectin-like characteristics facilitates its immune defense function.